Universidad de Huelva

Departamento de Ingeniería Química, Química Física y Ciencias de los Materiales

Freeze drying process design of pharmaceutical dispersions

Memoria para optar al grado de doctor
presentada por:

Getachew Weldeabezgi Assegehegn

Fecha de lectura: 10 de marzo de 2020

Bajo la dirección de los doctores:

José María Franco Gómez

Edmundo Brito de la Fuente

Huelva, 2020

University of Huelva

Department of Chemical Engineering, Physical Chemistry and Material Sciences

FREEZE DRYING PROCESS DESIGN OF PHARMACEUTICAL DISPERSIONS

Ph.D. Thesis

Doctoral Program in Industrial and Environmental Science and Technology

GETACHEW WELDEABEZGI ASSEGEHEGN

2020

Supervisors:

Prof. Dr. Edmundo Brito-de la Fuente

Prof. Dr. José María Franco Gómez

FREEZE DRYING PROCESS DESIGN OF PHARMACEUTICAL DISPERSIONS

Research memory presented by Getachew Weldeabezgi Assegehegn to apply for a doctoral degree at the University of Huelva.

Getachew Weldeabezgi Assegehegn

The present dissertation has been performed as a collaboration work between the department of Chemical Engineering, Physical Chemistry and Materials Science of the University of Huelva and the department of Innovation and Development Center of Fresenius Kabi Deutschland GmbH, under the supervision of Prof. Dr. Edmundo Brito-de la Fuente and Prof. Dr. José María Franco Gómez, who approve its defense.

Prof. Dr. Edmundo Brito-de la Fuente Prof. Dr. José María Franco Gómez

Huelva, 2020

Universidad de Huelva
Escuela de Doctorado

AUTORIZACIÓN PARA LA DEFENSA DE LA TESIS DOCTORAL EMITIDA POR EL DIRECTOR Y EL TUTOR Y POR LA COMISIÓN ACADÉMICA DEL PROGRAMA DE DOCTORADO

DATOS DEL DOCTORANDO:

Apellidos y nombre: Getachew W. Assegehegn	NIF/NIE/Pasaporte: EP3344643	Nacionalidad: Etíope
Dirección a efectos de notificaciones: Saalburgstrasse 160d, 61350 Bad Homburg, Alemania		
Teléfono: +4915231845666	EMAIL: felgech@gmail.com	

DATOS DE LA TESIS DOCTORAL:

Título: Freeze Drying Process Design of Pharmaceutical Dispersions
Programa Oficial de Doctorado al que se adscribe y órgano responsable: **Ciencia y Tecnología Industrial y Ambiental**
Línea de investigación a la que se adscribe y órgano responsable: **Ingeniería de procesos y productos químicos**
Rama de Conocimiento **(marcar casilla)**: ☐ Arte y Humanidades ☐ Ciencias ☐ Ciencias de la Salud ☐Ciencias Sociales y Jurídicas ☒ Ingeniería y Arquitectura

A CUMPLIMENTAR POR EL DIRECTOR Y POR EL TUTOR DE LA TESIS DOCTORAL: (en caso de que el Director y Tutor sean la misma persona, no es necesario cumplimentar los campos relativos al Tutor ni se precisa la firma de éste).

Director/es:	**Tutor/es:**
Dr./Dra.: José María Franco Gómez	Dr./Dra.:
Dr./Dra.: Edmundo Brito de la Fuente	Dr./Dra.:
Dr./Dra.:	Dr./Dra.:
como Director/Tutor de la Tesis Doctoral antes indicada **AUTORIZA** LA DEFENSA DE LA MISMA.	

En Huelva a, 7 de enero de 2020

Firma del/los Director/es de la Tesis Doctoral

Fdo.: José María Franco Gómez Fdo.: Edmundo Brito de la Fuente

Firma del/los Tutor/es de la Tesis Doctoral

Fdo.:_____ Fdo.:_____

A CUMPLIMENTAR POR LA COMISIÓN ACADÉMICA DEL PROGRAMA DE DOCTORADO:

Cumplidos los criterios de calidad aprobados para este Programa de Doctorado por el Comité de Dirección de la Escuela de Doctorado de la Universidad de Huelva y una vez valorada la Tesis Doctoral presentada por el Doctorando y haber incorporado éste las modificaciones y/o cambios que esta Comisión Académica le pudiera haber indicado, **se AUTORIZA** en reunión de fecha _____ **LA DEFENSA** de la misma.

En Huelva a, _____ de _____ de _____

Firma y sello del Presidente de la Comisión Académica

Fdo. Concepción Valencia Barragán

To my Parents

Table of Contents

Table of Contents

Acknowledgment

This PhD thesis has been completed as a collaboration work between the University of Huelva, Spain and Fresenius Kabi Deutschland GmbH, Germany.

First and foremost, I would like to express my sincere gratitude to Prof. Dr. Edmundo Brito-de la Fuente and Prof. Dr. Críspulo Gallegos-Montes for giving me the most precious opportunity to complete my Ph.D. thesis at Fresenius Kabi Deutschland GmbH. It has been a great honor to work with you and I am forever grateful for your continuous encouragement, support and timely review of all the papers throughout the journey of this work. With your help and supervision, I was able not only to advance my education and carrier but also to take the opportunity to build my personal competence.

Secondly, I would like to express my sincere gratitude to my academic supervisor at the University of Huelva, Prof. Dr. José Mª Franco Gómez, for accepting me to his team and for his continuous supervision, availability and timely review of my work throughout this project.

My wife, Felegehiwot Tekle Kahsay, has been a great support both mentally and physically, and I am highly grateful for that. Thank you for all the support, love and caring you showed me throughout our time together and I love you more.

The support and love of my family is the reason for me to reach the level where I am now. I would like to deeply thank my parents, Weldeabezgi Assegehegn and Ebabe Belay, for their encouragement and support since I was born. I would also like to thank my brothers Teklay, Emuru, Kokeb and Eyobed, and my sister Rosa. Thank you all for your encouragement and support throughout my years of study.

Finally, I would like to thank Dr. Lida Quinchia and Dr. Muhamad Anjum Nawaz for sharing their support and encouragement to take this challenging task. Especial thanks go to Marta Velasco for her unlimited help with Spanish related topics.

Nomenclature

API	Active pharmaceutical ingredient
Ave	Average
A_{con}	Area of contact between the vial bottom and the shelf
A_v	Outer surface area of a vial
C	Center vials
CQAs	Critical quality attributes
C	Mass fraction of solutes, Equation 7
C_g'	Mass fraction of solutes in the maximally freeze concentrated state
d	Thickness of the vial bottom
DoE	Design of Experiments
DS	Design space
DSC	Differential scanning calorimetry
FDM	Freeze drying Microscopy
FE	Front edge vials
FK1	Fresenius Kabi's drug formulation
GMP	Good Manufacturing Practice
G	Rate of crystal growth, Equation 8
IPEC	International Pharmaceutical Excipients Council
k	Thermal conductivity of a vial
K_c	Heat transfer coefficient contributed from direct conduction from a shelf to a vial glass at the point of contact
K_g	Heat transfer coefficient contributed from the conduction through the gas between a shelf and a vial bottom
K_r	Heat transfer coefficient contributed from a radiative heat transfer
K_{r1}	Radiation heat transfer coefficient from a chamber wall to a vial surface
K_{r2}	Radiation heat transfer coefficient from a shelf surface to a vial surface
K_v	Overall vial heat transfer coefficient
L_{R_p}	Dried layer thickness
Max	Maximum
MC	Moisture content
MF1	Model formulation 1 (10% (w/w) trehalose solution)
MF2	Model formulation 2 (20% (w/w) sucrose solution)
Min	Minimum

$\dot{m}$ in g/s	Overall mass transfer rate from a vial
$\dot{m}_{cn}$	Mass transfer rate through a condenser duct
$\dot{m}_p$	Mass transfer rate through a dried product
$\dot{m}_{st}$	Mass transfer rate through a semi-stopper opening
m_{wf}	Mass of freezable water
m_{wn}	Mass of water crystallized at nucleation
n	Experimental constants, Equation 8
PDS	Process design space
PEG	polyethylene glycol
PRT	Pressure rise test
P_{atm}	Atmospheric pressure
P_c	Chamber pressure
$P_c m1^0$	Maximum chamber pressure for primary drying
$P_c m2^0$	Maximum chamber pressure for secondary drying
$P_c t1^0$	Target chamber pressure for primary drying
P_{cn}	Ice condenser pressure
P_i	Vapor pressure of ice
$P_i(T_{cn})$	Vapor pressure of ice at ice condenser temperature
$P_i(T_p)$	Vapor pressure of ice (function of product temperature, T_p)
$P_i(T_p t1^0)$	Vapor pressure of ice at target product temperature for primary drying
P_v	Pressure inside a vial
QbD	Quality by design
QTPP	Quality target product profiles
$\dot{Q}$	Overall heat transfer rate to a given vial
$\dot{Q}_c$	Rate of heat transfer due to direct conduction
$\dot{Q}_g$	Rate of heat transfer due to conduction through the gas
$\dot{Q}_r$	Rate of heat transfer due to radiation
RSM	Response surface methodology
r	Pore radius of a dried product
R_{cn}	Ice condenser resistance to water vapor flow
R_p	Resistance to mass transfer of a dried product
$R_p(r)$	Resistance to mass transfer of a dried product (function of pore radius, r)
R_{st}	Stopper resistance to water vapor flow
RSC	Refrigerated cooling system
SD	Standard deviation

SSA	Specific surface area
TBA	Tert-butanol
TRA	Temperature ramp approach
T_c	Collapse temperature
T_{cn}	Ice condenser temperature
t_d	Drying time
T_{eu}	Eutectic temperature
T_f	Equilibrium freezing temperature of a solution
T_g	Glass transition temperature
$T_g(s)$	Glass transition temperature of a solute
$T_g(w)$	Glass transition of pure water
T_g'	Glass transition temperature of the maximally freeze-concentrated solution
$T_m(s)$	Melting or freezing temperature of a solute
$T_m(w)$	Melting or freezing temperature of pure water
T_n	Ice nucleation temperature
T_p	Product temperature
T_pave	Average product temperature during primary drying
T_pt	Target product temperature for primary drying
T_pt1^0	Target product temperature for primary drying
T_pt2^0	Target product temperature for secondary drying
T_{pc}	Product temperature due to heat transfer through direct conduction
T_{pg}	Product temperature due to heat transfer from conduction through the gas
T_s	Shelf temperature
T_{ss}	Shelf surface temperature
T_{vs}	Vial outer surface temperature
T_w	Freeze-dryer inner wall temperature
WFI	Water for injection
ΔH_m	Latent heat of fusion of water
ΔH_s	Heat of sublimation of ice
ΔT_s	degree of supercooling
β	Experimental constant, Equation 8
δ	*Stefan-Boltzmann* constant
ε	Radiative property of a surface termed as emissivity

Chapter 1: Introduction

Chapter 1: Introduction

Resumen

En general, en un proceso de liofilización, la formulación que se desea deshidratar o secar debe congelarse primero y, a continuación, el disolvente congelado se elimina mediante un proceso de sublimación a presión reducida, seguido de un proceso de desorción para la eliminación del disolvente no congelado. Por lo tanto, en el proceso de liofilización se llevan a cabo dos etapas importantes: (1) congelación, durante la cual la mayor parte del disolvente se convierte en sólido congelado; y (2) secado, durante el cual se elimina casi todo el disolvente (congelado y descongelado) de la formulación. Dependiendo del mecanismo de secado, el proceso de secado se divide en dos etapas, secado por sublimación (o secado primario) y secado por desorción (o secado secundario).

Aunque la aplicación de procesos de liofilización en la industria farmacéutica y bio-farmacéutica está siendo cada vez mayor, se trata de procesos altamente consumidores de energía y de tiempo. Dados los altos costes de inversión y de operación, existe una motivación económica considerable para diseñar procesos de liofilización fiables y que funcionen en condiciones óptimas de operación. Así, en el presente estudio se abordan tres cuestiones fundamentales que son pertinentes durante el diseño, optimización y escalado del proceso de liofilización: (1) comprensión de la etapa de congelación y su impacto en el proceso de secado posterior; (2) el análisis detallado y comprensión del proceso de transferencia de masa y de calor durante el secado primario; y (3) el análisis detallado, entendimiento y optimización de la etapa de secado secundario.

La etapa de congelación dicta la morfología de los cristales de hielo y el tamaño medio y la distribución de tamaños de los mismos que, a su vez, influye en varios parámetros críticos relacionados con la liofilización. El carácter aleatorio del grado

de sobre-enfriamiento durante la etapa de congelación afecta a las características del hielo, dando como resultado cierta heterogeneidad entre viales y lotes, lo que origina nuevos retos en el desarrollo, optimización y escalado del proceso de liofilización. Por lo tanto, comprender y controlar el paso de congelación es de suma importancia. En el presente estudio se discuten ampliamente diferentes tecnologías desarrolladas con el objetivo de controlar el grado de sobre-enfriamiento.

La etapa de secado primario es la más larga y crítica, influyendo significativamente en la calidad del producto y en la economía del proceso de liofilización. Los procesos de transferencia de calor y materia son los principios fundamentales que afectan el proceso de sublimación. Así, una mejor comprensión de la transferencia de materia y de calor durante el secado primario permite mejorar el diseño, optimización y escalado del proceso de liofilización. Se han realizado estudios de sublimación para estudiar la relación entre las variables independientes, a controlar, y las variables dependientes, o de salida, del secado primario. Además, los estudios sobre el efecto de la posición de los viales en las variables y parámetros del proceso de secado primario revelaron diferencias significativas entre los viales situados en el centro y en el borde del conjunto de viales colocados en las bandejas del liofilizador. El entendimiento de los procesos de transferencia de materia y de calor durante la fase de secado primario fue la base para el desarrollo de un nuevo enfoque, denominado enfoque de la rampa de temperatura (TRA), con el fin de diseñar un proceso de liofilización óptimo y fiable. El empleo de la aproximación TRA ha permitido optimizar el proceso de liofilización eficazmente para dos formulaciones modelo, aplicando relativamente pocos datos experimentales y condiciones de operación. Además, en el presente estudio se abordó la aplicación novedosa de un espacio de diseño de procesos (PDS) para la etapa de secado primario del proceso de liofilización.

Aunque la mayor parte del disolvente se elimina durante la fase de secado primario, es posible que aún quede una cantidad significativa de disolvente al final del secado primario, relacionada con el disolvente no congelado. Por lo tanto, es necesaria una etapa adicional de secado, a una temperatura elevada, para reducir el contenido de humedad residual del producto a un nivel aceptable. En el contexto de un proceso de liofilización, esta etapa adicional de secado se denomina secado secundario. En

este trabajo, se realizaron estudios experimentales de liofilización de una formulación de medicamento farmacéutico para estudiar la relación entre las variables a controlar y los parámetros del secado secundario o características finales del producto. Los resultados de estos estudios se utilizaron para desarrollar nuevamente un espacio de diseño de procesos (PDS), en este caso para la etapa de secado secundario, del cual se pudieron seleccionar las variables óptimas de procesado.

1.1. Summary

During a freeze-drying process, the formulation is first frozen and, then, the frozen solvent is removed by a sublimation process at a reduced pressure, followed by a desorption process for the removal of the unfrozen solvent. Therefore, two equally important major processes are taking place during a complete freeze-drying process: (1) freezing, during which the majority of the solvent is converted into a frozen solid; and (2) drying, during which almost all the solvent (frozen and unfrozen) is removed from the formulation. Depending on the drying mechanism, the drying process is further classified into two steps, namely; sublimation process (primary drying) and desorption process (secondary drying).

Although the use of a freeze-drying process in the pharmaceutical and biopharmaceutical industries is increasingly growing, it is an energy and time consuming process. Therefore, due to the high investment and running cost, there is a considerable economic motivation to design a robust and optimum freeze-drying process. With this regard, the present study addresses three key issues, which are relevant during freeze-drying process design, optimization and scale-up: (1) understanding of the freezing step and its impact on the subsequent drying process; (2) detailed analyses and understanding of mass and heat transfer during the primary drying; and (3) detailed analyses, understanding and optimization of the secondary drying step.

The freezing step dictates the ice crystal morphology, size, and size distribution, which, in turn, influences several freeze-drying related critical parameters. The

random nature of the degree of supercooling during the freezing step affects the ice habit and results in vial-to-vial and batch-to-batch ice habit heterogeneity. This, in turn, adds significant challenges during development, optimization, and scale-up of the freeze-drying process. Therefore, understanding and controlling the freezing step is of paramount importance. In the present study, several technologies, developed with the aim of controlling the degree of supercooling, have been extensively discussed.

The primary drying step is the longest and most critical step. Consequently, it significantly influences the product quality and process economy of the entire freeze-drying process. Heat and mass transfers are the core principles of the sublimation process. Thus, a better fundamental understanding of the mass and heat transfer during the primary drying allows a greater efficiency during the process design, optimization and scale-up. Sublimation studies were performed to examine and to establish a fundamental understanding of the relationship between the primary drying input and output parameters. Furthermore, studies on the effect of vial position on the primary drying output parameters revealed significant differences between vials located at the center and edge of the vial array. This fundamental understanding of the mass and heat transfer during the primary drying step was the foundation to the development of a novel approach, called temperature ramp approach (TRA), to design an optimum and robust freeze-drying process. Freeze-drying process design using the TRA for two model formulations demonstrated that an effective freeze-drying process could be designed using very few experimental setups. In addition, the present study discussed a novel approach for the development of a process design space (PDS) for the primary drying step a freeze-drying process.

Although most of the solvent is removed during the primary drying step, there might still be significant amount of solvent, related to the unfrozen solvent, remained at the end of the primary drying. Therefore, an additional drying step at an elevated temperature is necessary to reduce the residual moisture content of the product to an acceptable level. In the context of the freeze-drying process, this additional drying step is termed as secondary drying. Experimental studies using a pharmaceutical

drug formulation were performed to examine and to understand the relationship between the secondary drying input and output parameters. The results of these studies were then utilized to develop a process design space (PDS) for the secondary drying step, from which optimum processing parameters could be selected.

1.2. Justification

The majority of the existing literature focusses on mathematical modeling to design an optimized freeze-drying process, which requires additional expensive computer software. Furthermore, the mathematical models are developed based on several assumptions, and thus several experiments could be necessary to verify the resulting process parameters. Given the growing demand of the pharmaceutical and biopharmaceutical industries in implementing the freeze-drying process as a major drying unit operation, there exists a need for a systematic, scientific, and result-based process design and optimization approach. To address this point, this study aims on understanding the fundamentals of the freeze-drying process and developing different experimental-based approaches to design and optimize a freeze-drying process. Designing an optimum and robust freeze-drying process is certainly a high priority among pharmaceutical and biopharmaceutical industries, and thus the findings presented in this study will allow readers to understand the fundamentals of transport phenomena in a freeze-drying process and to apply scientific, easy-to-use and experimental-based approaches during freeze-drying process design and optimization. In doing so, the results and discussions presented in this research work advances the use of effective experimental-based approaches during freeze-drying process design, optimization, scale-up and transfer. Fresenius Kabi is a healthcare company, which implements the freeze-drying process as a major drying unit operation for some of its marketable products. Therefore, Fresenius Kabi would also significantly benefit from the research work presented in this thesis.

1.3. Objectives

Freeze-drying is commonly used in manufacturing labile pharmaceutical and biopharmaceutical products with the aim of extending their shelf life. However, freeze-drying process is a time and energy intensive process that could take from several days to weeks if the process is not well optimized. It is still common practice to design freeze-drying process using trial and error approach and, as a consequence, commercial freeze-drying processes are often neither robust nor efficient. Understanding formulation characteristics and their effect on freeze-drying processes, as well as a profound understanding of the heat and mass transfer processes during the freeze-drying process, allows greater efficiency in process development and optimization. Furthermore, designing a freeze-drying process based on a scientific understanding of the process minimizes problems encountered during scale-up and transfer. Therefore, a simplified approach based on a detailed heat and mass transfer analyses of different model pharmaceutical formulations will be developed for designing an effective and robust freeze-drying process. In addition, scaling-up a freeze-drying process from laboratory scale to manufacturing scale is another challenge during freeze-drying process design. Difference in mass and heat transfer between the different equipment is one critical scale-up issue. Laboratory and manufacturing scale freeze-dryers could have different design performances, which could cause variability in heat exchange and vapor transport systems. Differences in degree of supercooling during freezing arising due to differences in cleanness of manufacturing environments is another major factor during scale-up. Differences in degree of supercooling cause differences in vapor transport rate and significantly impacts drying temperature and time.

The main objectives of this thesis work are listed below:

- To develop a profound understanding of mass and heat transfer in freeze-drying process by performing sets of sublimation experiments using two model formulations and pure water using different process parameters (i.e., chamber pressure and shelf temperature). Mass and heat transfer

parameters will be calculated and the effect of the different process parameters on heat and mass transfer coefficients will be analyzed.

- To elucidate the effect of process parameters (i.e., chamber pressure and shelf temperature) on heat transfer uniformity across a shelf. This requires the calculation of overall heat transfer coefficient of vials at different positions (i.e., front edge, center, rear edge and side edge) and at different combinations of chamber pressure and shelf temperature. Understanding this relationship allows selection of process parameters that provide improved heat transfer uniformity as well as improved overall drying rate during the primary drying.

- To utilize the expertise and knowledge acquired from the above mentioned experiments and analyses to develop a novel and scientific approach, called “Temperature Ramp Approach”, for an effective, optimized and robust freeze-drying process design for any given formulation. The new approach will be tested experimentally for two model formulations and the resulting process parameters will be compared with the process parameters obtained using process design space approach of the same formulations.

- To develop a scientific approach for the construction of a process design space of the primary drying step of a freeze-drying process. The process design space is an important tool to study the dynamic relationship of the input process parameters with product temperature, sublimation rate, and product quality. Process design space sets process boundaries, within which process optimization and robustness studies can be performed without compromising product quality. The new approach will be tested experimentally using the two model formulations.

- To understand the influence of the critical input process parameters on the critical output parameters of the secondary drying step of a freeze-drying process. Furthermore, to optimize and construct a process design space of the secondary drying step for a drug formulation from Fresenius Kabi.

1.4. Thesis structure

The complete PhD thesis manuscript is divided in 5 main chapters.

This **first chapter** succinctly describes the summary, justification and objectives of the research work.

Chapter 2 presents the state of the art of the subject. Here, a detailed discussion of the fundamentals of the freeze-drying process, including an in-depth discussion of the three phases of the freeze-drying process, i.e., freeze, primary drying, and secondary drying phases are given. In the freezing sub-section, the physicochemical changes that occur during the freezing phase and their impact on the freeze-drying process are discussed. Furthermore, currently available alternative technologies for the application of controlled nucleation are discussed. In the primary drying sub-section, a detailed discussion on the heat and mass transfer during the primary drying phase is given. In the secondary drying sub-section, a brief discussion on the importance of the secondary drying phase is given. Furthermore, this chapter presents a detailed discussion on the overview of a freeze-drying equipment and on the relationship of formulation properties and a freeze-drying process.

Chapter 3 presents a detailed description of the experimental techniques employed in this work, including all the materials, methods and devices.

Chapter 4 presents the major findings, results and discussions of this work. In the first sub-section of this chapter, detailed analyses of the heat and mass transfer during the primary drying phase, focusing on the effect of input process parameters on output parameters are given. Such analyses provide fundamental understanding on the freeze-drying process. In the second sub-section, an innovative approach, called temperature ramp approach (TRA), for the design of a robust and optimum freeze-drying process of model formulations is discussed. In the third sub-section, another innovative approach for the construction of a process design space (PDS) is discussed. The PDS is a tool that could be used during process design, scale-up and transfer. In the last sub-section of this chapter, understanding and optimizing the secondary drying step is discussed. Furthermore, a detailed discussion on the

effect of the critical input parameters on the critical output parameters during the secondary drying is given. Also, construction of a process design space (PDS) for the secondary drying phase is discussed.

Chapter 5 presents the main conclusions of this research work.

Finally, the **Appendices** collected copies of articles already published (or submitted to publication) in peer-reviewed journals, including a review article on the importance of the freezing step in the freeze-drying process, which makes part of the state-of-the-art chapter, as well as a list of contributions and publications in international congresses and conferences on this topic.

Chapter 2: State of the art

Chapter 2: State of the art

2.1. Fundamentals of a freeze-drying process

Drying is one of the key unit operations in pharmaceutical and biopharmaceutical industries, especially used to remove solvents (usually water) from liquid drug formulations with the purpose of converting them into solid forms without compromising their pharmaceutical and therapeutic properties. The main reason behind this conversion is that a drug formulation in its solid state allows the immobilization of the active drug substance as well as the excipients, hence significantly reducing chemical and physical degradation pathways, such as hydrolysis, oxidation, isomerization, condensation, racemization and reactions with other components in solution [Franks, 2007]. An extended stability of the formulations containing active pharmaceutical ingredients (APIs), even at ambient temperature, is then achieved [Bosca & Fissore, 2014]. In addition to the stability benefits, drug formulations in solid forms have the advantages of easing handling and storage, and reducing transportation costs [Walters et al., 2014]. In contrast to the above advantages, solid or freeze dried products have some disadvantages, such as they are not as convenient to administer as a sterile, ready-to-use solution; freeze dried products require additional reconstitution and transfer steps during administration (because of this, sterility assurance may be compromised); and due to expensive equipment and manufacturing costs, freeze dried products are, generally, more expensive than ready-to-use solutions.

Several drying technologies are already in use or under development in pharmaceutical and biopharmaceutical industries. These include freeze-drying [Pikal, 2006; Bhatnagar et al., 2013; Kharaghani et al., 2017], foam drying [Ohtake et al., 2011; Jangle & Pisal, 2012], spray drying [Cheow et al., 2010; Ohtake et al., 2010; Cortés-Rojas et al., 2015], spray freeze-drying [Sonner et al., 2002; Cheow et al., 2011; Wanning et al., 2015; Ali & Lamprecht, 2017], supercritical fluid drying [Reverchon et al., 2009; Jin et al., 2012], convective drying [Gabel et al., 1998] ,

microwave drying [Farrel et al., 2005; de Jesus & Filho, 2011] and more recently electrostatic drying [Xie et al., 2015]. A detailed review of these drying technologies is given elsewhere [Walters et al., 2014]. Selection of an efficient drying process often presents challenges, because it requires the consideration and evaluation of many critical parameters. These include physical properties of the product, drying temperature, residual water content, quality and shelf-life of the dried product, ease of process design, scalability, capability to implement the technique in a GMP (Good Manufacturing Practice) environment, ease of control of critical process parameters, and investment and operational costs of the drying process. The challenges arise from the fact that all the available drying technologies only fulfill few of the factors listed above. Therefore, the selection process requires an intensive evaluation and comparison of the different drying technologies, especially considering the final product attributes. In addition to the above factors, the cost of raw materials might also have an impact on the selection of the drying process [Walters et al., 2014]. For instance, for high value products, as it is often the case with pharmaceuticals, the cost of the raw ingredients may be the primary driver that dictates the selection of a drying method, as low yield or product recovery less than 100% may not be acceptable [Walters et al., 2014].

Despite the abundance of drying technologies available, the vast majority of these techniques, in their current state, are not directly applicable for the processing of pharmaceutical and biopharmaceutical products due to many reasons, including: (1) unknown effect of energy source on structure/stability of the products, (2) energy efficiency, (3) scalability, and (4) inability to achieve low residual water content [Walters et al., 2014]. This might be the reason why the vast majority of the pharmaceutical and biopharmaceutical industries are currently using freeze-drying or lyophilization as a drying technique. Despite its shortcomings, such as high production costs, high investment and maintenance costs, and low throughput, freeze-drying is a well-established drying method that successfully passes regulatory bottlenecks. Some of the most important reasons that freeze-drying established itself as a common drying process are; (1) low temperature process is beneficial for most of the heat sensitive active pharmaceuticals, (2) it has long been accepted by national and international authorities, which regulate the granting of product licenses,

(3) the ability of running the process under conditions of absolute sterility, (4) the rapid reconstitution of the dried product at the point of use, and (5) freeze-dried products are widely recognized and accepted products in the market [Franks, 2007]. In this context, the main focus of industries is to optimize the drying process, so that an elegant product is obtained at the shortest possible processing time. Optimization of a freeze-drying process requires a detailed understanding of the formulation and the process itself. The broad use of freeze-drying process is supported by the fact that, in 1998, lyophilized pharmaceuticals accounted for 11.9% of all new injectable or infusible drugs, but, by 2015, they made up half of all such new drug introductions [Shanley, 2017].

The use of freeze-drying as a method of preservation is not a new idea and can be traced back to prehistoric times when, for example, the Eskimo preserved fish by dehydration in the cold Arctic winds. Given the complexity nature of a freeze-drying process as well as the limited knowledge of refrigeration and vacuum technologies, industrialization of freeze-drying process was not an easy task until 1930s, when the need arose to preserve large volumes of heat-sensitive blood products and the then newly discovered antibiotics [Ward, 1997]. Recently, advances in refrigeration and vacuum technologies have enabled freeze-drying process to expand within pharmaceuticals and biopharmaceuticals industries to encompass a wide range of products, such as vaccines, proteins, vitamins, therapeutic enzymes and many others. Through the years, it has become clear that freeze-drying process offers additional advantages compared to alternative drying methods in addition to stabilization. First, freeze-drying process allows heat-sensitive pharmaceutical drugs to be dried at low temperature, hence reducing the extent of degradation as well as therapeutic properties of the drugs. Second, freeze-dried products have a very high specific surface area, which enables a rapid and complete reconstitution of the products [Ward, 1997].

Freeze-drying is a drying unit operation with a core principle of removal of solvent from a liquid formulation, in which the formulation is first frozen and then the frozen solvent is removed by sublimation, at a reduced pressure, followed by a desorption process for the removal of the unfrozen solvent. Therefore, two equally important

major processes are taking place during a complete freeze-drying process; (1) *freezing*, during which the majority of the solvent, up to 95% [Tang & Pikal, 2004], is converted into frozen solid, and *(2) drying*, during which almost all the solvent (frozen and unfrozen) is removed from the formulation. The drying process is further classified into two steps, based on the mechanism of the drying process, namely sublimation (primary drying) and desorption (secondary drying).

During the *freezing phase*, the liquid formulation is frozen and eventually converted into a solid form. In the frozen solid form, a phase separation of the solvent, usually water, and the rest of the solutes occurs, which is a key phenomenon for a lyophilization process. This is because, if this separation does not occur, a fully solid frozen formulation with a greatly reduced vapor pressure will be formed and the formulation cannot be lyophilized [Kasper & Friess, 2011]. Most of the water (approximately 80% to 95% [Tang & Pikal, 2004], depending on the formulation) crystallizes into hexagonal ice crystals and the rest of the solvent (approximately 5% to 20%) remains unfrozen entrapped within the solutes. During the freezing process, the concentration of the solute increases to a maximum, as water is removed because of crystallization, above which a further increase in concentration is not possible. The solute at this state is termed as “maximally freeze-concentrated solute”.

During the *primary drying phase*, the frozen part of the solvent, mostly 80% to 95%, is removed from the formulation through a sublimation process. Sublimation is the process of converting a solid phase directly into gaseous phase without passing through the intermediate liquid phase. In freeze-drying, the driving force of the sublimation process is the pressure difference between the vapor pressure of ice at a given target product temperature and the ice condenser pressure, which is identical to the chamber pressure. The chamber pressure is, therefore, reduced to a pressure well below the vapor pressure of ice at the given target product temperature to initiate the sublimation process. Additionally, continuous heat supply is provided to compensate the heat removed by the sublimation process and to maintain the target product temperature during the entire primary drying phase.

During the *secondary drying phase*, the unfrozen part of the solvent, mostly 5% to 20% of the total solvent, is removed from the formulation through a desorption process. Desorption is the process of removal of liquid phase into gaseous phase via evaporation of the liquid. In freeze-drying, the driving force for the desorption process is the temperature difference between the product temperature and the evaporation temperature of water at a given pressure. In order to facilitate the evaporation of water at low temperatures, the chamber pressure is usually kept very low, mostly similar to the chamber pressure during primary drying. At the same time, the temperature during the secondary drying is increased to allow faster desorption rate. Depending on the heat sensitivity of the formulation, a secondary drying temperature as high as 45 °C could be used [Tang & Pikal, 2004].

A complete evolution of a freeze-drying process can be described using Figures 1 and 2. As illustrated in Figure 2, the freezing step consists of different physicochemical changes (cf. section 2.1.1). During the first change, the solution is cooled down to its equilibrium freezing temperature (T_f), point A, and the solution during this stage is called cold solution. Since solutions do not start freezing at their T_f, they remain liquid for certain degrees below their T_f (from point A to point B). The state of a solution during this stage is called supercooled solution, and the degree that a given solution retains its liquid state below T_f is called degree of supercooling. At point B, the supercooled solvent starts to freeze by creating a stable ice nucleus. The temperature at which the first ice nucleus starts is called nucleation temperature (T_n) and the process is called *primary nucleation*. Since crystallization is an exothermic process, the temperature of the solution increases rapidly to its T_f (point C). During the nucleation period, which is also called *secondary nucleation*, (point B to point C), many ice crystals are generated, encompassing the entire solution volume.

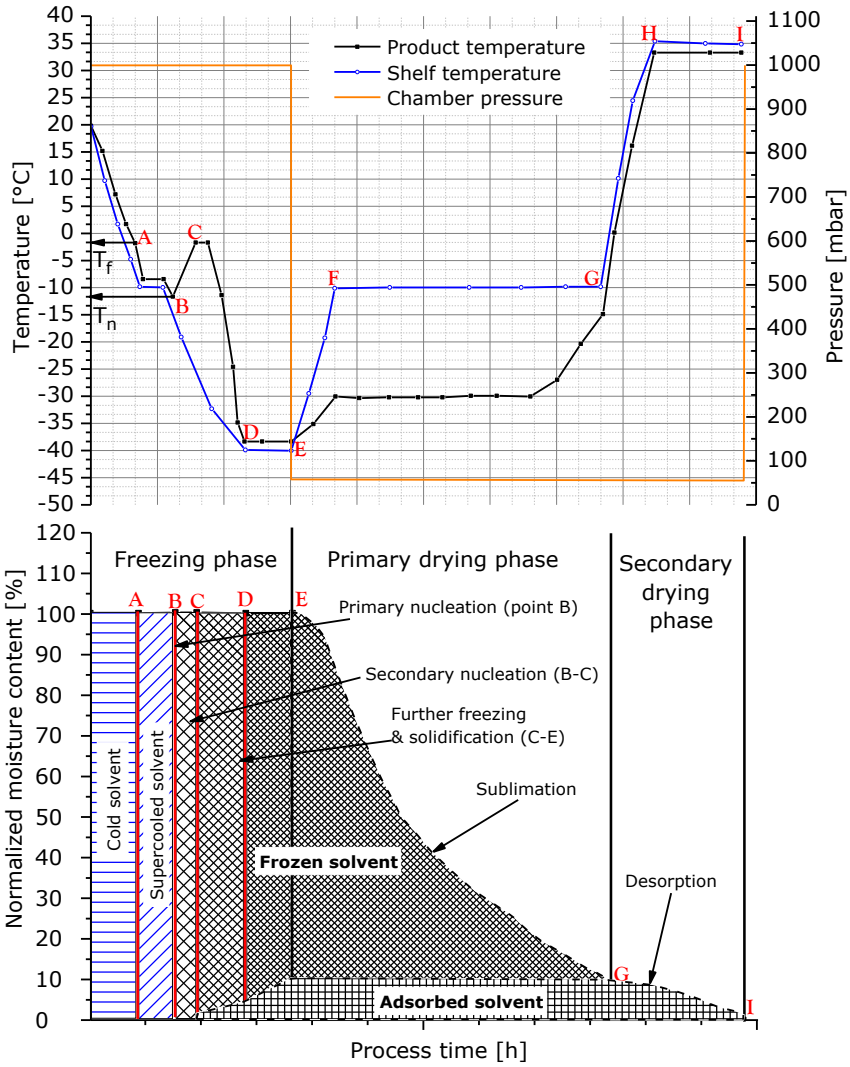

Figure 1. Graphical depiction of the freeze-drying process. Upper figure shows typical temperature and pressure profiles, while the lower figure shows how freezing, sublimation and desorption of a solution progresses with regard to the temperature and pressure profiles. T_f, equilibrium freezing temperature; and T_n, nucleation temperature.

The number of ice crystals formed during the secondary nucleation period are dependent on the degree of supercooling, which takes-up the heat generated during the exothermic crystallization process. Upon further cooling of the solution, the ice crystals, generated during the nucleation period, grow and the solution further freezes (from point C to point D). However, simply lowering the temperature to the

final freezing temperature does not guarantee complete solidification of the solution. Thus, a holding time at the final freezing temperature (from point D to point E) is necessary to allow complete solidification of the freezable solvent. During freezing of the solution, there is a significant increase in solute concentration, as the available liquid solvent decreases with freezing. This increase in solute concentration increases the amount of adsorbed solvent, as shown from point B to point E of the lower part of Figure 1. Both the freezing and adsorption interfaces progress until a critical concentration of the solute is achieved, above which further freezing or adsorption of the solvent is not possible. At this point, the solution is regarded as a completely solidified solution, denoted by point E. Analyzing point E, up to 10% of the initial water content remains unfrozen, bound or adsorbed within the solute matrix. The amount of unfrozen water depends on the type and concentration of the solute and it typically ranges from 5 to 20% [Tang & Pikal, 2004]. The freezing process is shown in the phase diagram of water (Figure 2) as liquid water crosses the melting/freezing interface and changes into frozen water, when temperature is decreased at atmospheric pressure (P_{atm}).

Once all the freezable liquid is solidified, the sublimation process is started by reducing the chamber pressure and increasing the shelf temperature into a predefined value (point F, Figures 1 and 2). During the sublimation process, strict control of the product temperature is required as this defines the product quality and drying rate. However, in a freeze-drying process, a direct control of the product temperature is not possible and this is usually done by a proper manipulation of the chamber pressure and shelf temperature. The optimum combination of chamber pressure and shelf temperature that produces the desired product temperature is then held until all the frozen solvent is sublimed, point G. As displayed in Figure 2, sublimation of the frozen water is triggered when the chamber pressure reaches a minimum pressure. At a target product temperature for primary drying ($T_p t1^0$), the maximum chamber pressure for primary drying ($P_c m1^0$) corresponds to the vapor pressure of ice at $T_p t1^0$. However, at this point, the driving force for sublimation, which is the pressure difference between the vapor pressure of ice at $T_p t1^0$ and chamber pressure is null, leading to an extremely slow or no sublimation process. To increase the sublimation process, the chamber pressure is further reduced to a

target chamber pressure for primary drying ($P_c t1^0$), while keeping $T_p t1^0$. At a given $T_p t1^0$, the lower the chamber pressure, the higher the driving force for the sublimation process, and hence the faster the drying rate. However, the minimum chamber pressure is limited by the capability of a freeze-drying equipment to properly maintain it during the entire primary drying phase [Ganguly et al., 2013 & 2017; Kshirsagar et al., 2019].

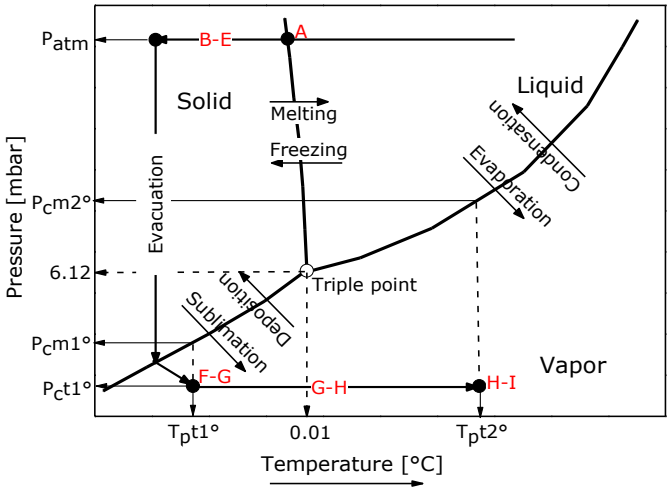

Figure 2. Progression of a freeze-drying process through a phase diagram of water. P_{atm}, atmospheric pressure; $P_c m2^0$, maximum chamber pressure for secondary drying; $P_c m1^0$, maximum chamber pressure for primary drying; $P_c t1^0$, target chamber pressure for primary drying; $T_p t1^0$, target product temperature for primary drying, and $T_p t2^0$, target product temperature for secondary drying. The letters A-I correspond to the same process phases as in Figure 1.

Once all frozen solvent is sublimed (Point G, Figure 1), product temperature is increased (point H, Figure 1), while keeping low chamber pressure, to remove adsorbed (unfrozen) solvent via desorption. Desorption is evaporation of adsorbed liquid solvent through the dried product. Desorption process continues until the desired final moisture content and glass transition temperature of the dried cake is achieved (point I, Figure 1). Figure 2 shows the desorption process of unfrozen water, in which product temperature is increased to a point beyond the triple point temperature of water. At a target product temperature for secondary drying ($T_p t2^0$), the maximum chamber pressure for secondary drying ($P_c m2^0$) corresponds to the

vapor pressure of liquid water at $T_p t2^0$. However, at this point, the driving force for evaporation, which is the temperature difference between actual product temperature ($T_p t2^0$) and the evaporation temperature at $P_c m2^0$ is null, leading to an extremely low or no desorption rate. To increase the desorption rate, the chamber pressure is kept as low as possible. Low chamber pressure decreases the evaporation temperature of liquid water, and hence at $T_p t2^0$, the driving force for evaporation is increased. In most cases, chamber pressures for primary and secondary drying are kept identical.

2.1.1. Freezing

The following sub-section has been published as a review article on the Journal of Pharmaceutical Sciences (see Appendix A.1). The structure of the published document has been slightly modified to fit to this particular document.

2.1.1.1. Introduction

Freeze-drying is a drying unit operation with a core principle of removal of solvent from a liquid formulation, in which the formulation is first frozen and then the frozen solvent is removed by sublimation, at a reduced pressure, followed by a desorption process for the removal of the unfrozen solvent. Therefore, 2 equally important major processes are taking place during a complete freeze-drying process; (1) freezing, during which most of the solvent, up to 95%, [Tang & Pikal, 2004] is converted into frozen solid, and (2) drying, during which almost all the solvent (frozen and unfrozen) is removed from the formulation. The drying process is further classified into 2 steps, based on the mechanism of the drying process, namely sublimation (primary drying) and desorption (secondary drying).

Freezing is the first operation in a freeze-drying process and is, of course, a critical step because if the product is impaired from the start, there is obviously no interest to go further [Rey, 2010]. During the freezing step, most of the water is converted into solid by forming a network of ice crystals and this step dictates ice crystal morphology, size, and size distribution, which, in turn, influence several critical parameters, such as dried product resistance, primary and secondary drying rates,

extent of product crystallinity, specific surface area, and reconstituability of the dried product [Searles et al., 2001a]. The influence of freezing on the subsequent drying process can be well described using the governing transport phenomena equations of a freeze-drying process. During the primary drying phase of a freeze-drying process, heat and mass transfer should take place in “close-equilibrium”, so that the change in product temperature during the entire primary drying period remains insignificant, usually within 2 °C–3 °C. Therefore, for the purpose of calculations, a pseudo steady-state in product temperature can be safely assumed, and hence the equilibrium in heat and mass transfer during primary drying is given as in Equation 1.

$$\dot{Q} = \Delta H_s \dot{m} \quad (1)$$

where, $\dot{Q}$[W] is the overall heat transfer rate to a given vial; ΔH_s[J/g] is the heat of sublimation of ice; and $\dot{m}$ [g/s] is the overall mass transfer rate from a vial.

Furthermore, the overall heat and mass transfer rates can be expressed as in Equations 2 and 3, respectively.

$$\dot{Q} = A_v K_v (T_s - T_p) \quad (2)$$

where, A_v[cm^2] is the outer surface area of a vial; K_v[W/cm^2.K] is the overall vial heat transfer coefficient; T_s[K] is the shelf temperature; and T_p[K] is the product temperature.

$$\dot{m} = \frac{P_i(T_p) - P_c}{R_p(r)} \quad (3)$$

where, $P_i(T_p)$[mbar] is the vapor pressure of ice (function of product temperature, T_p); P_c[mbar] is the chamber pressure; and $R_p(r)$[mbar.s/g] is the resistance to mass transfer of the dried product (function of pore radius, r).

Substituting Equations 2 and 3 into Equation 1 gives:

$$A_v K_v \left(T_s - T_p\right) = \Delta H_s \frac{P_i(T_p) - P_c}{R_p(r)} \quad (4)$$

All the parameters in Equation 4 are as described previously. Equation 4 can be used to analyze the effect of the freezing step on the primary drying of freeze-drying process.

Effect of freezing on resistance to mass transfer of the dried product ($R_p(r)$)

As mentioned earlier, the predominant and direct impact of the freezing step is on the formation of ice crystal habits, such as size and morphology, and this, in turn, impacts the pore size of the dried product after the ice crystals are sublimed. Large ice crystals leave large pore radius in the dried product and, consequently, they have low resistance to mass transfer. In contrast, small ice crystals leave small pore radius, which hinder the transport of water vapor significantly. Therefore, the resistance to mass transfer of the dried product is inversely related to the size of ice crystals that are formed during the freezing step.

Effect of freezing on product temperature (T_p) and vapor pressure of ice (P_i)

As mentioned in the previous section, the direct impact of the freezing step is on the resistance to mass transfer of the dried product, R_p, and, as a consequence of this, many other parameters, such as product temperature, T_p, vapor pressure of ice, P_i, overall vial heat transfer coefficient, K_v, and mass transfer rate, $\dot{m}$, are affected. Although the effect of the freezing step on these parameters is rather complex, it can be studied by evaluating the governing heat and mass transfer equations. Rearranging Equation 4 for product temperature, the following equation is obtained:

$$T_p = T_s - \frac{\Delta H_s(P_i(T_p) - P_c)}{A_v K_v R_p(r)} \qquad (5)$$

To evaluate the effect of the freezing step on product temperature, T_p, from Equation 5, the following condition must be met: The input process parameters, that means the shelf temperature, T_s, and the chamber pressure, P_c, should be kept unchanged. Now, let us consider 2 proprietary products, product A and product B. For product A, the freezing protocol produces few and large ice crystals, and hence low R_p. On other hand, the freezing protocol for product B produces many and small ice crystals, and

hence high R_p. According to Equation 5, this results in lower product temperature for product A than for product B. This is because, at low R_p, the endothermic mass transfer process is dominant, and thus takes up substantial energy from the process. If this substantial energy take-up is not compensated by increasing the heat transfer rate (rate limiting process), the product temperature decreases. At the same time, according to the phase diagram of water, the vapor pressure of ice, p_i, decreases as product temperature decreases. Consequently, the term $(P_i(T_p) - P_c)$ in Equation 5 decreases, resulting in a reduction of mass transfer rate. The reduction in mass transfer rate reduces the energy take-up from the process, and thus the product temperature slightly increases. This cycle repeats itself until a new equilibrium in heat and mass transfer rate is achieved. This analysis implies that, for product A (with low R_p), the energy input (i.e., the shelf temperature) can be increased to shift the heat transfer rate from a rate limiting process to a process in equilibrium with the mass transfer rate, so that the product temperature remains at the predefined target product temperature from the start of the process.

On the other hand, at high R_p, the endothermic mass transfer process becomes a rate limiting process, and the excess energy input from the dominant exothermic heat transfer process causes the product temperature to increase. At the same time, according to the phase diagram of water, the vapor pressure of ice, P_i, increases as product temperature increases. Consequently, the term $(P_i(T_p) - P_c)$ in Equation 5 increases, resulting in an increased forced mass transfer rate. Depending on the increase in the magnitude of the forced mass transfer rate and the product temperature, a microcollapse or a complete collapse of the product might occur. This analysis implies that, for product B (with high R_p), the energy input, that means the shelf temperature, might need to be decreased to shift the heat transfer rate from a dominant process to a process in equilibrium with the mass transfer rate, so that the product temperature remains at the predefined target product temperature, avoiding product damage. In general, the impact of the freezing step on the different parameters can be summarized as follows:

$$\left.\begin{array}{c} r \propto ice\ crystal\ size \\ R_p \propto \frac{1}{r} \\ R_p \propto T_p \\ P_i \propto T_p \\ T_p, P_i \propto \frac{1}{r} \\ \dot{m} \propto \frac{1}{R_p}, T_p \end{array}\right| \quad Provided\ T_s\ and\ P_c\ are\ kept\ unchanged \qquad (6)$$

Therefore, it is of paramount importance to study the nature of the freezing step during development, optimization, transfer and/or scale-up of the freeze-drying process.

Effect of freezing on mass transfer rate ($\dot{m}$)

The effect of the freezing step on mass transfer rate is not a straight forward relationship. On one hand, mass transfer rate is inversely related to the resistance to mass transfer of the dried product, R_p. On the other hand, mass transfer rate is directly related to the product temperature, T_p, and hence to the vapor pressure of ice, P_i, provided that the shelf temperature and chamber pressure are kept unchanged (Equation 6).

As can be deduced from Equation 6, large ice crystals are correlated with low dried product resistance and with low product temperature. Further, Equation 6 shows the relationship of dried product resistance and product temperature with mass transfer rate and, according to this equation, the lower the dried product resistance, the higher the mass transfer rate and, on the other hand, the lower the product temperature (or the vapor pressure of ice), the lower the mass transfer rate. Therefore, the overall effect of the freezing step on mass transfer rate is dependent on the relative effect of the freezing step on the dried product resistance and the product temperature. Therefore, the advantage of having high mass transfer rate due to low dried product resistance could be offset by the low product temperature, unless the processing parameters (shelf temperature and chamber pressure) are set to keep the product temperature at the predefined target product temperature.

In addition to the above impact of the freezing step on freeze-drying process, it is a critical step with regard to biological activity and stability of the active pharmaceutical ingredient, especially for pharmaceutical proteins [Carpenter et al., 1994; Bhatnagar et al., 2007 & 2008; Searles, 2010; Connolly et al., 2015]. Therefore, a thorough understanding of the physico-chemistry of the freezing process is essential for understanding how both formulation composition and process conditions influence the quality of the freeze-dried product [Nail et al., 2002].

The aim of the current review is to gather existing information on the physicochemical phenomena involved during the freezing process and how these phenomena impact the subsequent drying step of the freeze-drying process. In addition, modification of the freezing process and different techniques used to actively control the degree of supercooling during freezing will be reviewed and discussed along with their impact on freeze-drying process performance. In this sense, this review stresses the importance of understanding the fundamental principles of the freezing step during the freeze-drying process, as well as its significant impact on freeze-drying process development, optimization and scale-up. In addition, an update of the available techniques for the active control of the degree of supercooling is addressed.

2.1.1.2. The freezing process

In general, the freezing process consists of 3 stages namely, (1) *cooling stage*, in which the liquid formulation is cooled from its initial temperature to the freezing point temperature; (2) *phase change stage*, in which the first ice nucleus formation and ice crystal growth are taking place; and (3) *solidification stage*, in which all the ice crystals grow to an extent that no further ice crystal growth is possible [Dalvi-Isfahan et al., 2017].

2.1.1.2.1 Cooling stage

During the cooling stage, the temperature of the formulation is decreased until the first ice nucleus starts to be formed. The temperature at which the first ice nucleus is formed is known as ice nucleation temperature, T_n. When an aqueous system is cooled at atmospheric pressure, it does not freeze spontaneously at its equilibrium

freezing point [Kasper & Friess, 2011]; rather, it retains its liquid state to a certain degree. The equilibrium freezing of aqueous systems requires, among other things, that an ice crystal nucleus is made available at the equilibrium freezing point of the system and that appreciable temperature differences within the system do not exist. Supercooling arises when, at least, one of these conditions is not met [MacKenzie et al., 1997]. Supercooling is therefore defined as the ability of an aqueous system to retain its liquid state below its equilibrium freezing point. During the supercooling state, which is a nonequilibrium and metastable state, water molecules form clusters with relatively long-living hydrogen bonds with similar molecular arrangements to ice crystals [Kasper & Friess, 2011; Petzold & Aguilera, 2009]. Since this process is energetically unfavorable, the molecular clusters break up rapidly until an adequate amount of molecules associate in 3 dimensions to form a thermodynamically stable aggregate, so-called critical nucleus, which provides surfaces suitable for crystal growth [Dalvi-Isfahan et al., 2017]. Depending on the cooling rate used, 2 supercooling states can be observed. The first is global supercooling, in which the entire liquid volume achieves a similar level of supercooling, and the secondary nucleation zone encompasses the entire liquid volume. Solidification then progresses through the already nucleated volume [Searles et al., 2001a]. Slow cooling rates, such as shelf-ramp cooling, lead to global supercooling. The second is local supercooling, in which a small fraction of the volume is supercooled to the point of primary and secondary nucleation. The nucleation and solidification fronts are in close proximity in space and time, with the front moving into the non-nucleated liquid [Searles et al., 2001a]. Figure 3 shows a typical freezing curve of a pharmaceutical liquid formulation. The equilibrium freezing point of this formulation is shown as point A and, because freezing does not start at point A, the formulation retains its liquid state until point B, in which the first ice nucleus is formed. The state of the formulation from point A to point B is termed as supercooling state and the degree that the given formulation retains its supercooling state is termed as degree of supercooling. The degree of supercooling is quite variable and it is affected by several factors, such as foreign particles, container surface area, process conditions, sample volume, composition of the matrix, and contact area between sample and container [Dalvi-Isfahan et al., 2017]. The aforementioned and other factors are responsible for the random and stochastic nature of ice nucleation. As will be

discussed later more in detail, the variation in degree of supercooling from sample to sample affects the drying behavior of these samples during primary drying and this, in turn, hinders the effort to design robust and economically optimized freeze-drying processes. Therefore, the ability to control the degree of supercooling or ice nucleation during the freeze-drying process is essential to produce batches with consistent and similar freezing behaviors. Freezing methods aiming to control the ice nucleation during the freeze-drying process are currently available. Some of them have yielded successful experimental results at laboratory scale [Konstantinidis et al., 2011; Awotwe-Otoo et al., 2014; Esfandiary et al., 2016]. However, only limited data are still available at industrial scale [Chakravarty et al., 2012; Azzarella et al., 2016]. These methods will be discussed more in detail later in this review.

2.1.1.2.2 Phase change stage

Phase change stage (referring to a phase change from liquid to solid) starts once a formulation reaches its ice nucleation temperature (T_n), point B of Figure 3, in which the first ice nucleus appears. The appearance of the first ice nucleus is called primary nucleation.

Primary nucleation is an extremely fast process, and hence it is difficult to observe either by eye or on a cooling thermogram except as a starting point of the secondary nucleation [Searles et al., 2001a]. *Secondary nucleation* (from point B to C of Figure 3) immediately follows primary nucleation and it is characterized by the addition of ice nucleation sites.

Formation of ice crystals is an exothermic process and, for this process to continue, the heat given off must be removed. This heat is removed by the supercooled solution, which is at a certain degree below the equilibrium freezing temperature. During this process, the supercooled formulation only absorbs limited amount of heat, and hence the temperature of the solution increases quickly to its equilibrium freezing temperature where formation of ice crystals ceases, point C of Figure 3.

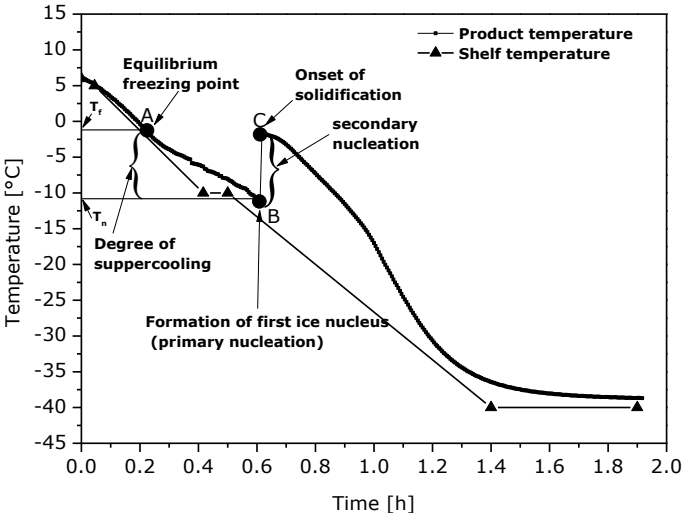

Figure 3. Freezing curve of a typical pharmaceutical formulation obtained during a shelf-ramp freezing experiment (authors' own results). T_f, equilibrium freezing temperature; and T_n, ice nucleation temperature.

The amount of heat absorbed during secondary nucleation determines the total number of ice crystals formed, which, in turn, depends on the degree of supercooling. Higher degree of supercooling allows bigger amount of heat to be absorbed during the exothermic crystallization process and this grants the formation of many ice crystals.

The mass fraction of freezable water that crystallizes during nucleation (x) can be calculated according to Equation 7, in which the extent of supercooling is used to absorb the heat of crystallization up to the equilibrium freezing point [Searles et al., 2001a]:

$$x = \frac{m_{wn}}{m_{wf}} = \frac{(T_f - T_n)\, C_{pw}}{\left(1 - {C}/{C_g'}\right) \Delta H_m} \qquad (7)$$

where, m_{wn} is the mass of water crystallized at nucleation; m_{wf} is the mass of freezable water; T_f is the equilibrium freezing temperature of water; T_n is the ice nucleation temperature; C_{pw} is the heat capacity of water (around 4.2 J/g.K); C is the mass fraction of solutes; C_g' is the mass fraction of solutes in the maximally freeze

concentrated state; and ΔH_m is the latent heat of fusion of water (334 J/g) [Kumano et al., 2007]. The amount of total crystallizable water and unfrozen water is mainly influenced by the composition of the formulation and is not influenced by the ice nucleation temperature [Geidobler & Winter, 2013].

In addition, the rate of ice crystal growth (freezing rate) is dependent on the degree of supercooling. At higher degree of supercooling (i.e., lower ice nucleation temperature), the ice crystal growth rate is faster. This is because the relatively colder shelves of the freeze dryer remove the heat generated during ice formation faster. The rate of crystal growth (G) can be expressed as a function of degree of supercooling, as shown in Equation 8 [Petzold & Aguilera, 2009]:

$$G = \beta(\Delta T_s)^n \tag{8}$$

where, $\Delta T_s = T_f - T_n$ (degree of supercooling); and β & n are experimental constants.

On the other hand, if a solution has a low degree of supercooling, meaning small temperature difference between the equilibrium freezing point temperature and the nucleation temperature, only a small amount of the heat of crystallization can be absorbed by the supercooled water. This results in the instantaneous freezing of only a small fraction of freezable water, and hence the formation of just a few ice crystals. In addition, the ice crystal growth rate of a solution with low degree of supercooling is slow, as the relatively warmer freeze dryer shelves have low driving force to remove the crystallization heat. A pictorial depiction of the freezing process at high and low degrees of supercooling is shown in Figure 4. Figure 4a shows the freezing phenomenon in the case of a high degree of supercooling (i.e., 13 °C). As discussed earlier, higher degree of supercooling leads to a higher amount of water to crystallize during secondary nucleation (cf. Eq. 7) and to faster rate of freezing (cf. Eq. 8). This, in turn, leads to the formation of many ice nucleation sites during secondary nucleation producing many small ice crystals. By contrast, Figure 4b shows an example of a low degree of supercooling (i.e., 3 °C). In this case, it is apparent that a lower amount of water crystallizes during secondary nucleation (cf. Eq. 7), yielding very few large ice crystals.

It is also known that ice crystal morphology is a function of the degree of supercooling. Generally, 3 different types of ice crystal morphologies can be observed during freezing of a solution [Petzold & Aguilera, 2009; Shibkov et al., 2003]: (1) at high degree of supercooling (Figure 4a), because of the fast freezing rate, the water molecules arrange randomly around the ice nuclei, creating irregular dendrites or needle-like crystals; (2) at low degree of supercooling (Figure 4b), the freezing rate is slower and the water molecules have sufficient time to arrange themselves to form regular hexagonal crystals, called dendrites; (3) at high cooling rates, many ice spears can originate from the center of crystallization without side branches, called spherulites.

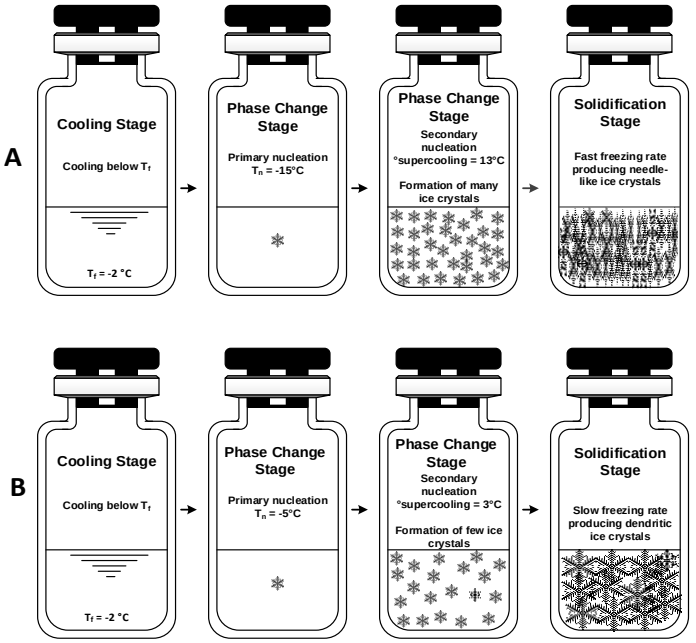

Figure 4. Pictorial depiction of the freezing phenomena: effect of the degree of supercooling on ice crystals size, number, and morphology. (a) Freezing phenomena with high degree of supercooling, and (b) freezing phenomena with low degree of supercooling. T_f, equilibrium freezing temperature; and T_n, ice nucleation temperature [Geidobler & Winter, 2013].

Supporting this idea, Tammann reported the influence of nucleation temperature on ice crystal morphology [Knight, 1967]. Specifically, samples frozen at low degree of supercooling (i.e., warmer nucleation temperature) yield dendritic structures,

whereas samples frozen at high degree of supercooling (i.e., colder nucleation temperature) yield crystal filaments [Searles, 2010; Knight, 1967].

2.1.1.2.3 Solidification stage

Once stable ice nuclei are formed, their growth proceeds by the addition of water molecules to the interface, which is termed as solidification. Point C of Figure 3 shows the onset of solidification. During solidification, the ice crystals grow, reducing the availability of liquid water. This, in turn, increases the solute concentration in the formulation, which is referred to as freeze-concentration [Searles, 2010]. The increase in solute concentration during freezing is a function of temperature only and is independent of the initial concentration [Franks, 1998]. On further cooling, the solute concentration increases to a critical concentration, above which the concentrated solution undergoes either eutectic freezing or vitrification [Kasper & Friess, 2011].

A eutectic mixture is formed when a solute crystallizes from a freeze-concentrated solution [Nail et al., 2002]. For example, mannitol, glycine, sodium chloride, and phosphate buffers are known to crystallize on freezing if present as the major component [Searles, 2010]. The *eutectic temperature (T_{eu})* is the lowest temperature at which a solution remains liquid and, at this point, the freeze-concentrate saturates and eutectic freezing or solute crystallization occurs [Kasper & Friess, 2011]. It is only below the eutectic temperature that a crystalline system is considered completely solidified [Nail et al., 2002].

For binary mixtures, the eutectic temperature depends on the solubility of the solute and it could generally be said that the lower the solubility of a given solute, the higher is the eutectic temperature [Nail et al., 2002]. For multicomponent systems, the general rule is that the crystallization of any component is influenced or hindered by the presence of other component [Franks, 2007].

On the other hand, vitrification occurs in amorphous solutions where solutes do not crystallize during freezing. The fact that amorphous solutes do not crystallize at their eutectic temperature is due to their complex microstructures [Franks, 2007].

Freezing of water and, consequently, increase in solution concentration cease when the solution viscosity is close to 102 Pa·s [Blond et al., 1997]. At this viscosity level, the state of the freeze-concentrated solution is expected to change from a rubbery to a glassy solid, a process known as glassification or vitrification [Blond et al., 1997]. The temperature at which this transition occurs is referred to as the *glass transition temperature of the maximally freeze-concentrated solution (T_g')*. T_g' is shown in the supplemented phase diagram, Figure 5, as the intersection of the freezing point depression curve of water in the presence of amorphous solute and the glass transition curve. T_g' is the point on the glass transition curve, representing a reversible change between a viscous rubberlike liquid and a rigid glassy system [Nail et al., 2002; Kasper & Friess, 2011]. T_g' depends on the composition of the solution, but is independent of the initial solute concentration [Franks, 1998; Hatley & Mant, 1993; Her & Nail, 1994].

The most important difference between freeze-drying a crystalline solution and an amorphous solution concerns the definition of the maximum allowable product temperature during primary drying. In a crystalline solution, complete solidification of the solution occurs below the eutectic temperature, and hence the eutectic temperature is defined as the maximum allowable product temperature during primary drying. On the other hand, complete solidification of an amorphous solution occurs below the glass transition temperature of the maximally freeze-concentrated solution (T_g'). Although, in most cases, T_g' is used to define the maximum allowable product temperature during primary drying, the collapse temperature (T_c) of an amorphous solution more precisely defines the temperature at which a structural loss of the product occurs. In addition, T_c is several degrees higher than T_g', as the high viscosity of the sample at a temperature close to T_g' prevents viscous flow [Tang & Pikal, 2004]. Thus, to maximize process efficiency, T_c can be used to define the maximum allowable product temperature during primary drying. Eutectic melting temperatures are relatively high compared to glass transition temperatures, allowing a higher product temperature during primary drying and resulting in much shorter drying processes [Kasper & Friess, 2011]. If the product temperature during primary drying exceeds either the eutectic temperature (for a crystalline solution) or the

collapse temperature (for amorphous solutions), a structural breakdown of the dried product occurs. This structural breakdown is commonly known as meltback (for a crystalline solution) or collapse (for amorphous solutions) [Nail et al., 2002]. In relation to this, the physical state of some drugs, that means crystalline versus amorphous, may have a significant effect on drug potency loss; crystalline drugs are more prone to lose potency [Gupta et al., 2004; Connelly et al., 2015]. Drug potency and insolubility share a common origin: structural and thermodynamic drug properties. A potent drug forms a stable complex, that is, a complex with an unfavorable free energy of dissociation. Similarly, an insoluble drug forms a stable crystal, that is, a crystal with an unfavorable free energy of dissolution [Gupta et al., 2004; Connelly et al., 2015]. Because amorphous drugs are markedly more soluble than their crystalline counterparts, they represent the most energetic solid state of a material, and thus they provide the biggest advantage in terms of solubility and bioavailability [Hancock & Parks, 2000; Rumondor et al., 2016]. The higher aqueous solubility can potentially translate into higher bioavailability compared to a formulation consisting of the crystalline form of the drug substance. Recently, amorphous solid dispersions have been used as formulation solutions to improve drug solubility and bioavailability [Purohit et al., 2018].

Moreover, the microstructural differences between crystalline and amorphous frozen solutions result in significantly different behaviors during the freeze-drying process. Thus, the interstices among the ice crystal matrices of a crystalline solution consist of an intimate mixture of small crystals of ice and solute, whereas the interstitial region in amorphous solutes consists of solid solution and unfrozen, amorphous water. Therefore, in a crystalline solution, nearly all water is frozen and can be easily removed during primary drying without requiring secondary drying. However, in an amorphous solution, up to 20% of unfrozen water is associated with the solid solution, which must be removed by desorption during secondary drying [Nail et al., 2002]. Characterization of a lyophilization formulation is therefore essential to better understand the effect of the freezing step on the subsequent drying process. Several techniques are available to characterize a lyophilization formulation in its frozen state. Differential scanning calorimetry, modulated differential scanning calorimetry, and differential thermal analysis are used for the determination of glass transition

temperature of the maximally freeze-concentrated solution (T_g'), and eutectic temperature (T_{eu}), [Her & Nail, 1994; Ma et al., 2001; Schawe, 2006; Sacha & Nail, 2009; Ward & Matejtschuk, 2010; Knopp et al., 2016] whereas freeze-drying microscopy is used for the determination of the collapse temperature (T_c) [Passot et al., 2006; Meister & Gieseler, 2009; Depaz et al., 2016; Horn & Friess, 2018].

It is common that crystalline bulking agents, such as mannitol, polyethylene glycol (PEG), and glycine, are added to amorphous lyophilization formulations to facilitate the primary drying [Johnson et al., 2002]. In such circumstances, a thorough understanding of the extent of crystallinity of the crystalline bulking agents is crucial in terms of process performances as well as storage stability. Bhatnagar et al. [Bhatnagar et al., 2011] studied the effect of sucrose concentration on the crystallization of PEG. They reported that sucrose concentration above 5 (% w/v) effectively hindered PEG crystallization during freeze-drying, whereas PEG was crystallized in a formulation with sucrose concentration up to 10 (% w/v) when PEG was covalently linked with recombinant human growth hormone. While PEG crystallization during freezing allows primary drying to be performed at elevated temperature and decreases primary drying time, failure of PEG crystallization during freeze-drying leads to crystallization during storage, which might affect protein stability. Low temperature Xray powder diffractometry is one of the techniques used for qualitative determination of crystallinity on mixed frozen formulation [Cavatur & Suryanarayanan, 1998].

The illustration of the supplemented phase diagram (see Figure 5) summarizes all the physicochemical changes that occur during freezing and the subsequent drying process for a selected proprietary formulation, named as A.

As can be observed in Figure 5, a solution “A”, having a certain initial solute weight fraction, is cooled down according to a typical freezing protocol (red broken line starting at “A”).

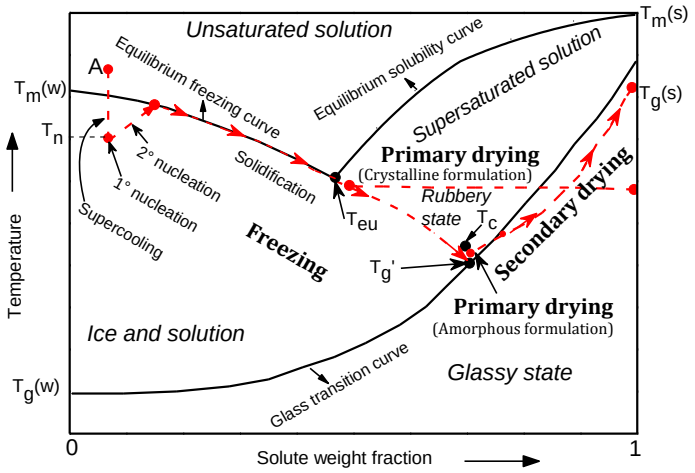

Figure 5. Supplemented phase diagram describing the low temperature behavior of a selected proprietary solution "A". $T_m(w)$, melting or freezing temperature of pure water; T_n, ice nucleation temperature; $T_g(w)$, glass transition of pure water; $T_m(s)$, melting or freezing temperature of solute; $T_g(s)$, glass transition temperature of solute; T_g', glass transition temperature of maximally freeze-concentrated solution (for an amorphous solution); T_c, collapse temperature; and T_{eu}, eutectic temperature of a frozen crystalline solution [Searles, 2010; Kasper & Friess, 2011; MacKenzie et al., 1997; Franks, 1998; Liu, 2006].

The freezing line crosses the equilibrium freezing curve, demonstrating the fact that solutions do not instantaneously freeze at their equilibrium freezing temperatures. As discussed in section 2.1.1.2.1, the solution passes through a supercooling state before the formation of the first ice nucleus. After the formation of the first ice nucleus, additional ice crystals are created during the secondary nucleation, until the temperature of the supercooled water reaches the equilibrium freezing curve. The number of ice crystals formed during the secondary nucleation is dependent on the degree of supercooling (cf. section 2.1.1.2.2).

Once the secondary nucleation is completed, additional heat is removed by cooling the solution further and the remaining water freezes and solidifies when the previously formed ice crystals grow [Kasper & Friess, 2011]. If the cooling rate is slow, the solidification process follows the equilibrium freezing curve of the solution until it intersects the equilibrium solubility curve and this demonstrates that solidification is only proceeding by the growth of ice crystals formed during

secondary nucleation. During the solidification process, the concentration of the solution increases as more water is removed by ice crystal growth and this increase in concentration is independent of the initial concentration (it only depends on temperature) [Blond et al., 1997]. At the point of intersection of the equilibrium freezing curve and the equilibrium solubility curve, the solution reaches a critical concentration, above which the supersaturated solution undergoes, depending on the nature of the formulation, either eutectic freezing or vitrification.

Crystalline formulations undergo eutectic freezing, in which the solute crystallizes below the eutectic temperature. During the eutectic freezing, the unfrozen water is released from the supersaturated solution as the solute continues crystallizing and this free water immigrates to the frozen water and further crystallizes. If 100% solute crystallization is assured, it could be concluded that all the available water is also frozen. This means that, during freeze-drying of a crystalline formulation, all the water can be removed by sublimation, as shown in Figure 5. Crystalline formulations can be freeze-dried a few degrees below their eutectic temperatures without the need for secondary drying.

Amorphous formulations, on the other hand, undergo vitrification, in which the solute concentration continues to increase as more water freezes below the eutectic temperature. Freezing of water ceases when the freeze-concentrated solution changes from a rubbery to a glassy solid. This transition is marked by the intersection of the freezing curve and the glass transition curve in Figure 5. The temperature at which a transition from rubbery state to glassy solid is taking place is known as the glass transition of the maximally freeze-concentrated solution, T_g'. In amorphous formulations, the glassy solid consists of amorphous solutes and frozen (as well as unfrozen) water. Depending on the initial concentration of the solute, the unfrozen water in the glassy solid can be as high as 20% [Nail et al., 2002].

Primary drying of amorphous formulations can be performed at a few degrees below T_c (as seen in Figure 5) until all the frozen water is removed. At the end of primary drying, the water content of the dried product is still significantly high, which accounts for the unfrozen water. During the freeze-drying process, the unfrozen water is removed by a desorption process (more commonly known as secondary drying).

During the secondary drying, the temperature of the formulation is increased to facilitate desorption of unfrozen water through the pores of the dried cake. It is, however, important to note here that the increase in temperature during the secondary drying should not lead to a temperature of the sample above the glass transition temperature, and hence the secondary drying curve should remain below the glass transition curve during the complete process (Figure 5).

As demonstrated in Figure 4 and in the above sections, the random nature of the degree of supercooling is the main factor for the formation of heterogeneous ice habits during freezing. These heterogeneous ice crystals have significant effect during the drying process, as they impose differences in resistance to water vapor flow, which lead to heterogeneous product temperatures and drying behaviors. In addition, freezing may affect the physicochemical properties of a formulation, such as protein denaturation, pH shifts, and degradation reaction. Therefore, the knowledge of the freezing step and its impact on the product quality and process performance is a critical step for a successful process development and scale-up. In this context, the ability to control the degree of supercooling during the freezing step is essential in achieving consistent ice crystal habits, and hence drying behaviors. Several technologies are available with the aim of controlling the degree of supercooling (nucleation) during the freezing step of a freeze-drying process, which will be discussed in the next section in detail.

2.1.1.3. Technological alternatives for the active control of ice nucleation and their impact on the freeze-drying process

The impact of the freezing step on the whole freeze-drying process is yet the least understood topic mainly because: (a) freezing a given formulation is not the final goal of a freeze-drying process and, as a consequence, it may be thought that achieving just a solidified formulation is sufficient for the subsequent drying process. This leads to the exclusion of the freezing step from discussions of freeze-drying process optimizations and failures; (b) the freezing step accounts, in most of the cases, for less than 15% of the total freeze-drying time and this turns the attention of many product development engineers and scientists to the optimization of the primary and secondary drying steps, neglecting the potential impact of the freezing step; and (c)

the complexity of the freezing process, lack of variety of freezing methods equipped with freeze dryers, and the difficulty of controlling the ice nucleation make it difficult to investigate the effect of different freezing methods on the freeze-drying process. This is why many freeze-drying process designers use the most easily available freezing method, the shelf ramp method.

Nevertheless, the freezing step has been identified by some researchers as a particularly important step, which must also be monitored and controlled, as it impacts both the primary and the secondary drying steps. With this regard, there are several studies that deal with the effect of the freezing step on the freeze-drying process [Searles et al., 2001a; Konstantinidis et al., 2011; Esfandiary et al., 2016; Roy & Pikal, 1989; Searles et al., 2001b; Pikal et al., 2002; Lu & Pikal, 2004; Rambhatla et al., 2004; Liu et al., 2005; Abdelwahed et al., 2006; Hawe & Friess, 2006; Nakagawa et al., 2006 & 2009; Petersen et al., 2006a; Hottot et al., 2007 & 2008; Passot et al., 2009; Awotwe-Otoo et al., 2013; Geidobler et al., 2013; Kuu et al., 2013; Ullrich et al., 2015; Pisano & Capozzi, 2017; Fang et al., 2018]. The primary reasons that explain this influence rely on the structure (morphology), size, and number of ice crystals formed during freezing (cf. Figure 4). When the ice crystals sublime during primary drying, they leave a porous structure behind, through which water vapor flows. The size of the pores determines the resistance to water vapor flow (mass transfer) during primary and secondary drying, as shown in Equation 6. Larger ice crystals leave larger pores behind, and during primary drying, this means less resistance to mass transfer and faster drying rate. On the other hand, larger pore sizes reduce the surface area available for diffusion of the unfrozen solvent and decrease the rate of desorption during secondary drying.

The correlation between ice nucleation temperature (T_n) and ice crystal size or morphology was established many years ago. In 1925, Tammann reported that samples frozen at a high nucleation temperature yielded dendritic ice crystals, whereas samples frozen at low nucleation temperature yielded crystal filaments [Knight, 1967]. In 1969, Thijssen and Rulkens reported that the freezing rate is an important determinant of pore size and drying rate in freeze-drying of liquid food products. For a 20% dextran solution freeze-dried in slabs, a faster cooling rate

during freezing resulted in smaller pores and therefore higher resistance and slower drying rates [Thijssen & Rulkens, 1969]. Roy and Pikal [Roy & Pikal, 1989] reported that the ice nucleation temperature in vials with thermocouples was higher than in vials without thermocouples, resulting in a higher primary drying rate. Recently, Searles et al. [Searles et al., 2001a] demonstrated a strong correlation between the ice nucleation temperature and primary drying rate. They showed that an increase in ice nucleation temperature by approximately 12 °C increased the primary drying rate of a model formulation by approximately 37%. A decrease in product resistance with increasing ice nucleation temperature has been reported by Rambhatla et al. [Rambhatla et al., 2004] In their study, they used the ice fog method to obtain different ice nucleation temperatures for 4 model formulations. They observed up to 38% reduction in product resistance when increasing the ice nucleation temperature by 8 °C. Nakagawa et al. [Nakagawa et al., 2006] demonstrated a clear relationship between ice nucleation temperature and ice morphology. In their study, they used ultrasounds to control the ice nucleation temperature. They reported that an increase in nucleation temperature from -8 °C to -2 °C changed the ice habit from small, many, and heterogeneous ice crystals to large and dendrite ice crystals. Similarly, Awotwe-Otoo et al. [Awotwe-Otoo et al., 2014] and Esfandiary et al. [Esfandiary et al., 2016] observed a significant primary drying time reduction because of a higher ice nucleation temperature achieved by using the controlled ice nucleation method.

During freezing, the cooling rate and the ice nucleation temperature can be controlled by means of different technologies, aiming to improve the impact of the freezing step on the subsequent primary and secondary drying processes, as well as on the final product quality, such as physical state of the sample, residual moisture content, and reconstitution time. Various methods that allow for the direct control of the freezing step have been proposed. Although such methods have demonstrated potential for process improvement at laboratory and pilot plant scales, their applicability to commercial-scale manufacturing of regulated products seems to be very difficult to achieve, due to economic, sterility, and safety concerns [Awotwe-Otoo et al., 2014]. These different technological alternatives are discussed in detail in the following sections.

2.1.1.3.1 Precooled shelf freezing

In the precooled shelf freezing method, samples are placed on shelves, which are cooled to a predefined temperature. Searles et al. [Searles et al., 2011a] used shelves precooled between -40 °C and -44 °C and they found that the median nucleation temperature for the precooled shelf frozen samples was increased by around 3.5 °C as compared to samples frozen using a shelf ramp freezing. They also demonstrated that samples placed on a shelf at -44 °C nucleated over a wide range of temperature, indicating the limitation of the precooled shelf method to enable a consistent nucleation temperature across the vials. The effect of different loading shelf temperatures was studied by Hottot et al. [Hottot et al., 2007]. In their study, they measured the mean ice crystal size in the frozen matrix and reported insignificant effect of the loading temperatures on ice crystal sizes.

Comparing precooled shelf freezing to quench freezing, Dawson and Hockely demonstrated that 1% (w/v) trehalose formulation frozen by liquid nitrogen exhibited a fine filamentous directional network of ice crystals, had less resistance to vapor flow during drying and reconstituted faster, whereas freezing by placement on a -50 °C shelf yielded a leafy mixed-orientation appearance with a higher resistance to vapor flow compared to liquid nitrogen frozen samples [Dawson & Hockley, 1992].

In general, the effect of different loading temperatures on subsequent process parameters, such as nucleation temperature, ice morphology, and drying rates should be systematically assessed if this method is going to be used.

2.1.1.3.2 Freezing with annealing

Annealing is a process step in which samples are maintained at a specified temperature for a period. Annealing can be carried out as a holding temperature during the initial cooling but, more commonly, it is a postfreezing warming and holding step, followed by recooling [Searles, 2010; Randolph & Searles, 2002]. More often, annealing is used to facilitate crystallization of active or bulking agents, but it also has a profound effect on improving consistency in inter-vial ice crystal size and drying behaviors [Tang & Pikal, 2004; Searles, 2010; Liu, 2006; Searles et al.,

2001b]. The mechanism of ice crystal morphological change during annealing, as demonstrated by Searles [Searles, 2010], is due to the difference in surface free energy between small and large ice crystals. According to Kelvin's equation, ice crystals with smaller radii of curvature induce a higher vapor pressure, and hence on increased bulk mobility due to annealing, ice crystal regions with smaller radii will melt preferentially as a consequence of their higher vapor pressure, which induces higher free energy compared to ice crystal regions with larger radii [Randolph & Searles, 2002]. In addition, higher temperature during annealing increases the diffusional mobility of the annealed species and, in turn, increases the diffusion of the melted ice crystals into the surviving ice crystals in the time scale of the annealing process. Therefore, the choice of temperature and time during an annealing process is a critical step. Furthermore, annealing can also promote the completion of freeze concentrate (devitrification), as rewarming up to a temperature above T_g' allows amorphous water to crystalize [Kasper & Friess, 2011; Searles et al., 2001b]. However, annealing is not a suitable process for formulations susceptible for denaturation and degradation above their glass transition temperature. In addition, the benefits of shorter drying time may be offset by the additional time required for the annealing cycle.

The reported data on the impact of annealing on the subsequent drying processes are, until recently, controversial. Pikal et al. [Pikal et al., 1983] found that annealing resulted in larger ice crystal sizes for small (5 µL) samples that were frozen rapidly between glass coverslips. With sublimation studies in a 13-µL microbalance apparatus, Pikal et al. also showed that annealing resulted in circa 50% decrease in the area-normalized dry product resistance for an amorphous formulation and up to 60% for a crystalline formulation, but actual drying rates were not presented. However, annealing was not tested on products frozen and dried in vials. On the other hand, Lu and Pikal [Lu & Pikal, 2004] reported that annealing of a mannitol-trehalose sodium chloride formulation increased the dried product resistance, and hence the primary drying time. They hypothesized that the increase in dried product resistance of the annealed samples was because of the crystallization of solutes during annealing, preventing microcollapse during drying. Liu et al. [Liu et al., 2005] reported 10% and 17% primary drying time reduction when comparing a shelf ramp

freezing with freezing and annealing at -10 °C for 4 h and with freezing and annealing at -2.5 °C for 4 h, respectively. Unfortunately, the source of the reduction in primary drying time in the study by Liu et al. is not clear, as the average product temperatures during primary drying for the 3 freezing protocols were identical while using the same shelf temperature and chamber pressure. This is because if annealing had helped to reduce the resistance to vapor flow, one would expect to see a reduction in product temperature if the shelf temperature and chamber pressure were identical. Searles et al. [Searles et al., 2001b] reported that a 3.5-fold enhancement in primary drying rate can be achieved after annealing of amorphous sucrose, hydroxyethyl starch or mixture of both. On the other hand, a recent study by Esfandiary et al. [Esfandiary et al., 2016] showed that, compared to a freezing protocol without annealing, up to 20% increase in primary drying time was observed when the same formulation was annealed at -15 °C for 2 h. As demonstrated by these authors, the reason for this increase in primary drying time was the strong top crust formed in the annealed samples. In addition, our recent study showed insignificant effect of annealing on amorphous formulation with high solid content (18.5 wt%). It was showed that the increase in cycle time due to the annealing step was higher than any reduction in cycle time in the subsequent drying process.

2.1.1.3.3 Quench freezing

Quench freezing refers to the process of immersing sample containers either into liquid nitrogen, liquid propane, dry ice- acetone, or dry ice-ethanol for a period that assures complete solidification [Kasper & Friess, 2011]. Quench freezing is characterized by a fast cooling and fast freezing. Fast cooling tends to stabilize metastable states by retaining greater quantities of unfrozen water, whereas fast freezing tends to promote a finer subdivision of the ice. High cooling rates tend to increase both nucleation and crystal growth rates [MacKenzie et al., 1997]. It has also been reported that quench freezing results in a directional freezing. Thus, Hsu et al. [Hsu et al., 1995] observed that freezing of vials in dry ice-isopropanol yielded directional solidification. Dawson and Hockely also demonstrated that a 1% (w/v) trehalose formulation frozen by liquid nitrogen exhibited a fine filamentous directional network of ice crystals [Dawson & Hockley, 1992].

The impact of quench freezing on freeze-drying process optimization is not a well-studied subject yet; however, as the quench freezing promotes the formation of heterogeneous ice crystals, its applicability in manufacturing scale processes is minimal [Kasper & Friess 2011].

2.1.1.3.4 Vacuum-induced surface freezing

The concept of vacuum-induced surface freezing was introduced by Kramer et al., [Kramer et al., 2002] based on the mechanism that favors evaporation of cold water when the pressure of a solution is reduced at a given temperature. In these circumstances, the associated enthalpy of vaporization causes sufficient cooling of the solution surface to produce a thin film of ice. Kramer et al. proposed the following procedure to perform vacuum-induced surface freezing: the vials were placed on a precooled shelf at +10 °C and the chamber pressure was reduced to a predefined value required to cause incipient surface freezing of the solution. This pressure was determined by visual observations and they set it at 1 mbar. After 5 min under these conditions, the solution exhibited a surface freezing to form an ice layer thickness of 1-3 mm. To avoid further boiling of water and melting of the ice surface film, the chamber pressure was released to atmospheric pressure as quickly as possible and, simultaneously, the shelf temperature was reduced to 3 °C–4 °C below the onset of melting of ice in the frozen formulation. After holding the solution at these conditions for 1 h, ice crystal growth was completed and the shelf temperature was further reduced to -40 °C to complete the solidification phase of the freezing step. These authors claimed that the vacuum-induced surface freezing method produced large chimney-like ice crystals, which, in turn, yielded a reduction of up to 20% in primary drying time.

Liu et al. [Liu et al., 2005] also studied the impact of vacuum-induced surface freezing on subsequent primary drying. They reported up to 12% primary drying time reduction compared to a standard shelf ramp freezing. Contrary to the method by Kramer et al. described previously, Liu et al. modified the vacuum-induced surface freezing method as follows: the shelf temperature was first lowered down to -10 °C and the chamber pressure to 0.8 mbar. After a visual observation of ice crystals on the top surface, the freezing step was completed by quickly lowering the shelf

temperature to -45 °C and holding. The reason for the lower shelf temperature, as compared to the original procedure, was because the latent heat of vaporization at higher shelf temperatures was not sufficient to lower the temperature of the sample at the bottom of the vial. In this case, complete nucleation might take longer than 5 min and “puff-off” of the sample could take place.

A recent study by Oddone et al. [Oddone et al., 2014 & 2016] reported that the vacuum induced surface freezing method improves intra-vial and inter-vial drying behavior uniformity, as well as moisture content of model formulations. These authors also reported that the effective pressure to induce ice nucleation was formulation dependent. In addition, Oddone et al. [Oddone et al., 2017] studied the effect of vacuum-induced surface freezing on secondary drying. Although the time required to achieve the same moisture content during secondary drying was longer for samples frozen using vacuum-induced surface freezing as compared to normal freezing, the overall time (primary and secondary) was shorter. In addition, consistency in vial-to-vial moisture content was improved using vacuum-induced surface freezing as freezing protocol.

In general, this method is associated with a high water boiling risk if some processing parameters, such as shelf temperature and chamber pressure, are not carefully selected. Moreover, only few experimental results are available so far to support its effectiveness and scalability.

2.1.1.3.5 Ice fog freezing technique

The use of ice fog to nucleate ice crystals was first proposed by Rowe [Rowe, 1990] and implemented for the freeze-drying process by Rambhatla et al. [Rambhatla et al., 2004] The concept of ice fog technique relies on the use of cold nitrogen as a heat exchange medium. When cold nitrogen gas enters the product chamber, ice crystals are formed from the water vapor inside the chamber. These ice crystals are then forced into the vials, due to the slightly higher pressure outside the vials, and serve as nucleation seeds. The primary advantage of this technique is the improvement of the uniformity of ice nucleation among vials. In addition, Rambhatla et al. reported that the ice fog technique can also be used to perform freezing at a

defined nucleation temperature. With this aim, Rambhatla et al. used ice fog technique to nucleate samples at different nucleation temperatures ranging from -1 °C to -12 °C [Rambhatla et al., 2004]. As a first approach, they used nitrogen at -40 °C and reported a successful nucleation at 3 different temperatures (-3 °C, -7 °C, and -12 °C). However, complete nucleation of all vials took as long as 30 min. In addition, they found no significant differences in dried product resistance of the samples nucleated at the 3 nucleation temperatures, although a 10% increase in primary drying time, resulting from 8 °C increase in nucleation temperature, was reported [Rambhatla et al., 2004]. The reason for this, according to the authors, is that the long time required for complete nucleation of the samples at a temperature far above their T_g' favors annealing and Ostwald ripening, which increases the ice crystal size, and hence reduces the dried product resistance of samples nucleated at low temperatures. To tackle this problem, the same authors modified the technical setup of the ice fog technique and the temperature of the nitrogen entering the chamber was reduced from -40 °C to -50 °C. These improvements enabled them to achieve complete nucleation, in all the vials studied, in less than 5 min. Using this setup, they reported nearly 30% reduction in primary drying time when comparing samples nucleated at -11 °C with samples nucleated at -1 °C [Rambhatla et al., 2004].

In a follow-up study, Patel et al. [Patel et al., 2009] used a modified version of the ice fog technique called reduced pressure ice fog technique. In this technique, before the introduction of cold nitrogen, the pressure inside the chamber was evacuated at a desired nucleation temperature, as shown in Figure 6. Different reduced pressures, namely from 800 to 64 mbar, were tested. However, the results obtained at high pressures were not satisfactory at all. They reported that, in a pressure range from 66.7 to 64 mbar, complete nucleation of one shelf load was achieved in less than a minute.

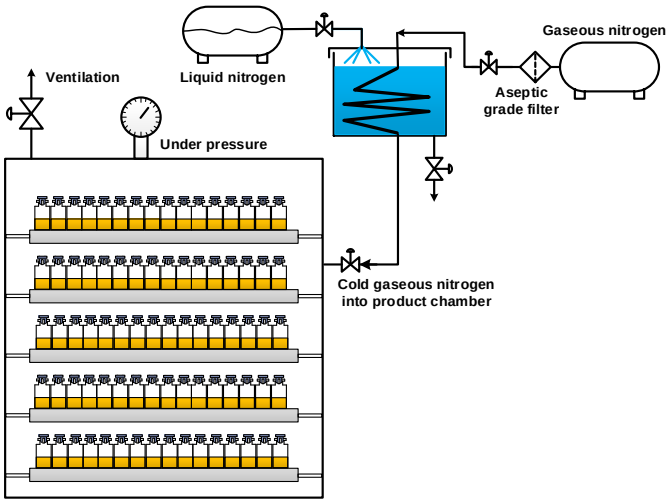

Figure 6. Pictorial depiction of the original ice fog method, as described by Patel et al. [Patel et al., 2009]. In this method, once the vials reach the desired nucleation temperature, cold nitrogen gas is introduced into the product chamber. The ice fog is generated from the humidity inside the chamber.

However, there was no explanation given on why the higher pressure range was not successful or why the reduced pressure technique shortened the nucleation time. The most probable reason could be that, owing to the large pressure difference between the cold nitrogen chamber and the drying chamber, the high suction power of the drying chamber was able to draw a large amount of cold nitrogen gas. This amount of cold nitrogen gas was then able to nucleate much more water vapor inside the chamber, which was sufficient to seed all the vials within short periods of time. This could also explain the reason why high drying chamber pressure ranges were not successful. High chamber pressure reduces the pressure difference between the cold nitrogen chamber and the drying chamber, thus limiting the amount of cold nitrogen entering into the drying chamber. Therefore, the amount of cold nitrogen introduced into the chamber, either via reduced drying chamber pressure or increased cold nitrogen chamber pressure, and the ability to uniformly distribute the nitrogen within the drying chamber, especially for manufacturing freeze-dryers with many and large shelves, define the success of the ice fog technique. The aforementioned reasoning is also supported by the full load experiment (3 fully loaded shelves) performed by Patel et al. [Patel et al., 2009], in which the reduced

pressure ice fog technique was not able to nucleate all the vials uniformly and in a short period, even at the lowest chamber pressure.

An industrial scale ice fog technique is currently available from Linde Gases, in collaboration with IMA Life North America, under the trade name of VERISEQ® nucleation technology [Chakravarty et al., 2012; Azzarella et al., 2016; Brower et al., 2015], and from Millrock Technology, Inc., under the trade name of FreezeBooster® Controlled Nucleation Technology. In the case of industrial scale ice fog method, the ice crystals are first formed by mixing cold nitrogen and water vapor in a device, such as an ejector, outside the product chamber. The ice fog is then introduced into the product chamber once the vials reach the desired nucleation temperature [Chakravarty et al., 2012], as shown in Figure 7.

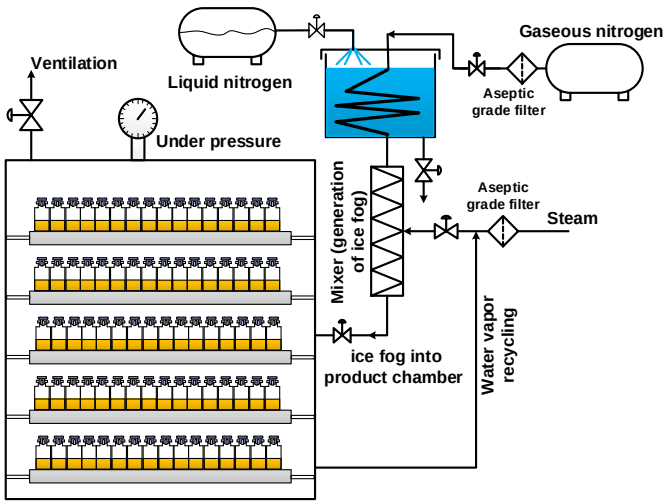

Figure 7. Pictorial depiction of the modified (industrial) ice fog method, as described by Chakravarty et al. [Chakravarty et al., 2012]. In this modified method, ice fog is generated outside the product chamber in a mixer, mixing cold nitrogen gas with water vapor. The ice fog is then introduced into the chamber once the vials reach the desired nucleation temperature.

It has been reported that, for freeze dryers having 1.1 m^2 and 2.5 m^2 shelf area, introduction of ice fog for 30–50 s was sufficient to nucleate all the vials [Chakravarty et al., 2012]. However, the number of vials used in these tests was far away from the full capacity of the freeze dryers and the success of ice fog technique cannot be guaranteed yet. In another study, Azzarella et al. [Azzarella et al., 2016] reported

successful ice fog controlled nucleation in industrial scale freeze dryers with shelf areas of 15 m^2, 39 m^2 (45,540 vials), and 56 m^2 (195,960 vials), yielding a reduction of up to 19% in product primary drying time and up to 40% improvement in batch homogeneity. They have also reported that, to successfully induce nucleation for bigger freeze dryers, jacketed walls are required to reduce thermal gradient across the shelf stacks.

In general, even though the ice fog freezing technique is a promising method for the active control of nucleation, especially from inter-vial and intra-vial homogeneity points of view, more studies are needed to support its success at industrial scale.

2.1.1.3.6 High-pressure shift or depressurization freezing

High-pressure shift freezing has been a common practice in freeze conservation of foods [Otero & Sanz, 2000]. In this method, the samples are exposed to high pressure while their temperature is lowered. According to the phase diagram of water, liquid water can be kept unfrozen well below its equilibrium freezing temperature under high pressure conditions. When the desired temperature is reached in the product, pressure is released, inducing uniform supercooling throughout the sample. This is due to the fact that the increase in pressure affects the whole sample instantaneously and at the same time. Thus, this supercooling induces uniform formation of nuclei throughout the sample (regardless of its shape or size), so that the latent heat is released, raising the sample temperature to the corresponding equilibrium freezing temperature. Freezing is then completed at constant pressure, usually at atmospheric conditions, and by lowering the shelf temperature. The higher the pressure and the lower the product temperature before expansion, the more is the ice formed [Otero & Sanz, 2000; Zhu et al., 2005; Fernandez et al., 2006; Otero et al., 2009]. This is consistent with the fact that a higher degree of supercooling produces many ice crystals.

The main advantage of high-pressure shift freezing in the food industries is related to the big amount of ice instantaneously formed after expansion [Otero et al., 2009]. By contrast, formation of few and large ice crystals is the main goal in the freeze-drying process. This can be achieved by manipulating the parameters of the high-

pressure shift freezing method, such as the pressure difference before and after expansion and the product temperature before expansion. A small pressure difference and high product temperature produce few and large ice crystals.

Application of high-pressure shift freezing to a freeze-drying process was first introduced by Gasteyer et al. [Gasteyer et al., 2007] The procedures of the freezing method they have used in their patent are identical to the one described previously, which comprise (1) cooling the materials to near or below their equilibrium freezing temperature in an elevated pressure; (2) decreasing the pressure to induce ice nucleation; and (3) further cooling the materials up to complete solidification. As described by these authors, the possible mechanisms for inducing ice nucleation using high-pressure shift freezing are (1) an initial elevated pressure increases the concentration of dissolved gas in a solution and a rapid decrease in pressure at low temperature reduces the gas solubility. As a consequence, the gas is released from the supercooled solution, forming cold bubbles, which trigger nucleation; (2) depressurization causes evaporation of some liquid in the solution and the resultant cooling from the endothermic evaporation process may initiate the nucleation; and (3) on depressurizing, the cold gas in a close proximity to the solution freezes some vapor and these ice crystals re-enter the solution and act as seeds or surfaces to initiate nucleation. As part of the patent supporting examples, Gasteyer et al. reported a reduction in primary drying time, stating an average difference in water loss of about 21% when comparing samples frozen using high pressure shift freezing with samples frozen using shelf-ramp freezing. The primary drying conditions in both freezing methods were identical [Gasteyer et al., 2007]. One of the main advantages of controlled ice nucleation is to improve vials freezing behavior consistency and, consequently, to achieve uniform ice sublimation. However, this was not achieved in the example provided by these authors [Gasteyer et al., 2007]. In their example, the averages plus or minus standard deviations of the water loss for the vials studied were 86.1 ± 3%, in the case of samples frozen using high-pressure shift freezing, and 65.2 ± 0.93%, in the case of shelf-ramp frozen samples. This demonstrates that shelf-ramp freezing produces a better ice sublimation uniformity than high-pressure shift freezing.

The applicability of high-pressure shift freezing was demonstrated both at laboratory (1 m^2 shelf area) and small industrial scale (5 m^2 shelf area) freeze dryers by performing repeated tests, where the ice nucleation temperature was controlled within 1 °C of their equilibrium freezing point [Bursac et al., 2009]. Bursac et al. [Bursac et al., 2009] reported a 27% decrease in primary drying time for 5 wt% sucrose freeze-dried by applying high-pressure shift freezing as compared to shelf-ramp freezing. In addition, the same authors reported improved dried product uniformity, demonstrating a reduction in absolute standard deviation in the residual moisture content of the sucrose cakes from 4.6% down to 2.1%. In another study, Konstantinidis et al. [Konstantinidis et al., 2011] reported 40% reduction in primary drying time for a 5 wt% mannitol solution when using high-pressure shift or depressurization controlled nucleation. In other more recent studies by Awotwe-Otoo et al., the advantage of controlling ice nucleation using high-pressure shift or depressurization technique has been demonstrated [Awotwe-Otoo et al., 2013 & 2014]. For the formulations studied, they reported up to 21% reduction in primary drying time, although the difference in residual moisture content was insignificant.

The high-pressure shift or depressurization freezing technique at industrial scale is available from Praxair, Inc., under the trade name of ControLyo™, Nucleation On-Demand Technology. However, experimental studies demonstrating the success of this technique at this scale are not yet available.

In general, it could be said that high-pressure shift or depressurization freezing technique is an effective tool for controlling the degree of supercooling or ice nucleation during the freeze-drying process. That is because this technique relies on inducing ice nucleation based on pressure manipulation, and the isostatic nature of pressure (i.e., even application of pressure to all containers under treatment) offers significant advantage in terms of (1) covering a wide range of sample sizes (potential for ease of scalability); and (2) inducing ice nucleation over a wide range of sample sizes instantaneously and simultaneously (potential for improving freezing uniformity within as well as between batches and potential for reducing freezing time). In addition, as described by Rampersad et al. [Rampersad et al., 2010], a freeze dryer

requires minimum adaptation to accommodate the high-pressure shift or depressurization freezing technique.

2.1.1.3.7 Ultrasound-powered freezing

The application of power ultrasounds for active control of freezing food products has been proven to be effective [Petzold & Aguilera, 2009; Li & Sun, 2002; Sun & Li, 2003; Kiani et al., 2013]. Many authors have reported that ultrasound vibration can be used to initiate ice nucleation at a desired freezing temperature [Nakagawa et al., 2006; Inada et al., 2001; Saclier et al., 2010; Kiani et al., 2012]. Ultrasound-powered freezing process is generally accomplished according to the following steps [Nakagawa et al., 2006; Hottot et al., 2008; Saclier et al., 2010]: (1) cooling the sample down to a desired nucleation temperature; (2) applying ultrasound power at a certain frequency and for a period; and (3) further reducing the temperature until complete solidification, as shown pictorially in Figure 8. The mechanism of inducing ice nucleation by using ultrasounds remains uncertain. However, regardless of the mechanism, it has been clearly demonstrated that the application of ultrasounds has a notable and quantifiable effect on ice nucleation [Saclier et al., 2010]. Different theories have been proposed to describe the mechanism of ultrasounds-induced ice nucleation. The first proposal was provided by Hickling [Hickling, 1965]. Based on this proposal, extensive collapse of cavitation bubbles produced by ultrasounds generates local zones of high pressure for a very short period of time. These high-pressure zones increase the local degree of supercooling, which acts as a driving force for ice nucleation. On the other hand, Zhang et al. [Zhang et al., 2003] reported a delay on the onset of ice nucleation after the application of ultrasound irradiation. They attributed this delay not only to the collapse of cavitation bubbles, but also to some other variables responsible for ice nucleation.

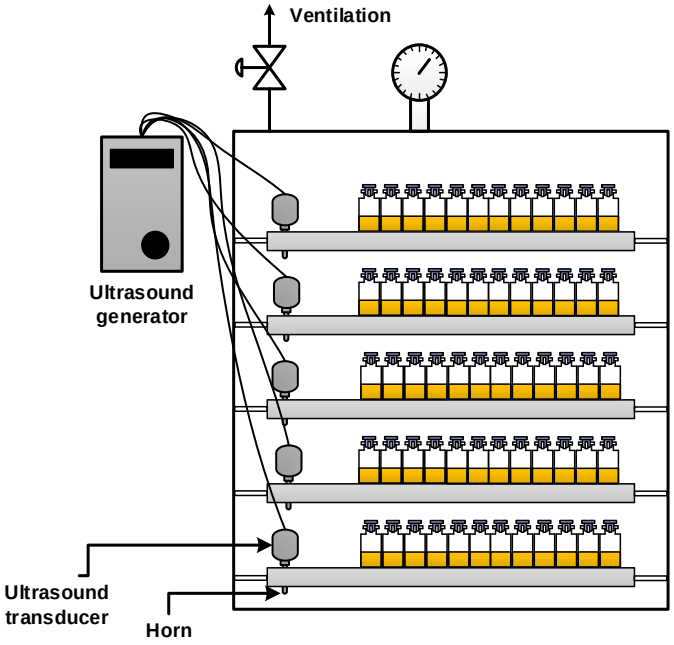

Figure 8. Pictorial depiction of ultrasound-powered freezing as described by Nakagawa et al. [Nakagawa et al., 2006]. In this method, controlled ultrasound power is applied to the shelves, once the vials reach the desired nucleation temperature [Nakagawa et al., 2006].

A complete different mechanism of ultrasound-triggered ice nucleation was reported by Dodds et al. [Dodds et al., 2007]. This mechanism is based on a molecular segregation theory, which explains that the driving force for nucleation is the pressure gradient around the cavitation bubble, resulting in a pressure-controlled diffusion of particles. These particles are composed of a number of molecules, which, on segregation, create a nucleus. In addition to the aforementioned mechanisms, Chow et al. [Chow et al., 2003, 2004 & 2005] reported that ultrasound irradiation may also trigger secondary nucleation. They hypothesized that the movement of fast and powerful cavitation bubbles fragments the ice crystals already created, producing additional new ice crystals (termed as secondary nucleation). Because of these phenomena, ultrasound irradiation creates numerous and small ice crystals even at relatively high ice nucleation temperature.

The use of ultrasound-powered controlled ice nucleation for freeze-drying applications was first reported by Nakagawa et al. [Nakagawa et al., 2006], who

implemented an ultrasound system to control the freezing step during freeze-drying of proteins in vials. These authors reported that ultrasound power can be used to initiate ice nucleation of model pharmaceutical formulations at a preselected ice nucleation temperature. However, the relationship between the ice nucleation temperature and the ultrasound process parameters was not described. Other studies suggested that pulse or acoustic power [Inada et al., 2001; Saclier et al., 2010; Kiani et al., 2012; Chow et al., 2003], ultrasound duration [Li & Sun, 2002; Kiani et al., 2012], number of cavitation bubbles [Chow et al., 2005], and initial oxygen content [Amira et al., 2014] influence the ice nucleation temperature, and ice crystal size and shape. Nakagawa et al. [Nakagawa et al., 2006] reported a clear correlation between ice nucleation temperature and ice crystal size during ultrasound-powered controlled ice nucleation. Small and numerous ice crystals were obtained at low nucleation temperature (higher supercooling degree), whereas large and directional ice crystals (dendrite type) were obtained at high nucleation temperature (lower supercooling degree). They also reported a significant reduction in primary drying time, up to 60%, when the ice nucleation temperature was increased from -8 °C to -2 °C. In another study, Passot et al. [Passot et al., 2009] reported an improved intra-vial homogeneity in sublimation by using ultrasound-controlled ice nucleation. In addition, up to 14% reduction in primary drying time was reported by changing the freezing protocol from shelf-ramp freezing to ultrasound controlled freezing [Passot et al., 2009].

In general, ultrasound-powered controlled ice nucleation could be considered a promising alternative for controlling ice nucleation during freeze-drying. However, some drawbacks associated with the ultrasound technology need to be addressed. These include (1) the heat dissipated during ultrasounds application may alter the freezing process. Hence, optimum acoustic power and duration should be determined, which could represent a challenge; (2) Nakagawa et al. [Nakagawa et al., 2006] reported that vials having poor mechanical contact with the shelf surface might be less affected by the ultrasound vibration. In addition to this, application of uniform ultrasound vibration across a single shelf surface, as well as across the shelf stack, might be a challenge in an industrial scale freeze dryer; (3) scalability of the freeze-drying process to industrial scale. In this regard, the optimum ultrasound

power and duration obtained in a laboratory scale freeze dryer might not be directly applied to an industrial scale freeze dryer. This means that scaling up the ultrasound process could present a huge challenge; and (4) the application of strong and intensive vibration on the freeze dryer shelves obviously creates particulate matters, which jeopardize the sterility of the process.

2.1.1.3.8 Electrofreezing

Although the effect of electrofreezing on the freezing of water droplets in the atmosphere was reported as early as 1861 [Dufour, 1862], the first trials to induce ice nucleation in supercooled water droplets by high-voltage electric fields were carried out by Rau [Rau, 1951] in 1951. Electrofreezing is generally carried out according to the following protocol [Shichiri & Araki, 1986; Petersen et al., 2006b]: (1) cooling the sample to a desired nucleation temperature; (2) applying an electric field, in a continuous or pulsed manner, to the supercooled sample to induce ice nucleation; and (3) further reducing the temperature up to complete solidification. Although many scientists tried to study the mechanism of electrofreezing to induce ice nucleation experimentally [Shichiri & Araki, 1986; Shichiri & Nagata, 1981; Mandal & Kumar, 2002; Hozumi et al., 2003] and theoretically [Xia & Berkowitz, 1995; Vaitheeswaran et al., 2005; Wei et al., 2005], the basic mechanism is still controversial. However, bubble formation and breakdown induced by the electric field are believed to be the most accepted mechanisms [Shichiri & Araki, 1986; Petersen et al., 2006b].

Application of electrofreezing in the freeze-drying process is still not a well-developed technology because of many drawbacks associated with an electrofreezing process in typical freeze-drying applications. These include its relative complexity and high costs associated to its implementation and maintenance, the invasive nature of the method, and the incompatibility with solutions containing ionic species (e.g., NaCl). In addition, the effectiveness of electrofreezing is also electrode-dependent [Hozumi et al., 2003], which adds more complexity to the method. In relation to the applicability of electrofreezing in the freeze-drying process, Petersen et al. [Petersen et al., 2006b] reported that

electrofreezing can be used to selectively choose nucleation temperature during the freezing step, and hence reduce the primary drying time.

In general, electrofreezing is a method that needs a thorough study for its applicability in freeze-drying application. This method requires the need of an electrode in each container system, questioning the application of this method in a freeze-drying process at industrial scale, as well as introducing apparent sterility concerns.

2.1.1.3.9 Ice crystals distribution from condensed frost

Controlled ice nucleation using pressure differential ice fog distribution from a cold condenser was first introduced by Ling [Ling, 2014a]. This method is based on the following steps: (1) cooling down a product placed inside a product chamber to a predetermined temperature; (2) creating sufficient volume of ice fog in a separate condenser chamber, which is connected to the product chamber using a vapor port; and (3) opening the vapor port between the condenser chamber (which is at a pressure higher than the product chamber pressure) and the product chamber. During this operation, ice fog from the condenser distributes rapidly and evenly through the vapor port into the product chamber, which acts as nucleating agent.

In the original ice fog method, the ice fog is created from the humidity inside the product chamber by introducing cold nitrogen gas, which, according to Ling, has some drawbacks. These include inability to nucleate large number of vials simultaneously at a controlled time and temperature, producing significant vial-to-vial heterogeneity in nucleation temperature (owing to the time difference between the first and the last frozen vials), and requirement of significant retrofit to implement it [Ling, 2014a]. Ling reported that creating a sufficient amount of ice fog, according to the size of the product, in an external chamber (such as a condenser chamber), resolves the aforementioned drawbacks of the original ice fog method. In contrast to the aforementioned advantage of ice fog from an external condenser chamber reported by Ling [Ling, 2014a], the same author [Ling, 2014b] reported, in an accompanying patent, that the amount of ice fog produced in a limited volume of condenser chamber was insufficient to nucleate large number of vials. In the new

patent, Ling reported that volume limitation of the condenser chamber can be tackled by producing a condensed frost (solid) instead of a suspended ice fog (gas) [Ling, 2014b], (Figure 9). During the opening of the isolation valve between the product chamber and the condenser chamber, the sudden change in pressure creates strong gas turbulence in the condenser chamber. This turbulence is capable of breaking any loosely attached condensed frost into ice crystals and these ice crystals travel to the product chamber and act as nucleating agent. However, Ling's patents [Ling, 2014a; Ling, 2014b] do not contain experimental results to support any of the claims and advantages, as well as to prove the effectiveness of the methods in a large-scale freeze-drying process.

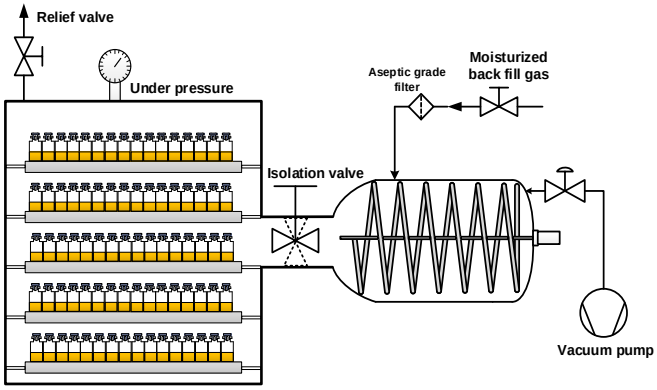

Figure 9. Pictorial depiction of ice crystals distribution from condensed frost, as described by Ling [Ling, 2014b]. In this method, the condenser chamber is used to create ice crystals by introducing moisturized gas after cooling it down to below -50 °C. Once the isolation valve is open, the ice crystals are distributed to the product chamber due to the pressure difference between the 2 chambers [Ling, 2014b].

With this regard, Geidobler et at. [Geidobler et al., 2012] reported a similar approach of controlled nucleation. This approach is based on the following steps: (1) cool down and equilibrate the product inside the product chamber to a desired temperature; (2) Cool down the condenser to around -50 °C to -80 °C and spray sterile water to load the condenser with ice; (3) depressurize the freeze dryer (both product and condenser chambers) to a predefined vacuum set point; (4) Re-pressurize the freeze dryer using a venting valve connected to the condenser. During re-pressurization, the venting gas passes through the cold condenser to the product chamber, carrying ice crystals [Geidobler et al., 2012]. According to these authors, the predominant

mechanism for induction of nucleation is that loosely attached ice from the condenser surface is blown into the product chamber during re-pressurization, even though in situ generated ice crystals might also have contribution [Geidobler et al., 2012]. The success of nucleation in this approach, according to these authors, was nearly 100% for small scale batch sizes. In addition, Geidobler et al. [Geidobler et al., 2013] reported a significant improvement in specific surface area and primary drying time of several formulations containing bovine serum albumin and monoclonal antibody, when comparing shelf ramp freezing and precooled shelf methods with the previously stated controlled nucleation approach.

The approach developed by Geidobler et al. [Geidobler et al., 2012] is under development by different companies, such as GEA Lyophil GmbH, under the trade name of LYOSPARK™ controlled nucleation, and Martin Christ Gefriertrocknungsanlagen GmbH, under the trade name of LyoCoN controlled nucleation. In general, the most significant limitation of this approach, as it is in almost all controlled nucleation techniques, is the ability to uniformly and instantly trigger nucleation at large-scale freeze dryers. It is therefore crucial that freeze dryer manufacturing companies deliver reliable and useful experimental data regarding the effectiveness of this approach at industrial scale freeze dryers.

2.1.1.3.10 Gap freezing

Gap freezing is a relatively recent concept introduced by Kuu et al. [Kuu, 2012; Kuu et al., 2012], which is performed according to the following steps: (1) creating a gap between the cooling shelves and the vials by using low thermal conductivity spacers and a stainless steel tray; (2) placing the vials on the tray; and (3) applying a step change of temperature, usually directly up to the final temperature. During the step change in temperature, the actual cooling rate of the samples is determined by the heating and cooling capabilities of the freeze dryer [Kuu et al., 2013]. The gap freezing concept is designed to eliminate directional freezing of solutions, which, as the authors claim, happens when vials are directly sitting on the cooling shelves. This is due to the fact that the much higher heat transfer rate from the bottom shelf to the vials than from the top shelf to the vials causes freezing to start at the bottom of the vials, moving then upward. During this upward freezing phenomenon, solutes

are pushed upward in the vials, resulting in a solute concentration at the top of the vials, which can eventually form a “skin layer” at the cake surface and, subsequently, increasing the dried product resistance to vapor flow during primary drying [Kuu et al., 2013]. Therefore, Kuu et al. [Kuu et al., 2012 & 2013] reported that the gap freezing method can avoid the upward freezing phenomenon and promote a uniform freezing of solutions both from bottom and top directions, avoiding formation of a highly concentrated skin layer. Even though the exact mechanism for increasing the ice nucleation temperature was not described, the authors also reported an increase in ice nucleation temperature of samples frozen by using the gap freezing method as compared to samples frozen by conventional shelf ramp freezing [Kuu et al., 2013].

Kuu et al. [Kuu et al., 2013 & 2014] performed different studies to explain the effect of gap freezing on freeze-drying performance, mainly by comparing the results obtained with those from the conventional shelf ramp freezing method. However, more studies are still needed to explain the advantages of gap freezing over the other controlled ice nucleation methods, in terms of freeze-drying process performance, ease of scaling up, and ease of implementation in an industrial scale freeze-drying process.

2.1.1.4. Summary

Freeze-drying is a very commonly used drying unit operation in pharmaceutical and biopharmaceutical industries, mainly for the purpose of removing solvents from unstable liquid formulations. The shelf life of unstable liquid formulations can be significantly extended if the solvents, which facilitate chemical and physical degradation pathways, are removed from these formulations. During a freeze-drying process, the formulation is first frozen and, then, the frozen solvent is removed by a sublimation process at a reduced pressure, followed by a desorption process for the removal of the unfrozen solvent. Therefore, 2 equally important major processes are taking place during a complete freeze-drying process: (1) freezing, during which most of the solvent is converted into a frozen solid; and (2) drying, during which almost all the solvent (frozen and unfrozen) is removed from the formulation. The drying process is further classified into 2 steps, based on the mechanism of the

drying process, namely sublimation process (primary drying) and desorption process (secondary drying). Freezing is the first step in the freeze-drying process and the fundamental understanding of the physicochemical changes during freezing is of paramount importance due to the fact that the freezing step dictates ice crystal morphology, size, and size distribution, which, in turn, influence several critical parameters, such as dried product resistance, primary and secondary drying rates, extent of product crystallinity, and reconstituability of the dried product. In addition, freezing is a critical step with regard to biological activity and stability of the APIs, especially pharmaceutical proteins.

Physical changes during freezing take place in 3 distinct phases: (1) cooling stage; (2) phase change stage; and (3) solidification stage. During the cooling stage, the temperature of the solution is lowered below its equilibrium freezing temperature until the first ice nucleus starts to be formed. The temperature at which the first ice nucleus is formed is known as ice nucleation temperature. The physical state of a solution below its equilibrium freezing temperature is called supercooling and the degree to which a solution retains its supercooling state before formation of the first ice nucleus is called degree of supercooling. In other words, the degree of supercooling is the temperature difference between the equilibrium freezing temperature and the ice nucleation temperature. The degree of supercooling determines the number, size, and morphology of ice crystals and, consequently, many other critical parameters during the drying phase of the freeze-drying process. The degree of supercooling is quite variable and it significantly differs from container to container, being affected by several factors such as foreign particles, container surface area, process conditions, sample volume, composition of the matrix, and contact area between sample and container. This random nature of the degree of supercooling affects the ice habit and results in vial-to-vial and batch-to-batch ice habit heterogeneity. This, in turn, adds a significant challenge during development, optimization, and scale-up of the freeze-drying process. In addition, the degree of supercooling at different manufacturing scales can be affected due to the differences in particulate levels, which adds additional challenges to the scale-up of a freeze-drying process. During the phase change stage, formation of ice nuclei is taking place. The number of ice nuclei formed, the rate of ice growth, and the ice crystals

size depend on the degree of supercooling. The higher the degree of supercooling, the more crystallization heat can be absorbed by the supercooled solution, and the more fraction of water instantly freezes, resulting in many ice crystals. Solutions with small degree of supercooling, on the other hand, absorb only a small amount of the heat of crystallization. This results in a small fraction of freezable water to instantly freeze, and hence the formation of very few ice crystals is favored. During the solidification stage, the ice crystals formed during the phase change stage grow in size, increasing the concentration of the solution. Solidification stops when, for a crystalline solution, all the solute and the solvent crystallize, whereas, for an amorphous solution, the increase in concentration of the solution prevents further growth of ice. For crystalline solutions, complete solidification is achieved below the eutectic temperature of the solution, whereas, for amorphous solutions, complete solidification is achieved below the glass transition temperature of the maximally freeze-concentrated solution.

The variation in degree of supercooling is the major challenge during the freeze-drying process development and scale-up. Therefore, its control during the freezing step is of paramount importance. Several alternative technologies, developed with the aim of controlling the degree of supercooling during the freeze-drying process, have been reviewed here and are summarized in Table 1.

Most of these technologies have been successfully tested at laboratory scale, but their potential use at industrial scale is still under progress. The lack of experimental data concerning the effectiveness of these technologies at industrial scale, as well as the potential expensive investment are the major factors preventing companies from implementing them. It is therefore evident that more research and experimental data are necessary to justify their effectiveness, especially at industrial scale.

Table 1. Summary of alternative freezing technologies and their advantages and disadvantages with regard to the active control of ice nucleation for freeze-drying applications

Freezing methodologies	Method description	Advantages[a]	Disadvantages[a]	References
Pre-cooled shelf freezing	Vials are placed on shelves cooled to a pre-defined temperature	Increases T_n Easy to scale up Non-invasive Retrofit not needed	Inability to select T_n Formation of heterogeneous ice crystals	[Searles et al., 2001a; Hottot et al., 2007]
Freezing with annealing	Vials are held at a specified temperature above T_g' during cooling or re-warmed after freezing	Increases ice crystals size Increases drying rate Increases Intra- and inter-batch ice crystal homogeneity Easy to scale up Non-invasive Retrofit not needed	Inability to select T_n Sensitive to annealing temperature and time May promote degradation of sensitive APIs Additional process time due to annealing step	[Tang & Pikal, 2004; Searles, 2010; Esfandiary et al., 2016; Cavatur & Suryanarayanan, 1998; Searles et al., 2001b; Lu & Pikal, 2004; Liu et al., 2005; Randolph & Searles, 2002; Pikal et al., 1983]
Quench freezing	Vials are immersed in a cold bath	Increases T_n Non-invasive	Inability to select T_n Difficult to scale up Formation of heterogeneous ice crystals Retrofit needed	[MacKenzie et al., 1977; Dawson & Hockley, 1992; Hsu et al., 1995]
Vacuum induced surface freezing	Vials are placed on a pre-cooled shelf and chamber pressure is reduced to promote surface freezing of the solution	Increases T_n Increases drying rate Increases Intra- and inter-batch ice crystal homogeneity Retrofit not needed Non-invasive	Inability to select T_n Risk of "puff-off" and boiling Difficult to scale up	[Liu et al., 2005; Kramer et al., 2002; Oddone et al., 2014, 2016 & 2017]
Ice fog freezing technique	Ice fog is injected into cold vials as nucleating agents	Ability to select T_n Increases drying rate Increases Intra- and inter-batch ice crystal homogeneity Good repeatability Possible to scale up	Retrofit needed Invasive Less effective at industrial scale (needs more experimental support) Expensive	[Chakravarty et al., 2012; Azzarella et al., 2016; Rambhatla et al., 2004; Patel et al., 2009; Brower et al., 2015]
High pressure shift /depressurization freezing	Instant nucleation is induced by reducing the pressure after vials are cooled to a desired nucleation temperature at an elevated pressure	Ability to select T_n Increases drying rate Increases Intra- and inter-batch ice crystal homogeneity Good repeatability Easy to scale up Could be effective at industrial scale (needs more experimental support)	Retrofit needed Invasive Expensive	[Konstantinidis et al., 2011; Awotwe-Otoo et al., 2013 & 2014; Gasteyer et al, 2007; Bursac et al., 2009; Rampersad et al., 2010]
Ultrasound powered freezing	Instant nucleation is induced by applying ultrasound power after vials are cooled to a desired nucleation temperature	Ability to select T_n Increases drying rate	Retrofit needed Strong vibration creates particulate matter and thus sterility concern Difficult to scale up Difficult to optimize the process	[Petzold & Aguilera, 2009; Nakagawa et al., 2006; Hottot et al., 2008; Passot et al., 2009; Li & Sun, 2002; Sun & Li, 2003; Inada et al., 2001; Saclier et al., 2010]
Electrofreezing	Nucleation is induced by applying electric pulse after vials are cooled to a desired nucleation temperature	Ability to select T_n Increases drying rate	Retrofit needed Invasive Incompatibility with solutions containing ionic species Expensive	[Shichiri & Araki, 1986; Petersen et al., 2006b; Hozumi et al., 2003]
Ice crystals distribution from condensed frost	Ice crystals are injected into cold vials as nucleating agents	Ability to select T_n Increases drying rate Increases Intra- and inter-batch ice crystal homogeneity Good repeatability Possible to scale up	Retrofit needed Invasive Less effective at industrial scale (needs more experimental support) Expensive	[Geidobler et al., 2012 & 2013; Ling, 2014a & 2014b]
Gap freezing	Vials are placed and cooled in a stainless tray, which is in a certain gap from the shelf	Reduces "skin layer" at the top Increases drying rate Possible to scale up	Inability to select T_n Slow freezing process might offset benefits of drying rate Retrofit needed Increases equipment height	[Kuu, 2012; Kuu et al., 2012; 2013 & 2014]

T_n, ice nucleation temperature; T_g', glass transition temperature of the maximally freeze concentrated solution

[a] Advantages and disadvantages sections include author's opinion.

2.1.2. Primary drying

Primary drying is a term that represents the first drying step during the freeze-drying process. During this step, sublimation of the frozen solvent (usually water) is carried out. Sublimation is a process of converting a solid phase into a vapor phase without passing through the intermediate liquid phase. As displayed in Figure 10, the sublimation interface of water lies below the triple point of the phase diagram, which consists of low pressure and low temperature. To perform the primary drying, the ice condenser temperature is reduced to below -60 °C, and the system pressure is evacuated to a pressure below the vapor pressure of ice at a target product temperature for primary drying, $P_i(T_p t1^0)$.

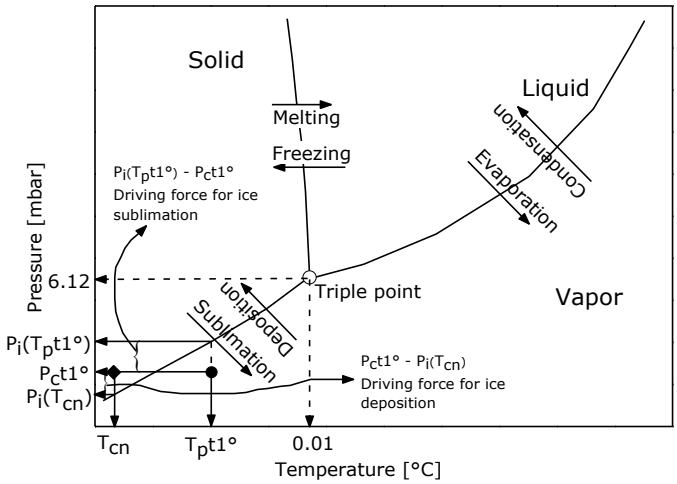

Figure 10. Phase diagram of water. Demonstration of sublimation and deposition. $T_p t1^0$, target product temperature during primary drying; T_{cn}, ice condenser temperature; $P_i(T_{cn})$, vapor pressure of ice at ice condenser temperature; $P_c t1^0$, target chamber pressure during primary drying (equivalent to the pressure at the ice condenser chamber); and $P_i(T_p t1^0)$, vapor pressure of ice at a target product temperature for primary drying.

As shown in Figure 10, sublimation continues as long as the target chamber pressure during primary drying, $P_c t1^0$, remains below the vapor pressure of ice at the target product temperature, $P_i(T_p t1^0)$ (i.e., $P_c t1^0 << P_i(T_p t1^0)$, circular symbol in Figure 10). However, sublimation of frozen water releases significant amount of water vapor, which leads to an instant increase in chamber pressure. If this water vapor is not

removed, the system reaches dynamic equilibrium and ice sublimation ceases. Thus, the continuous removal of water vapor is vital for the continuity of the ice sublimation. The purpose of the ice condenser is to continuously remove the water vapor generated during the sublimation process and to maintain the chamber pressure. The underlying principle of water vapor removal through ice condenser is that, at the ice condenser temperature (typically from -60 °C to -80 °C) and pressure (typically from 0.20 mbar to 0.05 mbar), water exists as a solid phase (diamond symbol in Figure 10). Therefore, any available water vapor is immediately converted into ice at the condenser coils through a process known as de-sublimation or deposition. Therefore, not only the continuous removal of water vapor is important during primary drying, but also the rate and the capacity of ice deposition are equally important. The rate of ice deposition is dependent on the temperature of the ice condenser. Low ice condenser temperature means that the difference between ice condenser pressure (equivalent to $P_c t1^0$) and vapor pressure of ice at ice condenser temperature, $P_i(T_{cn})$, is large (i.e., $P_c t1^0$ >> $P_i(T_{cn})$), which allows higher ice deposition rate. On the other hand, the capacity of ice deposition is dependent on the available total surface area of the ice condenser coils.

Sublimation of ice is an endothermic process, and thus takes up energy from the system. This energy take-up reduces the shelf surface temperature where the vials rest and, subsequently, the product temperature decreases. If proper energy is not supplied during the sublimation period, the product temperature will decrease until a point where its corresponding vapor pressure and the chamber pressure reach dynamic equilibrium. At this point, there is no net ice sublimation. Therefore, it is vital to maintain the product temperature at a predefined target value for the continuity of the ice sublimation. Freeze-drying equipment are supplied with product shelves, which are designed in such a way that the heat transfer fluid circulating through them is capable of precisely controlling the temperature of the product shelves in the range of -55 °C to +55 °C [Nail et al., 2002]. This feature is used to supply all necessary energy to compensate the energy take-up due to the endothermic sublimation process. Once the chamber pressure is reduced to its set value, the shelf temperature is increased to supply energy to the product and, consequently, the product temperature increases, increasing the sublimation rate of the frozen ice. The

increase in sublimation rate, in turn, increases the energy consumption from the system and reduces the product temperature. This cycle continues until the energy consumption from the sublimation of ice and the energy supply from the heating shelves reach equilibrium. At this point, the product temperature reaches quasi steady-state condition and stays fairly constant throughout the entire primary drying period, provided that the shelf temperature and chamber pressure have not been modified. A well-designed freeze-drying process is a process that balances the energy consumption and supply, so that the product temperature stays constant within pre-defined target product temperature throughout the entire primary drying period.

Primary drying is completed once all the frozen water is sublimed. There are several ways of detecting the completion of primary drying [Patel et al., 2010]. Some of the most common are: comparative pressure measurement of pirani and capacitance manometer, product temperature or shelf surface temperature response, and pressure rise test.

Comparative pressure measurement of Pirani and capacitance manometer

The difference in working principle between a Pirani gauge and a Baratron MKS capacitance manometer gives the opportunity to use these vacuum gauges as an indication for the completion of primary drying. A Pirani vacuum gauge works on the principle of measuring the thermal conductivity of the gas in the drying chamber, whereas a Baratron MKS manometer measures the absolute pressure in the drying chamber, independent of the gas composition [Patel et al., 2010]. The Pirani gauge reads about 60% higher than the Baratron MKS capacitance manometer during primary drying when essentially all of the gas in the chamber is water vapor. This is because the thermal conductivity of water vapor is ~1.6 times the thermal conductivity of nitrogen [Patel et al., 2010]. Such differences can be used to detect the end of primary drying, which is the point where the Pirani pressure starts to sharply decrease (i.e., onset), indicating that the gas composition is changing from mostly water vapor to nitrogen (i.e., sublimation is “essentially” complete) [Patel et al., 2010].

Product temperature or shelf surface temperature response

The most widely used method to detect the end of primary drying is the product temperature response. As discussed previously, the product temperature stays fairly constant during the primary drying phase for as long as there is sublimation of ice. The product temperature starts increasing toward the shelf temperature set point, indicating the completion of ice sublimation. In most cases, the point at which the product temperature crosses the shelf temperature set point is taken as an indication for the completion of primary drying [Patel et al., 2010]. Although primary drying can be completed in the monitored vial (s) even just slightly after the product temperature starts to increase, the monitored vials might not be representative of the whole batch. In addition, thermocoupled vials nucleate at higher temperature, resulting in low product resistance, and hence faster drying rate [Patel et al., 2010]. Thus, primary drying times from product temperature response may be seriously biased, and the actual primary drying time may be much longer.

To minimize the biased response of product temperature, an alternative approach is to use shelf surface temperature response. During primary drying, the shelf surface temperatures are certain degrees (depending on the sublimation rate) below the shelf temperature set point. The difference in shelf temperature set point and shelf surface temperature is solely due the presence of ice sublimation, which consumes energy from the shelves. Similar to the product temperature response, the shelf surface temperature starts increasing toward the shelf temperature set point, indicating the completion of ice sublimation. The advantage of this approach over the product temperature response is that the temperature measurement is not invasive, avoiding the effect of temperature sensors on nucleation temperature. Moreover, unlike the product temperature response, which is based on a single vial measurement, the shelf surface temperature response is the effect of several vials surrounding the point of measurements, giving better representation of the whole batch.

Pressure rise test (PRT)

The PRT is a test on the rise (increase) of pressure when the drying chamber is isolated from the condenser. As mentioned earlier, during the ice sublimation period, there is a continuous generation of water vapor, which is continuously removed by the condenser. During the pressure rise test, the condenser is briefly isolated (for ca. 25 s) from the drying chamber and, during this brief isolation time, water vapor accumulates inside the drying chamber as long as there is ice sublimation. The accumulation of water vapor yields a momentarily rise in chamber pressure and this rise in chamber pressure is analyzed to evaluate the completion of primary drying. The PRT is performed several times during the primary drying period and primary drying is marked as completed when there is little or no pressure rise. This is because, at the end of primary drying, there is no accumulation of water vapor to cause pressure rise, as all the ice is sublimed.

2.1.2.1. Transport phenomena during primary drying

As mentioned previously, primary drying is a term given to a process of conversion of frozen solvent (mostly water) directly into vapor via sublimation. Therefore, during the primary drying, there is a transport of mass (i.e., water vapor) from the ice. The mass vapor transport is an endothermic process, and hence it consumes energy from the system. It is therefore necessary to have an exothermic process to counterbalance the energy consumption due the mass transport and to keep the system in an ***energy equilibrium state***. An *energy equilibrium state* is a state where the input and output energy are equilibrated to keep the system at a constant product temperature (T_p). The exothermic process during the primary drying refers to an energy transport, in a form of heat, to the system. This is usually performed by manipulating the shelf temperature (T_s) on which the sublimating product rests.

The driving force for the vapor mass transport during primary drying is the pressure difference between the vapor pressure of ice (P_i) and the condenser pressure (P_{cn}). While P_{cn} (which is equivalent to P_c) is a user defined value, P_i is a value that depends on the product temperature of the frozen materials (T_p). Therefore, it is extremely important to consider here that the energy equilibrium state alone does not have a

relevant meaning during the primary drying, unless the concept of T_p and P_{cn} is included. To put this in other words, regardless of the user defined process parameters during the primary drying (i.e., T_s and P_c), energy equilibrium state will always be achieved, but the T_p at which the energy equilibrium state is achieved is the most important factor. This is because the T_p at which the energy equilibrium is achieved defines both the process efficiency and product quality during the primary drying. Because T_p is influenced by both user defined processing parameters (i.e., T_s and P_c), the energy equilibrium state during the primary drying is simultaneously affected by heat and mass transfer phenomena. Heat and mass transfer during the primary drying will be discussed more in detail below.

2.1.2.1.1 Heat transfer

The underlining principle of a freeze-drying process lies on a heat transfer both from and to the product. During the freezing step, heat is transferred from the product to the system, reducing the temperature of the product; whereas, during the drying step, heat is transferred from the system to the product to increase and maintain the temperature of the product. In either case, the source of the heat transfer is the temperature of the heat transfer fluid, which circulates and controls the T_s.

During the primary drying, heat is transferred from the system to the product; thus, the temperature difference between T_s and T_p is the driving force for heat transfer. In general, the overall heat transfer rate from a given vial during the primary drying can be expressed as (Equation 9):

$$\dot{Q} = A_v K_v (T_s - T_p) \quad (9)$$

where, $\dot{Q}$[W] is the overall heat transfer rate to a given vial; A_v[cm^2] is the outer surface area of a vial; K_v[W/cm^2·K] is the overall vial heat transfer coefficient of a vial; T_s[K] is the shelf temperature; and T_p[K] is the product temperature.

As reported in the literature [Pikal et al., 1984] and shown in Figure 11, there are three different mechanisms of heat transfer during the primary drying, namely direct conduction, conduction through the water vapor gas and radiation. Therefore, the

overall vial heat transfer coefficient, K_v, may be expressed as the sum of the three heat transfer contributions (Equation 10) [Pikal et al., 1984]:

$$K_v = K_c + K_g + K_r \quad (10)$$

where, K_c[W/cm^2·K] is the heat transfer coefficient contributed from direct conduction from the shelf to the vial glass at the point of contact; K_g[W/cm^2·K] is the heat transfer coefficient contributed from the conduction through the gas between the shelf and the vial bottom; and K_r[W/cm^2·K] is the heat transfer coefficient contributed from the radiative heat transfer.

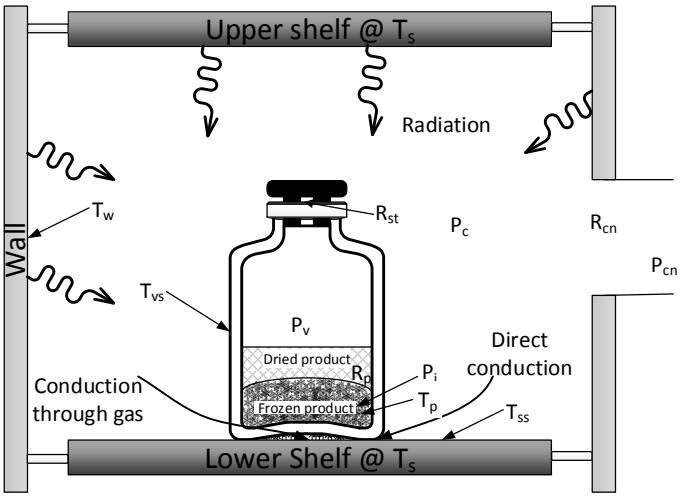

Figure 11. Heat and mass transfer from and to a vial during the primary drying step of a freeze-drying process. T_s, shelf temperature; T_w, freeze-dryer inner wall temperature; T_{vs}, vial outer surface temperature; T_{ss}, shelf surface temperature; T_p, product temperature; P_i, vapor pressure of ice; P_c, chamber pressure; P_{cn}, ice condenser pressure; P_v, pressure inside a vial; R_p, dried product resistance to water vapor flow; R_{st}, stopper resistance to water vapor flow; and R_{cn}, ice condenser resistance to water vapor flow.

Heat transfer through direct conduction is directly proportional to the contact area of a vial and the shelf. Attributed to the design of the vials, the contact area is much smaller than the total area of the vial bottom. The contact area of a vial can be determined using a print test [Pikal et al., 1984] or a detailed analysis of the vial bottom. Theoretically, heat transfer by direct conduction can be estimated using

Equation 11, provided that the area of contact, the thermal conductivity of the vial, and the thickness of the vial bottom are known.

$$\dot{Q}_c = A_{con} \frac{k}{d} (T_s - T_{pc}) \quad (11)$$

where, $\dot{Q}_c$[W] is the rate of heat transfer due to direct conduction; A_{con}[cm^2] is the area of contact between the vial bottom and the shelf; k[W/cm·K] is the thermal conductivity of the vial; d[cm] is the thickness of the vial bottom; and T_{pc}[K] is the product temperature due to heat transfer through direct conduction.

However, in practice, calculation of $\dot{Q}_c$ is not possible, as determination of T_{pc} cannot be realized.

Heat transfer from conduction through the gas is caused due to energy transfer from the gas molecules inside the chamber to the vial surface. The gas molecules inside the chamber are in constant movement. During this movement, they carry some kinetic energy and, upon collision with the vial surface, some energy might be transferred from the gas molecules to the vial surface. The heat contribution from conduction through the gas can be given as (Equation 12):

$$\dot{Q}_g = K_g (T_s - T_{pg}) \quad (12)$$

where, $\dot{Q}_g$[W] is the rate of heat transfer due to conduction through the gas; K_g[W/cm^2·K] is the heat transfer coefficient due to conduction through the gas; and T_{pg}[K] is the product temperature due to heat transfer from conduction through the gas.

As in the case of heat transfer via direct conduction, it is difficult to estimate the relative contribution of heat transfer from conduction through the gas to the total heat transfer. However, it has been reported that $\dot{Q}_g$ is dependent on the gas (chamber) pressure and on the separation distance between the vial bottom and the shelf [Pikal et al., 1984]. Thus, $\dot{Q}_g$ increases with increasing chamber pressure and with decreasing the separation distance.

Thermal radiation is energy emitted by matter that is at non-zero temperature [Incropera et al., 2007]. While the transfer of energy by conduction or convection requires the presence of a material medium, the energy transfer through radiation is transported by electromagnetic waves. Thus, energy transfer through radiation does not require the presence of a material medium. In fact, radiation transfer occurs most effectively in a vacuum [Incropera et al., 2007]. Radiation heat transfer is a function of the difference in the fourth powers of the absolute temperatures of the two surfaces in question. In freeze-drying, radiation heat transfer is a sum of two contributions; radiative heat transfer between the walls of the product chamber and the vial surfaces and radiative heat transfer between the shelf surfaces and the vial surfaces. The total rate of radiation heat transfer can be expressed as (Equation 13):

$$\dot{Q}_r = A_v \varepsilon \delta \, (T_w^4 - T_{vs}^4) + A_v \varepsilon \delta (T_{ss}^4 - T_{vs}^4) \qquad (13)$$

where, $\dot{Q}_r$[W] is the rate of heat transfer due to radiation; ε is a radiative property of a surface termed as emissivity. ε values are given in the range of 0 and 1 and they provide a measure of how efficiently a surface emits energy relative to a black body. A block body has an ε value of 1 and it is regarded as an ideal emitter. ε strongly depends on the surface material and finish. δ is the *Stefan-Boltzmann* constant (δ = 5.67 X 10^{-8} W/m^2·K^4); T_w[K] is the freeze-dryer inner wall temperature; T_{vs}[K] is the vial outer surface temperature; and T_{ss}[K] is the shelf surface temperature.

Equation 13 can be further simplified as:

$$\dot{Q}_r = A_v K_{r1} \, (T_w - T_{vs}) + A_v K_{r2} \, (T_{ss} - T_{vs}) \qquad (14)$$

where, K_{r1}[W/m^2·K] and K_{r2}[W/m^2·K] are, respectively, the radiation heat transfer coefficient from the chamber wall to the vial surface and from the shelf surface to the vial surface, and given as:

$$K_{r1} \cong \varepsilon \delta \, (T_w + T_{vs})(T_w^2 + T_{vs}^2) \qquad (15)$$

$$K_{r2} \cong \varepsilon \delta \, (T_{ss} + T_{vs})(T_{ss}^2 + T_{vs}^2) \qquad (16)$$

K_{r1} and K_{r2} strongly depend on the temperature of the surfaces.

The magnitude of the energy transferred via radiation is highly dependent on the temperature difference, emissivity and the surface area of the surfaces.

It has been reported that the relative contribution of the three different heat transfer mechanisms is dependent on T_s and P_c [Pikal et al., 1984]. However, regardless of the relative contribution of the different heat transfer mechanisms, knowledge of the overall vial heat transfer coefficient, K_v (cf. Equation 10), is the most important factor to analyze the overall heat transfer rate to a vial. K_v strongly depends on T_s, P_c, and vial characteristics (i.e., vial thickness, vial surface area, and vial bottom curvature).

2.1.2.1.2 Mass transfer

As discussed previously, mass transfer during the primary drying is characterized by water vapor flow from the frozen water interface to the condenser coils. The flow of water vapor in a freeze-drying process overcomes different resistances to mass transfer. These resistances include resistance due to the dried product, R_p; resistance due to a vial stopper, R_{st}; and resistance due to the ice condenser, R_{cn} (cf. Figure 11). The driving force for water vapor flow during the primary drying phase is the pressure difference between the vapor pressure of ice, P_i, and the ice condenser pressure, P_{cn}. The overall mass transfer rate from a given vial can be expressed as (Equation 17):

$$\dot{m} = \frac{P_i(T_p) - P_{cn}}{R_p(r) + R_{st} + R_{cn}} \quad (17)$$

where, $\dot{m}$[g/s·vial] is the overall mass transfer rate from a given vial; $P_i(T_p)$[mbar] is the vapor pressure of ice (function of product temperature, T_p); P_{cn}[mbar] is the ice condenser pressure; $R_p(r)$[mbar·s/g] is the resistance to mass transfer of the dried product (function of pore radius of the dried product, r); R_{st}[mbar·s/g] is the resistance to mass transfer of a vial stopper; and R_{cn}[mbar·s/g] is the resistance to mass transfer of an ice condenser.

The vapor transport through the dried product can be expressed as follows (Equation 18):

$$\dot{m}_p = \frac{P_i(T_p) - P_v}{R_p(r)} \quad (18)$$

where, $\dot{m}_p$[g/s·vial] is the mass transfer rate through the dried product; and P_v[mbar] is the pressure inside a vial.

Analyzing Equation 18, a high $R_p(r)$ hinders vapor transport, and thus the energy consumption from the system is reduced, increasing T_p. An increase in T_p increases P_i and, according to Equation 18, $\dot{m}_p$ increases, provided that P_{cn} is held constant. However, since the high $R_p(r)$ hinders any increase in vapor transport, the net result of this process is that the water vapor forces itself through the dried product, generating a so called micro-collapse. If the micro-collapse is not sufficient to establish energy equilibrium state in the system (i.e., a balance in energy input and output in the system), a further increase in T_p occurs. This leads to an eventual collapse or melt-back of the product. To avoid such product damage, the energy supply must be reduced (i.e., reducing T_s), so that an energy equilibrium state is reached at a target T_p. In conclusion, in a product with a high $R_p(r)$, the mass transfer rate through the dried product is a rate limiting factor. Thus, the heat transfer rate should be adjusted, so that the system reaches an energy equilibrium state before product damage occurs.

On the other hand, a low $R_p(r)$ promotes vapor transport, and thus the energy consumption from the system increases, decreasing T_p. A decrease in T_p decreases P_i and, according to Equation 18, $\dot{m}_p$ decreases, provided that P_{cn} is held constant. Unless the energy supply to the system is increased (i.e., increasing T_s), T_p continues decreasing until an energy equilibrium state in the system has been reached. To avoid such unwanted decrease in mass transfer rate, the energy supply to the system must be increased (i.e., increasing T_s), so that the energy equilibrium state of the system is reached at a target T_p. In conclusion, in a product with a low $R_p(r)$, the heat transfer rate is a rate limiting factor. Thus, the heat transfer rate should be adjusted, so that the system reaches an energy equilibrium state at the highest possible mass transfer rate (i.e., corresponding to target T_p).

The vapor transport through the vial stoppers can be expressed as follows (Equation 19):

$$\dot{m}_{st} = \frac{P_v - P_c}{R_{st}} \quad (19)$$

where, $\dot{m}_{st}$[g/s·vial] is the mass transfer rate through the semi-stopper opening; and P_c[mbar] is the chamber pressure.

During a freeze-drying process, vials are closed using stoppers in a so called semi-stoppered position. Although the opening of the semi-stoppered stoppers is sufficient to allow vapor transport without imposing significant resistance, differences in stopper design and wrong stoppering might impose differences in vapor transport rate during the primary drying.

Analyzing Equation 19, a high R_{st} hinders vapor transport from inside the vial to the chamber, and thus increases P_v. An increase in P_v increases $\dot{m}_{st}$, but decreases $\dot{m}_p$ (cf. Equation 18). However, if $\dot{m}_p$ is greater than $\dot{m}_{st}$, there will be a continuous increase in P_v, resulting in a continuous decrease in $\dot{m}_p$, until it equals $\dot{m}_{st}$. As analyzed previously, a decrease in $\dot{m}_p$ reduces the energy consumption from the system, and thus T_p increases, unless the energy supply is adjusted. This may lead to product damage or even to stopper removal if there is a significant increase in P_v.

On the other hand, if $\dot{m}_p$ is less than $\dot{m}_{st}$, the resistance due to stoppers will be negligible. Therefore, the limiting mass transfer resistance becomes the resistance from the dried product. For a typical freeze-drying process, $\dot{m}_p$ is much less than $\dot{m}_{st}$, and thus the resistance to vapor transport due to the stoppers can be safely assumed negligible, unless the opening of a semi-stoppered vial is wrongly decreased.

The vapor transport through the condenser duct can be expressed as follows (Equation 20):

$$\dot{m}_{cn} = \frac{P_c - P_{cn}}{R_{cn}} \quad (20)$$

where, $\dot{m}_{cn}$[g/s·vial] is the mass transfer rate through the condenser duct; and P_{cn}[mbar] is the ice condenser pressure.

The resistance of the condenser to vapor transport is a contribution of two factors: resistance to vapor flow through the condenser duct, and deposition rate and capacity of the condenser coils.

If the condenser duct imposes resistance to vapor transport, there will be an increase in P_c. Furthermore, if the deposition rate of the condenser coils is less than the vapor transport rate, there will be an increase in both P_c and P_{cn}. A resistance to vapor transport due to the condenser can be easily identified by observing the P_c. If the P_c stays at the set point during the entire primary drying period, the resistance to vapor transport due to the condenser can be considered negligible.

In general, as reported by Pikal et al., [Pikal et al., 1984], the major resistance to vapor transport during the primary drying period comes from the dried product and the overall mass transfer rate from a given vial during the primary drying can be expressed as (Equation 21):

$$\dot{m} = \frac{P_i(T_p) - P_{cn}}{R_p(r)} \qquad (21)$$

All the parameters are as defined previously.

As mentioned previously, after some transient time during the initial period of a primary drying, an energy equilibrium state must be reached. During the energy equilibrium sate, the energy input and output are in equilibrium, and thus the product temperature becomes fairly constant. The energy equilibrium state during the primary drying can be expressed as follows (Equation 22):

$$\dot{Q} = \Delta H_s \dot{m} \qquad (22)$$

where, ΔH_s[J/g] is the heat of sublimation of ice.

Substituting Equation 9 for $\dot{Q}$ and Equation 21 for $\dot{m}$, Equation 22 can be expressed as follows (Equation 23):

$$A_v K_v (T_s - T_p) = \Delta H_s \frac{P_i(T_p) - P_{cn}}{R_p(r)} \quad (23)$$

All the parameters are as defined previously.

For known $\dot{m}$, T_p, and P_{cn} (or P_c), Equation 21 can be used to calculate $R_p(r)$. Furthermore, Equation 23 can be rearranged to calculate K_v at any given T_s and P_{cn}. Note that P_{cn} is equivalent to P_c.

2.1.3. Secondary drying

For amorphous formulations, the amount of water remained after completion of the primary drying is significantly high, which could potentially affect the storage stability. The remaining water after the primary drying for amorphous formulations are attributed to the unfrozen water, which remains adsorbed within the solute matrix (cf. Figure 1). The unfrozen water for amorphous formulations could range from 5–20% (depending on the solid content of the formulation) of the initial water content [Tang & Pikal, 2004]. On the other hand, the water content of fully crystalline formulations after the completion of the primary drying is insignificant, which is attributed to the fact that all available water might be crystallized during the freezing step. With this regard, Pikal et al. reported that unfrozen water adsorbed on the surface of the crystalline product might be responsible for some water content of crystalline formulations after the primary drying [Pikal et al., 1990].

In either case, removal of any residual water content after the end of the primary drying is essential to reduce the residual moisture content, and hence to increase the glass transition temperature of the dried product (T_g). T_g is strongly related to the storage stability of the product. It is important to store a dried product at a temperature well-below its T_g, otherwise the dried product may be meltdown and damaged during storage. Furthermore, the T_g is strongly dependent on the residual moisture content of the dried product. The presence of water in a dried product acts as a plasticizer and enhances mobility of the dried product. This, in turn, significantly reduces the T_g of the dried product.

In a freeze-drying process, the secondary drying is a term used to describe the process of removal of any adsorbed (unfrozen) water through a desorption process. The following processes are taking place during a complete desorption process [Pikal et al., 1990]: (1) adsorbed water is diffused from the interior matrix of an amorphous solid to the surface of the solid; (2) evaporation of the water from the solid surface; and (3) vapor transport from the interior of the dried product all the way to the ice condenser. The first two processes, i.e., diffusion of adsorbed water to the surface and evaporation of water from the surface, are believed to be the rate limiting processes during the secondary drying. Therefore, to overcome the previously mentioned rate-limiting factors, the temperature during the secondary drying period is increased to a temperature as high as 40 °C [Colandene et al., 2007; Abdul-Fattah et al., 2008]. The maximum temperature during the secondary drying is limited by two factors: (1) the temperature sensitivity of formulation components, in which case, some formulation components cold lose their therapeutic properties or other functionalities at high processing temperatures; and (2) glass transition temperature of the formulation, mainly for amorphous formulations. Because of the significant amount of water content left after the completion of the primary drying, the T_g of product is very low. Therefore, both the heating rate and the final drying temperature of the secondary drying should be chosen, so that the actual product temperature always stays below the momentary glass transition temperature of the product. The T_g of the product increases with continuous loss of water; therefore, secondary drying is often performed at a final temperature as high as 40 °C [Colandene et al., 2007; Abdul-Fattah et al., 2008]. The product is held at the final drying temperature for as long as the final residual moisture content reaches an acceptable level, usually less than 2 wt% on a dry basis.

From process efficiency perspective, performing the secondary drying at high temperature–short time rather than low temperature–long time is advantageous. However, both the ramp rate and the final drying temperature for the secondary drying step should be chosen considering the characteristics of a given formulation.

2.2. Overview of a freeze-drying equipment

The entire freeze-drying process is a combination of three distinct processes, which involves freezing of a liquid formulation and drying through sublimation and desorption processes, with the latter two processes usually performed under reduced pressures. In the majority of freeze-drying processes, the liquid formulation is filled into a primary packaging container (e.g. vials or blisters) and loaded onto the shelves of a freeze dryer. The shelves are then gradually cooled down until the liquid formulation is completely solidified. Once solidified, the chamber pressure is reduced and the shelf temperature is raised, which initiates the sublimation process. The sublimation process continues until all the frozen solvents are removed. After the sublimation process has been completed, the shelf temperature is further increased to facilitate the removal of unfrozen solvent through a desorption process. To accomplish these three distinct processes in a single equipment, a synchronized operation of several devices is necessary. The different devices of a freeze dryer equipment, grouped into components, are displayed in Figure 12 and are discussed below.

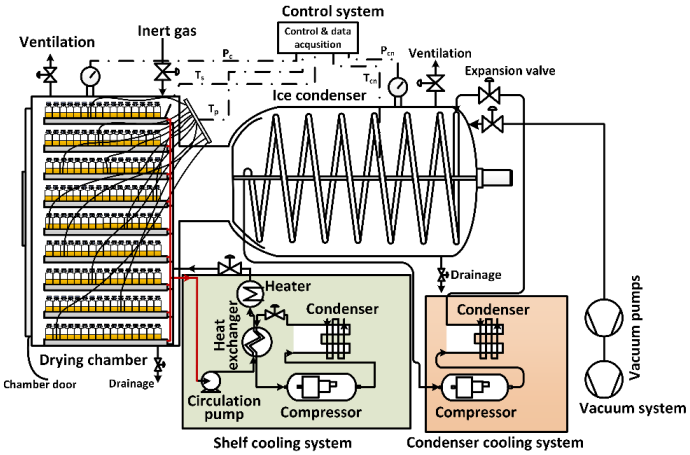

Figure 12. Schematic of a typical industrial freeze-drying equipment, showing the major components. T_s, shelf temperature; T_p, product temperature; P_c, chamber pressure; T_{cn}, ice condenser temperature; and P_{cn}, ice condenser pressure.

The *drying chamber* is usually a square cylindrical chamber, which contains several heat transfer shelves. The heat transfer shelves, or simply known as product

shelves, are designed in such a way that a heat transfer fluid is uniformly circulating through them. The heat transfer fluid is used to precisely control the temperature of the product shelves during the freezing and drying processes, which ranges from approximately -55 °C to +55 °C [Nail et al., 2002]. The flow rate of the heat transfer fluid to the shelves is controlled by temperature measurement thermocouples located at the inlet and outlet of the heat transfer fluid. The drying chamber also contains several thermocouples for product temperature measurement (non-aseptic process), a pressure and vacuum tight door to load and unload the products, pressure gauges for chamber pressure measurement, and different ports, such as ventilation port, pressure back-filling port, and drainage port.

The *ice condenser cooling* system is a sub-component of the refrigeration component of a freeze-drying equipment. The ice condenser cooling system consists of mainly a compressor, a condenser, and an expansion valve. This component is used to cool the ice condenser coils down to a required temperature, usually from -60 °C to -80 °C. The refrigeration method used in the ice condenser cooling system is known as “direct expansion”. In this method, the ice condenser coils serve as an evaporator and the refrigerant evaporates directly into these coils. Some advantages of the direct expansion method are: simple to manufacture, energy efficient, and can achieve low temperatures. These advantages of direct expansion make it suitable to cool the condenser, but its limited accuracy, which is usually within ~5 °C, makes it unsuitable for shelf cooling system [Ward, 1997].

The *shelf cooling system* is another sub-component of the refrigeration component of a freeze-drying equipment with core purposes of providing and maintaining the shelves at predefined temperatures. As displayed in Figure 12, the shelf cooling system contains a refrigeration process, in which a refrigerant fluid is circulating through a compressor, a condenser, an expansion valve and a heat exchanger. Additionally, it contains a separate process fluid or heat transfer fluid, usually silicon oil, which circulates through the heat exchanger, an electrical heater, and the shelves with the aid of a circulation pump. Since the direct expansion method used in the condenser cooling system does not provide a well controllable cooling system, the shelf cooling system uses a method known as “diatherm fluid circulation” [Ward,

1997]. In this method, the heat exchanger serves as an evaporator and the heat transfer fluid, which passes through the heat exchanger is used to cool or heat the shelves. With this method, the shelves can be maintained to typically within ±1 °C, in a temperature range of between -55 °C and +55 °C [Ward, 1997; Nail et al., 2002]. One disadvantage of this method is that it must necessarily include a pump to force the diatherm fluid around the circuit.

This pump produces heat, which is dissipated back into the system, thus reduces the efficiency of the cooling system. A second disadvantage of the diatherm fluid circulation cooling mechanism is that the process fluid, silicone oil, becomes highly viscous below temperatures of around -50 °C, resulting in pumping difficulties. However, since most freeze-drying processes do not require such low shelf temperatures, this method is often the method of choice for shelf cooling systems where strict temperature control is the main priority [Ward, 1997]. Since the diatherm fluid is not subjected to high pressures, flexible tubing may be used which enables the movement of shelves within the freeze-dryer, thus allowing shelf-stoppering mechanisms to be used.

In some cases, a single refrigeration system can be used, in which the refrigerant is shared between the condenser and the shelves. During the freezing phase of the process, full capacity of the refrigeration system is directed toward the shelves, ensuring maximum cooling of the shelves. During ice condenser cooling period, the entire capacity of the refrigeration system is switched to the ice condenser expansion valve, again ensuring maximum cooling of the ice condenser. During this period, the shelf temperature might increase a few degrees. Although this increase in shelf temperature has insignificant effect on the process, a short ice condenser pull-down time is required in order to prevent significant increase in shelf temperature. Modern freeze dryers have an ice condenser pull-down time of less than 30 minutes for a temperature range from +20 °C to -45 °C. During drying period, the capacity of the refrigeration system is shared between the ice condenser and the shelves, in which the majority of the refrigeration capacity is used to maintain the temperature of the ice condenser, whereas a small fraction of the refrigerant is reserved for precise shelf temperature control. It is important to note here that the cooling mechanisms of the

ice condenser and the shelves do not change even if a single refrigeration system is used. This means that a direct expansion cooling mechanism is employed for the ice condenser and a diatherm fluid circulation cooling mechanism is employed for the shelves.

The primary purpose of the *ice condenser* is to remove the water vapor generated during the drying process. Before the first sublimation process is started, the pressure inside the product container, in the drying chamber and in the ice condenser is the same. Once sublimation starts, the pressure in the product container increases due to a continuous accumulation of water vapor and this creates a pressure difference between the product container and the drying chamber. Due to this pressure difference, the water vapor flows from the product container to the drying chamber and the drying chamber pressure starts to increase. This again creates pressure difference between the drying chamber and the ice condenser and the water vapor flows from the drying chamber to the ice condenser. It is therefore critically important to remove the water vapor in the ice condenser in order to keep the pressure differences and to ensure the progression of the sublimation process. This is done by cooling the ice condenser to a very low temperature (usually down to -80 °C), so that the water vapor is condensed and converted into ice on the ice condenser coils. The ice condenser capacity in terms of ice deposition rate as well as total ice deposition capacity should match with the sublimation rate and with the total water vapor, which sublimates during a single freeze-drying process. To put it in other words, the ice condenser should be able to depose all the water vapor at the same rate as the maximum possible sublimation rate during a drying process. If water vapor is not removed from the drying chamber, the chamber pressure increases until it equilibrates the vapor pressure of ice and the sublimation process reaches a dynamic equilibrium.

The *vacuum system* is an integral part of a freeze-drying equipment, which could consist of redundant vacuum pumps. The vacuum system is used to evacuate the pressure in the drying chamber and in the ice condenser to any desired value. The sublimation process can only start when the chamber pressure is lower than the vapor pressure of ice at the desired product temperature. For example, the vapor

pressure of ice at -30 °C is 0.380 mbar and, for sublimation process to take place, the chamber pressure should be kept at a pressure below 0.380 mbar. The vacuum system should be too robust to maintain the chamber pressure at a user defined pressure during the entire process.

Finally, the *control system* is equipped with many communication and instrumentation lines to serve as a communication interface between the user and the freeze dryer. All necessary parameters, such as shelf temperature, chamber pressure, cooling rates, heating rates, holding times, and others are provided from the user. The control system uses these input parameters to precisely control the operation of the different parts of the equipment. Additionally, the control system registers different process output parameters, such as shelf temperature (T_s), product temperature (T_p), chamber pressure (P_c), ice condenser temperature (T_{cn}), ice condenser pressure (P_{cn}), and others.

2.3. Formulation design and the freeze-drying process

Freeze-drying is an energy intensive, time consuming, and economically expensive process [Pikal, 1985; Nail & Gatlin, 1993; Rambhatla & Pikal, 2003; Patel et al., 2010; Mortier et al., 2016]. Therefore, rational design and optimization of the freeze-drying process is of a paramount importance. The freeze-drying process usually consists of three steps: *freezing*, in which a liquid formulation is converted into a frozen solid state; *primary drying*, during which the frozen solvent is removed from the product via sublimation; and *secondary drying*, during which the unfrozen solvent is removed from the product via desorption. It is understandable that deeper knowledge of a formulation and its critical parameters, such as freezing behavior of the formulation (phase separation, protein denaturation, and pH shifting), glass transition temperature of the maximally freeze-concentrated solute (T_g'), collapse temperature of the formulation (T_c), eutectic temperature of the formulation (T_{eu}), stability of the active ingredient during preparation, and properties of the excipients are essential for the efficient and rational design of a freeze drying process [Tang & Pikal, 2004; Liu, 2006; Wang, 2000; Carpenter et al., 1997].

Characterizing and developing a rational lyophilization formulation have been a practice for the design of efficient and robust lyophilization process. As early as 1972, MacKenzie discussed how the freeze-drying process could be affected by different formulations by measuring melting temperature (T_m), eutectic temperature (T_{eu}), glass transition temperature (T_g), glass transition temperature of the freeze concentrate solute (T_g') of a water/sucrose system and collapse temperatures (T_c) of NaCl/sucrose system [MacKenzie, 1972]. Pikal reported that, because eutectic and collapse temperatures vary over an enormous range, determining the maximum allowable product temperature during primary drying is extremely important and is the first step in formulation and process development [Pikal, 1990a; Pikal, 1990b; Pikal & Shah, 1990]. Franks pointed out that an understanding of a freeze-drying formulation can remove most of the empiricism from the freeze-drying cycle development [Franks, 1992 & 1989]. In addition, many research and review articles demonstrated the importance of formulation characterization for the design of a freeze-drying process [Carpenter et al., 2002; Wang, 2010; Ward & Matejtschuk, 2010 & 2019; Passot et al., 2005 & 2010; Remmele et al., 2012]. There is therefore a significant interest in understanding the interrelationship between the formulation characteristics and the freeze-drying process parameters. With this aim, the objective of this section is to present a more detailed discussion of critical formulation properties and on how these critical properties could be applied for a rational freeze-drying process design and optimization.

2.3.1. Interrelationship between formulation properties and the freeze-drying process

When the topic of freeze-drying process design and optimization is raised, it is more than clear that the next question to follow is about the formulation properties, such as, among others, T_g', T_c, and T_{eu}. This demonstrates that a rational design of a lyophilization formulation is indispensable for the rational, economical, and robust freeze-drying process design. During the primary drying phase of a freeze-drying process, the sublimation rate is limited by the maximum allowable product temperature, which, in turn, defines the pressure difference for mass transfer. The maximum allowable product temperature of a formulation is defined from the

knowledge of T_g' or T_c of an amorphous formulation and from T_{eu} of a crystalline formulation. For example, an amorphous formulation with a T_c of -45 °C limits the maximum allowable product temperature during the primary drying phase to a maximum of -45 °C. At a T_p of -45 °C, the corresponding vapor pressure of ice of this formulation is 0.072 mbar, which is very close to the minimum value of P_c that most modern freeze dryers support at their full load capacity. This extremely small pressure difference means that the sublimation rate during the primary drying is very slow. The slow sublimation rate combined with other factors, such as total solid content, fill volume, and fill height could significantly extend the drying time of the formulation. Therefore, in this case, modification of the formulation to improve the T_c is necessary.

The interrelationship of formulation properties and freeze-drying process parameters is depicted in Figure 13.

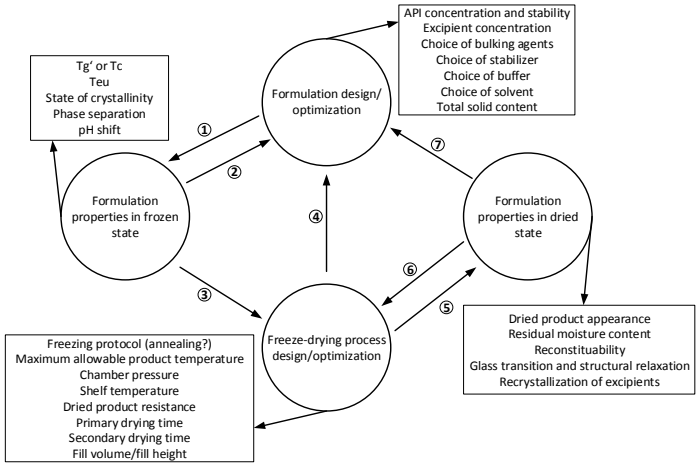

Figure 13. Interrelationship between formulation and the freeze-drying process and its role during process design and optimization. T_g', glass transition temperature of the maximally freeze-concentrated solute; T_c, collapse temperature; and T_{eu}, eutectic temperature.

As illustrated in Figure 13, the development of a lyophilization formulation starts by defining the appropriate Active Pharmaceutical Ingredient(s) (APIs) and their concentrations. In most cases, the APIs need additional constituents that provide them a stable environment during processing and storage. Therefore, the first step is to design a lyophilization formulation that contains all the required APIs, excipients

and their concentrations. The selection of the composition and concentration of the excipients requires a comprehensive understanding of the physical, chemical, and biological properties of the active ingredient. Once a lyophilization formulation is designed, the next step is to characterize the formulation in a frozen state, indicated by number 1 in Figure 13. Characterization of the formulation in its frozen state provides critical formulation properties, such as T_g' or T_c of an amorphous formulation, T_{eu} of a crystalline formulation, degree of crystallinity of a formulation, phase separation, and pH shifts. It is critical for both the process and formulation stability that these properties lie within acceptable ranges. If the excipients yield a significant deviation on the formulation properties, formulation optimization should be considered before starting designing the freeze-drying process. This is indicated by number 2 in Figure 13. For example, a formulation with a very low T_g' or T_c might need to be reformulated with the addition of collapse temperature modifiers aiming to facilitate the sublimation rate during the primary drying. Alternatively, crystalline bulking agents with high T_{eu} can be added to support the amorphous formulation. With such modification, the primary drying could be performed at a T_p higher than T_g' or T_c and the processing time can be shortened [Depaz et al., 2016; Bjelošević et al., 2018]. Furthermore, a significant pH shift during the freezing step could influence protein stability, and thus re-designing the formulation with alternative buffering agent should be considered.

Designing a freeze-drying process for an optimized formulation requires the knowledge of the critical formulation properties as well as the process itself. As indicated by number 3 in Figure 13, the critical formulation properties could be obtained from the characterization of the frozen formulation. For example, if a formulation is predominantly crystalline, annealing might be important to assure complete crystallization of the excipients. The maximum target product temperature during the primary drying step is defined based on T_g' or T_c for amorphous formulations and based on T_{eu} for crystalline formulations. The optimum critical process parameters, such as P_c, T_p, and drying time (t_d), can then be defined from the knowledge of heat and mass transfers in the freeze-drying process. As indicated by number 4 of Figure 13, the results from the freeze-drying experiments, such as

t_d, could provide useful information to further optimize the formulation. Examples of formulation optimizations include: (1) decreasing the excipients concentration to reduce total solid content of the formulation; and (2) increasing the APIs concentration to reduce the total fill height of the formulation, while keeping the same APIs concentration per vial.

Once the freeze-drying process is performed, the freeze dried products are characterized to obtain critical product quality attributes of the dried product. These include product appearance, residual moisture content, reconstituability, storage stability, glass transition of the dried product, and pH shift during storage (number 5 of Figure 13). Analyzing the storage stability data is critical to draw valid conclusions on the effect of the freeze-drying process on storage stability of the formulation [Abdul-Fattah et al., 2007a & 2007b]. For example, a dried product with a high moisture content (higher than 5 wt%) might lose its rigidity during storage, which leads to product damage and APIs degradation. In this case, re-designing the secondary drying processing conditions (i.e., drying temperature and time) is necessary. In addition, crystalline excipients, such as mannitol, might form crystal hydrates during storage, which could significantly affect storage stability of proteins [Yu et al., 1999, Hawe & Friess, 2006]. In such circumstances, re-designing the annealing step should be considered to allow complete crystallization of crystalline solutes during the freezing step (number 6 of Figure 13).

In addition to the effect of the freeze-drying process on storage stability, the formulation itself can impose long term stability issues on freeze dried formulations [Pikal et al., 1991], such as pH shift of the formulation and interaction of the formulation components during storage. Thus, formulation related stability issues can be minimized by re-formulating as indicated by number 7 of Figure 13.

2.3.2. Formulation design and optimization

Application of the freeze-drying process lies in a wide range of materials; however, the most widely used application involves products of pharmaceuticals and biopharmaceuticals industries. These products mainly comprise proteins, enzymes, hormones, vitamins, biologicals, vaccines, and antibiotics. These products are

commonly prepared as an aqueous formulation, and, unless stored at very low temperature (-70 °C), their shelf life is limited to a matter of days or weeks [Jennings, 2008]. Freeze-drying provides a means by which the shelf life of these products can be greatly extended without compromising their therapeutic properties.

Every lyophilization formulation consists of, at least, one key component with a therapeutic or diagnostic property, termed as Active Pharmaceutical Ingredient (API). The API requires, for various reasons, the addition of other components, which are termed as excipients. During formulation development, the main purpose of the excipients is usually directed to the preparation of a stable environment for the API [Jennings, 2008].

2.3.2.1. API concentration and stability

The concentration of the API is usually defined based on the therapeutic efficiency, purity, and the required final dose of the API. It is important to note here that the stability of the API should be maintained prior to lyophilization (i.e., during preparation and freezing) as well as in the dried product (i.e., during storage). To achieve such stability, the API may require other constituents or excipients. The addition of excipients may be required to provide [Jennings, 2008]: (a) correct range of pH values; (b) additional bulk to prevent physical loss of the active ingredient; (c) a stabilizing environment for the active ingredient in both its liquid and dried states; (d) protection of the active ingredient during the freezing process; and (e) protection against oxidation. The selection of the composition and concentration of the excipients requires a comprehensive understanding of the physical, chemical, and biological properties of the active ingredient.

2.3.2.2. Excipients

Excipients are defined, according to International Pharmaceutical Excipients Council (IPEC), as substances other than API, which have been appropriately evaluated for safety and are intentionally included in a drug delivery system for the following purposes: to aid in the processing of the formulation during its manufacture; to protect, support or enhance stability, bioavailability, or patient acceptability; and/or

to enhance any other attributes of the overall safety and effectiveness of the final product during storage or use [The International Pharmaceutical Excipients Council, 2017].

Table 2. Thermal properties of some of the most commonly used bulking agents and stabilizers in lyophilization

Excipients		T_g'[°C]	T_c [°C]	T_g [°C]	References
Sugars	Sucrose	-32	-31	+75	[Chang & Randall, 1992; Taylor & Zografi, 1998; Franks, 1992; Her & Nail, 1994; Adams & Ramsay, 1996]
	Trehalose	-29	-28.5	+118	
	Lactose	-28	-30.5	+114	
	Maltose	-30		+100	
Polyols	Mannitol	-35	-1.4	+13	[Chang & Randall, 1992; Adams & Ramsay, 1996; Yu et al., 1998; Her & Nail, 1994]
	Sorbitol	-46	-54	-1.6	
	Inositol				
Amino acids	Glycine	-62	-4	+30	[Passot et al., 2005; Lueckel et al., 1998; Chang & Randall, 1992; Mattern et al., 1999]
	Analine	-65			
	Arginine			+42	
	Histidine	-33		+37	
Polymers	Polyethlene glycol (PEG)	-25	-13	+180	[Bell et al., 1995; Levine & Slade, 1998; Adams & Ramsay, 1996; Willemer, 1999]
	Dextran		-11		
	Polyvinylpyrrolidone (PVP)		-24		
	Ficoll				
	Polyvinylalcohol (PVA)				
Buffering agents	Acetic acid	-53		+11	[Chang & Randall, 1992; Franks, 2007]
	Citric acid				
	Potassium phosphate dibasic	-65			
	Potassium acetate				
	Potassium citrate				
	Sodium acetate	-64			
	Sodium Chloride dihydrated	-60			
	Sodium citrate	-41		+69	
	Tris base	-51			
	Tris HCl	-65			
	Zinc chloride	-88			

T_g', glass transition temperature of the maximally freeze-concentrated solution; T_c, collapse temperature; T_g, glass transition temperature

In freeze-drying application, excipients are classified, based on the purpose they provide, as follows: *solvents* (water, oil or organic solvents), *bulking agents* (mannitol, glycine, hydroxyethyl starch or bovine serum albumin (BSA)), *stabilizers* (disaccharide, such as sucrose or trehalose), *buffering agents* (tris, histidine, or citrate), *collapse temperature modifiers* (dextran, maltodextrin, or polyvinylpyrrolidone (PVP)) and *miscellaneous agents* (tonicifying agents and

antimicrobial agents). The most widely used excipients used in freeze-drying process are listed in Table 2.

2.3.2.3. Solvents

The selection of a solvent for a formulation requires the same degree of awareness as for the other excipients in the formulation. In the case of hydrophilic constituents, water is the most preferred solvent system. However, there may be instances where freeze-drying from other solvent systems, such as organic solvents or mixtures of water and organic solvent, may offer advantages over simply drying from an aqueous solution [Teagarden et al., 2010; Vessot & Andrieu, 2012; Kunz & Gieseler, 2018; Kunz et al., 2018 & 2019]. In some instances, solubility of a drug substance in water may only be achieved at a pH value that could result in significant degradation during the time frame of dissolution of the formulation components, filtration, filling, and freezing. In such instances, the addition of an organic solvent may increase the solubility of the drug at a formulation pH that provides adequate stability prior to freeze-drying [Wittaya-Areekul & Nail, 1998]. One significant concern of using organic solvent systems is the residual amount of the solvent that could have a significant impact on the toxicity of the final product. In the case of tert-butanol (TBA), for example, the initial concentration of TBA has a significant impact on the residual TBA level in an amorphous formulation. Wittaya-Areekul and Nail demonstrated that, in a 5% sucrose formulation, the threshold TBA concentration for eutectic crystallization is about 2%. Below this concentration, the TBA remains dispersed in the amorphous phase, whereas, above the threshold concentration, it is primarily present as part of the eutectic mixture [Wittaya-Areekul & Nail, 1998]. Since removal of TBA from an amorphous phase is relatively more difficult than from a crystalline phase, the highest level of residual TBA was observed at an initial TBA concentration just below the threshold level [Wittaya-Areekul & Nail, 1998]. On the other hand, the residual level of TBA showed no dependence on the initial TBA concentration in a glycine/TBA/water system. This is consistent with TBA being present as crystalline material regardless of its concentration, since both glycine and TBA appear to crystallize readily in the presence of the other solutes. The potential advantages and

disadvantages of using organic solvents in freeze-drying application are given elsewhere [Teagarden & Baker, 2002; Teagarden et al., 2010].

2.3.2.4. Bulking agents

Most pharmaceutical formulations contain a very low amount of active constituent and, as a result, the percentage of solid in the formulation may be significantly small. When a formulation with small solid content (less than 2 wt%) is lyophilized, some of the product might be carried out of the container as a result of the flow of water vapor during the drying phase [Jennings, 2008]. Therefore, to prevent such a loss in product, to provide product elegance, as well as to increase the mechanical strength of a formulation, its solid content is increased by the addition of a bulking agent.

Amorphous bulking agents, such as glucose, maltose, and lactose are less preferred due to their low T_c, which results in an extended drying time.

Crystalline bulking agents, such as mannitol and glycine are perhaps the most commonly used bulking agents in lyophilization. The main advantage of these bulking agents is that, if crystallization of the formulation during freezing is assured, the crystalline structure provides a strong supporting structure to the active constituents and prevents product loss from the container. Moreover, the crystalline structure of the formulation allows the sublimation process to be carried out at a T_p higher than T_c of the amorphous part, and hence shortens the drying time.

Depending on the freezing protocol, a potential annealing step and the processing conditions during primary and secondary drying steps, mannitol can crystallize in the α-, β-, δ-modifications or as a mannitol hydrate [Cannon & Trappler, 2000; Pyne et al., 2002; Lu & Pikal, 2004]. Moreover, the presence of other excipients, like buffering agents and lyoprotectants or proteins can both inhibit and promote mannitol crystallization [Pikal et al., 1991; Kim et al., 1998; Lueckel et al., 1998]. The presence of mannitol hydrate can lead to stability problems during storage, due to the release of hydrate water upon its conversion into the anhydrous crystal forms [Hawe & Friess, 2006]. In addition to the main application of mannitol as a bulking agent, several approaches have been described the use of amorphous state mannitol as

lyoprotectant to adequately stabilize active protein via molecular interactions [Izutsu et al., 1994; Costantino et al., 1998]. Crystallization of mannitol can be retarded and amorphous mannitol can be produced, for example, by adding NaCl, boric acid or sodium tetraborate [Telang et al., 2003; Yoshinari et al., 2003; Izutsu et al., 2004; Srinivasan et al., 2017]. Therefore, the use of mannitol as crystalline bulking agent, in combination with an amorphous lyoprotectant (stabilizer), could present a versatile solution during freeze-drying formulation design [Johnson, et al., 2002; Horn et al., 2018a].

In addition to mannitol and glycine, crystalizing amino acids have also demonstrated a potential for alternative bulking agents [Horn et al., 2018b]. According to Horn et al., unlike mannitol and glycine, amino acids can crystalize at low amino acid to sugar ratio [Horn et al., 2018b]. This promotes the use of less excipient concentration, and hence less solid content in a lyophilization formulation.

In general, while the principal role of the bulking agents is to provide supporting structure for the active constituent, interaction between the bulking agent and the active constituent is possible [Jennings, 2008]. As a result, the bulking agent must be selected with consideration of the possible interactions between the bulking agent and the active constituent or other excipients in the formulation.

2.3.2.5. Stabilizers

While labile pharmaceutical products are generally quite stable in aqueous solution for short time, a pharmaceutical product must have adequate stability over storage periods of many months, typically several years. Thus, labile pharmaceutical products are typically freeze-dried in an attempt to achieve adequate storage stability [Pikal, 2010]. However, the process itself presents significant stress on the active constituents, which may cause instability problems by, for example, inducing conformational changes in many proteins subjected to freezing, drying and rehydration [Ward, 1997]. Such stability problems are normally minimized by a combination of proper process control and formulation optimization.

Stabilizers are usually added to lyophilization formulations in order to suppress the instability problems of active constituents during the freeze-drying process. Even though the mechanism of stabilization is not completely understood, it is suggested that the mechanism of proteins stabilization by adding a stabilizer falls into two general classifications; “thermodynamic mechanisms” and “pure kinetic mechanisms” [Pikal, 2010]. A stabilizer that functions by increasing the free energy of denaturation operates via a thermodynamic stabilization mechanism. Stability is conferred by shifting the equilibrium between “stable” native conformation and “unstable” unfolded conformation toward the native state. The “solute exclusion hypothesis”, generally believed to be a major factor in stabilization during freezing, and the “water substitute hypothesis”, often used to rationalize the stabilizing effect of saccharides during drying, are examples of thermodynamic stabilization mechanisms. Conversely, a stabilization strategy that functions by slowing the rate of the degradation process, without significantly affecting the equilibrium constants, operates via a pure kinetic mechanism [Pikal, 2010].

The *solute exclusion hypothesis* is a stabilization hypothesis for the stabilization of proteins during freezing. Solutes that stabilize protein during freezing, generally termed as “cryoprotectants”, are those solutes (such as polyols, sugars, amino acids and polyethylene glycol (PEGs)) that stabilize the native conformation of protein at the freezing temperature and concentration. Such solutes tend to be “excluded” from the surface of the protein and therefore induce “preferential hydration” of the protein. The thermodynamic consequence of “solute exclusion” and “preferential hydration” is to increase the chemical potential of the native protein. That is, as the solute is excluded from the protein interface, the surface tension of the solution is increased and the proteins are preferentially bound to the water rather than to the solute. Therefore, the free energy of unfolding is increased by the solute, which is equivalent to stabilization of the native conformation [Pikal, 2010].

The *water substitution hypothesis* is a stabilization hypothesis for the stabilization of proteins during drying. Solutes that stabilize proteins during drying are termed as “lyoprotectant” (such as trehalose, sucrose, and lactose). During drying, the critical stress factor is the reduction of water to low levels, thereby removing the assumed

stabilizing influence of hydrogen bond interactions between protein and water. This hypothesis states that stabilizers can form hydrogen bonds at specific sites on the surface of the proteins and substitute the thermodynamic stabilization function of water that is lost during drying. Therefore, unfolding of the protein is thermodynamically inhibited during the drying process (i.e., the free energy of unfolding is increased by the hydrogen bonding), and enhanced storage stability is the result of native structure preservation [Chang et al., 2005].

Regardless of the mechanism, a stabilizer or combination of stabilizers should be chosen taking into considerations factors, such as stabilizing performance during freezing as well as drying, interaction with the active constituent or other excipients, and their acceptance as excipients in pharmaceutical products.

2.3.2.6. Buffering agents

Control of pH is crucial in the lyophilization of formulations as the pH of a formulation is strongly correlated to the pharmaceutical stability of the active constituent. For this reason, buffering agents are added to freeze-drying formulations in order to suppress any pH change during processing as well as storage. A buffer solution is defined as a solution consisting of a weak acid and its salt formed by a strong base, or a weak base and its salt formed by a strong acid. The main function of a buffer solution is to resist changes in the pH of the solution [Jennings, 2008]. As most therapeutic agents are stable in a very narrow pH range, selection of a suitable buffering solution and its concentration are particularly important during formulation design.

During selection of an appropriate buffering solution, the following important properties should be considered: (1) high collapse temperature, which allows higher T_p during the primary drying, and hence faster drying rate; (2) non-volatile, to avoid buffer evaporation during processing, thus to avoid significant pH shifts; and (3) high glass transition temperature. Higher glass transition temperature of the buffer solutions assures better storage stability of the lyophilized products [Shalaev, 2005].

Crystallization of buffer components, resulting in massive pH shifts, may also present significant stress for active components, especially proteins [Pikal-Cleland et al., 2002; Sundaramurthi & Suryanarayanan, 2011]. Shalave et al. studied citrate, succinate and tartrate buffer solutions for their crystallization behavior and their effect on pH of the formulation. They had reported that the pH shift of citrate buffer was insignificant owing to the amorphous nature of the buffer solution, whereas the pH shift of succinate and tartrate was found to be significant, which is attributed to the crystallization of the buffer solutions during lyophilization [Shalaev et al., 2002]. Therefore, if the pharmaceutical stability of an active constituent is sensitive to pH shifts, buffer crystallization must be avoided. One way of minimizing buffer crystallization is to formulate with a very low weight ratio of buffer to other solutes [Pikal et al., 1991]. In addition, buffer crystallization could be inhibited using amorphous excipients [Sundaramurthi & Suryanarayanan, 2011].

2.4. References

[1]. Abdelwahed W, Degobert G, Fessi H. Freeze-drying of nano-capsules: impact of annealing on the drying process. *Int J Pharm.* 2006;324:74–82.

[2]. Abdul-Fattah AM, Lechuga-Ballesteros D, Kalonia DS, Pikal MJ. The impact of drying method and formulation on the physical properties and stability of methionyl human growth hormone in the amorphous solid state. *J. Pharm. Sci.* 2008;97(1):163–184.

[3]. Abdul-Fattah AM, Truong-Le V, Yee L, Nguyen L, Kalonia DS, Cicerone MT, Pikal MJ. Drying-induced variations in physico-chemical properties of amorphous pharmaceuticals and their impact on stability (I): stability of a monoclonal antibody. *J Pharm Sci.* 2007a;96(8):1983–2008.

[4]. Abdul-Fattah AM, Truong-Le V, Yee L, Pan E, Ao Y, Kalonia DS, Pikal MJ. Drying-induced variations in physico-chemical properties of amorphous pharmaceuticals and their impact on stability II: stability of a vaccine. *Pharm Res.* 2007b;24(4):715–727.

[5]. Adams GDJ, Ramsay JR. Optimizing the lyophilization cycle and the consequences of collapse on the pharmaceutical acceptability of *Erwinia L-Asparaginase*. *J Pharm Sci.* 1996;85(12):1301–1305.

[6]. Ali ME, Lamprecht A. Spray freeze drying as an alternative technique for lyophilization of polymeric and lipid-based nanoparticles. *Int J Pharm.* 2017;516(1-2):170–177.

[7]. Amira JH, Romann P, Pierre L. Ultrasonically triggered freezing of aqueous solutions: influence of initial oxygen content on ice crystals' size distribution. *J Cryst Growth.* 2014;402:78–82.

[8]. Awotwe-Otoo D, Agarabi C, Khan MA. An integrated process analytical technology (PAT) approach to monitoring the effect of supercooling on lyophilization product and process parameters of model monoclonal antibody formulations. *J Pharm Sci.* 2014;103(7):2042–2052.

[9]. Awotwe-Otoo D, Agarabi C, Read EK, Lute S, Brorson KA, Khan MA, Shah RB. Impact of controlled ice nucleation on process performance and quality attributes of a lyophilized monoclonal antibody. *Int J Pharm.* 2013;450(1-2):70–78.

[10]. Azzarella J, Mudhivarthi VK, Wexler E, Ganguly A. Increasing vial-to-vial homogeneity: an analysis of using VERISEQ® nucleation on production-scale freeze dryers. *BioPharm Int.* 2016;29(12):36–41.

[11]. Bell L, Hageman M, Muraoka, L. Thermally induced denaturation of lyophilized bovine somatotropin and lysozyme as impacted by moisture and excipients. *J Pharm Sci.* 1995;84:707–712.

[12]. Bhatnagar BS, Bogner RH, Pikal MJ. Protein stability during freezing: separation of stresses and mechanisms of protein stabilization. *Pharm Dev Technol.* 2007;12(5):505–523.

[13]. Bhatnagar BS, Martin SWH, Hodge TS, Das TK, Joseph L, Teagarden DL, Shalaev EY, Suryanarayanan R. Investigation of PEG crystallization in frozen and freeze-dried PEGylated recombinant human growth hormone-sucrose systems: implications on storage stability. *J Pharm Sci.* 2011;100(8):3062–3075.

[14]. Bhatnagar BS, Pikal MJ, Bogner RH. Study of the individual contributions of ice formation and freeze-concentration on isothermal stability of *Lactate Dehydrogenase* during freezing*. J Pharm Sci.* 2008;97(2):798–814.

[15]. Bhatnagar BS, Tchessalov S, Lewis LM, Johnson R. Freeze drying of biologics. In: Swarbrick J, ed. *Encyclopedia of pharmaceutical science and technology, 4th ed*., New York City: Taylor and Francis; 2013:1673–1722.

[16]. Bjelošević M, Seljak KB, Trstenjak U, Logar M, Brus B, Ahlin Grabnar P. Aggressive conditions during primary drying as a contemporary approach to optimise freeze-drying cycles of biopharmaceuticals. *Eur J Pharm Sci.* 2018;122:292–302.

[17]. Blond G, Simatos D, Catte M, Dussap CG, Gros JB. Modeling of the water-sucrose state diagram below 0 °C. *Carbohydr Res.* 1997;298:139–145.

[18]. Bosca S, Fissore D. Monitoring of a pharmaceuticals freeze-drying process by model-based process analytical technology tools. *Chem Eng Technol.* 2014;37(2):240–248.

[19]. Brower J, Lee R, Wexler E, Finley S, Caldwell M, Studer P. New developments in controlled nucleation: commercializing VERISEQ® nucleation technology. In: Varshney D, Singh M., eds., *Lyophilized Biologics and Vaccines: Modality Based Approach*, New York: Springer Science+Business Media; 2015:73–90.

[20]. Bursac R, Sever RR, Hunek B. A practical method for resolving the nucleation problem in lyophilization. *Bioprocess Int.* 2009;7:66–72.

[21]. Cannon AJ, Trappler EH. The influence of lyophilization on the polymorphic behavior of mannitol. *PDA J Pharm Sci Technol.* 2000;54(1):13–22.

[22]. Carpenter JF, Chang BS, Garzon-Rodriguez W, Randolph TW. Rationale design of stable protein formulations: theory and practice. In: Carpenter JF & Manning MC., eds. *Rationale design of stable protein formulations-theory and practice.* New York: Kluwer Academic/Plenum Publishers; 2002:109–133.

[23]. Carpenter JF, Pikal MJ, Chang BS, Randolph TW. Rational design of stable freeze-dried protein formulations: Some practical advice. *Pharm Res.* 1997;14:969–975.

[24]. Carpenter JF, Prestrelski SJ, Anchordoguy TJ, Arakawa T. Interactions of stabilizers with proteins during freezing and drying. In: Jeffrey LC, Robert L, eds. *Formulation and Delivery of Proteins and Peptides, Volume 567*, Washington D.C.: American Chemical Society; 1994:134–147.

[25]. Cavatur RK, Suryanarayanan R. Characterization of frozen aqueous solutions by low temperature X-ray powder diffractometry. *Pharm Res.* 1998;15:194–199.

[26]. Chakravarty P, Ron L, DeMarco F, Renzi E. Ice fog as a means to induce uniform ice nucleation during lyophilization. *BioPharm Int.* 2012;25(1):33–38.

[27]. Chang BS, Randall CS. Use of sub-ambient thermal analysis to optimize protein lyophilization. *Cryobiology.* 1992;29:632–656.

[28]. Chang L, Shepherd D, Sun J, Ouellette D, Grant KL, Tang XC, Pikal MJ. Mechanism of protein stabilization by sugars during freeze-drying and storage: native structure preservation, specific interaction, and/or immobilization in a glassy matrix? *J Pharm Sci.* 2005;94(7):1427–1444.

[29]. Cheow WS, Li S, Hadinoto K. Spray drying formulation of hollow spherical aggregates of silica nanoparticles by experimental design. *Chem Eng Res Des.* 2010;88(5-6):673–685.

[30]. Cheow WS, Ng ML, Kho K, Hadinoto K. Spray-freeze-drying production of thermally sensitive polymeric nanoparticle aggregates for inhaled drug delivery: Effect of freeze-drying adjuvants. *Int J Pharm.* 2011;404(d1-2):289–300.

[31]. Chow R, Blindt R, Chivers R, Povey M. A study on the primary and secondary nucleation of ice by power ultrasound. *Ultrasonics.* 2005;43:227–230.

[32]. Chow R, Blindt R, Chivers R, Povey M. The sono-crystallisation of ice in sucrose solutions: primary and secondary nucleation. *Ultrasonics.* 2003;41:595–604.

[33]. Chow R, Blindt R, Kamp A, Grocutt P, Chivers R. The microscopic visualisation of the sono-crystallisation of ice using a novel ultrasonic cold stage. *Ultrason Sonochem.* 2004;11:245–250.

[34]. Colandene JD, Maldonado LM, Creagh AT, Vrettos JS, Goad KG, Spitznagel TM. Lyophilization cycle development for a high-concentration monoclonal antibody formulation lacking a crystalline bulking agent. *J Pharm Sci.* 2007;96(6):1598–1608.

[35]. Connelly PR, Snyder PW, Zhang Y, McClain B, Quinn BP, Johnston S, Medek A, Tanoury J, Griffith J, Patrick Walters W, Dokou E, Knezic D, Bransford P. The potency-insolubility conundrum in pharmaceuticals: Mechanism and solution for hepatitis C protease inhibitors. *Biophys Chem.* 2015;196:100–108.

[36]. Connolly BD, Le L, Patapoff TW, Cromwell ME, Moore JMR, Lam P. Protein aggregation in frozen trehalose formulations: effects of composition, cooling rate, and storage temperature. *J Pharm Sci.* 2015;104(12):4170–4184.

[37]. Cortés-Rojas DF, Fernandes Souza CR, Pereira Oliveira W. Optimization of spray drying conditions for production of *Bidens pilosa L.* dried extract. *Chem Eng Res Des.* 2015;93:366–376.

[38]. Costantino HR, Andya JD, Nguyen PA, Dasovich N, Sweeney TD, Shire SJ, Hsu CC, Maa YF. Effect of mannitol crystallization on the stability and aerosol performance of a spray-dried pharmaceutical protein, recombinant humanized anti-IgE monoclonal antibody. *J Pharm Sci.* 1998;87(11):1406–1411.

[39]. Dalvi-Isfahan M, Hamdami N, Xanthakis E, Le-Bail A. Review on the control of ice nucleation by ultrasound waves, electric and magnetic fields. *J Food Eng.* 2017;195:222–234.

[40]. Dawson P, Hockley D. Scanning electron microscopy of freeze-dried preparations: relationship of morphology to freeze-drying parameters. *Dev Biol Stand.* 1992;74:185–92.

[41]. de Jesus SS, Filho RM. Optimizing drying conditions for the microwave vacuum drying of enzymes. *Drying Technol.* 2011;29(15):1828–1835.

[42]. Depaz RA, Pansare S, Patel SM. Freeze-drying above the glass transition temperature in amorphous protein formulations while maintaining product quality and improving process efficiency. *J Pharm Sci.* 2016;105(1):40–49.

[43]. Dodds J, Espitalier F, Louisnard O, Grossier R, David R, Hassoun M, Baillon F, Gatumel C, Lyczko N. The effect of ultrasound on crystallization-precipitation processes: some examples and a new segregation model. *Part Part Syst Charact.* 2007;24(1):18–28.

[44]. Dufour L. Über das Gefrieren das Wassers and Über die Bildung des Hagels. *Annalen der Physik.* 1862;114:530–554.

[45]. Esfandiary R, Gattu SK, Stewart JM, Patel SM. Effect of freezing on lyophilization process performance and drug product cake appearance. *J Pharm Sci.* 2016;105(4):1427–1433.

[46]. Fang R, Tanaka K, Mudhivarthi V, Bogner RH, Pikal MJ. Effect of controlled ice nucleation on stability of lactate dehydrogenase during freeze-drying. *J Pharm Sci.* 2018;107(3):824–830.

[47]. Farrel G, McMinn WAM, Magee TRA. Microwave-vacuum drying kinetics of pharmaceutical powders. *Drying Technol.* 2005;23(9):2131–2146.

[48]. Fernandez PP, Otero L, Guignon B, Sanz PD. High-pressure shift freezing versus high-pressure assisted freezing: effects on the microstructure of a food model. *Food Hydrocoll.* 2006;20:510–522.

[49]. Franks F. Freeze-drying of bioproducts: putting principles into practice. *Eur J Pharm Biopharm.* 1998;45:221–229.

[50]. Franks F. Freeze-drying of pharmaceuticals and biopharmaceuticals. The Royal Society of Chemistry, Cambridge: RSC Publishing, Cambridge, UK; 2007.

[51]. Franks F. Freeze-drying: from empiricism to predictability. The significance of glass transition temperature. *Dev Biol Stand.* 1992;74:9–18.

[52]. Gabel RD, Mattern M, Winter G, Wirl A, Woog H. Process for the manufacture of dry, amorphous products comprising biologically active material by means of convection drying and products obtainable by the process. *Patent* 1998: *EP0913178*.

[53]. Ganguly A, Alexeenko AA, Schultz SG, Kim SG. Freeze-drying simulation framework coupling product attributes and equipment capability: toward accelerating process by equipment modifications. *Eur J Pharm Biopharm.* 2013;85(2):223–35.

[54]. Ganguly A, Varma N, Sane P, Bogner R, Pikal MJ, Alexeenko A. Spatial variation of pressure in the lyophilization product chamber part 1: computational modeling. *AAPS PharmSciTech.* 2017;18(3):577–585.

[55]. Gasteyer TH, Sever RR, Hunek B, Grinter N, Verdone ML. Lyophilization system and method, *Patent Application Publication*, US 2007/0186437 A1; 2007.

[56]. Geidobler R, Konrad I, Winter G. Can controlled ice nucleation improve freeze-drying of highly-concentrated protein formulations? *J Pharm Sci.* 2013;102(11):3915–3919.

[57]. Geidobler R, Mannschedel S, Winter G. A new approach to achieve controlled ice nucleation of supercooled solutions during the freezing step in freeze-drying. *J Pharm Sci.* 2012;101(12):4409–4413.

[58]. Geidobler R, Winter G. Controlled ice nucleation in the field of freeze-drying: fundamentals and technology review. *Eur J Pharm Biopharm.* 2013;85:214–222.

[59]. Gupta P, Chawla G, Bansal AK. Physical stability and solubility advantage from amorphous celecoxib: the role of thermodynamic quantities and molecular mobility. *Mol Pharm.* 2004;1(6):406–413.

[60]. Hancock BC, Parks M. What is the true solubility advantage for amorphous pharmaceuticals? *Pharm Res.* 2000;(4):397–404.

[61]. Hatley RHM, Mant A. Determination of the unfrozen water content of maximally freeze-concentrated carbohydrate solutions. *Int J Biol Macromol.* 1993;15:227–232.

[62]. Hawe A, Friess W. Impact of freezing procedure and annealing on the physico-chemical properties and the formation of mannitol hydrate in mannitol-sucrose-NaCl formulations. *Eur J Pharm Biopharm.* 2006;64:316–325.

[63]. Her LM, Nail SL. Measurement of glass transition temperatures of freeze-concentrated solutes by differential scanning calorimetry. *Pharm Res.* 1994;11:54–59.

[64]. Hickling R. Nucleation of freezing by cavity collapse and its relation to cavitation damage. *Nature.* 1965;206:915–917.

[65]. Horn J, Friess W. Detection of collapse and crystallization of saccharide, protein, and mannitol formulations by optical fibers in lyophilization. *Front Chem.* 2018;6:4, doi: 10.3389/fchem.2018.00004.

[66]. Horn J, Schanda J, Friess W. Impact of fast and conservative freeze-drying on product quality of protein-mannitol-sucrose-glycerol lyophilizates. *Eur J Pharm Biopharm.* 2018a;127:342–354.

[67]. Horn J, Tolardo E, Fissore D, Friess W. Crystallizing amino acids as bulking agents in freeze-drying. *Eur J Pharm Biopharm.* 2018b;132:70–82.

[68]. Hottot A, Nakagawa K, Andrieu J. Effect of ultrasound-controlled nucleation on structural and morphological properties of freeze-dried mannitol solutions. *Chem Eng Res Des.* 2008;86(2):193–200.

[69]. Hottot A, Vessot S, Andrieu J. Freeze drying of pharmaceuticals in vials: influence of freezing protocol and sample configuration on ice morphology and freeze-dried cake texture. *Chem Eng Process.* 2007;46:666–674.

[70]. Hozumi T, Saito A, Okawa S, Watanabe K. Effects of electrode materials on freezing of supercooled water in electric freeze control. *Int J Refrig.* 2003;26(5):537–542.

[71]. Hsu CC, Nguyen HM, Yeung DA, Brooks DA, Koe GS, Bewley TA, Pearlman R. Surface denaturation at solid-void interface: a possible pathway by which opalescent particulates form during the storage of lyophilized tissue-type plasminogen-activator at high-temperatures. *Pharm Res.* 1995;12(1):69–77.

[72]. Inada T, Zhang X, Yabe A, Kozawa Y. Active control of phase change from supercooled water to ice by ultrasonic vibration 1. Control of freezing temperature. *Int J Heat Mass Transf.* 2001;44:4523–4531.

[73]. Incropera FP, DeWitt DP, Bergman TL, Lavine AS. Fundamentals of heat and mass transfer, 6th ed. John Wiley & Sons, Inc.; NJ, USA; 2007.

[74]. Izutsu K, Ocheda SO, Aoyagi N, Kojima S. Effects of sodium tetraborate and boric acid on nonisothermal mannitol crystallization in frozen solutions and freeze-dried solids*. Int J Pharm.* 2004;273(1-2):85–93.

[75]. Izutsu K, Yoshioka S, Terao T. Effect of mannitol crystallinity on the stabilization of enzymes during freeze-drying. *Chem Pharm Bull (Tokyo)*. 1994;42(1):5–8.

[76]. Jangle RD, Pisal SS. Vacuum foam drying: an alternative to lyophilization for biomolecule preservation. *Indian J Pharm Sci.* 2012;74(2):91–100.

[77]. Jennings TA. *Lyophilization: Introduction and Basic principles.* Informa Healthcare, NY, USA; 2008.

[78]. Jin HY, Xia F, Zhao YP. Preparation of hydroxypropylmethyl cellulose phthalate nanoparticles with mixed solvent using supercritical anti-solvent process and its application in co-precipitation of insulin. *Adv Powder Technol.* 2012;23(2):157–163.

[79]. Johnson RE, Kirchhoff CF, Gaud HT. Mannitol-sucrose mixtures-versatile formulations for protein lyophilization. *J Pharm Sci.* 2002;91(4):914–922.

[80]. Kasper JC, Friess W. The freezing step in lyophilization: Physico-chemical fundamentals, freezing methods and consequences on process performance and quality attributes of biopharmaceuticals. *Eur. J. Pharm. Biopharm.* 2011;78:248–263

[81]. Kharaghani A, Tsotsas E, Wolf C, Beutler T, Guttzeit M, Oetjen G. Freeze drying. In *Ullmann's Encyclopedia of Industrial Chemistry*, ed.; 2017. doi:10.1002/14356007.h12_h01.pub2.

[82]. Kiani H, Sun DW, Delgado A, Zhang Z. Investigation of the effect of power ultrasound on the nucleation of water during freezing of agar gel samples in tubing vials. *Ultrason Sonochem.* 2012;19(3):576–581.

[83]. Kiani H, Zhang Z, Sun DW. Effect of ultrasound irradiation on ice crystal size distribution in frozen agar gel samples*. Innov Food Sci Emerg Technol.* 2013;18:126–131.

[84]. Kim AI, Akers MJ, Nail SL. The physical state of mannitol after freeze-drying: effects of mannitol concentration, freezing rate, and a non-crystallizing co-solute. *J Pharm Sci.* 1998;87(8):931–935.

[85]. Knight CA. *The freezing of supercooled liquids*. Princeton: D. Van Nostrand and Co. Ltd.; 1967.

[86]. Knopp MM, Löbmann K, Elder DP, Rades T, Holm R. Recent advances and potential applications of modulated differential scanning calorimetry (mDSC) in drug development. *Eur J Pharm Sci.* 2016;87:164–173.

[87]. Konstantinidis AK, Kuu W, Otten L, Nail SL, Sever RR. Controlled nucleation in freeze-drying: effects on pore size in the dried product layer, mass transfer resistance, and primary drying rate. *J Pharm Sci.* 2011;100(8):3453–3470.

[88]. Kramer M, Sennhenn B, Lee G. Freeze-drying using vacuum-induced surface freezing. *J Pharm Sci.* 2002;91(2):433–443.

[89]. Kshirsagar V, Tchessalov S, Kanka F, Hiebert D, Alexeenko A. Determining maximum sublimation rate for a production lyophilizer: computational modeling and comparison with ice slab tests. *J Pharm Sci.* 2019;108(1):382–390.

[90]. Kumano H, Asaoka T, Saito A, Okawa S. Study on latent heat of fusion of ice in aqueous solutions. *Int J Refrig*. 2007;30(2):267–273.

[91]. Kunz C, Gieseler H. Factors influencing the retention of organic solvents in products freeze-dried from co-solvent systems. *J Pharm Sci.* 2018;107(8):2005–2012.

[92]. Kunz C, Schuldt-Lieb S, Gieseler H. Freeze-drying from organic co-solvent systems, part 1: thermal analysis of co-solvent-based placebo formulations in the frozen state. *J Pharm Sci.* 2018;107(3):887–896.

[93]. Kunz C, Schuldt-Lieb S, Gieseler H. Freeze-drying from organic co-solvent systems, part 2: process modifications to reduce residual solvent levels and improve product quality attributes. *J Pharm Sci.* 2019;108(1):399–415.

[94]. Kuu WY, Doty MJ, Hurst WS, Rebbeck CL. Optimization of nucleation and crystallization for lyophilization using gap freezing. *Patent US2012/0192448 A1*; 2012.

[95]. Kuu WY, Doty MJ, Rebbeck CL, Hurst WS, Cho YK. Gap-freezing approach for shortening the lyophilization cycle time of pharmaceutical formulations-demonstration of the concept. *J Pharm Sci.* 2013;102(8):2572–2588.

[96]. Kuu WY. Optimization of nucleation and crystallization for lyophilization using gap freezing. Patent *US2012/0077971A1;* 2012.

[97]. Kuu, WY, Doty MJ, Nisipeanu E, Rebbeck CL, Cho YK, Smit MH. Modeling of heat and mass transfer processes for the gap-lyophilization system using the mannitol-trehalose-NaCl formulation. *J Pharm Sci.* 2014;103(9):2784–2796.

[98]. Levine H, Slade L. Principles of “cryostabilization” technology from structure/property relationships of carbohydrate/water systems-a review. *Cryo Lett.* 1998;9:21–63.

[99]. Li B, Sun DW. Effect of power ultrasound on freezing rate during immersion freezing of potatoes. *J Food Eng.* 2002;55(3):277–282.

[100]. Ling W. Controlled nucleation during freezing step of freeze drying cycle using pressure differential ice fog distribution. Patent *US2014/8839528B2;* 2014a.

[101]. Ling W. Controlled nucleation during freezing step of freeze drying cycle using pressure differential ice crystals distribution from condensed frost. Patent *US2014/8875413B2;* 2014b.

[102]. Liu J, Viverette T, Virgin M, Anderson M, Dalal P. A study of the impact of freezing on the lyophilization of a concentrated formulation with a high fill depth. *Pharm Dev Technol.* 2005;10:261–272.

[103]. Liu J. Physical characterization of pharmaceutical formulations in frozen and freeze-dried solid states: techniques and applications in freeze-drying development. *Pharm Dev Technol.* 2006;11:3–28.

[104]. Lu X, Pikal MJ. Freeze-drying of mannitol-trehalose-sodium chloride-based formulations: the impact of annealing on dry layer resistance to mass transfer and cake structure. *Pharm Dev Technol.* 2004;9(1):85–95.

[105]. Lueckel B, Bodmer D, Helk B, Leuenberger H. Formulations of sugars with amino acids or mannitol-influence of concentration ratio on properties of the freeze-concentrate and the lyophilisate. *Pharm Dev Technol.* 1998:3:325–336.

[106]. Ma X, Wang DQ, Bouffard R, MacKenzie A. Characterization of murine monoclonal antibody to tumor necrosis factor (TNF-MAb) formulation for freeze-drying cycle development. *Pharm Res.* 2001;18:196–202.

[107]. MacKenzie AP, Derbyshire W, Reid DS. Non-equilibrium freezing behavior of aqueous systems. *Phil Trans R Soc Lond B.* 1977;278(959):167–189.

[108]. MacKenzie AP. Freezing, freeze-drying and freeze-substitution. Proceedings of the workshop on biological specimen preparation techniques for scanning electron microscopy. *IIT Research Institute*. 1972.

[109]. Mandal G, Kumar PP. A laboratory study of ice nucleation due to electrical discharge. *Atmos Res.* 2002;61:115–123.

[110]. Mattern M, Winter G, Kohnert U, Lee G. Formulation of proteins in vacuum-dried glasses II. Process and storage stability in sugar-free amino acid systems. *Pharm Dev Technol.* 1999;4:199–208.

[111]. Meister E, Gieseler H. Freeze-dry microscopy of protein/sugar mixtures: drying behavior, interpretation of collapse temperatures and a comparison to corresponding glass transition data. *J Pharm Sci.* 2009;98(9):3072–3087.

[112]. Mortier STFC, Van Bockstal PJ, Corver J, Nopens I, Gernaey KV, De Beer T. Uncertainty analysis as essential step in the establishment of the dynamic Design Space of primary drying during freeze-drying. *Eur J Pharm Biopharm*. 2016; 103:71–83.

[113]. Nail SL, Gatlin LA. Freeze-drying: principles and practice. In: Avis KE, Lieberman HA & Lachman L., eds. *Pharmaceutical Dosage Forms: Parenteral Medications, 2nd ed., Vol. 2.* New York: Marcel Dekker Inc., 1993:163–233.

[114]. Nail SL, Jiang S, Chongprasert S, Knopp SA. Fundamentals of freeze drying. In: Nail SL, Akers MJ, eds., *Development and Manufacture of Protein Pharmaceuticals*, New York: Kluwer Academic/Plenum Publisher; 2002:281–360.

[115]. Nakagawa K, Hottot A, Vessot S, Andrieu J. Influence of controlled nucleation by ultrasounds on ice morphology of frozen formulations for pharmaceutical proteins freeze-drying. *Chem Eng Process.* 2006;45:783–791.

[116]. Nakagawa K, Murakami W, Andrieu J, Vessot S. Freezing step controls the mannitol phase composition heterogeneity. *Chem Eng Res Des.* 2009;87(8):1017–1027.

[117]. Oddone I, Barresi AA, Pisano R. Influence of controlled ice nucleation on the freeze-drying of pharmaceutical products: the secondary drying step. *Int J Pharm.* 2017;524(1-2):134–140.

[118]. Oddone I, Pisano R, Bullich R, Stewart P. Vacuum induced nucleation as a method for freeze-drying cycle optimization. *Ind Eng Chem Res.* 2014;53:18236–18244.

[119]. Oddone I, Van Bockstal PJ, de Beer T, Pisano R. Impact of vacuum-induced surface freezing on inter-and intra-vial heterogeneity. *Eur J Pharm Biopharm.* 2016;103:167–178.

[120]. Ohtake S, Martin RA, Saxena A, Lechuga-Ballesteros D, Santiago AE, Barry EM, Truong-Le V. Formulation and stabilization of *Francisella Tularensis* live vaccine strain. *J Pharm Sci.* 2011;100(8):3076–3087.

[121]. Ohtake S, Martin RA, Yee L, Chen D, Kristensen DD, Lechuga-Ballesteros D, Truong-Le V. Heat-stable measles vaccine produced by spray drying. *Vaccine.* 2010;28(5):1275–1284.

[122]. Otero L, Sanz PD, Guignon B, Aparicio C. Experimental determination of the amount of ice instantaneously formed in high-pressure shift freezing. *J Food Eng.* 2009;95(4):670–676.

[123]. Otero L, Sanz PD. High pressure shift freezing. Part 1. Amount of ice instantaneously formed in the process. *Biotechnol Prog.* 2000;16:1030–1036.

[124]. Passot S, Fonseca F, Alarcon-Lorcab M, Rolland D, Marina M. Physical characterization of formulations for the development of two stable freeze-dried proteins during both dried and liquid storage. *Eur J Pharm Biopharm.* 2005;60:335–348.

[125]. Passot S, Tréléa IC, Marin M, Fonseca F. The relevance of thermal properties for improving formulation and cycle development: application to freeze-drying of proteins. In Rey L, May, JC., eds. *Freeze-Drying/Lyophilization of Pharmaceutical and Biological Products, 3rd Ed*. London: Informa Healthcare; 2010:136-166.

[126]. Passot S, Tréléa IC, Marin M, Galan M, Morris GJ, Fonseca F. Effect of controlled ice nucleation on primary drying stage and protein recovery in vials cooled in a modified freeze-dryer. *J Biomech Eng.* 2009;131(7):74511–74515.

[127]. Patel SM, Bhugra C, Pikal MJ. Reduced pressure ice fog technique for controlled ice nucleation during freeze-drying. *AAPS Pharm SciTech.* 2009;10:1406–1411.

[128]. Patel SM, Doen T, Pikal MJ. Determination of end point of primary drying in freeze-drying process control. *AAPS PharmSciTech*. 2010;11(1):73–84.

[129]. Patel SM, Jameel F, Pikal MJ. The effect of dryer load on freeze drying process design. *J Pharm Sci.* 2010; 99:4363–4379.

[130]. Petersen A, Schneider H, Rau G, Glasmacher B. A new approach for freezing of aqueous solutions under active control of the nucleation temperature. *Cryobiology.* 2006a;53:248–257.

[131]. Petersen A, Rau G, Glasmacher B. Reduction of primary freeze-drying time by electric field induced ice nucleus formation. *Heat Mass Transfer.* 2006b;42:929–938.

[132]. Petzold G, Aguilera J. Ice morphology: fundamentals and technological applications in foods. *Food Biophys.* 2009;4:378–396.

[133]. Pikal MJ. Mechanisms of protein stabilization during freeze-drying storage: the relative importance of thermodynamic stabilization and glassy state relaxation dynamics. In Rey L, May, JC., eds. *Freeze-Drying/Lyophilization of Pharmaceutical and Biological Products, 3rd Ed*. London: Informa Healthcare; 2010:198–232.

[134]. Pikal MJ, Dellerman KM, Roy ML, Riggin RM. The effects of formulation variables on the stability of freeze-dried human growth hormone. *Pharm Res.* 1991;8(4):427–436.

[135]. Pikal MJ, Rambhatla S, Ramot R. The impact of the freezing stage in lyophilization: effects of the ice nucleation temperature on process design and product quality. *Am Pharmaceut Rev.* 2002;5:48–52.

[136]. Pikal MJ, Roy ML, Shah S. Mass and heat transfer in vial freeze-drying of pharmaceuticals: role of the vial*. J Pharm Sci.* 1984;73:1224–1237.

[137]. Pikal MJ, Shah S, Roy ML, Putman R. The secondary drying stage of freeze drying: drying kinetics as a function of temperature and chamber pressure. *Int J Pharm.* 1990;60(3):203–217.

[138]. Pikal MJ, Shah S, Senior D, Lang JE. Physical chemistry of freeze-drying: measurement of sublimation rates for frozen aqueous solutions by a microbalance technique. *J Pharm Sci.* 1983;72(6):635–650.

[139]. Pikal MJ, Shah S. The collapse temperature in freeze-drying: dependence on measurement methodology and rate of water removal from the glassy phase. *Int J Pharm.* 1990;62:165–186.

[140]. Pikal MJ. Freeze drying. In: Swarbrick J, ed. *Encyclopedia of pharmaceutical technology*, *3rd ed*., New York City: Informa Healthcare, Inc.; 2006:1807–1833.

[141]. Pikal MJ. Freeze-drying of proteins. Part I: Process design. *BioPharm.* 1990a;3:18–27.

[142]. Pikal MJ. Freeze-drying of proteins. Part II: Formulation selection. *BioPharm.* 1990b:10:26–30.

[143]. Pikal MJ. Use of laboratory data in freeze drying process design: heat and mass transfer coefficients and the computer simulation of freeze drying. *PDA J Pharm Sci and Tech.* 1985;39:115–139.

[144]. Pikal-Cleland KA, Cleland JL, Anchordoquy TJ, Carpenter JF. Effect of glycine on pH changes and protein stability during freeze-thawing in phosphate buffer systems. J *Pharm Sci.* 2002;91(9):1969–1979.

[145]. Pisano R, Capozzi LC. Prediction of product morphology of lyophilized drugs in the case of vacuum induced surface freezing. *Chem Eng Res Des.* 2017;125:119–129.

[146]. Purohit HS, Trasi NS, Sun DD, Chow ECY, Wen H, Zhang X, Gao Y, Taylor LS. Investigating the impact of drug crystallinity in amorphous tacrolimus capsules on pharmacokinetics and bioequivalence using discriminatory in vitro dissolution testing and physiologically based pharmacokinetic modeling and simulation. *J Pharm Sci.* 2018;107(5):1330–1341.

[147]. Pyne A, Surana R, Suryanarayanan R. Crystallization of mannitol below Tg' during freeze-drying in binary and ternary aqueous systems. *Pharm Res*. 2002;19(6):901–908.

[148]. Rambhatla S, Pikal MJ. Heat and mass transfer scale-up issues during freeze-drying, I: atypical radiation and the edge vial effect. *AAPS Pharm Sci Tech,* 2003;4(2):1–10.

[149]. Rambhatla S, Ramot R, Bhugra C, Pikal MJ. Heat and mass transfer scale-up issues during freeze drying: II. Control and characterization of the degree of supercooling. *AAPS Pharm Sci Tech.* 2004:5(4) Article 58:1–9.

[150]. Rampersad BM, Sever RR, Hunek B, Gasteyer TH. Freeze-dryer and method of controlling the same, *Patent Application Publication*, US 2010/0242301 A1; 2010.

[151]. Randolph TW, Searles JA. Freezing and annealing phenomena in lyophilization: Effect upon primary drying rate, morphology, and heterogeneity. *Am Pharmaceut Rev.* 2002;5(4):40–46.

[152]. Rau W. Eiskeimbildung durch Dielektrische Polarisation. *Z Naturforschg A.* 1951;6:649–657.

[153]. Remmele RL, Krishnan S, Callahan WJ. Development of stable lyophilized protein drug products. *Curr Pharm Biotechnol*. 2012;13(3):471–496.

[154]. Reverchon E, Adami R, Cardea S, Della Porta G. Supercritical fluids processing of polymers for pharmaceutical and medical applications. *J Supercrit Fluids.* 2009;47(3):484–492.

[155]. Rey L. Glimpses into the realm of freeze-drying: classical issues and new ventures. In: Louis R, Joan CM, eds. *Freeze Drying/Lyophilization of Pharmaceutical and Biological Products, 3rd ed.,* London: Informa Healthcare; 2010:1–28.

[156]. Rowe TD. A technique for the nucleation of ice, in: *International Symposium on Biological Product Freeze-Drying and Formulation*, Geneva: 1990.

[157]. Roy M, Pikal MJ. Process control in freeze-drying: determination of the end point of sublimation drying by an electronic moisture sensor. *PDA J Pharm Sci Technol.* 1989;43(2):60-66.

[158]. Rumondor ACF, Dhareshwar SS, Kesisoglou F. Amorphous solid dispersions or prodrugs: complementary strategies to increase drug absorption. *J Pharm Sci.* 2016;105(9):2498–2508.

[159]. Sacha GA, Nail SL. Thermal analysis of frozen solutions: multiple glass transitions in amorphous systems. *J Pharm Sci.* 2009;98(9):3397–3405.

[160]. Saclier M, Peczalski R, Andrieu J. Effect of ultrasonically induced nucleation on ice crystals' size and shape during freezing in vials. *Chem Eng Sci.* 2010;65:3064–3071.

[161]. Schawe EK. A quantitative DSC analysis of the metastable phase behavior of the sucrose-water system. *Thermochim Acta.* 2006:451:115–125.

[162]. Searles JA, Carpenter JF, Randolph TW. The ice nucleation temperature determines the primary drying rate of lyophilization for samples frozen on a temperature-controlled shelf. *J Pharm Sci.* 2001a;90(7):860–871.

[163]. Searles JA, Carpenter JF, Randolph TW. Annealing to optimize the primary drying rate, reduce freezing-induced drying rate heterogeneity, and determine Tg' in pharmaceutical lyophilization. *J Pharm Sci.* 2001b;90(7):872–887.

[164]. Searles JA. Freezing and annealing phenomena in lyophilization. In: Louis R, Joan CM, ed. *Freeze Drying/Lyophilization of Pharmaceutical and Biological Products, 3rd ed*., London: Informa Healthcare; 2010:52–81.

[165]. Shalaev E. The impact of buffer on processing and stability of freeze-dried dosage forms, part 1. Solution freezing behaviour. *Am Pharm Rev.* 2005;8:80–87.

[166]. Shalaev EY, Johnson-Elton TD, Chang L, Pikal MJ. Thermophysical properties of pharmaceutically compatible buffers at sub-zero temperatures: implications for freeze-drying. *Pharm Res.* 2002;19(2):195–201.

[167]. Shanley A. Modernizing lyophilization. *BioPharm Int.* 2017;30(12):50–52.

[168]. Shibkov AA, Golovin YL, Zheltov MA, Korolev AA, Leonov AA. Morphology diagram of non-equilibrium patterns of ice crystals growing in supercooled water. *Physica A Stat Mech Appl.* 2003;319:65–79.

[169]. Shichiri T, Araki Y. Nucleation mechanism of ice crystals under electrical effect. *J Cryst Growth.* 1986;78:502–508.

[170]. Shichiri T, Nagata T. Effect of electric currents on the nucleation of ice crystals in the melt. *J Cryst Growth.* 1981;54:207–210.

[171]. Sonner C, Maa YF, Lee G. Spray-freeze-drying for protein powder preparation: particle characterization and a case study with trypsinogen stability. *J Pharm Sci.* 2002;91(10):2122–2139.

[172]. Srinivasan JM, Wegiel LA, Hardwick LM, Nail SL. The influence of mannitol hemihydrate on the secondary drying dynamics of a protein formulation: a case study. *J Pharm Sci.* 2017;106(12):3583–3590.

[173]. Sun DW, Li B. Microstructural change of potato tissues frozen by ultrasound-assisted immersion freezing. *J Food Eng*. 2003;57(4):337–345.

[174]. Sundaramurthi P, Suryanarayanan R. The effect of crystallizing and non-crystallizing co-solutes on succinate buffer crystallization and the consequent pH shift in frozen solutions. *Pharm Res.* 2011;28(2):374–385

[175]. Tang X, Pikal MJ. Design of freeze-drying processes for pharmaceuticals: practical advice. *Pharm Res.* 2004;21(2):191–200.

[176]. Taylor L, Zografi G. Sugar-polymer hydrogen bond interactions in lyophilized amorphous mixtures. *J Pharm Sci.* 1998;87:1615–1621.

[177]. Teagarden DL, Baker DS. Practical aspects of lyophilization using non-aqueous co-solvent systems. *Eur J Pharm Sci.* 2002;15(2):115–133.

[178]. Teagarden DL, Wang W, Baker DS. Practical aspects of freeze-drying of pharmaceutical and biological products using non-aqueous co-solvent systems. In Rey L, May, JC., eds. *Freeze-Drying/Lyophilization of Pharmaceutical and Biological Products, 3rd Ed*. London: Informa Healthcare; 2010:233–253.

[179]. Telang C, Yu L, Suryanarayanan R. Effective inhibition of mannitol crystallization in frozen solutions by sodium chloride. *Pharm Res.* 2003;20(4):660–667.

[180]. The International Pharmaceutical Excipients Council. *The Joint Good Manufacturing Practices Guide for Pharmaceutical Excipients,* Brussels: IPEC Federation and Pharmaceutical Quality Group; 2017.

[181]. Thijssen H, Rulkens W. Effect of freezing rate on rate of sublimation and flavor retention in freeze-drying. *Int J Refrig.* 1969;10:99–113.

[182]. Ullrich S, Seyferth S, Lee G. Measurement of shrinkage and cracking in lyophilized amorphous cakes. Part IV: Effects of freezing protocol. *Int J Pharm.* 2015;495(1):52–57.

[183]. Vaitheeswaran S, Yin H, Rasaiah JC. Water between plates in the presence of an electric field in an open system. *J Phys Chem B.* 2005;109(14):6629–6635.

[184]. Vessot S, Andrieu J. A review on freeze drying of drugs with tert-butanol (TBA) + water systems: characteristics, advantages, drawbacks. *Drying Technol*. 2012;30(4):377–385.

[185]. Walters RH, Bhatnagar B, Tchessalov S, Izutsu K, Tsumoto K, Ohtake S. Next generation drying technologies for pharmaceutical applications. *J Pharm Sci.* 2014;103(9):2673–2695.

[186]. Wang DQ. Formulation characterization. In Rey L, May, JC., eds. *Freeze-Drying/Lyophilization of Pharmaceutical and Biological Products, 3rd Ed*. London: Informa Healthcare; 2010:233–253.

[187]. Wang W. Lyophilization and development of solid protein pharmaceuticals. *Int J Pharm.* 2000;203:1–60.

[188]. Wanning S., Sueverkruep R. Lamprecht A. Pharmaceutical spray freeze drying. *Int J Pharm*. 2015;488(1-2):136–53.

[189]. Ward KR, Matejtschuk P**.** The use of microscopy, thermal analysis, and impedance measurements to establish critical formulation parameters for freeze-drying cycle development. In Rey L, May JC., eds. *Freeze-Drying/Lyophilization of Pharmaceutical and Biological Products, 3rd Ed*. London: Informa Healthcare; 2010:112–135.

[190]. Ward KR. Freeze-drying: a rational approach to process development and product formulation using model polymeric proteins and drug microcarrier systems. PhD thesis, the University of Aston in Birmingham; 1997.

[191]. Ward KR, Matejtschuk P. Characterization of formulations for freeze-drying. In: Ward KR, Matejtschuk P., eds. *Lyophilization of Pharmaceuticals and Biologicals: Methods in Pharmacology and Toxicology*. New York: Humana Press; 2019: 1–32.

[192]. Wei S, Zhong C, Su-Yi H. Molecular dynamics simulation of liquid water under the influence of an external electric field. *Mol Simul.* 2005;31(8):555–559.

[193]. Willemer H. Experimental freeze-drying: procedure and equipment. In: Rey L & May JC., eds. *Freeze-Drying/Lyophilization of Pharmaceutical and Biological product*. New York: Marcel Dekker, Inc.; 1999:79–122.

[194]. Wittaya-Areekul S, Nail SL. Freeze-drying of tert-butyl alcohol/water co-solvent systems: Effects of formulation and process variables on residual solvents. *J Pharm Sci.* 1998;87(4):491–495.

[195]. Xia X, Berkowitz ML. Electric-field induced restructuring of water at a platinum-water interface: a molecular dynamics computer simulation. *Phys Rev Lett.* 1995;74(16):3193–3196.

[196]. Xie J, Jiang J, Davoodi P, Srinivasan MP, Wang CH. Electrohydrodynamic atomization: A two-decade effort to produce and process micro-/nanoparticulate materials. *Chem Eng Sci.* 2015;125:32–57.

[197]. Yoshinari T, Forbes RT, York P, Kawashima Y. Crystallization of amorphous mannitol is retarded using boric acid. *Int J Pharm.* 2003;258(1-2):109–120.

[198]. Yu L, Milton N, Groleau EG, Mishra DS, Vansickle RE. Existence of a mannitol hydrate during freeze-drying and practical implications. *J Pharm Sci.* 1999;88(2):196–198.

[199]. Yu L, Mishra D, Rigsbee D. Determination of the glass properties of D-mannitol using sorbitol as an impurity. *J Pharm Sci.* 1998;87:774–777.

[200]. Zhang X, Inada T, Tezuka A. Ultrasonic-induced nucleation of ice in water containing air bubbles. *Ultrason Sonochem.* 2003;10(2):71–76.

[201]. Zhu S, Ramaswamy HS, Le Bail A. Ice crystal formation in gelatin gel during pressure shift versus conventional freezing. *J Food Eng.* 2005;66(1):69–76.

Chapter 3: Materials and methods

Chapter 3: Materials and Methods

3.1. Materials and equipment

3.1.1. Materials and formulation preparation

Model formulation 1 (MF1) was prepared from trehalose, purchased from Pfanstiehl, Inc. (Pfanstiehl, Inc., Waukegan, IL, USA), and water for injection (WFI) obtained from Fresenius Kabi Deutschland GmbH (Fresenius Kabi Deutschland GmbH, Friedberg, Germany). To prepare MF1, the required amount of trehalose and WFI were weighed using a precision balance (Sartorius AG, Göttingen, Germany) and dissolved using a laboratory magnetic stirrer (IKA-Werke, Staufen, Germany). Trehalose was used as received. In all the experiments of this study, MF1 was filtered using 0.22 µm pore-size filters (PALL Corporation, Port Washington, NY, USA) prior to filling the vials. The filtration setup used in this study is displayed in Figure 14.

Figure 14. Filtration setup used in this study.

Model formulation 2 (MF2) was prepared from sucrose, purchased from VWR (VWR, Darmstadt, Germany), and water for injection (WFI), obtained from Fresenius Kabi Deutschland GmbH (Fresenius Kabi Deutschland GmbH, Friedberg, Germany). To prepare MF2, the same procedure as for MF1 was used. In all the experiments of this study, MF2 was filtered using 0.22 µm pore-size filters (PALL Corporation, Port Washington, NY, USA) prior to filling the vials.

Fresenius Kabi drug formulation (FK1) was prepared from a preparation protocol provided by Fresenius Kabi. For confidentiality reasons, the detail composition of FK1 will not be given here. However, lyophilization relevant properties of FK1 are summarized in Table 3.

In addition to the 3 previously mentioned formulations, WFI was used to perform some sublimation experiments. The formulations and their relevant characteristics used in this study are summarized in Table 3.

Table 3. Summary of formulations used in this study and their critical properties relevant to the lyophilization process. The values of T_g' and T_c presented herein were obtained from this study

Formulation	Excipient	APIs	Solvent	Solid content [wt%]	T_g' [°C]	T_c [°C]
Model Formulation 1 (MF1)	Trehalose	Non	WFI	10	-29.2	-27.5
Model Formulation 2 (MF2)	Sucrose	Non	WFI	20	-32.4	-31.1
Fresenius Kabi drug Formulation (FK1)	Trehalose, emulsifier, and co-emulsifier,	Several APIs (confidential)	WFI and oil	18.5	-35.2	-29.0
Water for Injection	-	Non	WFI	0	-	-

T_g', glass transition temperature of the maximally freeze concentrated solution; T_c, collapse temperature of the frozen solutions; and WFI, water for injection.

3.1.2. Container-closure system

The container-closure system of a lyophilization process consists of elastomeric stoppers, glass vials and aluminum crimps. As discussed previously, lyophilization is a process based on heat and mass transfer. Thus, the type and design of the glass vial and the stoppers have significant influence on the outcome of the process. Considering the glass vial, side and bottom thickness, and bottom flatness or concavity are the major factors that lead to heterogeneity in heat transfer [DeGrazio, 2010]. In the case of the stoppers, design of the venting system plays a critical role for the vapor transport during the drying period of the lyophilization process. In this sense, the total area available for water vapor transport is a critical design factor for freeze-drying stoppers, as differences in the venting area could lead to differences in the resistance to the water vapor transport.

To avoid differences in heat and mass transfer due to the container-closure system, identical glass vials and stoppers were used throughout the experimental studies of this thesis. The glass vials were clear 10-mL tubing vials purchased from SCHOTT AG (SCHOTT AG, Mainz, Germany) and were used as received.

Figure 15. Container-closure system (10-mL vials and igloo single vented stoppers) used in all freeze-drying experiments.

The elastomeric stoppers were ready-to-sterilize Igloo single vented stoppers from West Pharmaceutical Services, Inc. (West Pharmaceutical Services, Inc., Exton, PA,

USA). The stoppers were also used as received. The container-closure system used in this study is displayed in Figure 15.

3.1.3. Freeze-dryer

The freeze-dryer used in this study was a four-shelf model purchased from HOF (HOF Sonderanlagenbau GmbH, Lohra, Germany), which has an internal condenser configuration system, as displayed in Figure 16. The shelves, the chamber walls and the condenser are manufactured from stainless steel, whereas the chamber door is manufactured from acrylic Plexiglas.

Figure 16. HOF laboratory freeze dryer used throughout the studies.

The dimension of each shelf is 300 mm X 300 mm, giving a total usable shelf area of 0.36 m^2, with a shelf spacing fixed at 75 mm. The condenser has a capacity of 6 kg of ice. The refrigeration system of the freeze dryer consists of two small duty compressors, working with R404A refrigerant. The condenser is cooled using a direct expansion system, providing an ultimate condenser temperature of -75 °C, whereas the shelves are cooled indirectly using silicon oil as a thermal fluid. In the case of the shelves, the refrigerant is used to cool the silicon oil in a separate heat exchanger, which then flows through an electrical heater where a precise control of the heating and cooling rates of the shelves is taking place. The silicon oil circulates in a closed loop with the help of a circulation pump.

The temperature range of the shelves is between -55 °C and +50 °C, and the electrical heater provides up to 1.2 °C/min cooling and heating rates. The temperatures of the silicon oil at the inlet to and outlet from each shelf are measured and the overall average temperature is taken to monitor the shelf set point temperature. Each shelf has a capacity for 176 vials (based on 10-mL tubing vials). The vacuum system of the freeze dryer is controlled by a Leybold oil sealed vacuum pump, which provides an ultimate vacuum up to 10 µbar on a dry run basis. The vacuum is controlled using a Pirani vacuum gauge, which measures from 100 to 0.001 mbar.

The HOF freeze dryer can be operated on manual mode or on fully automatic mode using a Siemens controller. The automatic control system has 15 freezing steps, 1 evacuation step and 23 drying steps. The set point vacuum during the drying step is controlled via a nitrogen bleed valve and the vacuum pump. Moreover, the freeze dryer is equipped with a proper alarm system, to ensure that the user is provided with an accurate failure message. The freeze dryer does not have an automatic stoppering system. Thus, the vials were taken out of the chamber and stoppering was performed manually outside the freeze dryer.

Product temperature measurements were performed using 3 type K thermocouples, which are connected to the freeze dryer, and 8 wireless thermologgers (Lives International, Timis, Romania). The wireless thermologgers and the positioning of the temperature probes inside vials are displayed in Figure 17. All data from the freeze dryer were obtained from a printout of a Yokogawa chart recorder and the minimum printing speed of the chart recorder was 1 set of data per hour. For this reason, product temperatures from the wireless thermologgers were used to analyze all experimental results of this study. The wireless thermologgers have a dedicated software that enables to remotely activate the thermologgers before the start of an experiment and to extract the data after the experiment. In this study, product temperatures using the wireless thermologgers were measured every 20 s.

Figure 17. Wireless thermologgers used for product temperature measurements throughout the studies.

3.2. Methods

3.2.1. Formulation characterization using differential scanning calorimetry (DSC)

DSC is a thermal analysis method that measure the difference in heat flow rate (in Watt) between a sample and a reference material as a function of time and temperature, whilst the sample and the references are subjected to a controlled and identical temperature program. During a controlled temperature program, a physical change in the sample could lead a heat to flow into the sample or out of the sample, resulting in enthalpy or heat capacity change of the sample. Heat flows into the sample as a result of physical changes that require energy (endothermic process), such as glass transition, melting and evaporation. Conversely, heat flows out of the sample as a result of physical changes that dissipates energy (exothermic process), such as crystallization, curing, and oxidation.

In the present study, the glass transition temperature of frozen formulations (T_g') and dried products (T_g) were determined using a TA Instruments Q2000 series differential scanning calorimetry with refrigerated cooling system (RCS) (TA Instruments, New Castle, DE, USA), as depicted in Figure 18. All analyses were performed using Universal Analysis software (TA Instruments, New Castle, DE, USA). Glass transition temperatures were reported as the midpoint of the glass transition curve.

For frozen formulations, the following protocol was applied: (i) a sample of 10–15 mg was weighed into aluminum sample pans, which were then hermetically sealed. An empty, hermetically sealed, pan was used as a reference; (ii) the RCS was set on continuous mode and the nitrogen supply was set to 50 mL/min; (iii) the solution samples were first equilibrated at 40 °C for 2 min and then frozen to -60 °C at a rate of 20 °C/min; (iv) the frozen samples were held at -60 °C for 10 min before heating to 40 °C at a rate of 10 °C/min.

Figure 18. Q2000 series differential scanning calorimetry used throughout the studies.

For dried products, the following protocol was followed: (i) a sample of 8–10 mg was weighed into aluminum sample pans, which were then hermetically sealed. An empty, hermetically sealed, pan was used as a reference; (ii) the RCS was set on continuous mode and the nitrogen supply was set to 50 mL/min; (iii) the dried

products were first equilibrated at 40 °C for 2 min and then cooled down to 0 °C at a rate of 5 °C/min; (iv) the samples were held at 0 °C for 2 min before heating to 100 °C at a rate of 10 °C/min.

3.2.2. Formulation characterization using freeze drying microscopy (FDM)

In most cases, the glass transition temperature of the maximally freeze concentrated solution (T_g') is used to define the maximum allowable product temperature during the primary drying period of a lyophilization process. However, it is currently a trend to use the collapse temperature (T_c) of an amorphous formulation. This is because, depending on the formulation, T_c can be several degrees higher than T_g', and thus the primary drying can be performed at a higher product temperature. Referring to Table 3, T_c for all the formulations studied in the present study was higher than T_g'; specifically, T_c for FK1 was 6 °C higher than T_g'. Performing the primary drying at a higher product temperature enhances the sublimation rate (cf. section 2.1.2), and thus significantly improves process efficiency.

Freeze drying microscopy (FDM) is a device used for the determination of the collapse temperature of amorphous formulations. An FDM consists of a cryo-stage, where sample temperature and pressure can be precisely controlled, and a microscope, through which the morphology of the sample during a controlled freeze-drying program may be observed. The cryo-stage consists of a cooling system, an electrical heater, a vacuum pump and a vacuum gauge. All these components of the FDM enable the user to program and to precisely control a temperature in the range of -90 °C to +40 °C, and a pressure up to 10 µbar. In addition, the cryo-stage consists of a quartz cover slip, a glass cover slip and a metal spacer for sample placement. The microscope, on the other hand, is equipped with a high speed digital camera to capture images of the sample during the experiment. A complete freeze-drying cycle can be programmed in a dedicate software, LinkSys 32 (Linkam Scientific Instruments, Surrey, UK), where all operations can be automatically and precisely controlled. The images are stored in the software database and can be used to determine the T_c of a sample from image analysis. The images were analyzed to

determine the collapse temperature (T_c), which was defined as the temperature where a clearly observable structural change on the interface of the dried and frozen formulation was observed.

The FDM used in the present study was a Lyostat 2 (Biopharma Technology Ltd., Winchester, UK) as displayed in Figure 19.

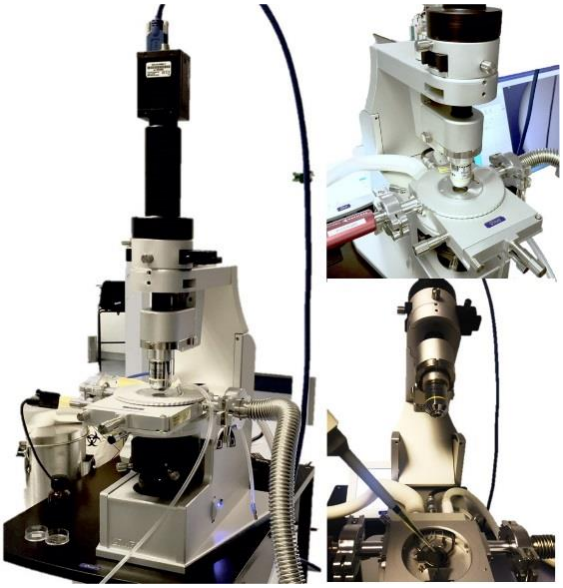

Figure 19. Lyostat freeze drying microscopy used for the determination of collapse temperature (T_c) of samples used in this study. Image courtesy: Biopharma Technology Ltd.

The following program was used to determine the T_c of the formulations studied: (i) a sample of 2 µL was placed on a quartz cover slip and covered using a glass cover slip. To allow sublimation of the sample, a 70 µm thick metal spacer was placed between the quartz and glass cover slips; (ii) the solution samples were frozen to -40°C at a rate of 20°C/min and held for 5 min to allow complete solidification; (iii) after freezing, the vacuum was reduced to approximately 0.1 mbar and maintained at this condition until an approximately 2–3 mm dry layer thickness was achieved; (iv) the samples were further heated at 5 °C/min to a temperature marginally lower than the T_g' obtained from DSC, and then the heating rate was decreased to 0.5 °C/min, aiming to observe a structural change at a higher temperature resolution; (v) the samples were heated until complete structural damage was observed and images of the samples were captured throughout the experiment.

3.2.3. Residual moisture content determination using Karl Fischer titration

The Karl Fischer titrator is commonly used to determine water content of solid or liquid samples, with water content values as low as 1 ppm. The basis for water content determination of the Karl Fischer titrator is based on the reaction of iodine with water in the presence of sulfur dioxide and a reagent. Initially, Karl Fischer used pyridine as a reagent to neutralize the acids formed during the reaction of iodine with water and sulfur dioxide [Fischer, 1935]. However, the Karl Fischer reaction based on pyridine was highly dependent on pH value of the medium, and hence Scholz developed a pyridine-free Karl Fischer reagent with imidazole as a base [Scholz, 1982].

Scholz proposed the following reaction scheme to be used for the Karl Fischer water content analyses [Scholz, 1982]:

1. $ROH + SO_2 + RN \longrightarrow (RNH)\cdot SO_3 R$

2. $(RNH)\cdot SO_3 R + 2RN + I_2 + H_2O \longrightarrow (RNH)SO_4 R + 2(RNH)I$

This results in the following general chemical equation, which is currently in use for water content analysis based on Karl Fischer reaction:

$$\mathbf{ROH + SO_2 + 3RN + I_2 + H_2O \longrightarrow (RNH)\bullet SO_4\, R + 2(RNH)I}$$

According to the above reaction, the I_2 reacts quantitatively with H_2O and serves as a basis for the water content determination. In a coulometric Karl Fischer titration, the necessary iodine is directly and electrochemically generated at a generator electrode according to the following half-reaction:

$$2I^- \longrightarrow I_2 + 2e^-$$

The amount of water titrated by coulometric technique is determined from the amount of electrical current given in Coulomb, designated as C, used to generate iodine and from the stoichiometric reaction of iodine and water. For an electrochemically optimized Karl Fischer cell, the current conversion efficiency for

iodine production is assumed to be 100%. Since current and time can be accurately measured, no standardization of the coulometric Karl Fischer reagents is necessary. For this reason, coulometry is designated as absolute method. Coulometric Kar Fischer analysis is suitable for samples where residual water content is in the range of 1 ppm to 5 wt%.

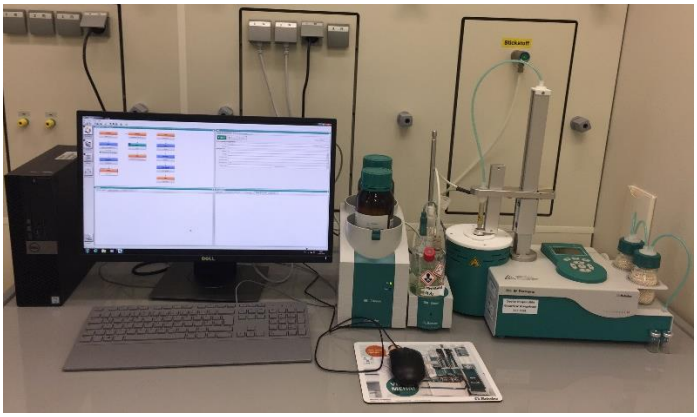

Figure 20. Karl Fischer coulometric titrator with thermoprep oven used throughout the studies.

The Karl Fischer titrator used in the present study was a coulometric titrator with thermoprep oven (Metrohm, Herisau, Switzerland), as displayed in Figure 20. In this setup, a sample is heated in the thermoprep oven, releasing its moisture. The moisture is then conveyed to the measuring cell with the aid of a gas flow, where it is reacted with iodine. The Karl Fischer titrator is controlled using a dedicated software, Tiamo™ 2.5 (Metrohm, Herisau, Switzerland). The following water content determination program was used throughout the study: (i) measure a blank vial to consider water content from the vial and the serum stopper; (ii) measure a standard sample to check the functionality of the device. In the present study, a standard sample with 1 wt% water content was used; (iii) a sample of 70–100 mg was weighed in a vial and immediately sealed using the serum stopper; (iv) the sample vial was inserted into the thermoprep oven, heated to 100 °C; (v) continuous measurement for a minimum extraction time of 10 min. However, the stop criteria for the measurement was set based on a drift value of 5 µg/min, and hence the actual measurement duration could last longer than 10 min. A drift indicates the quantity of

water that enters the measurement cell over a defined time and with a drift value of 5 µg/min, it could be assumed that all the residual water in the sample was removed.

3.2.4. Other experimental details

Other specific characterization techniques and experimental protocols are provided in each section of the Results & Discussion chapter.

3.3. References

[1]. DeGrazio FL. Closure and container considerations in lyophilization. In Rey L, May, JC., eds. *Freeze-Drying/Lyophilization of Pharmaceutical and Biological Products, 3rd Ed*. London: Informa Healthcare; 2010:396–412.

[2]. Fischer K. Neues Verfahren zur massanalytischen Bestimmung des Wassergehaltes von Flüssigkeiten und festen Körpern. *Angew Chem*. 1935;48:394–396.

[3]. Scholz E. Karl-Fischer Reagentien ohne Pyridin. zweikomponenten Reagentien mit Imidazol, Fresenius Z. *Anal Chem*. 1982;312:460–464.

Chapter 4: Results and Discussion

Chapter 4: Results and Discussion

4.1. Heat and mass transfer analyses during primary drying

4.1.1. Background

Sublimation of a frozen sample is the core process principle of the drying step of a freeze-drying process. Sublimation is an exothermic process, and hence it requires a sustained source of energy to maintain the process. During the drying step, energy is supplied, in a form of heat, to the system through the product shelves, which could be heated to and maintained at any desired temperature. Thus, a better understanding of the combined mass and heat transfer during the drying step allows a greater efficiency during the design, optimization, and scale-up of a freeze-drying process. Further, it minimizes problems that could be encountered at industrial scale.

The aim of this section is to evaluate the effect of different input processing conditions (i.e., shelf temperature (T_s) and chamber pressure (P_c)) on different output parameters, such as product temperature (T_P), sublimation rate ($\dot{m}$), overall vial heat transfer coefficient (K_v), and resistance to mass transfer of the dried product (R_p). Furthermore, the effect of vial position on the previously mentioned output parameters is discussed. Such knowledge enables to establish a fundamental understanding of the interactions between input and output parameters during the freeze-drying process.

4.1.2. Experimental details

Sublimation experiments using model formulation 1 (MF1) and model formulation 2 (MF2) were performed. Table 3 shows some details of the model formulations. The product temperature (T_P) and the sublimation rate ($\dot{m}$) were directly determined from the sublimation experiments. Whereas, the resistance to mass transfer of the dried

product (R_p) and the overall vial heat transfer coefficient (K_v) were calculated from the mass and heat transfer equations as given in Equations 24 and 25, respectively.

$$R_p = \frac{P_i(T_p) - P_c}{\dot{m}} \quad (24)$$

where, R_p[mbar·s/g] is the resistance to mass transfer of the dried product; P_i[mbar] is the vapor pressure of ice calculated from the product temperature (T_p); P_c[mbar] is the camber pressure; and $\dot{m}$[g/s] is the sublimation rate obtained gravimetrically from the sublimation experiments.

$$K_v = \Delta H_s \frac{\dot{m}}{A_v(T_s - T_p)} \quad (25)$$

where, K_v[cal/s·cm^2·K] is the overall vial heat transfer coefficient; A_v[cm^2] is the outer surface area of the vials used in this study, T_s[K] is the shelf temperature; T_p[K] is the product temperature; and ΔH_s[cal/g] is the heat of sublimation of ice. There are some differences in the literature reported ΔH_s values. 660 cal/g, [Pikal et al., 1985; Kuu et al., 2009], 667 cal/g [Tang et al., 2005], 676 cal/g [Rambhatla et al., 2006], 680 cal/g [Pikal et al., 2005; Zhai et al., 2005]. Further, Feistel and Wagner determined a value for ΔH_s of approximately 679 cal/g for a product temperature in the range -35 °C to -10 °C, which is relevant during the primary drying phase of the freeze-drying process [Feistel & Wagner, 2007]. Considering all the above reported ΔH_s values, an average value of 670 cal/g was used throughout this study.

The sublimation rate was determined gravimetrically. For this purpose, 50 selected sample vials were weighed before and after the freeze-drying experiments. The sample vials were systematically placed to represent different vial groups, which could have different sublimation rates and product temperatures, within the vial array. Figure 21 displays the placement of the sample vials and thermocoupled vials for all the experiments performed in this study. For example, in Figure 21, vials numbered 1–8 represent a vial group referred to as “front edge”, vials 9–17 represent “side edge outer”, vials 18–26 represent “side edge inner”, vials 27–42 represent “center”, and vials 43–50 represent “rear edge”. The sublimation rates obtained from the numbered vials of the same group were used to calculate the average

sublimation rates of their corresponding group. A laboratory analytical balance (Sartorius AG, Göttingen, Germany) was used to weigh the sample vials. The sublimation process was terminated by backfilling the product chamber using dry nitrogen and the vials were heated to 20 °C before the product chamber door was opened. This step was included to prevent condensation from the surrounding moisture from forming on the cold stoppers and penetrating into the extremely hygroscopic dried product. Once the product chamber door was opened, the sample vials were immediately fully stoppered and re-weighed.

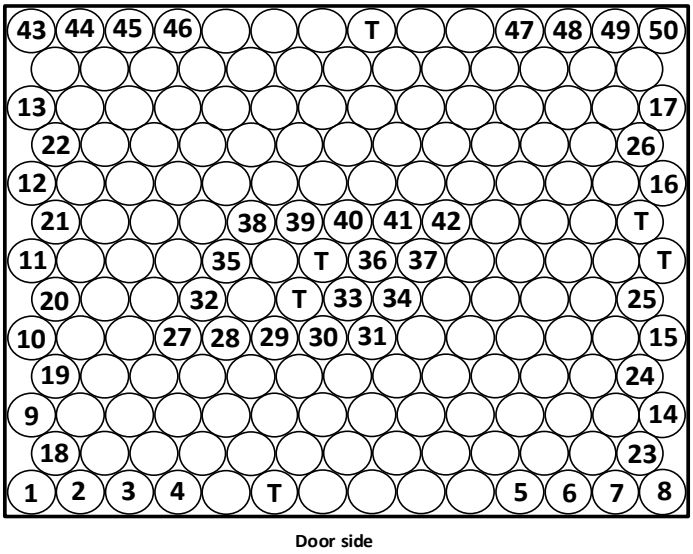

Figure 21. Vial placement for the sublimation experiments of this study. “Numbered vials” represent vials weighed before and after the freeze-drying experiment. “T-signed vials” represent vials with thermocouples for product temperature measurement of the different groups of vial arrays.

It is well known that dried product resistance and product temperature increase when product dried layer thickness increases [Fissore et al., 2011; Kodama et al., 2014; Scutellà, 2018]. Therefore, to include the maximum effect of the dried product resistance during the determination of the sublimation rate, the sublimation experiments were stopped once the frozen solution was almost completely sublimed. This was performed by visually observing the dried layer of the front edge vials. Thus, all the sublimation experiments were terminated once the dried layer of the front edge vials reach close to the vial bottom. The exact drying time for the calculation of

the sublimation rate was obtained from the product temperature profile of the wireless thermologgers. Primary drying time, by definition, starts when the shelf temperature attains the desired shelf set point temperature for primary drying. Thus, regardless of the product temperature, the starting time for the calculation of the sublimation rates was defined as the time at which the shelf temperature attained the desired set point temperature. It was experimentally determined that, at low chamber pressure and low shelf temperature, up to 4 hours were required to achieve a pseudo steady-state condition in product temperature. Whereas, up to 2 hours were required to attain a pseudo steady-state condition in product temperature at high chamber pressure and high shelf temperature conditions. Although the time required to achieve a pseudo steady state in product temperature was highly dependent on the processing conditions and formulation solid content, the values obtained in this study were significantly longer than the values reported in the literature [Pikal, 1985]. Therefore, the definition of the starting time used herein considers the real effect of different processing conditions and formulations on the sublimation rate, before the product temperature attained a pseudo steady-state condition.

4.1.3. Results and discussion

4.1.3.1. Effect of vial position on primary drying output parameters

The variation of the primary drying output parameters, such as product temperature (T_p), overall vial heat transfer coefficient (K_v), and sublimation rate ($\dot{m}$), with respect to vial position poses significant challenge during freeze-drying process design, optimization, scale-up, and transfer. Thus, to design a robust freeze-drying process that encompasses the entire vial position, a proper understanding of such variation is of paramount importance.

Figure 22 displays the effect of vial position on T_p, K_v, and $\dot{m}$, at constant and low P_c (P_c = 0.05 mbar) and different T_s values, for MF1. Compared to the rest of the vial groups, the center vials have the lowest T_p, K_v, and $\dot{m}$ values; whereas the front edge vials have the highest values (Figure 22a-d). This is attributed to three

important factors: (1) because the center vials are completely surrounded by other neighboring vials, the available surface area for heat transfer is smaller than the surface area of the edge vials. This limits the heat input to the center vials, reducing K_v although the processing conditions are the same for all vial groups; (2) the packing density (vials per shelf surface area) of the center vials is higher than those of the edge vials, and thus the center vials have higher heat demand per shelf surface area. This increases the heat consumption from the central part of the shelf and, in turn, reduces the shelf surface temperature.

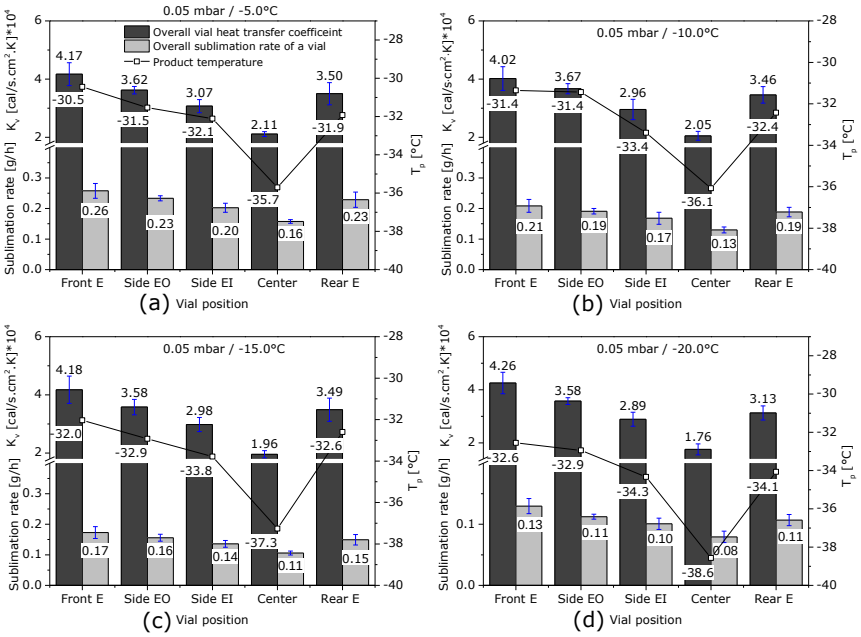

Figure 22. Effect of vial position on product temperature (T_p), overall vial heat transfer coefficient (K_v) and sublimation rate ($\dot{m}$) at low chamber pressure (P_c) (P_c = 0.05 mbar) and different shelf temperatures (T_s) for 10% trehalose solution (MF1).

Therefore, compared to the edge vials, the center vials run at lower shelf surface temperature, and thus at lower T_p; (3) the edge vials receive additional heat input from an atypical heat transfer via radiation from the walls and doors of the freeze dryer [Pikal et al., 2016]. This increases K_v, and hence T_p of the edge vials. Particularly, as the front edge vials are exposed to the acrylic freeze dryer door, which have higher temperature and emissivity compared to the side walls of the dryer, they receive higher heat input from the atypical radiation. Supporting this, the

experimental results (Figure 22a–d) demonstrated highest K_v and T_p values for front edge vials.

At constant P_c, an improvement in heat transfer uniformity was observed with an increase in T_s. Thus, at T_s = -5.0 °C, the percent differences[1] in T_p and K_v between the front edge and center vials were 15.7% and 65.6%, respectively (Figure 22a); whereas, at T_s = -20.0 °C, the percent differences in T_p and K_v between the front edge and center vials were 16.9% and 83.1%, respectively (Figure 22d). Despite the improvement in heat transfer uniformity at higher T_s, the percent difference in $\dot{m}$ between the front edge and center vials for the two shelf temperatures was identical (47.6%). Although increasing T_s did not improve the variation in sublimation rate among vials resting at different locations, it did significantly improve the values of the sublimation rates.

As with low P_c (Figure 22), intermediate P_c (P_c = 0.15 mbar) and different T_s showed similar trend (Figure 23) with regard to the effect of vial position on T_p, K_v, and $\dot{m}$. Thus, for all the T_s studied, the lowest and the highest primary drying output parameters correspond to the center and front edge vials, respectively.

Considering similar T_s and different P_c, for example Figure 22d and Figure 23b, the influence of vial position on T_p and K_v at low P_c was stronger than at high P_c. At P_c = 0.05 mbar, the percent difference in T_p between the front edge and center vials was16.9% (Figure 22d); whereas, at P_c = 0.15 mbar, the percent difference was 5.3% (Figure 23b). Also, the percent difference in K_v between the front edge and center vials, at P_c = 0.05 mbar, was 83.1% (Figure 22d); whereas, at P_c = 0.15 mbar, the percent difference was 58.3% (Figure 23b).

[1] The percent difference was calculated as: $\frac{[|value\ 1 - value\ 2|]}{\left[\frac{(value\ 1 + value\ 2)}{2}\right]} * 100$

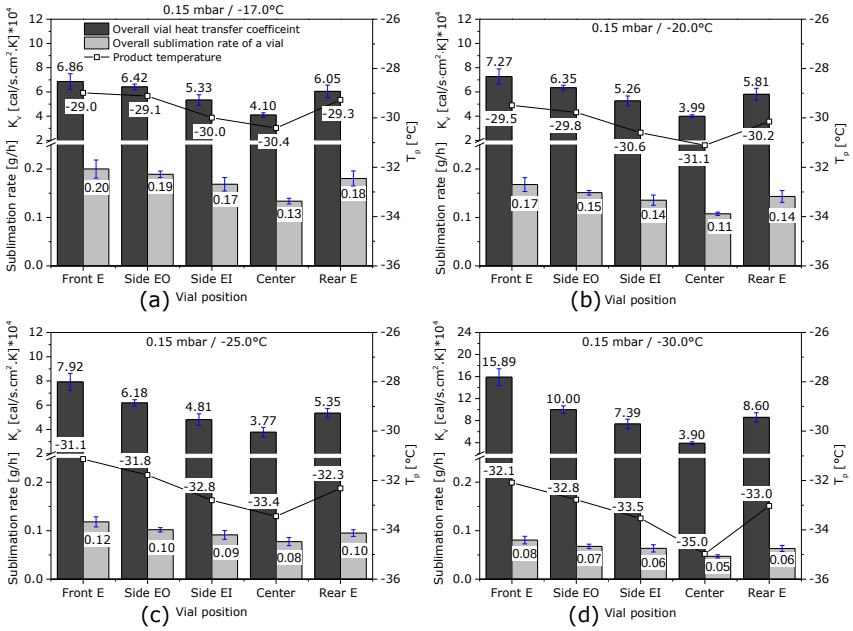

Figure 23. Effect of vial position on product temperature (T_p), overall vial heat transfer coefficient (K_v) and sublimation rate ($\dot{m}$) at intermediate chamber pressure (P_c) (P_c = 0.15 mbar) and different shelf temperatures (T_s) for 10% trehalose solution (MF1).

This clearly demonstrates that, at higher P_c, the variation in T_p and K_v with respect to vial position is minimized. These observations, which are in agreement with literature data [Pikal et al., 1984], are a direct result of the improved heat transfer due to conduction through the gas at high P_c. However, although high P_c improves the heat transfer uniformity and, consequently, improves the variation in T_p and K_v with respect to vial position, the corresponding improvement in sublimation rate ($\dot{m}$) variation was very small. Thus, the percent difference in $\dot{m}$ between the front edge and center vials at P_c = 0.05 mbar was 47.6% (Figure 22d), whereas, at P_c = 0.15 mbar, the percent difference was 42.9% (Figure 23b). This is because, while T_p and K_v are a direct result of the heat transfer part, $\dot{m}$ depends on both the heat transfer (through T_p) and the mass transfer (through P_c and R_p) (see Equation 24). Thus, although the T_p of the center vials at P_c = 0.05 mbar was very low (-38.6 °C) compared to the center vials T_p at P_c = 0.15 mbar (-31.1 °C), the driving force for sublimation (i.e., $P_i(T_p) - P_c$) at these two conditions was comparable. This is because, the low P_c compensates the decrease in P_i due to low T_p.

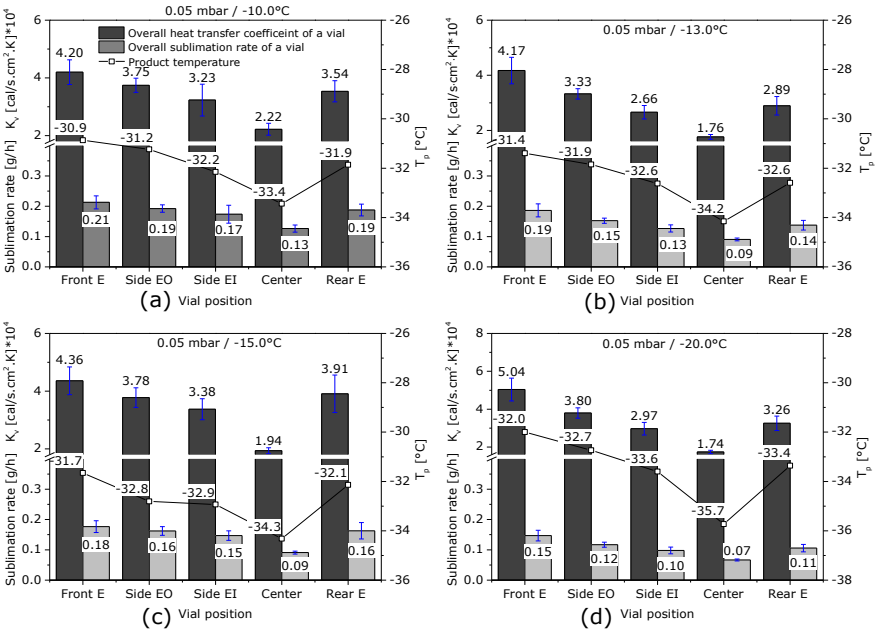

Figure 24. Effect of vial position on product temperature (T_p), overall vial heat transfer coefficient (K_v) and sublimation rate ($\dot{m}$) at low chamber pressure (P_c) (P_c = 0.05 mbar) and different shelf temperatures (T_s) for 20% (w/w) sucrose solution (MF2).

Figure 24 illustrates the effect of vial position on the primary drying output parameters at P_c = 0.05 mbar for MF2, showing similar trend to that observed in Figure 22 for MF1. While MF1 has 10% (w/w) solid content, MF2 has 20% (w/w) solid content, illustrating that MF2 imposes greater dried product resistance to water vapor flow during the primary drying phase, provided that there is no microcollapse in both formulations. Comparison of Figure 22d and Figure 24d illustrates that, at the same processing conditions (i.e., same T_s and P_c), a product with a higher dried product resistance yields smaller T_p difference between the front edge and center vials than a product with lower dried product resistance. For example, at P_c = 0.05 mbar and T_s = -20 °C, the percent differences in T_p and K_v between the front edge and center vials for MF1 were 16.9% and 83.1%, respectively (Figure 22d). Whereas, for MF2, the percent differences in T_p and K_v, at the same P_c and T_s, were 10.9% and 48.7%, respectively (Figure 24d). This demonstrates that, in a similar way to high P_c, high solid content improves the heat transfer uniformity within a vial array. However, the improvement in heat transfer uniformity in products with high solid

content did not guarantee an improvement in $\dot{m}$. Thus, the percent differences in $\dot{m}$, at P_c = 0.05 mbar and T_s = -20 °C, between the front edge and center vials for MF1 was 47.6%, whereas for MF2, it was 72.7% (cf. Figure 22d and Figure 24d).

In conclusion, it is extremely important to analyze the effect of vial position not only from the heat transfer perspective (i.e., T_p and K_v), but also from the mass transfer perspective (i.e., $\dot{m}$). In this sense, although certain processing conditions could yield significant improvement in heat transfer uniformity across a vial array, the corresponding center vials $\dot{m}$ (i.e., the minimum $\dot{m}$) could be smaller than at other processing conditions, where remarkable variation in T_p and K_v exists. Because $\dot{m}$ is an extremely important factor during freeze-drying process design and optimization, selection of an optimum processing condition, with regard to vial position, should be made considering a compromise between an improved heat transfer uniformity and the highest possible $\dot{m}$.

4.1.3.2. Effect of shelf temperature on primary drying output parameters

This section illustrates the relationship between T_s and the primary drying output parameters at constant chamber pressure. Figure 25 displays results of MF1 at a P_c = 0.05 mbar and P_c = 0.15 mbar for both front edge vials (FE) and center vials (C).

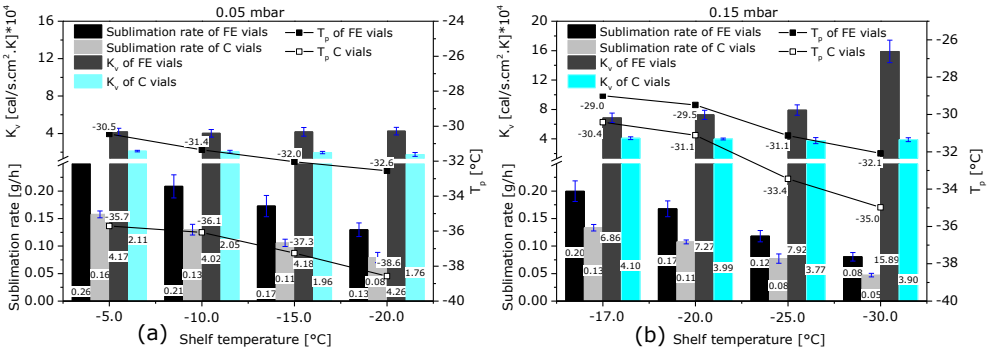

Figure 25. Dependency of primary drying output parameters on shelf temperature (T_s), at constant chamber pressure (P_c), for MF1. (a) at a P_c = 0.05 mbar and (b) at a P_c = 0.15 mbar. FE, front edge vials; C, center vials; T_p, product temperature; and K_v, overall vial heat transfer coefficient.

As illustrated in Figure 25, at a given P_c, a direct relationship between T_s and T_p for both vial groups was observed. This is consistent with the fact that reducing T_s, at a constant P_c, reduces the heat input to the system. Thus, the energy equilibrium state of the system is achieved at lower T_p. Further, at a given P_c, there is a direct relationship between T_p and $\dot{m}$. Thus, reducing T_s, at a constant P_c, reduces both T_p and $\dot{m}$.

Interestingly, the influence of T_s on T_p was found to be P_c dependent. Here, it is meaningful to compare the T_p of center vials, as the heat source of this vial group is predominantly the shelf temperature. Thus, while decreasing T_s by 15 °C, at P_c = 0.05 mbar, decreased T_p and $\dot{m}$ of center vials by 8.1% and 50%, respectively (Figure 25a), a decrease in T_s by 13 °C, at P_c = 0.15 mbar, decreased T_p and $\dot{m}$ of center vials by 15.1% and 61.5%, respectively (Figure 25b). This finding is relevant to the robustness of a freeze-drying process, and thus a freeze-drying process at low P_c is more robust to variations in T_s compared to a freeze-drying process at high P_c.

The relationship between T_s and K_v was rather complex. The calculation of K_v assumes that the driving force for the heat flow to the system during the primary drying is only the temperature difference between the shelf and the product (Equation 25). Thus, it only assumes that the source of energy for heat transfer is the T_s and neglects any additional energy source for heat transfer. Therefore, the validity of the assumption in Equation 25 is highly dependent on the relative contribution of T_s to K_v. At low T_s, the contribution of the direct conduction heat transfer mechanism (a direct result of the T_s) to K_v becomes weaker. Thus, the energy equilibrium state of the system is mainly sustained from the energy input via the conduction through the gas and radiation. Therefore, the interpretation of K_v values may require careful consideration when values at different processing conditions are compared. For example, K_v, T_p and $\dot{m}$ for front edge vials, at P_c = 0.15 mbar and at T_s = -30 °C, were 15.89*10^{-4} cal·s^{-1}·cm^{-2}·K, -32.1 °C and 0.05 g·h^{-1}, respectively. Whereas, at P_c = 0.15 mbar and at T_s = -20 °C, K_v, T_p and $\dot{m}$ for front edge vials were 7.27*10^{-4} cal·s^{-1}·cm^{-2}·K, -29.5 °C and 0.17 g·h^{-1}, respectively. Thus,

although the K_v values showed that the energy input to the front edge vials, at the former processing condition, was much higher than that of at the latter, the corresponding T_p and $\dot{m}$ showed the opposite evolution (Figure 25b).

On the other hand, K_v of the center vials, at a given P_c and different T_s, remained fairly constant, demonstrating that the source of the input energy to the center vials is predominantly from the product shelves.

4.1.3.3. Effect of chamber pressure on primary drying output parameters

As discussed previously, the driving force for the sublimation of ice is the pressure difference between the vapor pressure of ice (P_i) and the chamber pressure (P_c). Thus, variation in P_c has a direct influence on the sublimation of ice from the vials. As displayed in Figure 26, increasing P_c, at constant T_s, yields an increase in K_v, T_p and $\dot{m}$.

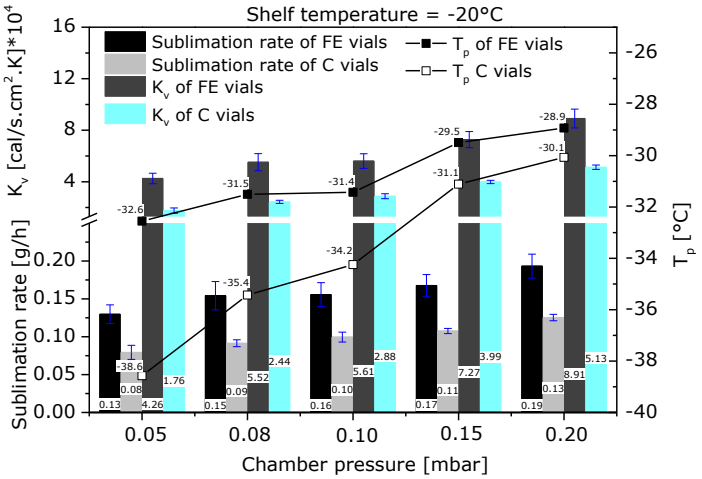

Figure 26. Dependency of primary drying output parameters on chamber pressure (P_c), at constant shelf temperature (T_s) (T_s = -20 °C), for MF1. FE, front edge vials; C, center vials; T_p, product temperature; and K_v, overall vial heat transfer coefficient.

Furthermore, a significant decrease in T_p difference between the front edge and center vials was observed as P_c increases. At low P_c, the driving force for the sublimation of ice (i.e., $P_i(T_p) - P_c$), even at low T_p, is large. Consequently, the energy consumption from the system becomes significant, yielding a shelf surface

temperature (T_{ss}) much lower than the corresponding shelf temperature (T_s). This mainly influences the center vials, where the primary energy source is T_{ss}. Conversely, the front edge vials could receive additional energy from atypical radiation, which could be significant if T_{ss} low. This leads to a large difference in T_p between the front edge and center vials at low P_c.

At high P_c, on the other hand, sublimation of ice does not start unless T_p is too high to yield a P_i greater than P_c. Thus, due the absence of sublimation at low T_p, the energy consumption from the system is very low. Consequently, most of the energy input at the start of the primary drying is utilized to increase T_p. In this case, T_p increases until the energy consumption from ice sublimation becomes significant to counter balance the energy input. Therefore, the energy consumption from the system is only significant at high T_p. To produce such a high T_p of the center vials, the T_{ss} must also be high (only slightly lower than the corresponding T_s). At such high T_{ss}, the energy input from the direct conduction becomes more significant compared to the energy input from the atypical radiation. Furthermore, the relatively warm water vapor (attributed to the high T_p) significantly increases the energy input from the conduction through the gas. Consequently, the T_p difference between the front edge and center vials, at high P_c, becomes small.

Figure 27 demonstrates the influence of P_c for a formulation with high solid content (MF2), which shows a similar trend to a formulation with low solid content (MF1, Figure 26). However, at a given P_c, the T_p difference between the front edge and center vials was smaller for MF2 than for MF1. This is attributed to the high solid content of MF2, which yields high dried product resistance during the primary drying phase. In this sense, the high dried product resistance of MF2 reduces the sublimation of ice, and thus the energy consumption from the system. Consequently, at similar processing conditions (i.e., T_s and P_c) to MF1, the energy equilibrium state of MF2 is achieved at higher T_p. Therefore, at similar processing conditions, the shelf surface temperature (T_{ss}) for MF2 is higher than for MF1. This increases the heat transfer contribution from the direct conduction and conduction through the gas, which, in turn, improves the heat transfer uniformity of MF2.

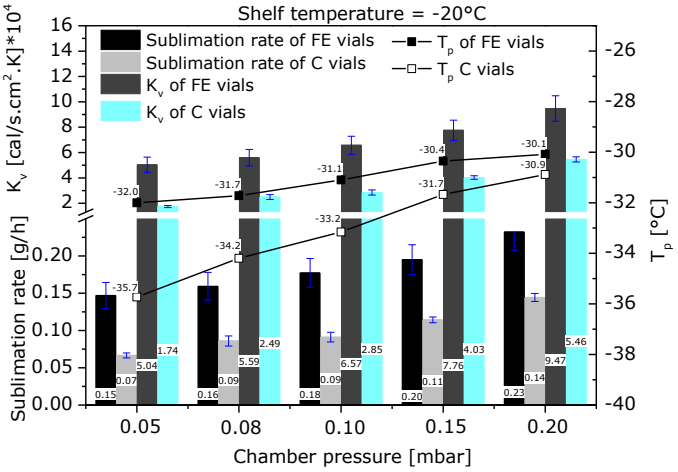

Figure 27. Dependency of primary drying output parameters on chamber pressure (P_c), at constant shelf temperature (T_s) (T_s = -20 °C), for MF2. FE, front edge vials; C, center vials; T_p, product temperature; and K_v, overall vial heat transfer coefficient.

4.1.3.4. Effect of shelf temperature and chamber pressure on primary drying output parameters at similar product temperature

As can be deduced from the previous discussions, different combinations of processing conditions may yield similar T_p; however, the corresponding $\dot{m}$ and K_v could be significantly different. Since the final goal of a freeze-drying process optimization is to identify the processing conditions that yield the desired T_p and the highest $\dot{m}$, identifying such processing conditions is very critical during freeze-drying process design and optimization. In this section, the effect of different processing conditions that yield similar T_p of the front edge vials (vials with the highest T_p in the array) on $\dot{m}$ and K_v will be discussed.

Similar T_p during the primary drying step could be obtained by proper manipulation of the processing conditions (i.e., T_s and P_c). Figures 28 and 29 illustrate that low P_c–high T_s and high P_c–low T_s combinations could yield similar T_p, although the exact value are formulation and container-closure system dependent.

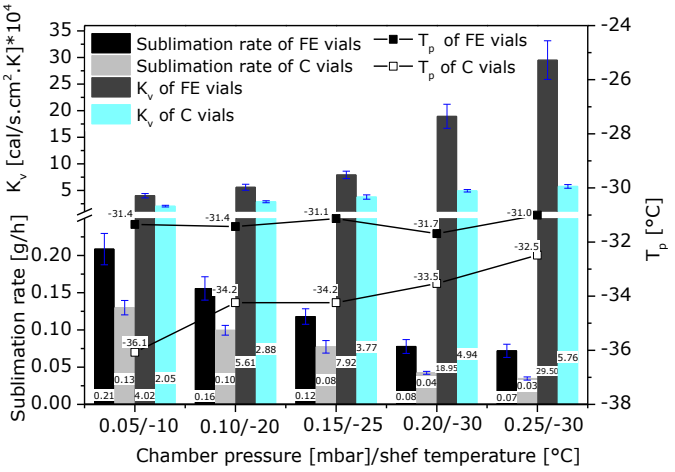

Figure 28. Dependency of primary drying output parameters on chamber pressure (P_c) and shelf temperature (T_s), at similar product temperature (T_p) of front edge vials, for MF1. FE, front edge vials; C, center vials; T_p, product temperature; and K_v, overall vial heat transfer coefficient.

As illustrated in Figure 28, there was a significant decrease in $\dot{m}$ of the front edge vials, as one goes from low P_c–high T_s combination to high P_c–low T_s combination. This demonstrates that, although similar T_p at all the P_c–T_s combinations were achieved, the high P_c–low T_s combination yielded lower $\dot{m}$. This is a direct result of the driving force for sublimation, $P_i(T_p) - P_c$. At similar T_p, P_i is also similar, and thus the driving force for sublimation decreases as P_c increases, which, in turn, decreases $\dot{m}$. On the other hand, T_p of the center vials increased from low P_c–high T_s combination to high P_c–low T_s combination. This is because, at an increased P_c, sublimation of ice does not start unless T_p is high enough, so that the corresponding P_i becomes greater than P_c. As illustrated in Figure 28, however, the $\dot{m}$ of the center vials were much lower at the high P_c–low T_s combinations than those of at the low P_c–high T_s combinations although the former produced higher T_p. This is because, the increase in P_i, due to increase in T_p, does not balance the increase in P_c, and thus $P_i(T_p) - P_c$ becomes small. A further increase in T_s, at a constant P_c, could increase T_p, which, in turn, increases P_i and $P_i(T_p) - P_c$. However, this would lead for T_p of the front edge vials to increase above the target T_p. This implies that, at a given T_p, high $\dot{m}$ are obtained at low P_c–high T_s combinations.

The increase in K_v when moving from low P_c–high T_s combination to high P_c–low T_s combination is related to the calculation of the K_v. Again, referring to Equation 25, the form of the equation assumes that the sublimation rate, $\dot{m}$, is generated because of an energy input derived from the temperature difference between the shelf and the product (i.e., $T_s - T_p$). At low P_c–high T_s combinations, the $T_s - T_p$ is very high (for example, at 0.05 mbar/-10 °C, $T_s - T_p$ for front edge vials is = 21.4 °C, Figure 28). Thus, $T_s - T_p$ could be the main driving force for the energy input to generate the corresponding sublimation rate. This is also supported by the insignificant sensitivity of K_v to changes in $T_s - T_p$. For example, a 3 °C decrease in $T_s - T_p$ at 0.05 mbar/-10 °C of the front edge vials (i.e., from 21.4 °C to 18.4 °C) changes K_v by only 14% (as calculated using Equation 25 and assuming the same $\dot{m}$). Conversely, at high P_c–low T_s combinations, $T_s - T_p$ is very low (for example, at 0.25 mbar/-30 °C, $T_s - T_p$ for front edge vials is = 1.0 °C, Figure 28).

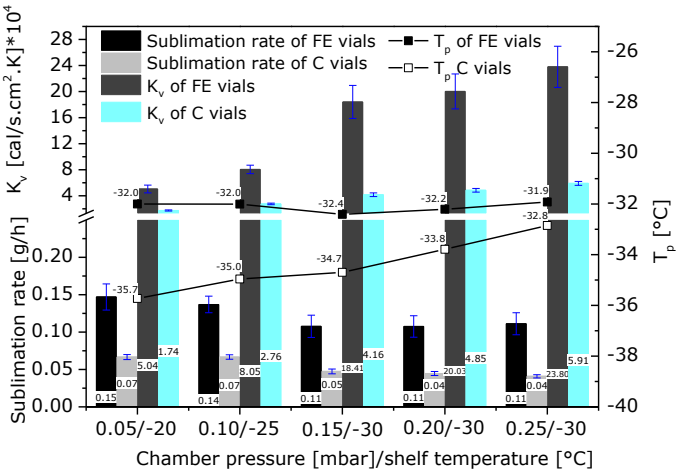

Figure 29. Dependency of primary drying output parameters on chamber pressure (P_c) and shelf temperature (T_s), at similar product temperature (T_p) of front edge vials, for MF2. FE, front edge vials; C, center vials; T_p, product temperature; and K_v, overall vial heat transfer coefficient.

Thus, the contribution of $T_s - T_p$ to the corresponding sublimation rate is very little. Hence, other source of energy input, such as radiation and conduction through the gas could also be responsible to generate the sublimation rate. Therefore, at high P_c–low T_s combinations, the validity of Equation 25 to calculate K_v is very weak. This

is supported by the significant sensitivity of K_v to changes in $T_s - T_p$. For example, a 3 °C increase in $T_s - T_p$ at 0.15 mbar/-30 °C of the front edge vials (i.e., from 1.0 °C to 4.0 °C) changes K_v by 75% (as calculated using Equation 25 and assuming the same $\dot{m}$).

As displayed in Figure 29, the dependency of $\dot{m}$ and K_v on T_s and P_c for MF2 was similar to the dependency observed for MF1.

In conclusion, at a given T_p of the front edge vials, low P_c–high T_s combinations yield the highest $\dot{m}$ for the front edge vials. However, $\dot{m}$ of the center vials (vials with the lowest $\dot{m}$ in the vial array) is the limiting factor during the freeze-drying process design and optimization. Therefore, selection of the optimum processing condition for the freeze-drying process should yield the maximum allowable product temperature of the front edge vials and the maximum possible sublimation rate of the center vials.

4.1.3.5. Effect of shelf temperature and chamber pressure on resistance to mass transfer of the dried product (R_p)

The resistance to mass transfer of the dried product (R_p) is dependent on several parameters, namely: (1) the freezing step, which is related to the formation of different ice crystal sizes and morphology; (2) the formulation, which is related to the total solid content and total fill volume; (3) the container system, which is related to the available inner cross-sectional area; and (4) the processing conditions during primary drying, which is related to the possible formation of microcollapse. During the freezing step, the random nature of the ice nucleation event leads to the formation of different ice crystal sizes and morphologies, which, in turn, could lead to differences in R_p among vials of the same batch. Thus, formation of small and many ice crystals during the freezing step leads to high R_p, whereas formation of large and few ice crystals leads to small R_p (cf. section 2.1.1.2.2). The total solid content is another important factor that could influence R_p. Thus, a formulation with high solid content could impose high R_p compared to a formulation with low solid content. The influence of fill volume on R_p is related to the total length of the dried

product. In this sense, R_p increases as the length of the dried product increases. The available inner cross-sectional area of a container system is also another factor that could influence R_p. In this regard, assuming similar vapor flow rates, large inner cross-sectional area imposes low overall R_p as the vapor flow rate is distributed across the cross-sectional area. The primary drying processing conditions are responsible to cause variations in R_p, mainly on vials rested at the different locations of a vial array. In this sense, if the primary drying processing condition yields a T_p close to the T_c of a given formulation, vials located at the edge of the vial array could form microcollapse, as they have higher T_p compared to vials located at the center. Formation of microcollapse could significantly reduce the R_p of the product.

Assuming the same formulation (i.e., solid content and fill volume) and the same container system (i.e., inner cross-sectional area), the uncontrollable freezing event and the primary drying processing conditions could cause variations in R_p.

Figure 30 displays R_p values for MF1 at different processing conditions.

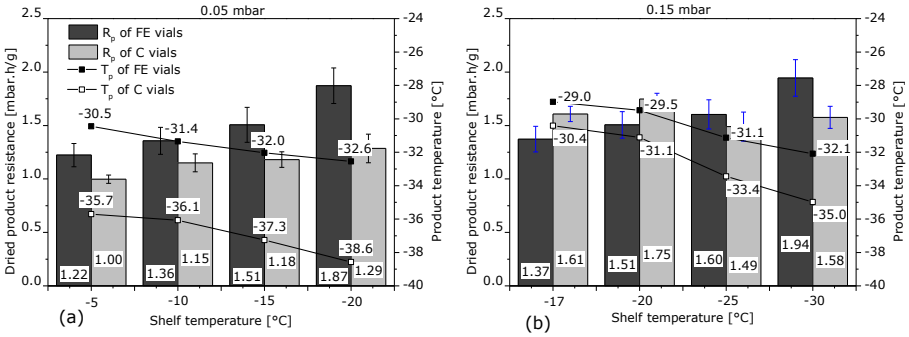

Figure 30. Influence of primary drying processing conditions and vial positions on resistance to mass transfer of the dried product (R_p) for MF1. (a) at a P_c = 0.05 mbar and (b) at a P_c = 0.15 mbar. FE, front edge vials; C, center vials; T_p, product temperature; and P_c, chamber pressure.

Although the formulation and container system in all these experiments were identical, there was observable differences in R_p with regard to different processing conditions and vial positions. As displayed in Figure 30a, the R_p of the front edge vials was larger than that of the center vials in all the processing conditions studied

herein. It is well known that R_p increases as the dried layer thickness increases. Thus, because the dried layer thickness of the front edge vials was larger than that of the center vials when the sublimation experiments were stopped (attributed to the faster sublimation rate of the front edge vials), their corresponding R_p was larger than the R_p of center vials. Also, noticeable differences in R_p among the front edge vials at the different processing conditions (Figure 30a) were observed. This could be due to the possible formation of microcollapse at high T_p range, which could further reduce R_p.

Conversely, Figure 30b displays a mixed trend in R_p with regard to vial position. At T_s of -17 °C and -20 °C, the front edge vials had smaller R_p than that of the center vials, whereas, at T_s of -25 °C and -30 °C, R_p of the front edge vials was larger than R_p of the center vials. At the former processing conditions, the T_p of the front edge vials was very close to the collapse temperature of MF1 (-27.5 °C), and hence there is a high probability of microcollapse formation. The formation of microcollapse could be responsible for the smaller R_p values of the front edge vials although they had a large dried layer thickness compared to the dried layer thickness of the center vials. Furthermore, the larger R_p of the front edge vials at the latter processing conditions showed the absence of microcollapse, which is in agreement with their T_p being much lower than the collapse temperature of MF1 (-27.5 °C).

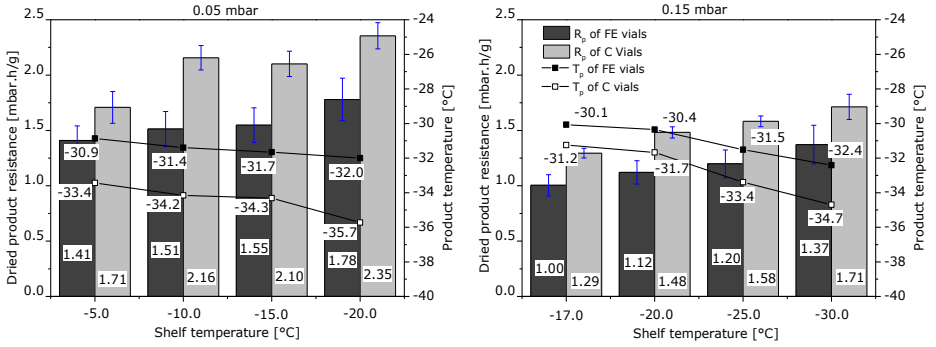

Figure 31. Influence of primary drying processing conditions and vial positions on resistance to mass transfer of the dried product (R_p) for MF2. (a) at a P_c = 0.05 mbar and (b) at a P_c = 0.15 mbar. FE, front edge vials; C, center vials; T_p, product temperature; and P_c, chamber pressure.

Unlike MF1 (Figure 30), MF2 (Figure 31) showed a trend where R_p values of the front edge vials were smaller than that of the center vials at all the processing conditions studied herein. This clearly demonstrated the presence of microcollapse in the front edge vials at all the processing conditions. This is also in agreement with the T_p of the front edge vials being very close to or even slightly higher than the collapse temperature of MF2 (-31.1 °C).

In general, assuming other factors, such as formulation solid content, fill volume, and container system are fixed, the R_p of a given formulation could be significantly influenced by the processing conditions. That is, unless the T_p of all the vials remains sufficiently below the collapse temperature of the formulation at all possible processing conditions, the presence of microcollapse could yield a significant variation in R_p.

4.1.4. Conclusions

As the core principle of the drying phase of a freeze-drying process involves mass and heat transfer, a proper understanding of these combined transport phenomena allows greater efficiency during freeze-drying process design, optimization, and scale-up. With this regard, the influence of the primary drying input parameters (i.e., shelf temperature and chamber pressure) on the output parameters, such as product temperature, sublimation rate, overall vial heat transfer coefficient, and resistance to mass transfer of the dried product, have been extensively discussed. Furthermore, the influence of vial position on the primary drying output parameters has been discussed.

In all the combinations of shelf temperature and chamber pressure studied, the highest product temperature, sublimation rate, and overall vial heat transfer coefficient were observed in the front edge vials, whereas the lowest were observed in the center vials. Considering different processing conditions with regard to the influence of vial position, high chamber pressure–high shelf temperature combination improves the uniformity of product temperature and overall vial heat transfer coefficient. However, high chamber pressure–high shelf temperature

combination might not represent the most optimum processing condition with regard to the highest possible sublimation rate. In this regard, the highest sublimation rate, at a given T_p, was observed at low chamber pressure–high shelf temperature combinations. Furthermore, a freeze-drying process at low P_c was found to be more robust to variations in T_s compared to a freeze-drying process at high P_c.

Finally, although the drying section of the freeze-drying process is simultaneously influenced by several parameters, the ultimate goal of the optimization process should yield the maximum allowable product temperature of the front edge vials (vial group with the highest product temperature) and the maximum possible sublimation rate of the center vials (vial group with the lowest sublimation rate).

4.1.5. References

[1]. Feistel R, Wagner W. Sublimation pressure and sublimation enthalpy of H_2O ice Ih between 0 and 273.16 K. *Geochimica et Cosmochimica Acta.* 2007;71(1):36–45.

[2]. Fissore D, Pisano R, Barresi AA. Advanced approach to build the design space for the primary drying of a pharmaceutical freeze-drying process. *J Pharm Sci.* 2011;100:4922–4933.

[3]. Kodama T, Sawada H, Hosomi H, Takeuchi M, Wakiyama N, Yonemochi E, Teradad K. Optimization of primary drying condition for pharmaceutical lyophilization using a novel simulation program with a predictive model for dry layer resistance. *Chem Pharm Bull.* 2014;62(2):153–159.

[4]. Kuu WY, Nail SL, Sacha G. Rapid determination of vial heat transfer parameters using Tunable Diode Laser Absorption Spectroscopy (TDLAS) in response to step-changes in pressure set-point during freeze-drying. *J Pharm Sci.* 2009;98(3):1136–1154.

[5]. Pikal MJ, Bogner R, Mudhivarthi V, Sharma P, Sane P. Freeze-drying process development and scale-up: scale-up of edge vial versus center vial heat transfer coefficients, Kv. *J Pharm Sci.* 2016;105(11):3333–3343.

[6]. Pikal MJ, Cardon S, Bhugra C, Jameel F, Rambhatla S, Mascarenhas WJ, Akay HU. The non-steady state modeling of freeze drying: in-process

product temperature and moisture content mapping and pharmaceutical product quality applications. *Pharm Dev Technol.* 2005;10(1):17–32.

[7]. Pikal MJ, Roy ML, Shah S. Mass and heat transfer in vial freeze-drying of pharmaceuticals: Role of the vials. *J Pharm Sci.* 1984;73(9):1224–1237.

[8]. Pikal MJ. Use of laboratory data in freeze drying process design: heat and mass transfer coefficients and the computer simulation of freeze drying. *J Parenter Sci Technol.* 1985;39(3):115–139.

[9]. Rambhatla S, Tchessalov S, Pikal MJ. Heat and mass transfer scale-up issues during freeze-drying, III: control and characterization of dryer differences via operational qualification tests. *AAPS PharmSciTech.* 2006;7(2):E39.

[10]. Scutellà B, Tréléa IC, Bourlès E, Fonseca F, Passot S. Determination of the dried product resistance variability and its influence on the product temperature in pharmaceutical freeze-drying. *Eur J Pharm Biopharm.* 2018;128:379–388.

[11]. Tang XC, Nail SL, Pikal MJ. Freeze-drying process design by manometric temperature measurement: design of a smart freeze-dryer. *Pharm Res.* 2005;22(4):685–700.

[12]. Zhai S, Su H, Taylor R, Slater NKH. Pure ice sublimation within vials in a laboratory lyophilizer; comparison of theory with experiment. *Chem Eng Sci.* 2005;60(4):1167–1176.

4.2. Freeze drying process design using a temperature ramp approach (TRA)

The following sub-section has been submitted in a form of research article to International Journal of Pharmaceutics (see Appendix A.2). The structure of the published document has been slightly modified to fit this particular document.

4.2.1. Introduction

Although the entire freeze-drying process is an energy intensive, time consuming, and economically expensive process, the primary drying step is the longest and most

critical step [Patel et al., 2010; Mortier et al., 2016]. As a result, this step significantly influences the product quality and process economy of the freeze-drying process. Consequently, there is a growing interest in the pharmaceutical and biopharmaceutical industries to optimize the primary drying step with regard to both product quality and processing time. Optimization of the primary drying step requires significant knowledge of the process, the formulation, and the interrelationship between the process and the formulation.

Figure 32 displays the interrelationship between the formulation properties and the freeze-drying process. As shown in Figure 32, there are several formulation properties and process parameters that could play an important role during the optimization of the primary drying step.

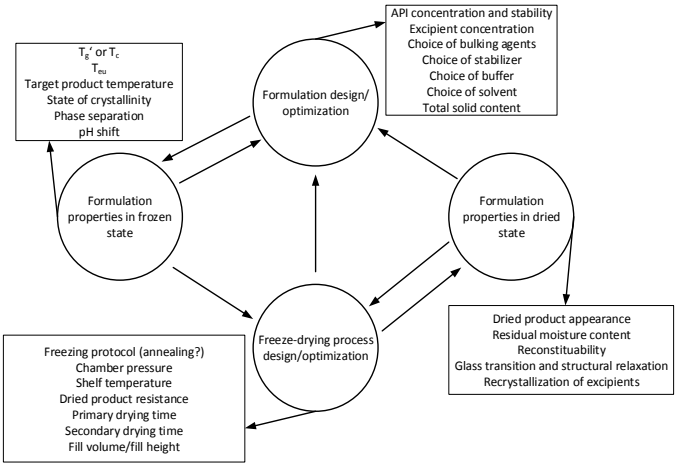

Figure 32. Interrelationship between a formulation and freeze-drying process, and its role during the freeze-drying process design and optimization.

As displayed in Figure 32, characterization of the formulation in its frozen state provides critical formulation properties, such as the glass transition temperature of the maximally freeze-concentrated solution, T_g', collapse temperature of an amorphous formulation, T_c, eutectic melting temperature of a crystalline formulation, T_{eu}, and degree of crystallinity of the formulation. Such information is useful to define the target product temperature for the primary drying step ($T_p t$). A formulation with very low T_g' or T_c might need to be reformulated with the addition of collapse temperature modifiers to facilitate the sublimation rate during primary drying.

Alternatively, crystalline bulking agents with high T_{eu} can be added to support the amorphous formulation. With such modifications, primary drying can be performed at product temperatures higher than T_g' or T_c, and the processing time can be shortened [Depaz et al., 2016; Bjelošević et al., 2018; Horn et al., 2018; Anko et al., 2019; Pansare & Patel, 2019].

Freeze-drying process design and optimization could be initiated once the optimum formulation is defined. Notably, understanding the freezing step is also essential to design and optimize the primary drying step [Kasper & Friess, 2011; Awotwe-Otoo et al., 2015; Ullrich et al., 2015; Esfandiary et al., 2016; Fonte et al., 2016; Goshima et al., 2016; Pisano & Capozzi, 2017; Assegehegn et al., 2019a; Colucci et al., 2019; Vollrath et al., 2019]. From the perspective of a freeze-drying process, optimization of the primary drying step implies working at a chamber pressure (P_c) and a shelf temperature (T_s) that yield the $T_p t$ of a given formulation. Performing the primary drying above $T_p t$ leads to product damage and, hence, to the rejection of the product. Whereas, performing the primary drying below the $T_p t$ leads to an unnecessarily long drying time and to an unoptimized and economically expensive freeze-drying process.

Heat and mass transfers are the core principle of the sublimation process during the primary drying step. The driving force for the mass transfer is the pressure difference between the ice vapor pressure at the sublimation front (P_i) and the chamber pressure (i.e., $P_i(T_p) - P_c$). To initiate the vapor mass transport during the primary drying, the P_c is lowered to a pressure less than the P_i at a target product temperature ($T_p t$). The sublimation of ice is an endothermic process, and thus it takes up energy from the system. It is therefore necessary to have an exothermic process to counterbalance the energy consumption due to the mass transfer process and to keep the system in an energy equilibrium state. An energy equilibrium state is a state where the input and output energies are equilibrated to keep the system at a constant T_p. The exothermic process during the primary drying refers to an energy transport, in the form of heat, to the system. This is usually performed by manipulating the temperature of the shelves (T_s) on which the sublimating product rests. The driving

force for the heat transfer is the temperature difference between T_s and T_p (i.e., $T_s - T_p$). To initiate heat transfer during primary drying, T_s is increased above T_p. However, depending on the processing conditions (i.e., T_s and P_c), the formulation (i.e., solid content), and the freezing step (i.e., ice crystal size and morphology), the energy equilibrium state could be achieved at a T_p far from $T_p t$. Therefore, the aim of the primary drying optimization is to achieve the energy equilibrium state of the system at $T_p t$. In the freeze-drying process, T_p is indirectly controlled through the manipulation of the processing conditions (i.e., T_s and P_c). In the majority of cases, the optimum processing conditions are achieved through a trial and error approach, which leads to unnecessarily long experimental setups. Furthermore, the resulting freeze-drying processes are neither robust nor efficient. In an attempt to minimize the trial and error experiments, researchers have developed mathematical models for the determination of the optimum processing conditions based on the governing heat and mass transfer equations [Schoen et al., 1995; Brülls & Rasmuson, 2002; Pikal et al., 2005; Gieseler et al., 2007; Velardi & Barresi, 2008; Kuu & Nail, 2009; Giordano et al., 2011; Koganti et al., 2011; Fissore et al., 2011; Bosca et al., 2013; Kodama et al., 2013 & 2014; Fissore & Pisano, 2015; Chen et al., 2015; Mortier et al., 2016; Zhu et al., 2018; Sharma et al., 2019]. The mathematical models provide an opportunity to simulate several combinations of input process parameters during the freeze-drying process design; however, their success is highly dependent on the accuracy of model input parameters and on the assumptions of the model equations. Furthermore, since some input parameters are obtained from non-drug experimental trials, verification of the resulting optimum processing conditions may require the execution of several freeze-drying experiments using the actual drug formulation.

Considering the broad use of the freeze-drying process in the pharmaceutical and biopharmaceutical industries [Shanley, 2017], there is a huge interest to develop a simple-to-use and reliable approach to design an optimum and robust freeze-drying process for any given drug formulation. To address this issue, this study presents a novel approach, called *Temperature Ramp Approach (TRA).* This simple-to-use experimental-based TRA could be applied to design an effective freeze-drying process using a few experimental setups. The TRA considers some important general issues and experimental procedures, as described below:

- Defining the target product temperature for the primary drying step. As discussed previously, knowledge of a formulation and its critical properties are vital during freeze-drying process design. The sublimation rate is dependent on several parameters, namely P_i or T_p, P_c, and the resistance to mass transfer of the dried product. To maximize the sublimation rate during primary drying, it is important to work at the highest P_i (this corresponds to the highest T_p) and at the lowest P_c. However, the maximum allowable T_p during the primary drying is limited by the T_c of amorphous formulations or by the T_{eu} of crystalline formulations. Such parameters are obtained from formulation characterization in its frozen state (cf. Figure 32). Several techniques are available to characterize a lyophilization formulation in its frozen state. Differential scanning calorimetry, modulated differential scanning calorimetry, and differential thermal analysis are used for the determination of T_g' and T_{eu} [Her & Nail, 1994; Ma et al., 2001; Schawe, 2006; Sacha & Nail, 2009; Knopp et al., 2016; Ward & Matejtschuk, 2019], whereas freeze-drying microscopy is used for the determination of T_c [Passot et al., 2005; Meister & Gieseler, 2009]. On the other hand, the minimum P_c is limited by the capability of the freeze-drying equipment [Ganguly et al., 2013 & 2017; Kshirsagar et al., 2019]. Patel and Pikal reported that most manufacturing dryers cannot control chamber pressures below 0.06 mbar and there is no additional advantage in sublimation rate for chamber pressures above 0.40 mbar [Patel & Pikal, 2013].

- Designing experimental setups to perform the temperature ramp experiments. An effective design of experiments (DoE) is essential to avoid repeated experimental setups. Thus, it is recommended to gather literature knowledge about similar formulations and, if necessary, to perform some preliminary freeze-drying experiments. This study demonstrated that, using an effective DoE, only three temperature ramp experiments are needed to design an optimum freeze-drying process of a model formulation.

- Defining optimum processing conditions after analysis of the results obtained from the temperature ramp experiments. It is well-known that vials

located at the periphery of a tray, commonly known as edge vials, have higher T_p and sublimation rate compared to vials located at the center of a tray [Pikal et al., 2016; Scutellà et al., 2017a; 2017b & 2018a; Pikal et al., 2018]. These heterogeneities in T_p and drying rate pose significant challenges during freeze-drying process design and scale-up. On one hand, defining the process variables based on center vials T_p could cause the edge vials to exceed the maximum allowable T_p and, consequently, suffer product damage. On the other hand, defining the drying time based on the sublimation rate of the edge vials could cause significant damage to the center vials as they generally need longer drying times during the primary drying step. The approach detailed in this study incorporates such T_p and sublimation rate variations caused due to vial location on a shelf. This guarantees the robustness of the process and facilitates process scale-up and transfer.

- Performing a sublimation rate determination experiment. The purpose of this experiment is to define the optimum drying time (t_d) during the primary drying step. Because center vials have the lowest sublimation rate, a gravimetric approach could be utilized to determine the sublimation rate of the center vials at the previously defined optimum processing conditions.

- Performing a verification experiment. This experiment aims to verify the previously defined optimum T_s-P_c-t_d profile. Visual inspection of the dried products and product temperature profiles could be used to assess the success of the freeze-drying process.

Therefore, the primary objective of this study was to utilize the aforementioned TRA to design a freeze-drying process of two model formulations. It has been demonstrated that the successful design of a robust and optimum freeze-drying process using only three temperature ramp experiments was possible for the two model formulations studied. Thus, compared to expensive and time-consuming trial and error experimental approach, the TRA detailed in this study has several advantages with respect to development time and material savings. Furthermore,

considering the simple and effective design strategy of the TRA, developmental engineers and scientists at any level of experience and lyophilization knowledge could utilize it to design an effective freeze-drying process for any given drug formulation.

4.2.2. Materials and methods

4.2.2.1. Materials

All vials used in this study were 10-mL tubing vials purchased from SCHOTT AG (SCHOTT AG, Mainz, Germany). The stoppers were Igloo single vented gray stoppers from West Pharmaceutical Services, Inc. (West Pharmaceutical Services, Inc., Exton, PA, USA). The temperature ramp approach was used to design a freeze-drying process of two model formulations. Model formulation 1 (MF1) represents a formulation with an intermediate solid content and is a solution containing 10% (w/w) trehalose. Trehalose was purchased from Pfanstiehl, Inc. (Pfanstiehl, Inc., Waukegan, IL, USA). The second model formulation (MF2) represents a formulation with a high solid content and is a solution containing 20% (w/w) sucrose. Sucrose was purchased from VWR (VWR, Darmstadt, Germany). The two model formulations were prepared using water for injection obtained from Fresenius Kabi Deutschland GmbH (Fresenius Kabi Deutschland GmbH, Friedberg, Germany). The trehalose and sucrose powders were used without further treatment. All the solutions used in this study were filtered using 0.22-µm pore size filters (PALL Corporation, Port Washington, NY, USA) before filling into the vials, aiming to remove any particulate matter that might have been introduced during preparation.

4.2.2.2. Methods

Differential Scanning Calorimetry (DSC)

A TA instruments Q2000 series differential scanning calorimetry (DSC) with a refrigerated cooling system (RCS) (TA Instruments, New Castle, DE, USA) was used to determine the T_g' of frozen samples. The following program was employed to determine the T_g' of MF1 and MF2. A nitrogen supply at 50 mL/min was provided to

the system using the continuous mode of the RCS. A sample of 10–15 mg of MF1 or MF2 was weighed into aluminum sample pans, and the pans were hermetically sealed. An empty hermetically sealed pan was used as a reference. The program detailed in section 3.2.1 was used for the determination of T_g' of the frozen formulations. The T_g' values were obtained during the heating period from -60 °C to 40 °C at a rate of 10 °C/min. These T_g' values were analyzed using Universal Analysis software, and they were reported as the midpoint of the glass transition curve.

Freeze-Drying Microscopy (FDM)

A Lyostat 2 freeze-drying microscopy (Biopharma Technology Ltd., Winchester, UK) was used to determine the T_c of the model formulations studied. The program detailed in section 3.2.2. was used to determine T_c of MF1 and MF2 samples. Images of the samples were captured throughout the experiment, and the T_c was defined as the temperature at which a clearly observable structural change of the frozen solution was observed.

Freeze-drying experiment

HOF laboratory freeze dryer (HOF Sonderanlagenbau GmbH, Lohra, Germany), as detailed in section 3.1.3, was used to perform all the freeze-drying experiments. All the freeze-drying experiments were carried out using 10-mL tubing vials, and for each of the experiments, 176 vials (one fully loaded shelf) were filled with 5-mL solution and placed on one of the four shelves of the freeze dryer. To reduce the effect of atypical radiation, a 4-mm thick polystyrene foam block and an aluminum foil were used to cover the acrylic chamber door of the dryer door. Product temperature measurement was performed using eight wireless thermologgers (Lives International, Timis, Romania), which were set to record product temperatures every 20 s. The freezing step was kept identical for all the TRA experiments, as follows: cooling from +5 °C to -10 °C at 1 °C/min, 90 min holding at -10 °C; further freezing to -40 °C at 1 °C/min and 240 min holding at -40 °C. During the primary drying, the shelf temperature was ramped down at 1 °C/min within the shelf temperature range given in the DoE (see Table 4). During the ramping down period, a 3-hour holding time was defined at different shelf temperature points, and the steady state product

temperature was recorded at these shelf temperature points (see Table 4). Product temperatures of the front edge vials and center vials were measured using four thermologgers for each vial group. At each of the shelf temperature points, the product temperature measurements obtained from the four thermologgers were used to calculate the minimum, maximum, average, and standard deviation of the product temperature.

Design of Experiments (DoE)

DoE allows the simultaneous determination of the effects of all potential input variables on the output responses. In addition, it allows investigations on how the process response changes as input variables fluctuate within allowable limits. DoE requires a profound scientific background of the formulation and the process. In addition, preliminary experiments using the specified drug formulation could be necessary to facilitate the development of an effective DoE. For the primary drying step of the freeze-drying process, the critical input process parameters are T_s and P_c, whereas the critical output parameters are T_p, t_d, and sublimation rate. Therefore, based on prior knowledge and some preliminary experiments using the model formulations, a customized DoE for both model formulations was developed and is presented in Table 4.

Table 4. Customized design of experiments (DoE) for MF1 and MF2

Experiment number	Primary drying input parameters		T_s points for TRA (°C)[a]
	P_c (mbar)	Range of T_s (°C)	
10% (w/w) trehalose solution (MF1)			
1	0.05	[0.0, -20.0]	0, -4, -8, -12, -16, and -20
2	0.10	[-5.0, -24.0]	-5, -10, -14, -18, -22, and -24
3	0.15	[-15.0, -33.0]	-15, -17, -21, -25, -29, and -33
20% (w/w) sucrose solution (MF2)			
1	0.05	[-8.0, -24.0]	-8, -10, -14, -18, -22, and -24
2	0.10	[-13.0, -31.0]	-13, -15, -19, -23, -27, and -31
3	0.15	[-15.0, -32.0]	-15, -17, -21, -25, -29, and -32

[a] T_s points are selected from the predefined range of T_s to perform a holding step during the TRA experiments. The quantity and value of the T_s points within a given range are user defined.
MF, model formulation; TRA, temperature ramp approach; P_c, chamber pressure; and T_s, shelf temperature

The biggest advantage of the TRA is that the T_s range during the DoE can be extended to any desired range, as long as the upper T_s limit does not lead to product

collapse. Furthermore, the entire TRA experiment should be completed before the frozen ice is completely sublimed.

Determination of sublimation rate

In order to define the optimum drying rate for any fill volume, determination of sublimation rate at the optimum processing conditions (processing conditions that yield the highest possible product temperature of the edge vials and, at the same time, the highest possible sublimation rate of the center vials) is important. Sublimation rate was determined gravimetrically. For this purpose, 16 selected sample vials, which were systematically placed to represent vial groups with the lowest sublimation rates, were weighed before and after the freeze-drying experiments. It has been experimentally determined that, at the optimum processing conditions, center vials yield the lowest product temperature, and thus the lowest sublimation rate. Therefore, the 16 sample vials were placed at the center of the vial array. A laboratory analytical balance (Sartorius AG, Göttingen, Germany) was used to weigh the sample vials. To stop the sublimation process immediately, the vacuum of the product chamber was released using dry nitrogen. At the end of the sublimation process, the product chamber was too cold to cause condensation of the surrounding moisture into the cold stoppers and into the extremely hygroscopic dried product. To prevent this issue, the vials were heated to 20 °C before the product chamber door was opened. Once the product chamber door was opened, the sample vials were immediately fully stoppered and re-weighed. The minimum sublimation rate of the 16 sample vials was taken to calculate the drying time of the primary drying step. To avoid any effect of the freezing step, the freezing protocol used during the TRA experiments and the sublimation experiments was identical.

It has been reported that the resistance of the dried product increases as the length of the dried layer of the product increases [Kuu et al., 2006; Fissore et al., 2011; Kodama et al., 2014; Scutellà et al., 2018b]. This implies that the sublimation rate decreases as the thickness of the dried product increases. Therefore, to consider the minimum sublimation rate, the sublimation process was stopped when a reasonable dried layer thickness of the center vials was achieved. Since the dried layer of the center vials was not visible, the dried layer of the front edge vials, which

was visible through the acrylic door of the dryer, was used as a guide to stop the sublimation process. Thus, the sublimation process was stopped after the dried layer of the front edge vials reached the vial bottom. The exact drying time for the calculation of the sublimation rate was obtained from the center vials product temperature profile. The definition of the starting and finishing time for the sublimation process is given in section 4.1.2.

4.2.2.3. Results and discussion

Characterization of frozen formulations

The T_g' of both model formulations, as determined using the DSC experiment described previously, were in excellent agreement with literature reported data [Her & Nail, 1994; Chang & Randall, 1992]. The T_c of the model formulations were determined from a subjective assessment of images that were captured during the experiment. Although the determination of the T_c values involves subjective evaluation of images, they provide important information on the structural change of a formulation at a microscopic scale, which is similar to a structural change that could occur during a freeze-drying process. Thus, the T_c can precisely define the $T_p t$ during the primary drying step of the freeze-drying process. The T_c of both model formulations were in excellent agreement with literature reported values [Adams & Ramsay, 1996]. The T_g', T_c, and $T_p t$ of both model formulations are summarized and presented in Table 5.

Table 5. Summary of formulation critical properties for MF1 and MF2.

Formulation	Solid content (mg/g)	T_g' (°C)	T_c (°C)	$T_p t$ (°C)
MF1	100	-29.2	-27.5	[-29.5, -28.5]
MF2	200	-32.4	-31.1	[-32.5, -31.0]

MF, model formulation; T_g', glass transition temperature of the maximally freeze-concentrated solution; T_c, collapse temperature of an amorphous formulation; and $T_p t$, target product temperature for primary drying

Optimization of primary drying using TRA

The main objective of optimizing the primary drying step of a freeze-drying process is to balance the heat and mass transfer of the process during the sublimation step

so that T_p remains within a desired range during the entire primary drying step. Even knowing T_g' and T_c, the optimization of the primary drying step is challenging. On one hand, T_p, which depends on formulation properties, processing conditions, and container-closure system, cannot be directly controlled during the primary drying step. This leads to several trial and error experimental studies aiming to achieve the optimum processing conditions. Although several mathematical models available today are helpful in reducing the experimental burdens necessary to optimize the primary drying step, several time- and material-consuming verification experimental studies could still be required. On the other hand, differences in product temperature and sublimation rate of vials located at the periphery and at the center of the vial array make the optimization effort even more challenging. In this sense, the challenge arises from defining an optimum T_s-P_c-t_d profile, considering all vials in the array. In addition to being optimum, robustness of the process is an important factor. Accordingly, the process should withstand small deviations in T_s and P_c, and considering such deviations, the drying time should allow all vials to complete the sublimation of the ice before proceeding to the secondary drying step.

The TRA developed in this study uses few experimental studies to define optimum processing conditions of a given formulation during primary drying. In addition, the approach is developed to consider the differences in product temperature and sublimation rate of vials at different locations. Because the TRA works better for formulations that show insignificant change in T_p as thickness of the dried layer (L_{R_p}) increases, determination of the relationship between T_p and L_{R_p} of a given formulation is an important part of the TRA. This could be easily performed by following the change in T_p during the progress of a primary drying at a selected T_s-P_c combination. As long as the T_p during this experiment stays lower than T_{eu}, T_g', or T_c of the formulation, any T_s-P_c combination can be used. For the two model formulations studied here, once the T_p reached pseudo steady-state condition, the change in T_p as a function of L_{R_p} was insignificant, demonstrating that the dried layer imposes similar resistance to vapor transport regardless of its thickness (see Figure 33). On the other hand, for formulations that show strong dependency of T_p on L_{R_p}, the TRA gives vital information to examine how T_p changes as L_{R_p} increases and T_s

decreases. In such circumstances, multiple T_s, during the primary drying, could be employed. The two model formulations described previously (cf. Table 4) were used to discuss the use of the TRA to design an effective freeze-drying process.

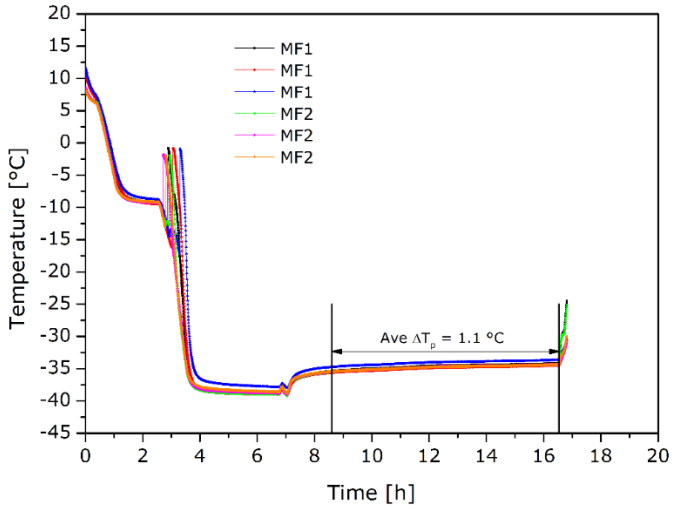

Figure 33. Dependency of product temperature (T_p) on dried layer thickness of model formulation (MF)1 and MF2.

Determination of product temperature (T_p): As discussed previously, T_p is a key variable during TRA process development. Thus, correct determination of the T_p is very important. Nail et al. described some recommended best practices for product temperature measurement [Nail et al., 2017]. The factors that significantly influence T_p are T_s and P_c, and the primary goal of TRA is to evaluate the effect of these factors on T_p for a given formulation and at a given container-closure system. The core advantage of TRA is its ability to analyze several combinations of T_s and P_c in a single experimental setup, thus minimizing the number of experimental studies. Some representative T_p profiles of both model formulations for front edge vials (FE) and center vials (C), measured during the TRA experiments, are displayed in Figure 34. In these experiments, the container-closure systems used were identical; therefore, the influence of variation in vial heat transfer coefficient on product temperature can be safely assumed as negligible.

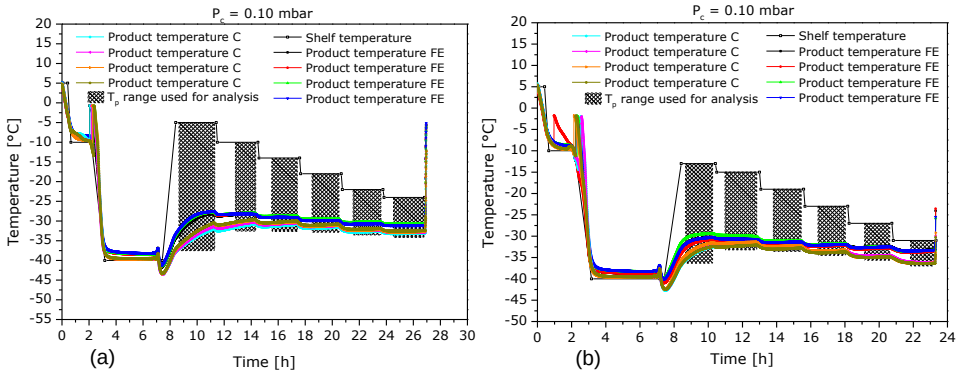

Figure 34. Product temperature profiles of selected temperature ramp approach experiments; (a) model formulation (MF)1 at P_c = 0.10 mbar, (b) MF2 at P_c = 0.10 mbar. C, center vials; FE, front edge vials, T_p, product temperature; and P_c, chamber pressure.

Table 6 presents results and statistical analyses of the T_p for FE and C of both model formulations. For each vial group, four thermologgers were used to measure T_p, from which the minimum (Min), maximum (Max), average (Ave), and standard deviation (SD) of the T_p were calculated (cf. Table 6).

The calculation of the Min, Max, Ave, and SD at each T_s point considers a pseudo steady-state condition in T_p (except at the first T_s point). Thus, because the first few T_p measurements at each T_s point showed transient behavior, they were not considered for the calculation of Min, Max, Ave, and SD. The T_p range used for the calculation of Min, Max, Ave, and SD at each T_s point are displayed in Figure 34. For each vial group and at each T_s point, the Min, Max, Ave, and SD were calculated from T_p measurements (approximately 1800 data points) obtained using the four thermologgers. Thus, in addition to being statistically significant, the reported T_p values are accurate representations of the experiments studied herein.

The statistical results (Table 6) show that regardless of the processing conditions and the formulation, the differences between the maximum and minimum T_p and the standard deviation at the first T_s point were higher than those at the rest of the T_s points. This was attributed to the longer time required to reach pseudo steady-state condition in T_p at the start of the primary drying. For this reason, the first T_s point was not included in further analysis of the TRA results. Differences in maximum and

minimum T_p at the rest of the T_s points (see Table 6) were consistent and small (less than 1 °C), demonstrating that at all T_s points, the change in T_p was insignificant. The SD of the T_p measures the precision or uniformity of the data points at each of the T_s points.

Table 6. Product temperature results and statistical analyses of MF1 and MF2 obtained from TRA experiments according to the DoE (Table 4). Statistical analysis includes minimum (Min), maximum (Max), average (Ave), and standard deviation (SD) of T_p at each T_s point studied

		Statistical analysis of product temperatures (°C)							
		Front edge vials				Center vials			
P_c (mbar)	T_s points (°C)	Min[a]	Max[b]	Ave[c]	SD[d]	Min[a]	Max[b]	Ave[c]	SD[d]
					MF1				
0.05	0.0	-34.8	-27.7	-30.4	1.90	-40.4	-33.2	-36.7	1.77
	-4.0	-28.8	-27.8	-28.2	0.23	-34.4	-31.2	-31.9	0.76
	-8.0	-29.0	-28.5	-28.8	0.16	-32.8	-31.1	-32.0	0.42
	-12.0	-29.8	-29.2	-29.5	0.18	-32.6	-31.5	-32.2	0.31
	-16.0	-30.6	-30.0	-30.3	0.26	-33.1	-32.3	-32.8	0.25
	-20.0	-31.4	-30.6	-31.0	0.29	-34.0	-33.2	-33.7	0.22
0.10	-5.0	-33.9	-27.5	-29.5	1.62	-37.6	-30.5	-33.7	1.81
	-10.0	-28.7	-28.0	-28.3	0.15	-31.3	-29.6	-30.3	0.50
	-14.0	-29.1	-28.7	-28.9	0.11	-31.5	-30.0	-30.6	0.40
	-18.0	-29.9	-29.4	-29.7	0.16	-31.9	-30.8	-31.3	0.30
	-22.0	-30.8	-30.2	-30.5	0.17	-32.8	-31.9	-32.4	0.26
	-24.0	-31.2	-30.6	-30.9	0.16	-33.2	-32.4	-32.8	0.23
0.15	-15.0	-33.2	-28.1	-30.3	1.24	-35.5	-31.0	-33.1	1.09
	-17.0	-28.8	-27.8	-28.2	0.27	-31.1	-29.4	-30.2	0.42
	-21.0	-29.5	-28.7	-29.0	0.22	-31.3	-30.2	-30.7	0.27
	-25.0	-30.5	-29.6	-30.0	0.24	-32.1	-31.4	-31.8	0.19
	-29.0	-31.6	-30.7	-31.1	0.23	-33.7	-33.2	-33.5	0.14
	-33.0	-33.2	-32.4	-32.8	0.23	-36.0	-35.5	-35.8	0.10
					MF 2				
0.05	-8.0	-35.1	-29.5	-30.8	1.26	-40.8	-32.9	-35.6	2.00
	-10.0	-30.3	-29.7	-30.1	0.13	-32.9	-32.0	-32.3	0.21
	-14.0	-31.1	-30.9	-30.9	0.05	-33.0	-32.5	-32.8	0.12
	-18.0	-31.5	-31.2	-31.3	0.08	-33.7	-33.2	-33.5	0.11
	-22.0	-31.9	-31.4	-31.8	0.12	-34.4	-34.1	-34.3	0.08
	-24.0	-32.1	-31.5	-31.9	0.19	-34.7	-34.4	-34.6	0.07
0.10	-13.0	-34.1	-30.3	-31.2	0.84	-36.8	-31.6	-33.7	1.26
	-15.0	-31.0	-30.6	-30.8	0.14	-32.5	-31.4	-32.0	0.34
	-19.0	-31.8	-31.1	-31.4	0.21	-33.1	-32.2	-32.7	0.25
	-23.0	-32.4	-31.7	-32.0	0.19	-33.9	-33.3	-33.6	0.18
	-27.0	-33.0	-32.4	-32.6	0.18	-35.0	-34.5	-34.8	0.14
	-31.0	-33.8	-33.2	-33.4	0.15	-36.4	-36.1	-36.3	0.09
0.15	-15.0	-30.5	-29.0	-29.6	0.34	-34.1	-30.9	-31.9	0.73
	-17.0	-30.1	-29.4	-29.7	0.24	-31.8	-31.1	-31.4	0.14
	-21.0	-31.1	-30.4	-30.7	0.26	-32.6	-32.1	-32.3	0.12
	-25.0	-31.9	-31.1	-31.6	0.25	-33.6	-33.1	-33.4	0.11
	-29.0	-32.8	-31.9	-32.4	0.23	-34.8	-34.4	-34.6	0.09
	-32.0	-33.4	-32.6	-33.1	0.23	-36.0	-35.6	-35.8	0.09

[a] Minimum value for each vial group represents the minimum T_p considering all four thermologgers used.
[b] Maximum value for each vial group represents the maximum T_p considering all four thermologgers used.
[c] Average value for each vial group represents the average T_p considering all four thermologgers used.
[d] Standard deviation value for each vial group represents the standard deviation considering all four thermologgers used.
MF, model formulation; TRA, temperature ramp approach; DoE, design of experiments; T_p, product temperature; T_s, shelf temperature; and P_c, chamber pressure

As presented in Table 6, the SD for all combinations of T_s and P_c studied, except for the first T_s point, was well below 1 °C. Since the SD values are calculated based on statistically significant numbers of data, the average product temperature (T_pave) values presented in Table 6 can be considered as accurate representation of the T_p at the given T_s and P_c values.

Determination of optimum processing conditions: As discussed previously, optimum processing conditions during primary drying define values of T_s and P_c, which allow the energy equilibrium of the system to be achieved at T_pt. As shown in Table 6 and reported in the literature [Pikal et al., 2016 & 2018; Scutellà et al., 2017a; 2017b & 2018a], the front edge vials have higher T_p compared to the center vials. Thus, the T_pave values of the front edge vials (Table 6) were utilized to analyze the T_pt during the primary drying step.

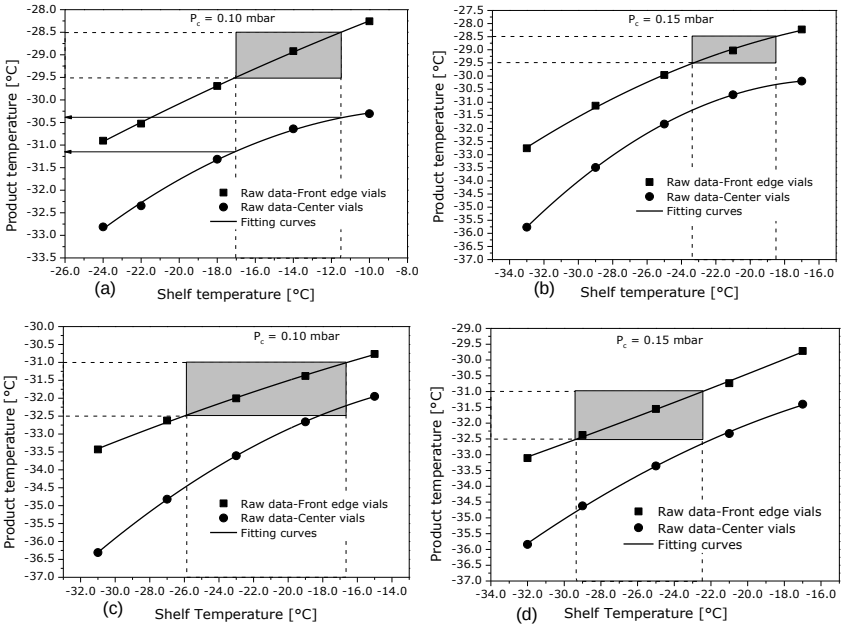

Figure 35. Product temperature dependence on shelf temperature for front edge and center vials at a selected chamber pressure; (a) Model formulation (MF)1 at P_c = 0.10 mbar, (b) MF1 at P_c = 0.15 mbar, (c) MF2 at P_c = 0.10 mbar, and (d) MF2 at P_c = 0.15 mbar. P_c, chamber pressure.

Evaluation of the optimum processing conditions was performed using regression analyses of the T_p of the front edge vials as a function of T_s at the P_c studied (Figure 35).

As can be deduced from Figure 35, the experimental data fit the regression analysis equations (polynomial curve fitting equations) fairly well ($R^2 \geq 0.97$). Thus, accurate determination of the optimum processing conditions is possible. The shade area of Figure 35 displays the range of $T_p t$, as defined previously (cf. Table 5), and the corresponding optimum T_s range at a given P_c. For example, the range of the $T_p t$ for MF1 was defined from -29.5 °C to -28.5 °C (cf. Table 5). As displayed in Figure 35a, the optimum range of T_s at a P_c of 0.10 mbar was obtained from -17.0 °C to -11.5 °C. The optimum range of T_s at a given P_c was defined on the basis that the T_p of the front edge vials remained within the predefined range of $T_p t$ (Figure 35). Similarly, at the optimum T_s, the range of T_p for the center vials varied between -31.1 °C and -30.4 °C (arrow lines, Figure 35a). Alternatively, the regression equations from Figure 35 could be used to calculate the optimum T_s at the corresponding P_c. Using similar analyses, the optimum range of T_s for MF1 and MF2, at all the P_c studied, are summarized and presented in Table 7.

Table 7. Range of optimum T_s as a function of the P_c studied and the corresponding range of T_p for MF1 and MF2 fluids

P_c (mbar)	Range of optimum T_s (°C)[a]	Range of T_p at optimum processing conditions (°C)[b]	
		Front edge vials	Center vials
		MF1	
0.05	[-12.0, -6.0]	[-29.5, -28.5]	[-32.3, -31.9]
0.10	[-17.0, -11.5]	[-29.5, -28.5]	[-31.1, -30.4]
0.15	[-22.5, -19.0]	[-29.5, -28.5]	[-31.1, -30.4]
		MF2	
0.05	[-28.5, -15.0]	[-32.5, -31.0]	[-35.8, -33.0]
0.10	[-26.0, -16.5]	[-32.5, -31.0]	[-34.5, -32.3]
0.15	[-29.5, -22.0]	[-32.5, -31.0]	[-34.9, -32.5]

[a] The range of optimum T_s was calculated using the regression equations (curve fitting equations) on the basis that the corresponding front edge vials T_p range remained within the predefined $T_p t$ (shaded area in Figure 35).
[b] The range for center vials T_p was calculated using the regression equations (curve fitting equations) in the optimum T_s range (cf. Figure 35a).
MF, model formulation; P_c, chamber pressure; T_s, shelf temperature; T_p, product temperature; and $T_p t$, target product temperature.

It is well known that the sublimation rate depends on P_c. Thus, depending on P_c, similar T_p values could produce different sublimation rates. Consider, for example, two optimum processing conditions of MF2 from Table 7: (1) P_c = 0.05 mbar and T_s = -28.5 (at this processing condition, T_p of the center vials was -35.8 °C); (2) P_c = 0.15 mbar and T_s = -29.5 (at this processing condition, T_p of the center vials was -34.9 °C). The driving force for the sublimation of ice ($P_i(T_p) - P_c$) for both selected processing conditions can be calculated from the knowledge of the ice vapor pressure (P_i) at the corresponding product temperatures (T_p). At processing condition 1, $P_i(T_p) - P_c$ = 0.155 mbar, whereas at processing condition 2, $P_i(T_p) - P_c$ = 0.076 mbar. Furthermore, for the same formulation and similar T_p, it could be safely assumed that the dried product resistance is the same. With such a valid assumption, the terms $P_i(T_p) - P_c$ and sublimation rate have similar qualitative and quantitative meanings. Thus, a higher $P_i(T_p) - P_c$ is directly translated into a higher sublimation rate. This analysis implies that although processing conditions 1 and 2 are defined as optimum processing conditions for MF2 from a T_p perspective, they yield significantly different sublimation rates. In this particular example, although the energy equilibrium state of the system at processing condition 2 is achieved within $T_p t$ (cf. Table 7), the corresponding sublimation rate is significantly lower than at processing condition 1. This leads to a prolonged primary drying time, and hence to an unoptimized primary drying step. Given the importance of such knowledge and information during the optimization of the primary drying step, it is therefore essential to identify the range of P_c that yields the highest sublimation rate. This is done by plotting the driving force for the sublimation of ice ($P_i(T_p) - P_c$) against T_p of the front edge vials, as displayed in Figure 36. It is important to mention here that because the center vials have the lowest T_p, and thus the lowest P_i in the vial array, the P_i values in Figure 36 were calculated from T_p of the center vials.

Figure 36 shows that for both model formulations, enhanced sublimation rates are obtained at lower P_c and higher T_p. Furthermore, $P_i(T_p) - P_c$ at P_c of 0.15 mbar was very low, suggesting that performing the primary drying at a chamber pressure above 0.10 mbar would not provide any advantage in terms of sublimation rate. Therefore,

the optimum chamber pressure for MF1 and MF2 could be defined in the range of 0.05 to 0.10 mbar (shaded area of Figure 36).

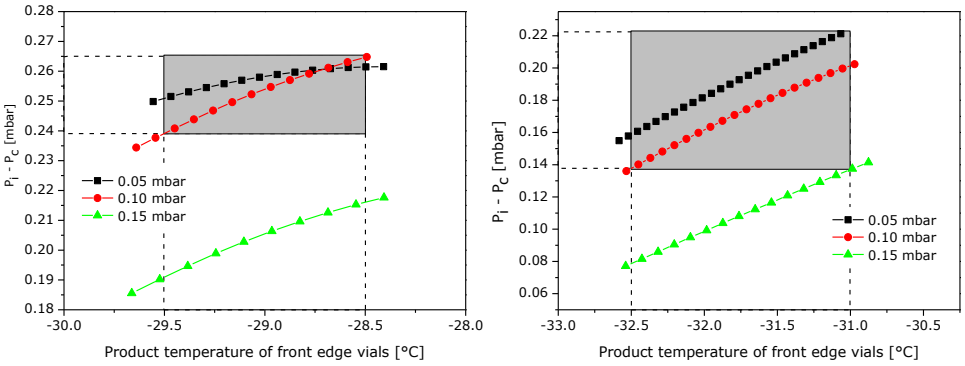

Figure 36. Dependency of the driving force for sublimation of ice, $P_i(T_p) - P_c$, on chamber pressure and product temperature; (a) Model formulation (MF)1 and (b) MF2. P_i, ice vapor pressure; T_p, product temperature; and P_c, chamber pressure.

Hence, referring to Table 7 and considering the aforementioned analyses, the final optimum processing conditions (i.e., T_s and P_c) for both model formulations were defined and are presented in Table 8.

Table 8. Final optimum processing conditions for MF1 and MF2

Optimum P_c (mbar)	Range of optimum T_s (°C)	Range of T_p at optimum processing conditions (°C)	
		Front edge vials	Center vials
	MF1		
0.05	[-12, -6.0]	[-29.5, -28.5]	[-32.3, -31.9]
0.10	[-17.0, -11.5]	[-29.5, -28.5]	[-31.1, -30.4]
	MF2		
0.05	[-28.5, -15.0]	[-32.5, -31.0]	[-35.8, -33.0]
0.10	[-26.0, -16.5]	[-32.5, -31.0]	[-34.5, -32.3]

MF, model formulation; P_c, chamber pressure; T_p, product temperature; and T_s, shelf temperature.

Determination of optimum primary drying time: Once the optimum processing conditions of a formulation were defined, the next step in the TRA scheme was to define the primary drying time of a given fill volume. Therefore, experimental determination of the sublimation rate at a set point, selected from any of the

previously defined ranges of optimum processing conditions (see Table 8), should be performed. In this study, the following set points were chosen to determine the primary drying time of MF1 and MF2:

- For MF1: P_c = 0.075 mbar, T_s = -7.0°C
- For MF2: P_c = 0.075 mbar, T_s = -16.0°C

As outlined in the materials and methods section, sublimation rates of the center vials were determined gravimetrically, and the results are presented in Table 9. As shown in Table 9, the $T_p ave$ of the front edge vials for both model formulations were well within the $T_p t$ ranges (cf. Table 5). This demonstrates the accuracy and reliability of the TRA design strategy, which was also supported by the fact that the standard deviations of the sublimation rate for both model formulations were also very low. Once reliable sublimation rates of the center vials were determined, the optimum primary drying time could be calculated either from the minimum or average sublimation rates.

Table 9. Results of the sublimation rate determination experiments at the selected processing set point

Formulation	Front edge vials		Center vials					
	T_p [a] (°C)		T_p [b] (°C)		$\dot{m}$ [c] (g/h·vial)			
	Ave	SD	Ave	SD	Min	Max	Ave	SD
MF1	-29.10	0.70	-32.44	1.51	0.130	0.151	0.140	0.007
MF2	-31.06	0.20	-32.94	1.09	0.086	0.105	0.095	0.005

[a] The average and standard deviation values were calculated from temperature measurements obtained from three thermologgers (approximately 4500 data points).
[b] The average and standard deviation values were calculated from temperature measurements obtained from four thermologgers (approximately 6000 data points).
[c] The Min, Max, Ave and SD of the sublimation rate were calculated from 16 center vials.
MF, model formulation; Ave, average; SD, standard deviation; Min, minimum; Max, Maximum; T_p, product temperature; and $\dot{m}$, overall mass transfer rate from a vial.

Verification experiment: Aiming to confirm the reliability of the freeze-drying process design strategy detailed in this study, the selected optimum processing conditions were experimentally verified. During the verification experiments, the previously selected optimum processing set point and the minimum sublimation rate (cf. Table 9) were employed. To assess the success and reliability of the TRA design

strategy, T_p was checked, and a visual inspection of the dried products was performed. To minimize possible variations in the drying behavior due to the freezing step, the freezing protocol during both verification and TRA experiments were kept identical.

Figure 37 shows product temperature profiles of the verification experiments. There are different techniques to define the end of primary drying, and hence to evaluate the adequacy of the selected primary drying time [Patel et al., 2010]. One technique is to use the product thermocouples response. In general, the point where the thermocouple response starts to offset from steady-state represents the end of the primary drying. However, a more conservative approach is to use the point where T_p approaches the shelf set point temperature. As shown in Figures 37a and 37b, the T_p responses of the center vials started to offset from their steady-state values before the start of the secondary drying, demonstrating that the drying time allocated to the process was adequate.

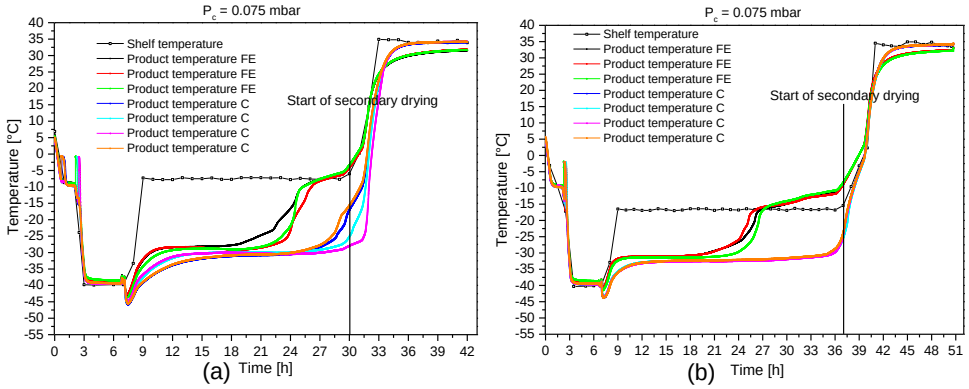

Figure 37. Experimental verification of the optimum processing conditions obtained using TRA. (a) Product temperature profiles of front edge vials (FE) and center vials (C) for model formulation (MF)1; (b) Product temperature profiles of front edge vials (FE) and center vials (C) for MF2. P_c, chamber pressure.

Furthermore, the completion of primary drying was supported by the physical appearance (damage-free) of the dried cakes, as displayed in Figure 38a and 38b. Although assessment of the physical appearance of a dried cake is subjective, some literature guidelines [Ullrich et al., 2015; Patel et al., 2017; Haeuser et al., 2018;

Ohori et al., 2019] have been followed to determine an acceptable appearance of a freeze-dried cake.

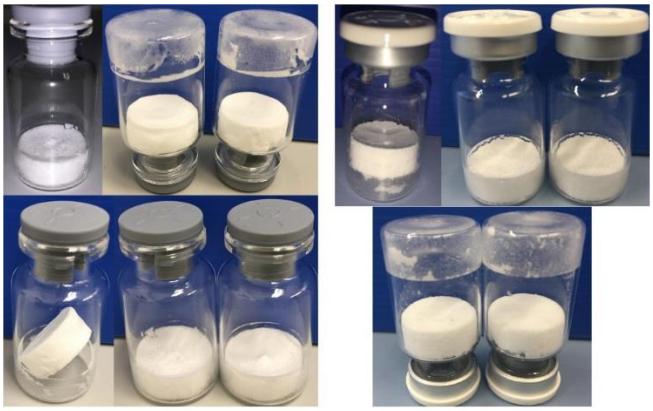

Figure 38. Physical appearance of the dried product after the verification experiments: (a) Model formulation (MF)1 and (b) MF2.

Table 10 presents the comparison between the T_p estimated from the TRA experiments and determined from the verification tests. The TRA estimated values presented in Table 10 represent the T_p values obtained from Table 8 at P_c = 0.10 mbar.

Table 10. Comparison of the TRA estimated and experimentally determined parameters at the selected optimum processing set point

Formulation	TRA estimated values		Experimentally determined values			
	Front edge vials	Center vials	Front edge vials T_p(°C)[a]		Center vials T_p(°C)[b]	
	T_p(°C)	T_p(°C)	Ave	SD	Ave	SD
MF1	[-29.5, -28.5]	[-31.1, -30.4]	-28.8	0.45	-31.1	1.35
MF2	[-32.5, -31.0]	[-34.5, -32.3]	-31.3	0.45	-32.4	1.09

[a] The average and standard deviation values were calculated from temperature measurements obtained from three thermologgers (approximately 4800 data points).
[b] The average and standard deviation values were calculated from temperature measurements obtained from five thermologgers (approximately 10300 data points).
TRA, temperature ramp approach; and T_p, product temperature.

As can be deduced from Table 10, the average T_p of both the front edge and center vials obtained from the verification experiment remained well within the range of the T_p values estimated from the TRA tests. This demonstrates that the TRA freeze-

drying process design strategy described in this study produces very accurate and reproducible results. This enables process scientists to design the freeze-drying process of a given pharmaceutical drug formulation based on a scientific and experimental-based approach rather than through a trial and error approach. Furthermore, the TRA employs a few and well-defined experimental runs, providing remarkable potential for savings in terms of development time and material.

4.2.3. Conclusions

The design strategy of a freeze-drying process for pharmaceuticals and biopharmaceuticals is far from optimum. In most cases, a trial and error experimental approach is employed during the designing, scaling-up, and transfer of the freeze-drying process. This approach is often material and time consuming, and the resulting freeze-drying processes are neither optimum nor robust. In this study, we described a novel simple-to-use and experimental-based approach, called temperature ramp approach (TRA), for the design of an optimum and robust freeze-drying process for any pharmaceutical and biopharmaceutical drug formulations. Proper formulation characterization and definition of a narrow range of target product temperatures during the primary drying step are necessary before performing the TRA experiments. An effective design of experiment (DoE) that contains a reliable range of process parameters (i.e., shelf temperature and chamber pressure) was developed based on a profound scientific understanding of the model formulations and the freeze-drying process. Furthermore, a few preliminary experiments were performed to better define the range of shelf temperatures at a given chamber pressure. One of the core advantages of the TRA is that a wide range of shelf temperatures can be tested in a single experiment, provided the complete TRA experiment is performed before the completion of the ice sublimation. The DoE was used to perform temperature ramp experiments, from which all necessary information to define optimum processing conditions for the primary drying step was obtained.

The proposed TRA considers variations in product temperatures and sublimation rates across a shelf. Accordingly, product temperature of the front edge vials and

sublimation rate of the center vials were used to define the optimum processing conditions. In this sense, the optimum processing condition was selected, so that product temperature of the front edge vials is kept within a pre-defined target product temperature and, at the same time, the highest possible sublimation rate of the center vials is achieved. This assures the effectiveness and robustness of the resulting freeze-drying process. Compared to the mathematical models that may require several freeze-drying experiments for optimization and verification, the TRA detailed in this study produced more realistic, reliable, and accurate results, demonstrating the potential for significant savings in terms of development time and material. Experimental verification with both model formulations, at the optimum processing conditions, showed excellent agreement between the TRA-estimated and the experimentally determined product temperature and sublimation rate values. Finally, coupled with an effective DoE, the proposed TRA for the freeze-drying process design considerably reduces development time and material, and, at the same time, significantly improves the effectiveness and robustness of the resulting freeze-drying process.

4.2.4. References

[1]. Adams GDJ, Ramsay JR. Optimizing the lyophilization cycle and the consequences of collapse on the pharmaceutical acceptability of *Erwinia L-Asparaginase*. *J Pharm Sci.* 1996;85:1301–1305.

[2]. Anko M, Bjelošević M, Planinšek O, Trstenjak U, Logar M, Ahlin Grabnar P, Brus B. The formation and effect of mannitol hemihydrate on the stability of monoclonal antibody in the lyophilized state. *Int J Pharm.* 2019;564:106–116.

[3]. Awotwe-Otoo D, Agarabi C, Read EK, Lute S, Brorson KA, Khan MA. Product and process understanding to relate the effect of freezing method on glycation and aggregation of lyophilized monoclonal antibody formulations. *Int J Pharm.* 2015;490(1-2):341–50.

[4]. Bjelošević M, Seljak KB, Trstenjak U, Logar M, Brus B, Ahlin Grabnar P. Aggressive conditions during primary drying as a contemporary approach to optimize freeze-drying cycles of biopharmaceuticals. *Eur J Pharm Sci.* 2018;122:292–302.

[5]. Bosca S, Barresi AA, Fissore D. Fast freeze-drying cycle design and optimization using a PAT based on the measurement of product temperature. *Eur J Pharm Biopharm.* 2013;85:253–62.

[6]. Brülls M, Rasmuson A. Heat transfer in vial lyophilization. *Int J Pharm*. 2002;246(1-2):1–16.

[7]. Chang BS, Randall CS. Use of sub-ambient thermal analysis to optimize protein lyophilization. *Cryobiology.* 1992;29:632–656.

[8]. Chen X, Sadineni V, Maity M, Quan Y, Enterline M, Mantri RV. Finite element method (FEM) modeling of freeze-drying: monitoring pharmaceutical product robustness during lyophilization. *AAPS PharmSciTech.* 2015;16:1317–1326.

[9]. Colucci D, Maniaci R, Fissore D. Monitoring of the freezing stage in a freeze-drying process using IR thermography. *Int J Pharm.* 2019;566:488–499.

[10]. Depaz RA, Pansare S, Patel SM. Freeze-drying above the glass transition temperature in amorphous protein formulations while maintaining product quality and improving process efficiency. *J Pharm Sci.* 2016;105:40–49.

[11]. Esfandiary R, Gattu SK, Stewart JM, Patel SM. Effect of freezing on lyophilization process performance and drug product cake appearance. *J Pharm Sci.* 2016;105:1427–1433.

[12]. Fissore D, Pisano R, Barresi AA. Advanced approach to build the design space for the primary drying of a pharmaceutical freeze-drying process. *J Pharm Sci.* 2011;100:4922–4933.

[13]. Fissore D, Pisano R. Computer-aided framework for the design of freeze-drying cycles: optimization of the operating conditions of the primary drying stage. *Processes.* 2015;3:406–421.

[14]. Fonte P, Lino PR, Seabra V, Almeida AJ, Reis S, Sarmento B. Annealing as a tool for the optimization of lyophilization and ensuring of the stability of protein-loaded PLGA nanoparticles. *Int J Pharm.* 2016;503(1-2):163–173.

[15]. Ganguly A, Alexeenko AA, Schultz SG, Kim SG. Freeze-drying simulation framework coupling product attributes and equipment

capability: toward accelerating process by equipment modifications. *Eur J Pharm Biopharm.* 2013;85:223–35.

[16]. Ganguly A, Varma N, Sane P, Bogner R, Pikal MJ, Alexeenko A. Spatial variation of pressure in the lyophilization product chamber. Part 1: Computational modeling. *AAPS PharmSciTech*. 2017;18:577–585.

[17]. Gieseler H, Kramer T, Pikal MJ. Use of Manometric Temperature Measurement (MTM) and SMART™ freeze dryer technology for development of an optimized freeze-drying cycle. *J Pharm Sci.* 2007;96:3402–3418.

[18]. Giordano A, Barresi AA, Fissore D. On the use of mathematical models to build the design space for the primary drying phase of a pharmaceutical lyophilization process. *J Pharm Sci*. 2011;100:311–324.

[19]. Goshima H, Do G, Nakagawa K. Impact of ice morphology on Design Space of pharmaceutical freeze-drying. *J Pharm Sci.* 2016;105:1920–1933.

[20]. Haeuser C, Goldbach P, Huwyler J, Friess W, Allmendinger A. Imaging techniques to characterize cake appearance of freeze-dried products. *J Pharm Sci.* 2018;107:2810–2822.

[21]. Her LM, Nail SL. Measurement of glass transition temperatures of freeze-concentrated solutes by differential scanning calorimetry. *Pharm Res.* 1994;11:54–59.

[22]. Horn J, Schanda J, Friess W. Impact of fast and conservative freeze-drying on product quality of protein-mannitol-sucrose-glycerol lyophilizates. *Eur J Pharm Biopharm.* 2018;127:342–354.

[23]. Kasper JC, Friess W. The freezing step in lyophilization: Physico-chemical fundamentals, freezing methods and consequences on process performance and quality attributes of biopharmaceuticals. *Eur J Pharm Biopharm.* 2011;78:248–263.

[24]. Knopp MM, Löbmann K, Elder DP, Rades T, Holm R. Recent advances and potential applications of modulated differential scanning calorimetry (mDSC) in drug development. *Eur J Pharm Sci.* 2016;87:164–167.

[25]. Kodama T, Sawada H, Hosomi H, Takeuchi M, Wakiyama N, Yonemochi E, Terada K. Determination for dry layer resistance of sucrose under various primary drying conditions using a novel simulation program for designing pharmaceutical lyophilization cycle. *Int J Pharm.* 2013;452:180–187.

[26]. Kodama T, Sawada H, Hosomi H, Takeuchi M, Wakiyama N, Yonemochi E, Teradad K. Optimization of primary drying condition for pharmaceutical lyophilization using a novel simulation program with a predictive model for dry layer resistance. *Chem Pharm Bull.* 2014;62:153–159.

[27]. Koganti VR, Shalaev EY, Berry MR, Osterberg T, Youssef M, Hiebert DN, Kanka FA, Nolan M, Barrett R, Scalzo G, Fitzpatrick G, Fitzgibbon N, Luthra S, Zhang L. Investigation of design space for freeze-drying: Use of modeling for primary drying segment of a freeze-drying cycle. *AAPS PharmSciTech.* 2011:12;854–861.

[28]. Kshirsagar V, Tchessalov S, Kanka F, Hiebert D, Alexeenko A. Determining maximum sublimation rate for a production lyophilizer: Computational modeling and comparison with ice slab tests. *J Pharm Sci.* 2019;108:382–390.

[29]. Kuu WY, Hardwick LM, Akers MJ. Rapid determination of dry layer mass transfer resistance for various pharmaceutical formulations during primary drying using product temperature profiles. *Int J Pharm.* 2006;313(1-2):99–113.

[30]. Kuu WY, Nail SL. Rapid freeze-drying cycle optimization using computer programs developed based on heat and mass transfer models and facilitated by Tunable Diode Laser Absorption Spectroscopy (TDLAS). *J Pharm Sci.* 2009;98:3469–3482.

[31]. Ma X, Wang DQ, Bouffard R, MacKenzie A. Characterization of murine monoclonal antibody to tumor necrosis factor (TNF-MAb) formulation for freeze-drying cycle development. *Pharm Res.* 2001;18:196–202.

[32]. Meister E, Gieseler H. Freeze-dry microscopy of protein/sugar mixtures: drying behavior, interpretation of collapse temperatures and a comparison to corresponding glass transition data. *J Pharm Sci.* 2009;98:3072–3087.

[33]. Mortier STFC, Van Bockstal PJ, Corver J, Nopens I, Gernaey KV, De Beer T. Uncertainty analysis as essential step in the establishment of the dynamic Design Space of primary drying during freeze-drying. *Eur J Pharm Biopharm*. 2016;103:71–83.

[34]. Nail S, Tchessalov S, Shalaev E, Ganguly A, Renzi E, Dimarco F, Wegiel L, Ferris S, Kessler W, Pikal MJ, Sacha G, Alexeenko A, Thompson TN, Reiter C, Searles J, Coiteux P. Recommended best practices for process monitoring instrumentation in pharmaceutical freeze drying-2017. *AAPS PharmSciTech.* 2017;18:2379–2393.

[35]. Ohori R, Akita T, Yamashita C. Mechanism of collapse of amorphous-based lyophilized cake induced by slow ramp during the shelf ramp process. *Int J Pharm.* 2019;564:461–471..

[36]. Pansare SK, Patel SM. Lyophilization process design and development: A single-step drying approach. *J Pharm Sci.* 2019;108:1423–1433.

[37]. Passot S, Fonseca F, Alarcon-Lorcab M, Rolland D, Marina M. Physical characterization of formulations for the development of two stable freeze-dried proteins during both dried and liquid storage. *Eur J Pharm Biopharm.* 2005;60:335–348.

[38]. Patel SM, Doen T, Pika MJ. Determination of end point of primary drying in freeze-drying process control. *AAPS PharmSciTech.* 2010;11:73–84.

[39]. Patel SM, Jameel F, Pikal MJ. The effect of dryer load on freeze-drying process design. *J Pharm Sci.* 2010;99:4363–4379.

[40]. Patel SM, Nail SL, Pikal MJ, Geidobler R, Winter G, Hawe A, Davagnino J, Rambhatla GS. Lyophilized drug product cake appearance: What is acceptable? *J Pharm Sci.* 2017;106:1706–1721.

[41]. Patel SM, Pikal MJ. Lyophilization Process Design Space. *J Pharm Sci.* 2013;102:3883–3887.

[42]. Pikal MJ, Bogner R, Mudhivarthi V, Sharma P, Sane P. Freeze-drying process development and scale-up: Scale-up of edge vial versus center vial heat transfer coefficients, Kv. *J Pharm Sci.* 2016;105:3333–3343.

[43]. Pikal MJ, Cardon S, Bhugra C, Jameel F, Rambhatla S, Mascarenhas WJ, Akay HU. The non-steady state modeling of freeze-drying: in-process product temperature and moisture content mapping and pharmaceutical product quality applications. *Pharm Dev Technol.* 2005;10:17–32.

[44]. Pikal MJ, Pande P, Bogner R, Sane P, Mudhivarthi V, Sharma P. Impact of natural variations in freeze-drying parameters on product temperature history: Application of quasi steady-state heat and mass transfer and simple statistics. *AAPS PharmSciTech.* 2018;19:2828–2842.

[45]. Pisano R, Capozzi LC. Prediction of product morphology of lyophilized drugs in the case of vacuum induced surface freezing. *Chem Eng Res Des.* 2017;125:119–129.

[46]. Sacha GA, Nail SL. Thermal analysis of frozen solutions: multiple glass transitions in amorphous systems. *J Pharm Sci.* 2009;98:3397–3405.

[47]. Schawe EK. A quantitative DSC analysis of the metastable phase behavior of the sucrose-water system. *Thermochimica Acta.* 2006;451:115–125.

[48]. Schoen MP, Braxton BK, Gatlin LA, Jefferis III RP. A simulation model for the primary drying phase of the freeze-drying cycle. *Int J Pharm*. 1995;114(2):159–170.

[49]. Scutellà B, Bourlès E, Plana-Fattori A, Fonseca F, Flick D, Tréléa IC, Passot S. Effect of freeze dryer design on heat transfer variability investigated using a 3D mathematical model. J *Pharm Sci.* 2018a;107:2098–2106.

[50]. Scutellà B, Passot S, Bourlés E, Fonseca F, Tréléa IC. How vial geometry variability influences heat transfer and product temperature during freeze-drying. *J Pharm Sci.* 2017b;106:770–778.

[51]. Scutellà B, Plana-Fattoric A, Passota S, Bourlès E, Fonseca F, Flick D, Tréléa IC. 3D mathematical modelling to understand atypical heat transfer observed in vial freeze-drying. *Appl Therm Eng.* 2017a;126:226–236.

[52]. Scutellà B, Tréléa IC, Bourlès E, Fonseca F, Passot S. Determination of the dried product resistance variability and its influence on the

product temperature in pharmaceutical freeze-drying. *Eur J Pharm Biopharm.* 2018b;128:379–388.

[53]. Shanley A. Modernizing lyophilization. *BioPharm Int.* 2017;30:50–52.

[54]. Sharma P, Kessler WJ, Bogner R, Thakur M, Pikal MJ. Applications of the tunable diode laser absorption spectroscopy: In-process estimation of primary drying heterogeneity and product temperature during lyophilization. *J Pharm Sci.* 2019;108:416–430.

[55]. Ullrich S, Seyferth S, Lee G. Measurement of shrinkage and cracking in lyophilized amorphous cakes. Part IV: Effects of freezing protocol. *Int J Pharm.* 2015;495(1):52–57.

[56]. Ward KR, Matejtschuk P. Characterization of formulations for freeze-drying. In: Ward KR, Matejtschuk P., eds. *Lyophilization of Pharmaceuticals and Biologicals: Methods in Pharmacology and Toxicology*. New York: Humana Press; 2019: 1–32.

[57]. Velardi SA, Barresi AA. Development of simplified models for the freeze-drying process and investigation of the optimal operating conditions. *Chem Eng Res Des.* 2008;86:9–22.

[58]. Vollrath I, Friess W, Freitag A, Hawe A, Winter G. Comparison of ice fog methods and monitoring of controlled nucleation success after freeze-drying. *Int J Pharm.* 2019;558:18-28.

[59]. Zhu T, Moussa EM, Witting M, Zhou D, Sinha K, Hirth M, Gastens M, Shang S, Nere N, Somashekar SC, Alexeenko A, Jameel F. Predictive models of lyophilization process for development, scale-up/tech transfer and manufacturing. *Eur J Pharm Biopharm.* 2018;128:363–378.

4.3. Freeze drying process design using a process design space (PDS) approach

The following sub-section has been published in a form of research article in Journal of Pharmaceutical Sciences (see Appendix A.3). The structure of the published document has been slightly modified to fit this particular document.

4.3.1. Introduction

Freeze-drying or lyophilization is a drying unit operation that is frequently used in pharmaceutical and biopharmaceutical industries to convert labile liquid formulations into a solid state with the aim of improving their long-term storage stability [Pikal, 1990a; 1990b]. Despite being a method of high relevance for these industries, freeze-drying is an energy intensive, time consuming, and economically expensive process [Patel et al., 2010; Mortier et al., 2016]. Therefore, the rational design and optimization of the freeze-drying process is of paramount importance. It is understandable that a sound knowledge of a formulation and its critical properties are essential for the efficient and rational design of a freeze-drying process [Tang & Pikal, 2004; Liu, 2006; Wang, 2010; Goldman et al., 2018; Ward & Matejtschuk, 2019]. Formulation critical properties include the freezing behavior of the formulation (phase separation, protein denaturation, and pH shift), glass transition temperature of the maximally freeze-concentrated solution (T_g'), collapse temperature of the amorphous formulation (T_c), eutectic temperature of the crystalline formulation (T_{eu}), stability of the active ingredients during preparation, and properties of the excipients. Knowledge of such formulation properties and the freeze-drying process itself significantly eases the design of a robust and optimum process. Whereas an optimum process minimizes the process time, a robust process addresses minor process deviations and maintains the predefined quality target product profiles (QTPP).

The primary drying step of the freeze-drying process is, typically, the most critical and longest processing step. Consequently, the majority of the optimization efforts are performed in this step. As reviewed in a previous paper [Goshima et al., 2016], the freezing step has a significant effect on the primary drying rate; this is attributed to the morphology, and the number and size of ice crystals formed during the freezing step. The ice crystals leave a porous structure of dried product upon sublimation, which determines the permeability and resistance to water vapor flow through the dried product. The larger the ice crystals formed during the freezing, the larger the pore radius of the porous dried product, and hence the lower the resistance to water vapor flow. This facilitates the drying rate during the sublimation step of the

freeze-drying process. In general, the influence of the freezing step on the different freeze-drying parameters can be summarized as shown in Equation 26. A more detailed analysis of Equation 26 is given in section 2.1.1.1.

$$\left.\begin{array}{c} r = f(ice\ crystal\ size) \\ R_p = f(\frac{1}{r}) \\ T_p = f(R_p, \frac{1}{r}) \\ P_i = f(T_p, R_p) \\ \dot{m} = f(\frac{1}{R_p}, T_p) \end{array}\right| \quad Provided\ T_s\ and\ P_c\ are\ held\ constant \qquad (26)$$

where, r[cm] is the pore radius of the dried product; R_p[mbar·s/g] is the resistance to mass transfer of the dried product; T_p[°C] is the product temperature; P_i[mbar] is the vapor pressure of ice; T_s[°C] is the shelf temperature; P_c[mbar] is the chamber pressure; and $\dot{m}$[g/s] is the overall mass transfer rate from a vial.

During the primary drying step, the chamber pressure, P_c, is reduced to trigger the sublimation of the ice crystals and, simultaneously, the shelf temperature, T_s, is increased to provide energy to the sublimation process. The endothermic sublimation of ice and the exothermic heat input processes are occurring in “close equilibrium”. Thus, the change in product temperature during the primary drying is insignificant, provided that the shelf temperature and chamber pressure are held constant. One major factor for a slight change in product temperature during the primary drying could be the increase in dried product resistance caused by an increase in dried layer thickness.

In a freeze-drying process, the product temperature is indirectly controlled through the manipulation of the shelf temperature and chamber pressure. In the majority of cases, the manipulation of the shelf temperature and chamber pressure is realized through a trial and error approach, which leads to unnecessary long experimental setups. Further, the resulting freeze-drying process is neither robust nor efficient. In an attempt to minimize the trial and error experiments, researchers have developed mathematical models for the determination of the optimum processing conditions based on the governing heat and mass transfer equations [Pikal et al., 2005;

Gieseler et al., 2007; Velardi & Barresi, 2008; Kuu & Nail, 2009; Sundaram et al., 2010; Giordano et al., 2011; Koganti et al., 2011; Fissore et al., 2011; Bosca et al., 2013; Kodama et al., 2013; Kodama et al., 2014; Fissore & Pisano, 2015; Chen et al., 2015; Mortier et al., 2016; Van Bockstal et al., 2017; Arsiccio & Pisano, 2018; Zhu et al., 2018; Sharma et al., 2019]. In these mathematical models, two input parameters, namely the overall vial heat transfer coefficient and the resistance to mass transfer of the dried product, are experimentally determined. The overall vial heat transfer coefficient is typically determined from a water sublimation test, whereas the resistance to mass transfer of the dried product is determined using the drug formulation. The determination of these parameters from a non-drug formulation and from a single experimental run could lead to a significant error during the optimization of the process [Kodama et al., 2014]. The authors' experimental results show up to 18% difference in the overall vial heat transfer coefficient determined from water sublimation tests and from drug formulation sublimation tests (see Table 11).

Table 11. Differences in vial heat transfer coefficients (K_v) of a drug formulation and water for injection. Note that the experiments were performed using identical vials and stoppers. Authors' own experimental results

P_c (mbar)	T_s (°C)	Overall vial heat transfer coefficient, K_v*10^4 (cal/s.cm^2·K)		
		Drug formulation	Water for Injection [WFI]	Difference (%)
0.05	-10.0	1.895	1.934	2.06
	-17.0	1.952	1.871	4.15
	-20.0	2.127	1.869	12.10
0.10	-10.0	3.044	3.044	0.00
	-15.0	2.847	3.093	8.64
	-20.0	3.131	3.165	1.09
	-24.0	2.764	3.182	15.10
0.15	-15.0	4.169	4.624	10.90
	-18.0	4.508	4.229	6.19
	-25.0	3.485	4.144	18.90

P_c, chamber pressure; and T_s, shelf temperature

Further, determination of the dried product resistance from a single experimental run may not represent different processing conditions. Processing at a product temperature close to the T_c could introduce a microcollapse on the dried structure, yielding a considerably reduced dried product resistance compared to the dried products without microcollapse.

Following the roll out of the International Conference on Harmonization (ICH) Q8(R2), the application of quality by design (QbD) has become an integral part of the formulation and process development for pharmaceutical products [Patel et al., 2015]. An essential feature of the QbD philosophy is the design space (DS), which is defined, according to ICH Q8(R2), as a multidimensional combination and interaction of input variables and process parameters that have been demonstrated to provide the assurance of critical product quality [https://www.ich.org/home.html]. Given the high interest of the pharmaceutical industries in implementing the QbD concept in their formulation and process development platforms, there exists a requirement for a systematic, scientific, and result-based DS construction strategy.

To address this point for a freeze-drying process, this study presents a new approach for the construction of a process design space (PDS) using a customized design of experiments (DoE). A PDS is a space enclosed by critical input process parameters of a given process, within which the output parameters and the critical quality attributes (CQAs) of the product remain within the desired limit. A PDS ensures both process efficiency and product quality, and hence its advantages and applications during the freeze-drying of pharmaceutical products are significant. Because freeze-drying is an energy intensive process, designing the most optimum freeze-drying process is certainly one of the highest priorities for pharmaceutical industries. In this regard, a PDS provides an opportunity to define optimum process parameters while maintaining product quality. Further, a PDS significantly eases the freeze-drying process scale-up and transfer, and ensures consistent product quality during large-scale commercial manufacturing. A PDS provides information on how possible process deviations during scale-up, transfer, or manufacturing influence the output parameters and CQAs, and offers an opportunity for an early and systematic mitigation system for the case where the output parameters and CQAs are outside

the PDS. Possible process deviations during scale-up, transfer, or manufacturing could be caused by differences in freezing conditions at lab and manufacturing scale, and differences in equipment design. In such circumstances, equipment characterization is necessary to assess the differences between equipment and to adjust the processing conditions. Adjustment of the processing conditions could be significantly facilitated using the PDS.

In a freeze-drying process, it is important to consider that a PDS contains the input parameters that provide the maximum possible sublimation rate during the primary drying step. As can be deduced from Equation 26, the sublimation rate is dependent on several parameters, namely, ice vapor pressure or product temperature, chamber pressure, and dried product resistance to mass transfer. To maximize the sublimation rate during primary drying, it is important to execute at the highest vapor pressure of ice (this corresponds to the highest product temperature) and at the lowest chamber pressure. However, the maximum product temperature during primary drying is limited by the T_c of an amorphous formulations or the T_{eu} of an crystalline formulations. Conversely, the minimum chamber pressure is limited by the capability of the freeze-drying equipment [Ganguly et al., 2013 & 2017; Kshirsagar et al., 2019]. In this sense, a PDS offers a method to identify the product and equipment limitations and to select the most optimized and robust process parameters for a given formulation.

Although profound prior scientific knowledge of both formulation and process is indispensable for building an effective DoE, it also significantly assists in minimizing the number of experiments necessary to construct a PDS. Using an effective DoE, less than 20 freeze-drying experiments can be performed to develop the PDS of a pharmaceutical formulation. As mentioned earlier, the primary drying is the most critical phase in terms of process economics and overall product quality. Thus, the focus of this study is on the construction of the PDS for the primary drying phase of the freeze-drying process. Although the mathematical models provide an opportunity to simulate several combinations of input process variables during the PDS construction, their success is highly dependent on the accuracy of the model input parameters and the assumptions of the model equations. In this sense, the

experimental-based PDS construction approach detailed in this study offers an alternative method for the construction of a freeze-drying PDS. In addition, although the mathematical models may need fewer experimental setups than the experimental approach presented herein, the advantages of the experimental approach over the mathematical models are several folds. These include: (i) the utilization of unique and easy procedures to construct a PDS using the data obtained solely from freeze-drying experiments of a given drug product. This eliminates the assumptions on heat transfer coefficient and dried product resistance, thus providing highly accurate results. For this reason, the PDS developed in this study is termed a product-based PDS; (ii) unlike the current representation of a freeze-drying PDS, this study uses shelf temperature versus chamber pressure curves with narrow ranges of product temperatures as contour lines. This facilitates the selection of the most effective and optimized process parameters for a given formulation; and (iii) the PDS presented herein incorporates the variation in product temperatures and sublimation rates of vials at different locations of a shelf. This guarantees the robustness of the process and facilitates the process scale-up and transfer. Moreover, presenting a product-based PDS offers more realistic and reliable results if there is an intention of using the PDS for regulatory purposes.

Finally, it is worth pointing out that Chang and Fischer reported construction of a freeze-drying PDS based on experimental approach, aiming to explain the use of a single-step freeze drying cycle for a crystalline formulation (i.e., use of high shelf temperature (as high as 40 °C) and low chamber pressure to avoid using secondary drying) [Chang & Fischer, 1995]. Consequently, it is apparent that the approach followed by Chang and Fischer is based on a rather different concept.

4.3.2. Materials and methods

4.3.2.1. Materials

Sucrose was purchased from VWR (VWR, Darmstadt, Germany) and trehalose was purchased from Pfanstiehl, Inc. (Pfanstiehl, Inc., Waukegan, IL, USA). The two raw materials were used without further treatment. Water for injection was obtained from Fresenius Kabi Deutschland GmbH (Fresenius Kabi Deutschland GmbH, Friedberg,

Germany). All vials used in this study were 10-mL tubing vials purchased from SCHOTT AG (SCHOTT AG, Mainz, Germany). The stoppers were Igloo single vented gray stoppers from West Pharmaceutical Services, Inc. (West Pharmaceutical Services, Inc., Exton, PA, USA).

Two model formulations were used for the development of the PDS. Model formulation 1 (MF1) was a 10% (w/w) trehalose solution; model formulation 2 (MF2) was a 20% (w/w) sucrose solution. Water for injection (WFI) was used to prepare all the solutions used in this study. Aiming to remove particulate matters that could be introduced during preparation, the model formulations were filtered using 0.22 µm pore-size filters (PALL Corporation, Port Washington, NY, USA) prior to filling the vials.

4.3.2.2. Methods

Differential Scanning Calorimetry (DSC)

The glass transition temperature of the frozen samples (T_g') was measured using a TA Instruments Q2000 series differential scanning calorimetry with refrigerated cooling system (RCS) (TA Instruments, New Castle, DE, USA). Sucrose and trehalose solutions were prepared as described previously and a sample of 10–15 mg was weighed into aluminum sample pans, which were then hermetically sealed. An empty, hermetically sealed, pan was used as a reference. The heating/cooling protocols applied were previously described in section 3.2.1. The T_g' values were determined using Universal Analysis software and were reported as the midpoint of the glass transition curve [Her & Nail, 1994].

Freeze-Drying Microscopy (FDM)

The collapse temperature (T_c) of the model formulations was determined using a Lyostat 2 freeze-drying microscopy (Biopharma Technology Ltd., Winchester, UK). Sucrose and trehalose solutions were prepared as described previously and a sample of 2 µL was placed on a quartz cover slip and covered using a glass cover slip. To allow sublimation of the sample, a 70-µm thick metal spacer was placed

between the quartz and glass cover slips. The experimental protocol was detailed in section 3.2.2. Images of the samples were captured throughout the experiment and the collapse temperature (T_c) was defined as the temperature where a clearly observable structural change of the frozen solution was observed.

Freeze-drying experiment

All freeze-drying experiments were performed using a HOF laboratory freeze dryer HOF Sonderanlagenbau GmbH, Lohra, Germany), as detailed in section 3.1.3. The freeze dryer was equipped with a Pirani gauge for chamber pressure control and three type K thermocouples for the measurement of the product temperature. Freeze-drying experiments of both model formulations were performed using 10-mL tubing vials. For each of the model formulations, 176 vials (one fully loaded shelf) were filled with 4 mL solution and placed on one of the four shelves of the freeze dryer. During the sublimation rate determination experiments, the fill volume was selected to be higher than the design fill volume (3 mL) to bring equivalence in dried product resistance and sublimation rate. For example, consider a sublimation experiment that was stopped after an average 60% of a given (5 mL) fill volume was sublimed. This is equivalent to a complete sublimation of 3 mL fill volume, and thus brings equivalence in dried layer thickness (i.e., dried layer resistance) and sublimation rate. The freeze dryer had an acrylic chamber door and to reduce the effect of radiation, the door was covered with a 4-mm thick polystyrene foam block and an aluminum foil. Eight wireless thermologgers (Lives International, Timis, Romania) and the three type K thermocouples were used to measure product temperatures.

Although the presence of temperature probes could impact the freezing and drying behavior of the probed vials, such impact could be minimized by using thin temperature probes. Thus, both the type K thermocouples sensors and wireless thermologgers used in this study were less than 1 mm thick. Product temperatures using the wireless thermologgers were measured every 20 s. The freezing step was held constant for all freeze-drying experiments as follows: 1 °C/min down to -10 °C and 90 min holding time; further freezing to -40 °C at 1 °C/min and 240 minutes

holding time. Conversely, the primary drying was changed according to the DoE, as indicated in Table 12.

Table 12. Custom designed full-factorial design of experiments (DoE) for model formulation 1 and model formulation 2

Experiment number	Primary drying input parameters		Primary drying output parameters
	P_c (mbar)	T_s (°C)	
1	0.05	-5.0[a]	• Product temperature of front edge and center vials • Sublimation rate of front edge and center vials
2		-10.0	
3		-13.0[b]	
4		-15.0	
5		-20.0	
6	0.08	-10.0	
7		-15.0	
8		-20.0	
9		-25.0	
10	0.10	-15.0	
11		-17.0	
12		-20.0	
13		-25.0	
14	0.15	-17.0	
15		-20.0	
16		-25.0	
17		-30.0	
18	0.20	-20.0	
19		-25.0	
20		-30.0	

[a] Experiment only for model formulation 1
[b] Experiment only for model formulation 2
P_c, chamber pressure; and T_s, shelf temperature

The shelf surface temperatures (Figure 42) were measured using the wireless thermologgers in a fully loaded shelf. For this purpose, the thermologgers were inserted into bottomless 10-mL vials and they were arranged to have a clear contact with the shelf surface.

Determination of sublimation rate

The sublimation rate was determined gravimetrically. For this purpose, 50 selected sample vials were weighed before and after the freeze-drying experiments. The sample vials were systematically placed to represent different vial groups, which could have different sublimation rates and product temperatures, within the vial array. Figure 39 displays the placement of the sample vials and thermocoupled vials for all the experiments performed in this study. For example, in Figure 39, vials numbered 1–8 represent a vial group referred to as "*front edge*", vials 9–17 represent

"*side edge outer*", vials 18–26 represent "*side edge inner*", vials 27–42 represent "*center*", and vials 43–50 represent "*rear edge*". Maximum, minimum, and average sublimation rates of each vial group were calculated from the sublimation rates obtained from the numbered vials of the same group (cf. Figure 39).

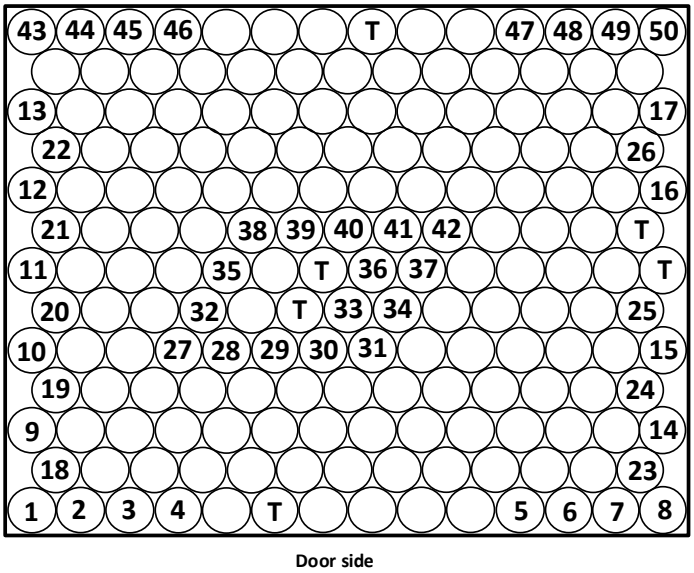

Figure 39. Vial placement for the sublimation experiments of this study. "Numbered vials" represent vials weighed before and after the freeze-drying experiment. "T-signed vials" represent vials with thermocouples for product temperature measurement of the different groups of vial arrays.

A laboratory analytical balance (Sartorius AG, Göttingen, Germany) was used to weigh the sample vials. The sublimation process was terminated by backfilling the product chamber using dry nitrogen and the vials were heated to 20 °C before the product chamber door was opened. This step was included to prevent condensation from the surrounding moisture from forming on the cold stoppers and penetrating into the extremely hygroscopic dried product. The freeze dryer available did not have an automatic stoppering mechanism. As a result, once the product chamber door was opened, the sample vials were taken out of the chamber, immediately fully stoppered and re-weighed.

It is well known that dried product resistance and product temperature increase as product dried layer thickness increases [Fissore et al., 2011; Kodama et al., 2014;

Scutellà et al., 2018a]. Therefore, to include the maximum effect of the dried product resistance during the determination of the sublimation rate, the sublimation experiments were stopped once the dried layer of the front edge vials was close to the vial bottom. This was performed by visually observing the dried layer of the front edge vials. At the end of the sublimation experiments, up to 70 wt% of the initial water content of the edge vials was removed, whereas, for center vials, up to 50 wt% of the initial water content was removed. Further, this procedure allows determination of consistent loss of water during the different sublimation experiments.

The exact drying time for the calculation of the sublimation rate was obtained from the product temperature profile of the wireless thermologgers, as detailed in section 4.1.2. Such definition of the starting time considers the real effect of different processing conditions and formulations on the sublimation rate, before the product temperature attained a pseudo steady-state condition. That is, the calculation of the sublimation rates considered the transition period at the beginning of the primary drying. Thus, any bias in sublimation rate calculation that could occur due to the transition period was avoided.

Design of Experiments (DoE)

DoE is a structured analysis of experiments wherein input parameters are changed, and differences and variations in output parameters are measured. DoE allows the simultaneous determination of the effects of all potential input variables on the output responses, as well as investigations on how the process response changes as input variables fluctuate (random and systematic variation of the process parameters) within allowable limits. This requires a profound scientific background of the formulation and process and, further, preliminary experiments using the specified drug formulation could be required to facilitate the development of an effective DoE. For a freeze-drying process, the critical process input and output parameters of the three steps are well known. They are depicted in Figure 40.

As the focus of this study was on the PDS development for the primary drying step, the DoE only considered the input and output parameters of the primary drying step

of the freeze-drying process. Based on prior knowledge and preliminary experiments using the model formulations, a customized full-factorial DoE for both model formulations was developed as displayed in Table 12.

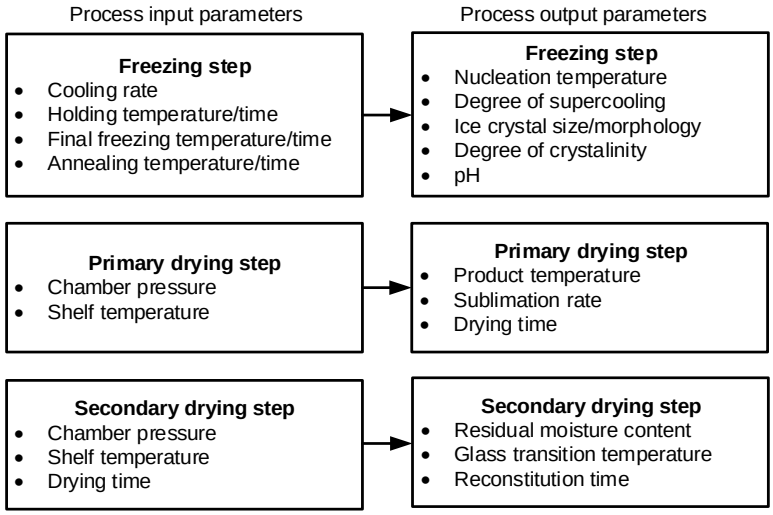

Figure 40. Critical input and output process parameters of a typical freeze-drying process.

4.3.3. Results and discussion

Characterization of frozen formulations

Representative DSC thermograms for MF1 and MF2 are displayed in Figure 41i. For MF1, T_g' was observed at a temperature of -29.2 °C; for MF2, T_g' was observed at a temperature of -32.4 °C. The T_g' values of MF1 and MF2 obtained in this study were in excellent agreement with previously reported values [Her & Nail, 1994; Chang & Randall, 1992].

Freeze-drying microscopy images of MF1 and MF2 are displayed in Figure 41ii. The T_c of both model formulations obtained in this study were also in excellent agreement with the values reported in the literature [Adams & Ramsay, 1996].

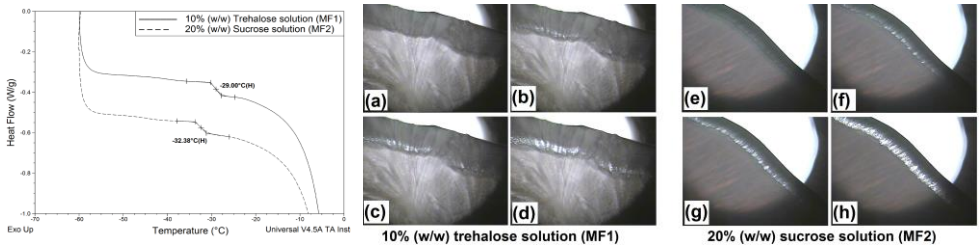

(i) (ii)

Figure 41. Characterization of frozen formulations. (i) DSC thermograms for MF1 (upper curve) and for MF2 (lower curve). (ii) Freeze-drying microscopy images for MF1: (a) intact structure at T = -28.5 °C, (b) onset of collapse at T = -28.0 °C, (c) collapse at T = -27.5 °C, (d) significant damage at T = -27.0 °C; and for MF2: (e) intact structure at T = -31.8 °C, (f) onset of collapse at T = -31.4 °C, (g) collapse at T = -31.1 °C, (h) significant damage at T = -30.6 °C.

Table 13 presents the results of T_g', T_c, and the range of maximum product temperature during primary drying for the two model formulations.

Table 13. Values of T_g', T_c, and the range of maximum product temperature during primary drying for MF1 and MF2

Formulation	T_g' (°C)	T_c (°C)	Range of maximum product temperature during primary drying (°C)
MF1	-29.2	-27.5	-28.5 to -29.5
MF2	-32.4	-31.1	-31.5 to -32.5

T_g', glass transition temperature of the maximally freeze-concentrated solution; and T_c, collapse temperature

Construction of Process Design Space (PDS) for MF1

During the construction of the freeze-drying PDS, the limitations imposed by the freeze-dryer and formulation were considered. Patel and Pikal reported that the majority of manufacturing dryers cannot control chamber pressures less than 0.06 mbar and that there is no additional advantage in sublimation rate for chamber pressures greater than 0.40 mbar [Patel & Pikal, 2013]. To verify these limitations, preliminary experiments were performed as follows: (i) a sublimation test using pure water at a chamber pressure of 0.05 mbar and a shelf temperature of -10 °C. This test provided an average sublimation rate of 0.319 g/h·vial, which exceeds the expected average sublimation rate of the model formulations at the same chamber pressure. Therefore, it can be safely assumed that 0.05 mbar and greater chamber pressures would not experience chocking flow for the expected sublimation rates of

the model formulations studied; (ii) sublimation tests using both model formulations at a chamber pressure of 0.25 mbar and a shelf temperature of -25 °C. Although these processing conditions yielded average product temperatures close to T_c (-29.7 °C for MF1 and -31.0 °C for MF2), the corresponding average sublimation rates (0.074 g/h·vial for MF1 and 0.089 g/h·vial for MF2) were considerably less than the sublimation rates obtained at lower chamber pressures and similar product temperatures. Therefore, chamber pressures greater than 0.25 mbar would have no benefit from a sublimation rate point of view.

The DoE displayed in Table 12 was developed considering the information obtained from the previously mentioned preliminary experiments. Representative results of the freeze-drying experiments are presented in Table 14. The results for all the processing conditions displayed in the DoE (Table 12) were obtained in a similar manner (not indicated herein) and further processed.

The results displayed in Table 14 indicate remarkable differences in T_pave and the sublimation rates between the front edge and center vials. As supported by the experimental results displayed in Figure 42 and in the literature [Pikal et al., 2016; Scutellà et al., 2017a; 2017b & 2018b], even in a freeze-drying process with a minimum effect of radiation, there could be significant spatial variation in the shelf surface temperature. Cold spots were observed at the center of the shelf, indicating a temperature of approximately 4 °C colder than the hot spots, which were observed at the front edge of the shelf. These spatial shelf surface temperature variations could be attributed to the large thermal demand of the vials located at the center of the shelf compared to the vials located at the edge. The center vials have a higher vial packing density (number of vials per unit area). Hence, they absorb much larger energy during ice sublimation compared to the edge vials. This, in turn, leads to different product temperatures and sublimation rates of the vials placed at different locations across a shelf (see Figure 42). Therefore, consideration of such variations during the construction of a PDS is critical in the design of a robust freeze-drying process. Further, as indicated in Table 14, the sublimation rate is dependent on the chamber pressure. Thus, depending on the chamber pressure, similar product temperatures can produce different sublimation rates.

Table 14. Results of average product temperatures and sublimation rates at selected combinations of chamber pressure and shelf temperatures for MF1 and MF2

P_c (mbar)	T_s (°C)	Formulation	Front edge vials				Center vials			
			T_pave[a] (°C)	Sublimation rate (g/h·vial)			T_pave[a] (°C)	Sublimation rate (g/h·vial)		
				Max[b]	Min[c]	Ave[d]		Max[b]	Min[c]	Ave[d]
0.10	-15.0	MF1	-30.1	0.229	0.170	0.191	-32.6	0.137	0.115	0.121
	-17.0		-30.7	0.202	0.147	0.171	-33.5	0.113	0.102	0.107
	-20.0		-31.7	0.181	0.137	0.156	-34.2	0.110	0.088	0.099
0.20	-25.0		-32.1	0.159	0.114	0.129	-36.6	0.087	0.069	0.076
	-20.0		-28.9	0.223	0.175	0.193	-29.9	0.134	0.120	0.125
	-25.0		-29.8	0.165	0.125	0.138	-31.4	0.085	0.081	0.078
	-30.0		-31.7	0.094	0.069	0.078	-33.5	0.046	0.026	0.042
	-35.0		-34.7	0.055	0.035	0.044	-36.6	0.018	0.015	0.016
0.10	-15.0	MF2	-30.3	0.258	0.201	0.221	-31.4	0.150	0.121	0.131
	-17.0		-30.7	0.231	0.173	0.193	-32.8	0.127	0.102	0.109
	-20.0		-31.1	0.210	0.160	0.177	-33.2	0.115	0.086	0.091
0.20	-25.0		-32.0	0.156	0.127	0.137	-35.0	0.072	0.059	0.067
	-20.0		-30.1	0.272	0.208	0.232	-30.8	0.153	0.138	0.144
	-25.0		-31.3	0.174	0.145	0.157	-32.3	0.105	0.081	0.092
	-30.0		-32.2	0.131	0.095	0.108	-33.8	0.052	0.041	0.045
	-35.0		-34.5	0.077	0.046	0.057	-36.7	0.018	0.014	0.016

[a] the average product temperatures (T_pave) for each vial group were calculated as the arithmetic average of the temperature measurements in the time range used for sublimation rate calculation.
[b] the maximum sublimation rates were the maximum value of the sublimation rates from each vial group.
[c] the minimum sublimation rates were the minimum value of the sublimation rates from each vial group.
[d] the average sublimation rates were calculated as the arithmetic average of the sublimation rates from each vial group.
P_c, chamber pressure; T_s, shelf temperature; and T_pav, average product temperature

As displayed in Table 14 for MF1, a similar T_pave for front edge vials was obtained at Condition 1 (T_s = -20 °C/P_c = 0.10 mbar) and Condition 2 (T_s = -30 °C/P_c = 0.20 mbar). Analyzing Conditions 1 and 2, similar T_pave were obtained at different T_s values. Thus, to yield similar T_pave, a higher P_c requires a lower T_s.

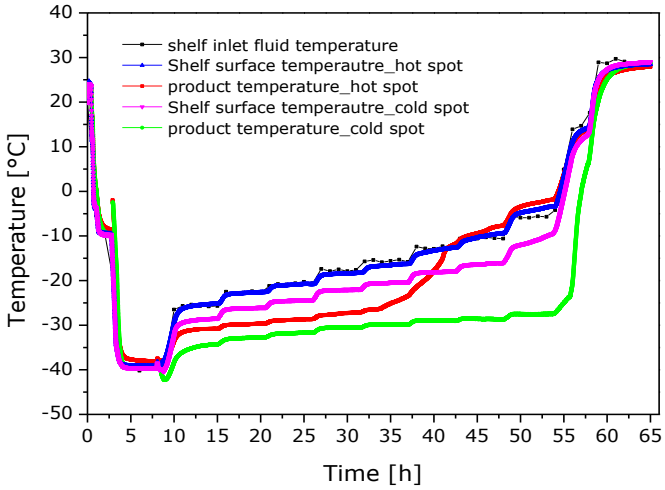

Figure 42. Experimental data showing significant spatial shelf surface temperature and product temperature differences across a shelf. Chamber pressure = 0.1 mbar.

This is because: (i) when the chamber pressure increases, the heat transfer rate due to gas conduction increases, leading to an increase in product temperature [Pikal et al., 1984]; and (ii) at constant P_i, high chamber pressures reduce the driving force for mass transfer rate, $P_i(T_p) - P_c$. The reduction in the endothermic mass transfer rate decreases the energy consumption from a vial, leading to an increase in product temperature, unless T_s is adjusted. It is important to note here that, although similar $T_p ave$ can be obtained at different P_c values, the corresponding sublimation rate values can be significantly different. Referring to the aforementioned conditions, the sublimation rates of the front edge vials under Condition 1 are significantly greater than under Condition 2. Similarly, although the center vials at Condition 1 had reduced $T_p ave$, their sublimation rates were considerably greater compared to the center vials under Condition 2. This is attributed to the fact that at a given T_p, the driving force for mass transfer rate, $P_i(T_p) - P_c$, decreases as P_c increases. Thus, for a given T_p, low P_c and high T_s produce a high mass transfer rate. Such knowledge and information for a specific drug product is essential to design the most optimized and robust freeze-drying process. A PDS can be used as a tool to choose the optimum process variables that yield the maximum possible mass transfer rate, without exceeding the maximum allowable product temperature during primary drying.

The construction of the PDS was started by plotting isotherms for the product temperature on a graph of shelf temperature versus chamber pressure, as displayed in Figure 43b. The product temperature isotherms were calculated from data obtained experimentally and represent the average product temperature of the front edge vials. The reason for selecting the front edge vials to define the product temperature was that this vial group had the highest product temperature in the vial arrays. Product temperatures were collected every 20 s. The average product temperature represents an average value of the product temperatures collected during the entire period of the sublimation test. Figure 43a presents the average product temperature of the front edge vials at the selected shelf temperature and chamber pressure. The results demonstrate an excellent linear relationship (R^2 > 0.94) of the average product temperature and shelf temperature at any given chamber pressure. Using regression analyses of the data points (solid lines, Figure 43a), possible combinations of chamber pressure and shelf temperature that produce any desired product temperature can be calculated. This information was used to construct the graph of chamber pressure versus shelf temperature with the isotherms of the product temperatures (Figure 43b).

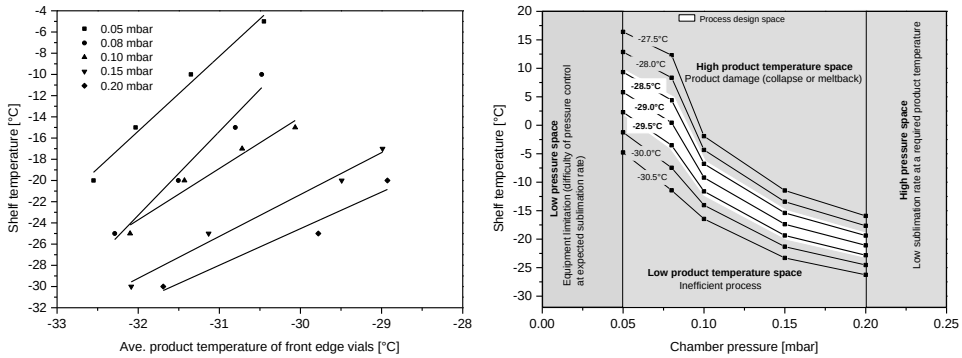

Figure 43. (a) Relationship between average product temperature of front edge vials and shelf temperature (at different chamber pressures) for MF1; and (b) PDS for primary drying of MF1 after formulation, process and equipment constraints.

As can be observed in Figure 43a, a change in the slope of the curves with increasing chamber pressure was observed. At relatively low chamber pressures, less than 0.08 mbar, the driving force for the sublimation rate is large, and thus the heat transfer becomes a rate-limiting factor of the drying process. In this case, as the

excess sublimation process consumes additional input energy, large changes in shelf temperature are required to produce an observable change in product temperature. Conversely, although high chamber pressures enhance the heat transfer rate, which is attributed to improved heat transfer via gas conduction [Pikal et al., 1984], they significantly reduce the driving force for mass transfer. Thus, the mass transfer becomes a rate-limiting factor of the drying process and any additional input energy, that is an increase in shelf temperature, has significant influence on the product temperature. This is evident from Figure 43a, where it can be observed that the curves at low chamber pressure have larger slopes than the curves at high chamber pressures. This fact has a quantifiable effect from a process robustness point of view. That is, a freeze-drying process designed at relatively low chamber pressure is more robust to small shelf temperature variations than a freeze-drying process designed at relatively high chamber pressure.

The range of maximum product temperature during primary drying for MF1 was defined from -29.5 °C to -28.5 °C (see Table 13). Further, lower and higher chamber pressure limits were defined based on the equipment and process constraints. This information was used to impose formulation, process, and equipment constraints, and the PDS was defined as displayed in Figure 43b. From Figure 43b, the process parameters that yielded a low product temperature space and high product temperature space can be easily identified. In the former, the product temperature is less than the desired range and leads to an unnecessarily long primary drying time (inefficient process), whereas in the latter, the resulting high product temperature leads to product damage (collapse or meltback), which compromises product CQAs. Although it has been reported that collapse does not lead to a loss of CQAs for drug products [Patel & Pika, 2013], additional experimental studies are required to study the effect of collapse on drug stability during storage [Wang et al., 2004; Schersch et al, 2010; 2012 & 2013; Ullrich et al., 2015; Patel et al., 2017; Duralliu et al., 2018; Haeuser et al., 2018]. Further, regulatory agencies require consistent, reproducible, and uniform cake appearance to ensure drug stability [Goldman et al., 2018].

From the PDS defined in Figure 43b, one would choose to use “high chamber pressure-low shelf temperature” or “low chamber pressure-high shelf temperature”

combinations to achieve the same product temperature. However, depending on the chamber pressure, the same product temperature can produce different sublimation rates. At a given product temperature, low chamber pressure yields a high sublimation rate. Thus, a further definition of the PDS including values for sublimation rate is necessary. To include such information, the data of sublimation rates are plotted against experimental product temperatures, as displayed in Figure 44a. Figure 44a contains the average product temperature of the front edge vials in the x-axis and the minimum sublimation rate of the center vials in the y-axis. As reported in the literature [Scutellà et al., 2017a; 2017b & 2018; Pikal et al., 2018] and determined experimentally in this study, the center vials have the lowest sublimation rate in the vial arrays. Therefore, Figure 44a allows consideration of the minimum sublimation rate during the construction of the PDS. This, in turn, avoids possible product damage due to premature change to the secondary drying step.

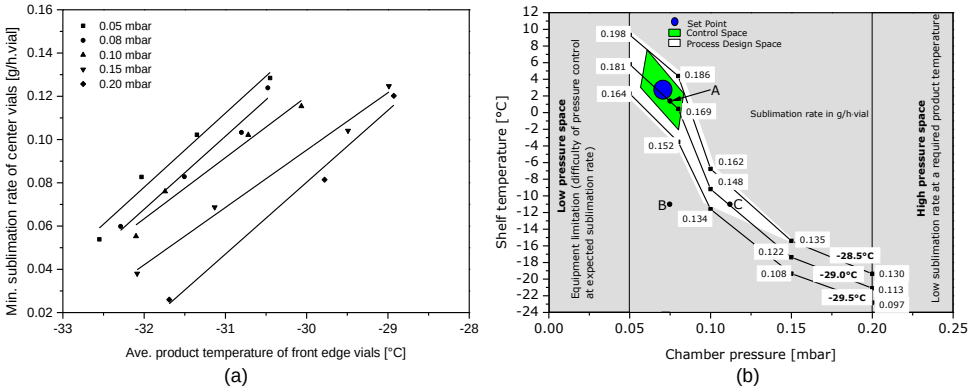

Figure 44. (a) Relationship of average product temperature of front edge vials and minimum sublimation rate of center vials (at different chamber pressures) for MF1. (b) Final PDS for primary drying of MF1, taking into consideration minimum sublimation rate of center vials. Relatively minimum values of sublimation rate (mostly in the region of high chamber pressure) were removed from the originally defined PDS (Figure 43b).

The choice of the average product temperature of the front edge vials in Figure 44a is because the product isotherms of the PDS (see Figure 43b) are based on this parameter. Therefore, information on the sublimation rate of the center vials, when the front edge vials achieve the target product temperature is required.

As indicated in Figure 44a, there is an excellent fitting of the experimental data (R^2 > 0.95) and regression analyses of the data were used to calculate the minimum sublimation rate of the center vials at a given chamber pressure and product temperature of the front edge vials. The initial PDS (Figure 43b) was re-defined after the sublimation rate values obtained from Figure 44a were included. The final PDS for MF1 is presented in Figure 44b.

The PDS defined in Figure 44b encompasses a wide range of T_s, P_c, and sublimation rate values. Thus, a control space within the PDS can be defined when the range of process parameters is small and well controlled. The control space is defined to encompass the highest sublimation rates within the PDS. However, it is recommended that the consideration of edge process parameters to account for batch-to-batch process variations be avoided. Process parameters for the primary drying step can be defined within the control space as a set point. The set point can be selected anywhere within the control space. However, to consider intra- and inter-batch variation in the process parameters, it is recommended to select the set point as the mid-point of the control space. At the set point, the minimum sublimation rate within the control space can be used to calculate the primary drying time.

Construction of Process Design Space (PDS) for MF2

The experimental data obtained for MF2 were analyzed in a similar manner to the method followed for MF1. Accordingly, the PDS for the second formulation was obtained. It is presented in Figure 45.

Experimental verification of the PDSs for MF1 and MF2

Because the calculations of the product temperatures and sublimation rates involve linear regression analyses, minor inaccuracies in the corresponding values could occur. Therefore, it is important to verify, experimentally, that the PDS obtained in this study yields the expected product temperatures and sublimation rates of the model formulations. Freeze-drying experimental runs were performed at selected set point values for both model formulations. The values of the set point parameters were selected from Figures 44b and Figure 45, as follows:

- For MF1: P_c = 0.075 mbar, T_s = 3 °C, Fill volume = 3 mL
- For MF2: P_c = 0.075 mbar, T_s = -16 °C, Fill volume = 3 mL

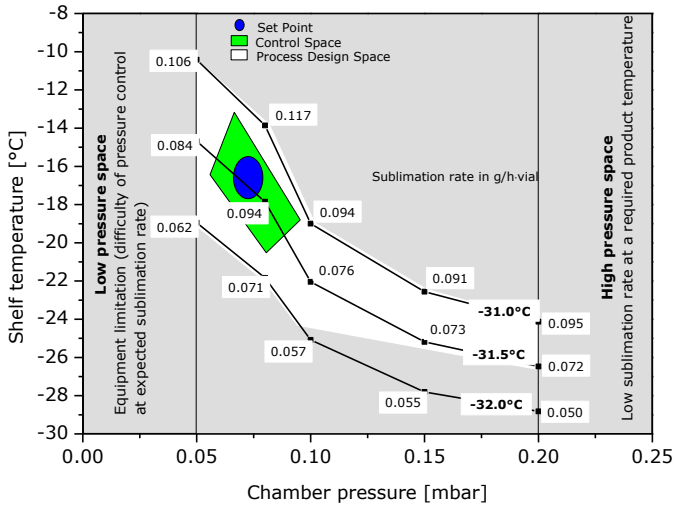

Figure 45. Final PDS for primary drying of MF2, taking into consideration the minimum sublimation rate. Relatively minimum values of sublimation rate (mostly in the region of high chamber pressure) were removed from the originally defined process design space.

The freezing protocol in these verification experiments was the same as the freeze protocol used for the construction of the PDS. This minimizes any possible variation of drying behavior due to the freezing protocol. The product temperatures of the center and front edge vials were measured using wireless thermologgers (four for each vial group). The sublimation rates of the center vials were determined gravimetrically and, for this purpose, 16 center vials were weighed before and after the experiment.

Figure 46 displays the product temperature profiles of MF1 and MF2 obtained from the verification experiments.

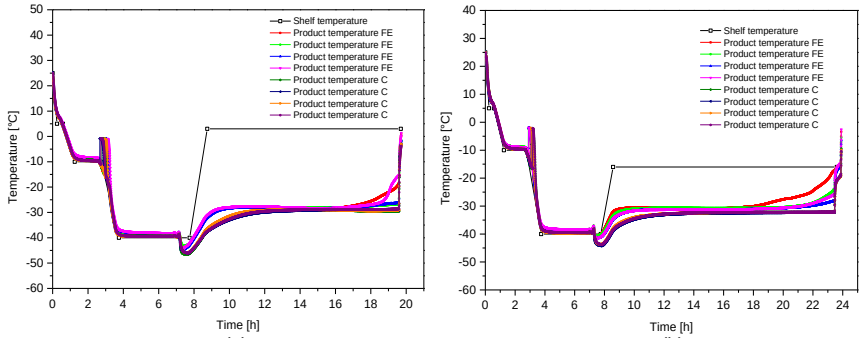

Figure 46. Experimental verification of the process design space. (a) Product temperature profiles of front edge vials (FE) and center vials (C) for MF1; (b) Product temperature profiles of front edge vials (FE) and center vials (C) for MF2.

Further, the estimated parameters from the PDS were compared to the parameters obtained from the verification experiments. They are presented in Table 15.

Table 15. Comparison of PDS-estimated and experimentally determined parameters at set point

Formulation	PDS estimated values				Experimentally determined values				Differences (%)			
	FE	C			FE	C			FE	C		
	$T_p ave$ (°C)	$T_p ave$ (°C)	$\dot{m}$ (g/h·vial)	t_d[c] (h)	$T_p ave$[a] (°C)	$T_p ave$[a] (°C)	$\dot{m}$[b] (g/h·vial)	t_d[d] (h)	$T_p ave$	$T_p ave$	$\dot{m}$	t_d
MF1	-28.7	-31.0	0.169	16.0	-28.4	-30.1	0.177	15.3	1.05	2.90	4.73	4.38
MF2	-31.2	-33.4	0.094	25.5	-31.3	-32.8	0.104	23.1	0.32	1.80	10.64	9.41

[a] $T_p ave$ was obtained by averaging product temperatures obtained from 4 thermologgers
[b] $\dot{m}$ is the minimum value of 16 sublimation rate values
[c] t_d is calculated based on the minimum sublimation rate within the control space and based on 3 mL fill volume
[d] t_d is calculated based on the minimum sublimation rate of the 16 experimentally determined sublimation rate values and based on 3 mL fill volume
$T_p ave$, average product temperature; $\dot{m}$, sublimation rate; t_d, drying time of primary drying; FE, front edge vials; and C, center vials

As indicated in Figure 46 and Table 15, there is an excellent agreement between the PDS-estimated and the experimentally determined values for both model formulations. This demonstrates that the procedures described in this paper for the construction of an effective and product-based PDS, coupled with an effective DoE, produce highly accurate and reproducible results. This can enable process scientists to design freeze-drying processes for a given pharmaceutical drug formulation based on a scientific approach, using limited well-defined experimental runs.

Utilization of the lab PDS for process scale-up and transfer

Equipment capability: Mainly due to their large capacity, chocking flow could be more pronounced at manufacturing scale freeze dryers. Therefore, it is critical to determine the capability of the target freeze dryer to control the P_c at full load capacity and at typical freeze-drying sublimation rates. The determination of the capability of a target freeze dryer could be done using a one-point water sublimation test as follows: (i) fully load the target freeze dryer with pure water placed on a tray made from plastic; (ii) freeze the water and allow complete solidification; (iii) set the P_c to 0 and increase the T_s to +30 °C or +40 °C; (iv) observe the minimum P_c, and its stability, attained by the freeze dryer after the T_s setpoint has been reached. Although the calculation of the exact value of the total vapor flow rate could be difficult, it could be assumed that the total vapor flow rate of pure water, at a T_s value ranging from +30 °C to +40 °C and a controllable low P_c, is much higher than most of the typical vapor flow rates obtained using drug formulations. Thus, if a freeze dryer is able to attain and control a minimum P_c of, for example, 50 µbar when pure water at a T_s of +30 °C or +40 °C is used, it could be safely concluded that the occurrence of chocked flow for P_c up to 50 µbar is highly unlikely when a drug formulation at typical primary drying T_s values is used.

Differences in resistance to mass transfer of the dried product (R_p) and overall vial heat transfer coefficient (K_v): The differences in R_p and K_v between laboratory and manufacturing scale freeze dryers are the major freeze-drying process scale-up and transfer factors. Differences in R_p could be caused by variations in the degree of supercooling, which could be affected by differences in cleanness between laboratory and manufacturing environments. On the other hand, differences in K_v could arise from differences in design and performance of the dryers. Differences in R_p and K_v during scale-up or transfer could be easily detected from T_p response, provided that identical primary drying processing conditions (i.e., T_s and P_c) are used. Thus, at the same processing conditions, an increase in R_p is reflected by an increase in T_p. Because the vapor flow is more restricted at higher R_p, there is less energy consumption from the system and most of the heat input is utilized to increase

the T_p. Conversely, at low R_p, most of the heat input is consumed by the relatively higher sublimation rate (attributed to the lower resistance to vapor flow), and hence the T_p becomes lower. An increase in K_v, at the same T_s and P_c, leads to an increase in T_p and vice versa. However, the influence of K_v on freeze-drying process scale-up and transfer could be significantly minimized by using the same container-closure system and a laboratory scale freeze dryer with similar design and performance to a manufacturing scale freeze dryer. Therefore, the most important factor that could cause differences in T_p during scale-up or transfer is R_p.

From the above discussion, the T_s (keeping P_c constant) at the target freeze dryer that is needed to obtain the $T_p t$ could be different, and thus determination of the new T_s and adjustment of the t_d would be the major scale-up or transfer experiments. With this regard, the PDS developed at lab scale provides important information that could be utilized during the scale-up or transfer experiments: (i) the range of possible T_s values that could be used to determine the new T_s; (ii) the robustness of the formulation to T_s changes; and (iii) variation of sublimation rates at different processing conditions. Considering possible variations in R_p, a T_s range from -12 °C to +12 °C at a P_c = 0.075 mbar could yield the $T_p t$ for MF1 (cf. Figure 44b). Such information could be utilized to perform a temperature ramp experiment using the target freeze dryer to obtain the new T_s value. Point A of Figure 44b shows that, at P_c = 0.075 mbar, a T_s around +1 °C was required to yield a T_p of -29.0 °C. Assuming that the new T_s value, at the target freeze dryer and P_c = 0.075 mbar, required to yield a T_p of -29.0 °C was -11 °C (Point B, Figure 44b), the corresponding differences in sublimation rates, and thus in t_d, of point A and point B could be adjusted using the PDS developed at lab scale. The reduction in sublimation rate caused by an increase in R_p (thus a decrease in T_s) at constant P_c (Point B, Figure 44b) is equivalent to a reduction in sublimation rate caused by an increase in P_c (thus a decrease in T_s) at constant R_p, provided that the T_p is the same for both cases. Considering the same formulation, product temperature, and processing environment, the R_p at laboratory scale can be assumed as fairly constant at the different processing conditions. Furthermore, assuming the reduction in T_s at the target freeze dryer is due entirely to the increase in R_p, the sublimation rate at the

new T_s value (i.e., -11 °C) and T_p = -29.0 °C from the PDS (point C, Figure 44b) could be used to adjust the sublimation rate and the t_d at the target freeze dryer.

4.3.4. Conclusions

A new step-by-step procedure for the construction of a product-based PDS for the primary drying step was described. An effective DoE was developed, which could then be used to experimentally determine the necessary information for the construction of the PDS. The development of an effective DoE requires a profound scientific understanding of the formulation and process, and perhaps requires only limited preliminary experiments. The proposed product-based PDS considers variations in product temperatures and sublimation rates within the vial arrays. With this regard, the product temperature of the front edge vials and sublimation rate of the center vials were used. This assures the effectiveness and the robustness of the PDS. Compared to the mathematical models that could require several freeze-drying experiments for optimization and verification, the product-based PDS detailed herein produced highly accurate results, demonstrating the potential for significant development time and material savings. Further, the PDS of a drug formulation based on experimental results presents more realistic and reliable data if there is an intention of using the PDS for regulatory agencies. Experimental verifications of the PDS for the two formulations studied in this research were performed and an excellent agreement between the PDS predicted values and experimentally determined values were achieved. Finally, coupled with an effective DoE, the proposed procedure for the construction of a product-based PDS considerably reduces development time and material requirements, and significantly improves the accuracy, effectiveness, and robustness of the resulting freeze-drying process. Thus, process scale-up problems are minimized with the development of a PDS. Further, the resulting optimum and robust freeze-drying process has significant advantages in process cost and energy savings, and in maintaining product quality consistency during a large-scale manufacturing process.

4.3.5. References

[1]. Adams GDJ, Ramsay JR. Optimizing the lyophilization cycle and the consequences of collapse on the pharmaceutical acceptability of *Erwinia L-Asparaginase*. *J Pharm Sci.* 1996;85:1301–1305.

[2]. Arsiccio A, Pisano R. Application of the Quality by Design approach to the freezing step of freeze-drying: building the design space. *J Pharm Sci.* 2018;107:1586–1596.

[3]. Bosca S, Barresi AA, Fissore D. Fast freeze-drying cycle design and optimization using a PAT based on the measurement of product temperature. *Eur J Pharm Biopharm*. 2013;85:253–62.

[4]. Chang BS, Fischer NL. Development of an efficient single-step freeze-drying cycle for protein formulations. *Pharm Res.* 1995;12: 831–837.

[5]. Chang BS, Randall CS. Use of sub-ambient thermal analysis to optimize protein lyophilization. *Cryobiology.* 1992;29:632–656.

[6]. Chen X, Sadineni V, Maity M, Quan Y, Enterline M, Mantri RV. Finite element method (FEM) modeling of freeze-drying: monitoring pharmaceutical product robustness during lyophilization. *AAPS PharmSciTech.* 2015;16:1317–1326.

[7]. Duralliu A, Matejtschuk P, Williams DR. Humidity induced collapse in freeze dried cakes: A direct visualization study using DVS. *Eur J Pharm Biopharm.* 2018;127:29–36.

[8]. Fissore D, Pisano R, Barresi AA. Advanced approach to build the design space for the primary drying of a pharmaceutical freeze-drying process. *J Pharm Sci.* 2011;100:4922–4933.

[9]. Fissore D, Pisano R. Computer-aided framework for the design of freeze-drying cycles: optimization of the operating conditions of the primary drying stage. *Processes.* 2015;3:406–421.

[10]. Ganguly A, Alexeenko AA, Schultz SG, Kim SG. Freeze-drying simulation framework coupling product attributes and equipment capability: toward accelerating process by equipment modifications. *Eur J Pharm Biopharm*. 2013;85:223–35.

[11]. Ganguly A, Varma N, Sane P, Bogner R, Pikal MJ, Alexeenko A. Spatial variation of pressure in the lyophilization product chamber part 1: Computational modeling. *AAPS PharmSciTech.* 2017;18:577–585.

[12]. Gieseler H, Kramer T, Pikal MJ. Use of Manometric Temperature Measurement (MTM) and SMART™ freeze dryer technology for development of an optimized freeze-drying cycle. *J Pharm Sci.* 2007;96:3402–3418.

[13]. Giordano A, Barresi AA, Fissore D. On the use of mathematical models to build the design space for the primary drying phase of a pharmaceutical lyophilization process. *J Pharm Sci.* 2011;100:311–324.

[14]. Goldman JM, More HT, Yee O, Borgeson E, Remy B, Rowe J, Sadineni V. Optimization of primary drying in lyophilization during early-phase drug development using a definitive screening design with formulation and process factors. *J Pharm Sci.* 2018;107:2592–2600.

[15]. Goshima H, Do G, Nakagawa K. Impact of ice morphology on design space of pharmaceutical freeze-drying. *J Pharm Sci.* 2016;105:1920–1933.

[16]. Haeuser C, Goldbach P, Huwyler J, Friess W, Allmendinger A. Imaging techniques to characterize cake appearance of freeze-dried products. *J Pharm Sci.* 2018;107:2810–2822.

[17]. Her LM, Nail SL. Measurement of glass transition temperatures of freeze-concentrated solutes by differential scanning calorimetry. *Pharm Res.* 1994;11:54–59.

[18]. Kodama T, Sawada H, Hosomi H, Takeuchi M, Wakiyama N, Yonemochi E, Terada K. Determination for dry layer resistance of sucrose under various primary drying conditions using a novel simulation program for designing pharmaceutical lyophilization cycle. *Int J Pharm.* 2013;452:180–187.

[19]. Kodama T, Sawada H, Hosomi H, Takeuchi M, Wakiyama N, Yonemochi E, Teradad K. Optimization of primary drying condition for pharmaceutical lyophilization using a novel simulation program with a predictive model for dry layer resistance. *Chem Pharm Bull.* 2014;62:153–159.

[20]. Koganti VR, Shalaev EY, Berry MR, Osterberg T, Youssef M, Hiebert DN, Kanka FA, Nolan M, Barrett R, Scalzo G, Fitzpatrick G, Fitzgibbon N, Luthra S, Zhang L. Investigation of design space for freeze-drying: Use of modeling

for primary drying segment of a freeze-drying cycle. *AAPS PharmSciTech.* 2011:12;854–861.

[21]. Kshirsagar V, Tchessalov S, Kanka F, Hiebert D, Alexeenko A. Determining maximum sublimation rate for a production lyophilizer: computational modeling and comparison with ice slab tests. *J Pharm Sci.* 2019;108:382–390.

[22]. Kuu WY, Nail SL. Rapid freeze-drying cycle optimization using computer programs developed based on heat and mass transfer models and facilitated by Tunable Diode Laser Absorption Spectroscopy (TDLAS). *J Pharm Sci.* 2009;98:3469–3482.

[23]. Liu J. Physical characterization of pharmaceutical formulations in frozen and freeze-dried solid states: techniques and applications in freeze-drying development. *Pharm Dev Technol.* 2006;11:3–28.

[24]. Mortier STFC, Van Bockstal PJ, Corver J, Nopens I, Gernaey KV, De Beer T. Uncertainty analysis as essential step in the establishment of the dynamic Design Space of primary drying during freeze-drying. *Eur J Pharm Biopharm*. 2016;103:71–83.

[25]. Patel S, Jameel F, Sane S, Kamat M. Lyophilization process design and development using QbD principles. In: Jameel F., Hershenson S., Khan M., Martin-Moe S., eds. *Quality by design for biopharmaceutical drug product development. AAPS Advances in the Pharmaceutical Sciences Series, vol 18.* Springer, New York, USA. 2015:303–329.

[26]. Patel SM, Jameel F, Pikal MJ. The effect of dryer load on freeze drying process design. *J Pharm Sci.* 2010;99:4363–4379.

[27]. Patel SM, Nail SL, Pikal MJ, Geidobler R, Winter G, Hawe A, Davagnino J, Rambhatla GS. Lyophilized drug product cake appearance what is acceptable? *J Pharm Sci.* 2017;106:1706–1721.

[28]. Patel SM, Pikal MJ. Lyophilization process design space. *J Pharm Sci.* 2013;102:3883–3887.

[29]. Pikal MJ, Bogner R, Mudhivarthi V, Sharma P, Sane P. Freeze-drying process development and scale-up: scale-up of edge vial versus center vial heat transfer coefficients, Kv. *J Pharm Sci.* 2016;105:3333–3343.

[30]. Pikal MJ, Cardon S, Bhugra C, Jameel F, Rambhatla S, Mascarenhas WJ, Akay HU. The non-steady state modeling of freeze-drying: in-process product temperature and moisture content mapping and pharmaceutical product quality applications. *Pharm Dev Technol.* 2005;10: 17–32.

[31]. Pikal MJ, Pande P, Bogner R, Sane P, Mudhivarthi V, Sharma P. Impact of natural variations in freeze-drying parameters on product temperature history: application of quasi steady-state heat and mass transfer and simple statistics. *AAPS PharmSciTech*. 2018;19:2828–2842.

[32]. Pikal MJ, Roy ML, Shah S. Mass and heat transfer in vial freeze-drying of pharmaceuticals: role of the vial. *J Pharm Sci.* 1984;73:1224–1237.

[33]. Pikal MJ. Freeze-drying of proteins. Part I: Process design. *BioPharm.* 1990a;3:18–27.

[34]. Pikal MJ. Freeze-drying of proteins. Part II: Formulation selection. *BioPharm.* 1990b;10:26–30.

[35]. Pikal MJ. Use of laboratory data in freeze-drying process design: heat and mass transfer coefficients and the computer simulation of freeze-drying. *J Parenter Sci Technol.* 1985;39:115–139.

[36]. Schersch K, Betz O, Garidel P, Muehlau S, Bassarab S, Winter G. Systematic investigation of the effect of lyophilizate collapse on pharmaceutically relevant proteins I: stability after freeze-drying. *J Pharm Sci.* 2010;99:2256–2278.

[37]. Schersch K, Betz O, Garidel P, Muehlau S, Bassarab S, Winter G. Systematic investigation of the effect of lyophilizate collapse on pharmaceutically relevant proteins, part 2: stability during storage at elevated temperatures. *J Pharm Sci.* 2012;101:2288–2306.

[38]. Schersch K, Betz O, Garidel P, Muehlau S, Bassarab S, Winter G. Systematic investigation of the effect of lyophilizate collapse on pharmaceutically relevant proteins III: collapse during storage at elevated temperatures. *Eur J Pharm Biopharm.* 2013;85:240-252.

[39]. Scutellà B, Plana-Fattoric A, Passot S, Bourlès E, Fonseca F, Flick D, Tréléa IC. 3D mathematical modelling to understand atypical heat transfer observed in vial freeze-drying. *Appl. Therm. Eng*. 2017a;126:226–236.

[40]. Scutellà B, Bourlès E, Plana-Fattori A, Fonseca F, Flick D, Tréléa IC, Passot S. Effect of freeze dryer design on heat transfer variability investigated using a 3D mathematical model. *J Pharm Sci.* 2018b;107:2098–2106.

[41]. Scutellà B, Passot S, Bourlés E, Fonseca F, Tréléa IC. How vial geometry variability influences heat transfer and product temperature during freeze-drying. How vial geometry variability influences heat transfer and product temperature during freeze-drying. *J Pharm Sci.* 2017b;106:770–778.

[42]. Scutellà B, Tréleéa IC, Bourlès E, Fonseca F, Passot S. Determination of the dried product resistance variability and its influence on the product temperature in pharmaceutical freeze-drying. *Eur J Pharm Biopharm*. 2018a;128:379–388.

[43]. Sharma P, Kessler WJ, Bogner R, Thakur M, Pikal MJ. Applications of the tunable diode laser absorption spectroscopy: in-process estimation of primary drying heterogeneity and product temperature during lyophilization. *J Pharm Sci.* 2019;108:416–430.

[44]. Sundaram J, Shay YHM, Hsu CC, Sane SU. Design space development for lyophilization using DOE and process modeling. *BioPharm Int.* 2010;23:26–36.

[45]. Tang X, Pikal MJ. Design of freeze-drying processes for pharmaceuticals: Practical advice. *Pharm Res.* 2004;21:191–200.

[46]. Ullrich S, Seyferth S, Lee G. Measurement of shrinkage and cracking in lyophilized amorphous cakes. Part I: final-product assessment. *J Pharm Sci.* 2015;104:155–164.

[47]. US Department of Health and Human Services, Food and Drug, Administration, Center for Drug Evaluation and Research (CDER), Center for Biologics Evaluation and Research (CBER). ICH Q8(R2) Pharmaceutical Development, 2009.

[48]. Van Bockstal PJ, Mortier STFC, Corver J, Nopens I, Gernaey KV, De Beer T. Quantitative risk assessment via uncertainty analysis in combination with error propagation for the determination of the dynamic Design Space of the primary drying step during freeze-drying. *Eur J Pharm Biopharm.* 2017;121:32–41.

[49]. Wang DQ, Hey JM, Nail SL. Effect of collapse on the stability of freeze-dried recombinant factor VIII and a-amylase. *J Pharm Sci.* 2004;93:1253–1263.

[50]. Wang DQ. 2010. Formulation characterization. In: Rey L, May JC., eds. *Freeze drying/lyophilization of pharmaceutical and biological products, 3rd Edition*. Informa Healthcare, London, UK. 2010: 233–253.

[51]. Ward KR, Matejtschuk P. Characterization of formulations for freeze-drying. In: Ward K, Matejtschuk P. eds. *Lyophilization of pharmaceuticals and biologicals. Methods in pharmacology and toxicology.* Humana Press, New York, USA. 2019:1–32.

[52]. Velardi SA, Barresi AA. Development of simplified models for the freeze-drying process and investigation of the optimal operating conditions. *Chem Eng Res Des.* 2008;86:9–22.

[53]. Zhu T, Moussa EM, Witting M, Zhou D, Sinha K, Hirth M, Gastens M, Shang S, Nere N, Somashekar SC, Alexeenko A, Jameel F. Predictive models of lyophilization process for development, scale-up/tech transfer and manufacturing. *Eur J Pharm Biopharm*. 2018;128:363–378.

4.4. Optimization of the secondary drying process: a case study

The following sub-section has been submitted for publication to Drying Technology in the form of a research article (see Appendix A.4).

4.4.1. Introduction

The freeze-drying process consists of two major process steps: (1) *freezing step*, in which a liquid formulation is converted into a frozen solid state; (2) *drying step*, during which the frozen and unfrozen solvent (usually water) is removed from the product. Depending on the drying mechanism, the drying step is further classified into two steps; primary drying and secondary drying. The primary drying step refers to the removal of the frozen solvent through a sublimation process. Therefore, at the end of the primary drying step, there could be a significant amount of residual solvent related to the unfrozen solvent. Most commonly, the unfrozen solvent is adsorbed in the highly concentrated solid phase of an amorphous formulation even though, in a rare occurrence, it may also adsorb, in the form of crystalline hydrates, on the surface of a crystalline product [Pikal et al., 1990]. In an amorphous formulation, the unfrozen water may account up to 20% of the total solvent [Nail et al., 2002]. Although

desorption of the unfrozen solvent could immediately follow the dried region during the primary drying step, the desorption rate is very low owing to the low process temperature during the primary drying step. Therefore, an additional drying step at an elevated temperature is necessary to reduce the moisture content (MC) of the product to an acceptable level. In the context of the freeze-drying process, this additional drying step is termed as secondary drying. The secondary drying step refers to a process step that involves removal of the unfrozen solvent (bound solvent) through a desorption process.

The complete desorption process consists of the following processes [Pikal et al., 1990]: (1) adsorbed solvent is diffused from the interior matrix of an amorphous solid to the surface of the solid; (2) evaporation of the solvent from the solid surface; and (3) vapor transport from the interior of the dried product all the way to the condenser. The first two processes, i.e., diffusion of adsorbed solvent to the surface and evaporation of the solvent from the surface, are believed to be the rate limiting processes during the secondary drying [Pikal et al., 1990]. Therefore, to overcome these rate-limiting factors, the temperature during the secondary drying step is increased to as high as 40°C [Colandene et al., 2007; Abdul-Fattah et al., 2008]. The maximum process temperature during the secondary drying is limited by the temperature sensitivity and the glass transition temperature (T_g) of the formulation components, especially for amorphous formulations. On one hand, some formulation components may not allow high processing temperature during the secondary drying. On the other hand, because of the significant amount of water content left after the completion of the primary drying, the T_g of the product is still very low. Therefore, both the heating rate and the final drying temperature of the secondary drying should be selected taking into account that the actual product temperature must always be kept below the momentary T_g of the product. The T_g of the product increases with continuous loss of water; therefore, the secondary drying process temperature could be slowly increased to a final drying temperature (T_d) without affecting the product quality. The product is held at the final T_d for as long as the final moisture content (MC) reaches an acceptable level, usually less than 2 wt% on a dry basis. The MC of a freeze dried product is strongly correlated to its T_g, which, in turn, is strongly related to the storage stability of the dried product. The presence of

residual moisture in a dried product acts as a plasticizer and enhances mobility of the dried product, significantly decreasing the T_g of the dried product. In this sense, it is important to store a dried product in a temperature well below its T_g, otherwise the dried product may be meltdown and damaged during storage.

Presumably because of its relatively short processing time, only limited studies [Pikal et al., 1990; Liapis & Bruttini, 1995; Sheehan & Liapis, 1998; Pikal et al., 2005; Schneid et al., 2011; Fissore et al., 2011; Pisano et al., 2012; Tréléa et al., 2016; Oddone et al., 2017; Sahni & Pikal, 2017] have been focused on the optimization of the secondary drying step. However, for amorphous drug formulations with high solid content and high fill-volume, the secondary drying processing time could be very long. In this case, optimization of the secondary drying could offer a significant economic advantage. With this aim, this study focuses on optimizing the secondary drying step of a highly complex and amorphous drug formulation obtained from Fresenius Kabi (FK1). For this purpose, a response surface methodology (RSM) technique was employed to develop an effective design of experiments (DoE) for the secondary drying step of FK1. The results obtained from the DoE were discussed to understand the influence of secondary drying input parameters on MC and T_g. Further, construction of a process design space (PDS) and its use in the optimization of the secondary drying step of FK1 was discussed. It was demonstrated that such experimental analyses significantly simplified the optimization of the secondary drying step for FK1. Therefore, the analyses presented in this study could be used to optimize the secondary drying step of other drug formulations in a result- and scientific-based approach.

4.4.2. Experimental details

4.4.2.1. Materials

A Fresenius Kabi drug formulation (FK1) was used for this study. FK1 was prepared in-house according to the preparation procedure provided by Fresenius Kabi Deutschland GmbH (Friedberg, Germany). FK1 is a complex and fully amorphous formulation (see Table 16 for more information). All vials used in this study were 10-

mL tubing vials purchased from SCHOTT AG (Mainz, Germany). The stoppers were Igloo single vented gray stoppers from West Pharmaceutical Services, Inc. (West Pharmaceutical Services, Inc., Exton, PA, USA).

Table 16. Composition and characteristics of FK1

Formulation	Solid excipients	Liquid excipients	APIs	Solid content [%]	Fill-volume [mL]	Crystallinity	T_g' [°C]	T_c [°C]
FK1	Trehalose, Emulsifier, and co-emulsifier	Water and oil	several different APIs	18.5	5	Fully amorphous	-35.2	-29.0

FK1, Fresenius Kabi's drug formulation; APIs, active pharmaceutical ingredients; T_g', glass transition temperature of the maximally freeze concentrate solution; T_c collapse temperature

4.4.2.2. Methods

Glass transition temperature (T_g)

The glass transition temperature of the dried cake (T_g) was measured using a TA instruments Q2000 series differential scanning calorimeter with refrigerated cooling system (RCS) (TA Instruments, New Castle, DE, USA). 10–15 mg of dried FK1 were weighed into aluminum sample pans and the pans were hermetically sealed. An empty, hermetically sealed, pan was used as a reference. The program detailed in section 3.2.1 was used for the determination of T_g the dried product. The T_g values were determined using Universal Analysis software of the DSC thermograms and they were reported as the midpoint of the glass transition curve. At each of the conditions studied, three different vials were used to perform triplicate measurements and the average T_g was used for further analyses.

Moisture content (MC)

Moisture content (MC) of the dried products was determined using a Karl Fischer titrator (Metrohm, Herisau, Switzerland). The Karl Fischer titrator used in the present study was a coulometric titrator with thermoprep oven. In this setup, a sample is heated in the thermoprep oven, releasing its moisture. The moisture is then

conveyed to the measuring cell with the aid of a gas flow, where it is reacted with iodine. The Karl Fischer titrator is controlled using a dedicated software, Tiamo™ 2.5 (Metrohm, Herisau, Switzerland). The water content determination protocol was described in section 3.2.3. At each of the conditions studied, three different vials were used to perform triplicate measurements and the average MC was used for further analyses.

Experimental freeze-drying procedure

All the freeze-drying experiments were performed using a HOF laboratory freeze dryer (HOF Sonderanlagenbau GmbH, Lohra, Germany), as detailed in section 3.1.3. A pirani gauge was used for vacuum control during the freeze-drying process. Freeze-drying experiments of FK1 were carried out in 10-mL tubing vials and, for each experiment, 176 vials (one fully loaded shelf) were filled with 5 mL FK1 and placed on one of the four shelves of the freeze dryer. Four wireless thermologgers (Lives International, Timis, Romania) were used to measure the product temperatures. The wireless themologgers were set to measure product temperatures every 20 s during the complete freeze-drying experiment. The primary drying step of FK1 was designed based on a procedure previously described in sections 4.2 and 4.3. Thus, the freezing and the primary drying steps were held constant for all the freeze-drying experiments as follows: *Freezing:* 1 °C/min down to -10 °C and 90 min holding time; further freezing to -40 °C at 1 °C/min and 240 min holding time; *Primary drying:* Evacuating chamber pressure to 0.10 mbar and heating shelf temperature to -10 °C at 1 °C/min and holding for 40 hours. Conversely, the secondary drying was performed as follows: Reducing chamber pressure to 0.05 mbar; heating shelf temperature to 5 °C at 0.05 °C/min; further heating shelf temperature to a designed drying temperature (T_d) at 1 °C/min and holding for a designed drying time (t_d). The designed T_d and t_d were varied according to the DoE presented in Table 17. Once the designed secondary drying was completed, the lyophilization process was terminated by backfilling the product chamber using dry nitrogen. Some selected vials were immediately sealed and used to analyze the MC and T_g.

To study the effect of vial position on the secondary drying output parameters, vial samples were taken from four different vial positions within a shelf. The placement of sample and thermocoupled vials is displayed in Figure 47. As shown in Figure 47, sample vials from center vials (C), front edge vials (FE), side edge vials (SE), and rear edge vials (RE) were taken to analyze the MC and T_g of their corresponding group. Product temperature of the front edge and center vials were measured using the wireless thermologgers.

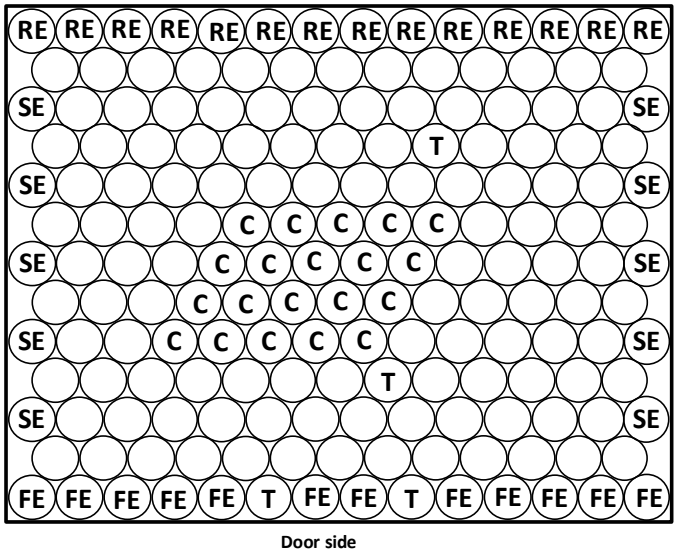

Figure 47. Sample vials placement to study the effect of vial position on the secondary drying output parameters. FE is front edge vials, C is center vials, SE is side edge vials and RE is rear edge vials. T-signed vials represent thermocoupled vials.

The effect of chamber pressure on secondary drying was studied separately as follows: (i) after the completion of the primary drying, the chamber pressure was reduced to 0.05 mbar and, at the same time, the shelf temperature was heated to 5 °C at 0.05 °C/min; (ii) further adjustment of the chamber pressure to a designed chamber pressure (P_c), at the same time, the shelf temperature was heated to 37 °C at 1 °C/min; (iii) the holding time at a designed P_c and 37 °C was 12 h. The T_d (37 °C) and t_d (12 h) were chosen as optimum process parameters from the analyses of the experiments presented in Table 17. The designed P_c studied here were 0.05, 0.20, and 0.40 mbar. During these experiments, the freezing and primary drying steps were kept identical to the main experiments, as described previously.

For the verification experiment, the lyophilizer was fully loaded with 5 mL FK1 (i.e., four fully loaded shelves) and identical freezing and primary drying process steps to the DoE experiments were employed. The optimum secondary drying processing parameters were obtained from the PDS (cf. results and discussion) and performed as follows: Reducing chamber pressure to 0.05 mbar; heating shelf temperature to 5 °C at 0.05 °C/min; further heating shelf temperature to the optimum drying temperature (T_d) at 1 °C/min and holding for the optimum drying time (t_d). Once the lyophilization process was completed, it was terminated by backfilling the product chamber using dry nitrogen. Some selected front edge and center vials were immediately sealed and used to analyze the MC and T_g.

Design of Experiments (DoE)

A response surface methodology (RSM) technique was employed to develop a DoE based on the knowledge of the critical input and output process parameters of the secondary drying (Figure 48) and the drug formulation.

As illustrated in Figure 48, chamber pressure is one of the critical input process parameters. However, to reduce the number of experiments, the influence of P_c on MC and T_g was studied once the optimum T_d and t_d has been defined, as previously described.

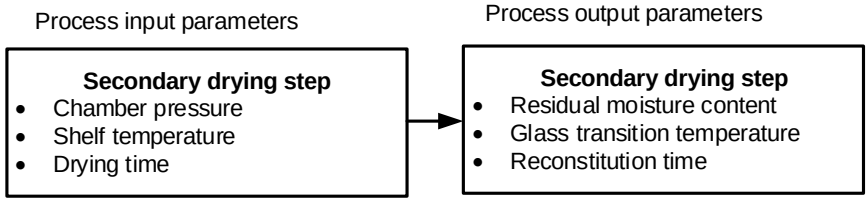

Figure 48. Critical input and output process parameters of the secondary drying step.

Therefore, only the shelf temperature (T_d) and t_d were considered during the development of DoE. The values of T_d and t_d were defined from preliminary experiments using FK1.

The DoE developed for this study is presented in Table 17.

Table 17. Response surface methodology-based DoE for the secondary drying of FK1.

Factors	t_d (h)	T_d (°C)	*Normalized values*
Levels	10.0	30.0	-1
	15.0	35.0	0
	20.0	40.0	1

Experiment number	Secondary drying input parameters			Secondary drying output parameters
	P_c (mbar)	t_d (h)	T_d (°C)	
1	0.05	0	1	MC, T_g
2		0	0	
3		1	1	
4		-1	0	
5		1	-1	
6		1	0	
7		0	0	
8		-1	1	
9		0	0	
10		-1	-1	
11		0	-1	

t_d, drying time; T_d, drying temperature; P_c, chamber pressure; MC, moisture content; T_g, glass transition temperature

4.4.3. Results and discussion

In the following sub-sections, the results of the center vials were used to analyze the influence of T_d and t_d on MC and T_g. This is because the center vials had the lowest MC and, consequently, the highest T_g compared to the edge vials (cf. *Influence of vial position on secondary drying output parameters* for details).

Influence of secondary drying temperature (T_d) on secondary drying output parameters: Figure 49 illustrates the influence of T_d on MC and T_g of center vials at different drying times. As seen in Figure 49, an increase in T_d from 30 °C to 40 °C yielded approximately 40% reduction in MC, regardless of the total t_d used.

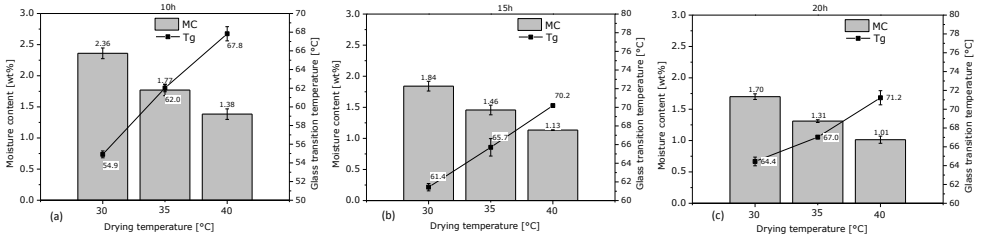

Figure 49. Influence of secondary drying temperature (T_d) on moisture content (MC) and glass transition temperature (T_g) of FK1 for center vials; (a) t_d = 10 h, (b) t_d = 15 h, and (c) t_d = 20 h. Error bars show standard deviation of three independent measurements. For all the experiments, P_c = 0.05 mbar; t_d, drying time; and P_c, chamber pressure.

This is because most of the unfrozen water is removed at the beginning of the secondary drying, reaching a plateau level in MC few hours after the start of the secondary drying [Pikal, 1990]. Since this plateau level decreases as T_d increases, the water removal rate after reaching the plateau level decreases as T_d increases (attributed to the low available MC). Thus, at high T_d, a further increase in t_d does not yield a significant reduction in MC. Conversely, owing to the slow water removal rate at low T_d, long t_d is needed to reach the plateau level in MC. Furthermore, the plateau level at low T_d is higher than that of at high T_d, and thus relatively faster water removal rate is possible even at prolonged t_d. This was the reason why the relative decrease in MC as T_d increased from 30 °C to 40 °C was similar at 10 h, 15 h, and 20 h drying times (cf. Figure 49). On the other hand, looking at the absolute MC values, a strong influence of T_d on MC was observed. In this sense, the MC value obtained at T_d = 30 °C and t_d = 20 h (Figure 49c) was similar to the MC value obtained at T_d = 35 °C and t_d = 10 h (Figure 49a).

Conversely, the effect of T_d on T_g was found to be slightly dependent on t_d. Thus, a 10 °C increase in T_d yielded 19% and 10% increase in T_g at t_d = 10 h and t_d = 20 h, respectively. Although the percent reduction in MC for 10 °C increase in T_d was similar (40%) at both drying times, the difference in percent increase in T_g demonstrates a non-linear T_g dependence on MC. The non-linear relationship between MC and T_g is consistent with the decreased dependence of T_g on MC at low

MC values. This provides an important information to select a critical MC, below which the increase in T_g is insignificant.

Influence of secondary drying time (t_d) on secondary drying output parameters: t_d is another important factor that defines both the economy of the process as well as the MC and T_g of the product. Figure 50 illustrates the effect of t_d on MC and T_g at different drying temperatures for center vials.

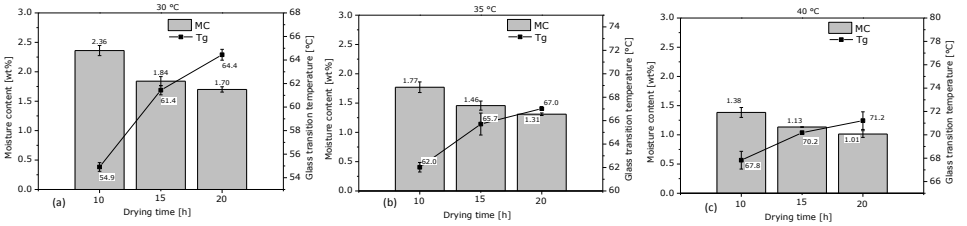

Figure 50. Influence of secondary drying time (t_d) on moisture content (MC) and glass transition temperature (T_g) of FK1 for center vials; (a) T_d = 30 °C, (b) T_d = 35 °C, and (c) T_d = 40 °C. Error bars show standard deviation of three independent measurements. For all the experiments, P_c = 0.05 mbar; T_d, drying temperature; and P_c, chamber pressure.

As displayed in Figure 50, a 10 h increase in t_d (from 10 h to 20 h) yielded approximately 28% reduction in MC regardless of the T_d used. However, the 28% reduction in MC at T_d = 30 °C yielded a 15% increase in T_g, whereas, at T_d = 35 °C and T_d = 40 °C, the increase in T_g was 8% and 5%, respectively. This is attributed to the weak dependence of T_g on the low MC obtained at T_d = 35 °C and T_d = 40 °C. Therefore, as discussed previously, high T_d could significantly reduce the time required to achieve a desired MC and T_g level. Although, both T_d and t_d exerted a significant effect on MC and T_g, T_d showed a stronger effect than t_d. For instance, at T_d = 30 °C and t_d = 20 h, the MC and T_g were, respectively, 1.70 wt% and 64.4 °C (Figure 50a), whereas, at T_d = 40 °C and t_d = 10 h, they were, respectively, 1.38 wt% and 67.8 °C (Figure 50c). Therefore, increasing T_d was found to have significant economic benefit for the secondary drying step of FK1.

Influence of chamber pressure (P_c) on secondary drying output parameters: Secondary drying chamber pressures, in the range from 0.05 mbar to 0.40 mbar, were applied to study the influence of chamber pressure on MC and T_g. For these

experiments, T_d and t_d were set to 37 °C and 12 h, respectively. The results displayed in Figure 51 showed minor influence of P_c on MC, whereas the influence on T_g was negligible.

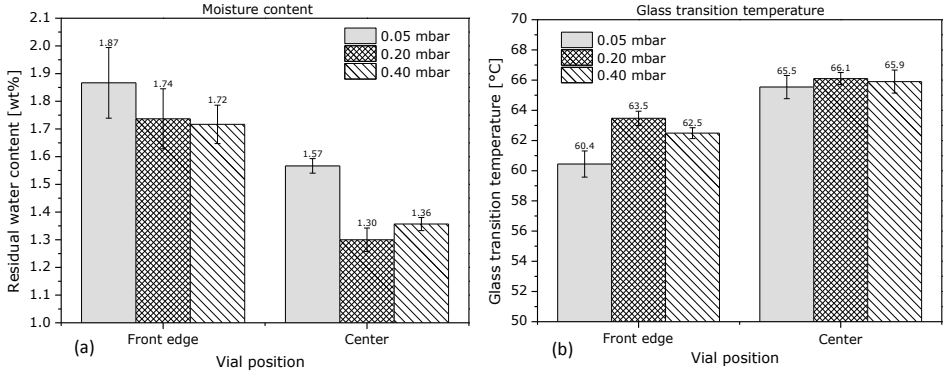

Figure 51. Influence of chamber pressure (P_c) on moisture content (MC) and glass transition temperature (T_g) of FK1 for front edge and center vials; (a) moisture content (MC) and (b) glass transition temperature (T_g). For all the experiments: T_d= 37 °C and t_d = 12 h. Error bars show standard deviation of three independent measurements. T_d, drying temperature; and t_d, drying time.

Although a small decrease in MC could be observed when increasing P_c from 0.05 mbar to 0.20 mbar, an insignificant change in MC was observed as P_c increased from 0.20 mbar to 0.40 mbar. The small decrease in MC with increasing P_c could be attributed to the improved heat transfer condition and thermal conductivity of the dried cake at higher P_c [Pikal et al., 1990]. Also, as displayed in Figure 52, high P_c improved both the rate of increase in product temperature (T_p) and the final value of T_p. That is, although the same heating rate was employed, significantly shorter time was required to increase T_p to the set point temperature when high P_c was used. Moreover, the final T_p value at high P_c was closer to the set point temperature than at low P_c (cf. Figure 52). Although such an improvement in heat transfer condition at high P_c, as compared to that of at low P_c, could be expected to yield a significant difference in MC and T_g, the results found in this study showed the contrary. This could be attributed to the influence of the rapid increase in T_p on the structure of the dried product. That is, the rapid increase in T_p could trigger the creation of microcollapse, which decreases the specific surface area (SSA) of the product. A

decrease in SSA is strongly linked to a decrease in water removal rate during the secondary drying phase [Rambhatla et al., 2004; Konstantinidis et al., 2011].

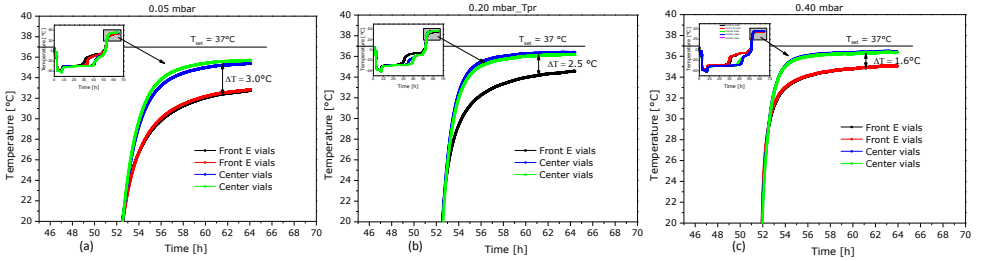

Figure 52. Influence of chamber pressure (P_c) on product temperature of front edge and center vials for FK1; (a) P_c = 0.05 mbar, (b) P_c = 0.20 mbar and (c) P_c = 0.40 mbar. For all the experiments: T_d = 37 °C and t_d = 12 h. T_d, drying temperature; and t_d, drying time.

In general, it could be concluded that the influence of secondary drying P_c on MC and T_g is minimal. Pikal et al. [Pikal et al., 1990] also demonstrated minimal influence of P_c on the secondary drying output parameters. However, at a given P_c, there was noticeable difference in MC and T_g between front edge and center vials at all the P_c studied (see Figure 51). This is contrary to the fact that the difference in T_p between front edge and center vials was decreased with increasing P_c (see Figure 52). It is, however, important to note that all the studies on the influence of P_c on the secondary drying output parameters presented here were based on a single T_d and t_d. The influence of P_c on MC and T_g could be different at different T_d and t_d combinations, although not significant differences to the results obtained here are expected.

Influence of vial position on secondary drying output parameters: The influence of vial position on MC and T_g has been extensively investigated in this study. For this purpose, vials were arranged as shown in Figure 47, and sample vials were taken for the measurement of MC and T_g. Representative results are displayed in Figures 53a-f. As illustrated in these figures, the edge vials generally had higher MC and lower T_g in all the drying conditions studied. This is attributed to 2 main factors: (1) during primary drying, the front edge vials have the highest T_p (see sections 4.2. and 4.3), which could lead to the occurrence of microcollapse if the lyophilization process is designed near the collapse temperature. Occurrence of microcollapse decreases the specific surface area (SSA), and hence decreases the secondary drying rate; (2)

contrary to the primary drying, the T_p of the front edge vials during the secondary drying was lower than that of the center vials.

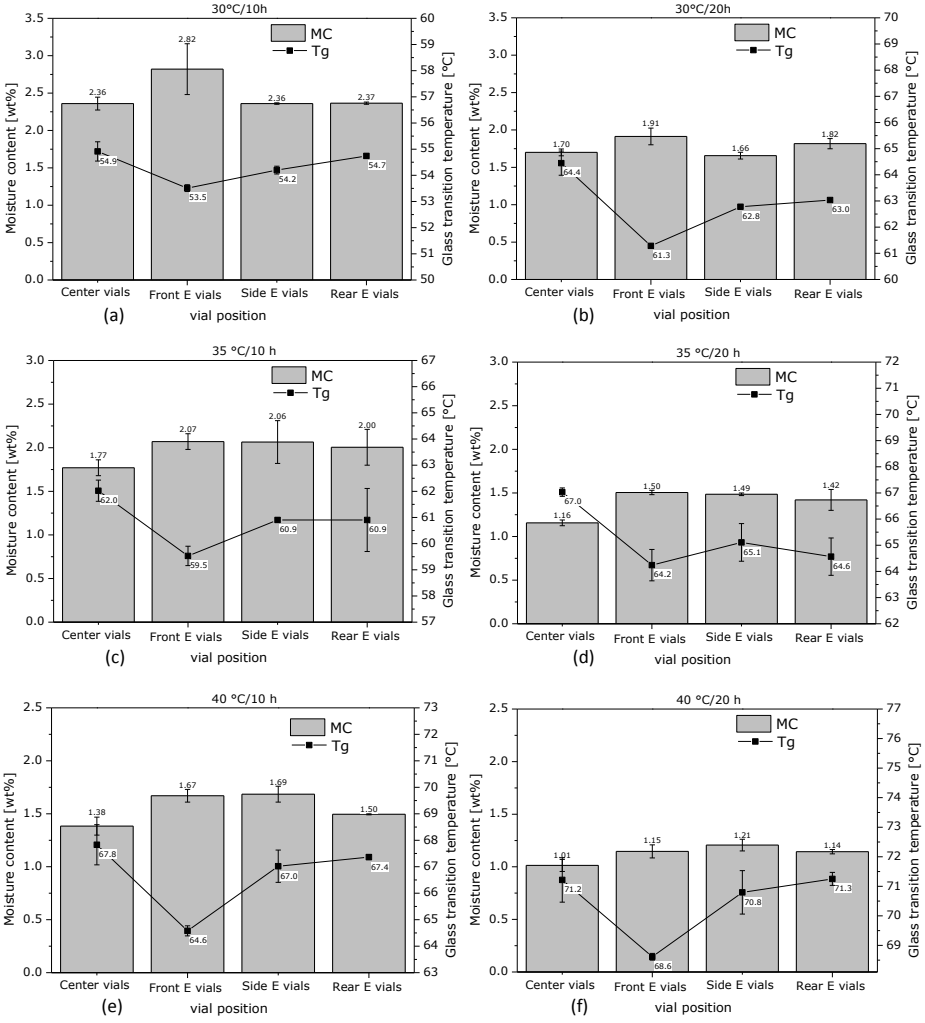

Figure 53. Influence of vial position on moisture content (MC) and glass transition temperature (T_g) of FK1; (a) T_d = 30 °C and t_d = 10 h, (b) T_d = 30 °C and t_d = 10 h, (c) T_d = 35 °C and t_d = 10 h, (d) T_d = 35 °C and t_d = 20 h (e) T_d = 40 °C and t_d = 10 h, and (f) T_d = 40 °C and t_d = 20 h. For all the experiments: P_c = 0.05 mbar. Error bars show standard deviation of three independent measurements. T_d, drying temperature; t_d, drying time; and P_c, chamber pressure.

This is due to the fact that the vial surface temperature of the front edge vials during the secondary drying phase is higher than those of the freeze dryer walls and door. Thus, the heat transfer due to atypical radiation flows from the vial surface to the freeze dryer walls and door, decreasing the T_p of the edge vials.

Figure 54 also shows that the difference in T_p between the front edge and center vials increases with increasing T_d. The difference in vial surface temperature and freeze dryer walls and door temperature increases as T_d increases, which in turn, increases the driving force for atypical radiation heat transfer. Thus, the large difference in T_p between the front edge and center vials, at high T_d, is attributed to the large driving force for atypical radiation. This, in turn, could lead to a tangible difference in MC and T_g among vials rested on different locations of a shelf.

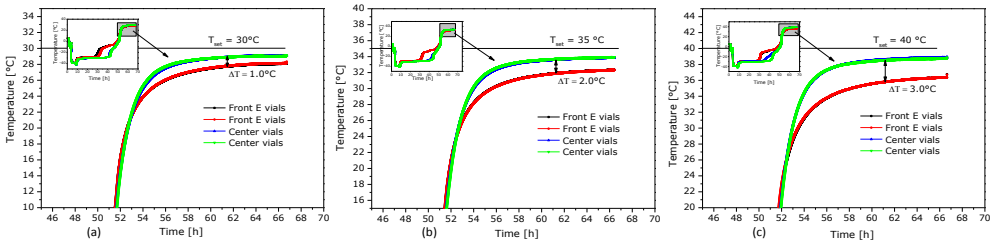

Figure 54. Influence of secondary drying temperature on product temperature of front edge and center vials of FK1; (a) T_d = 30 °C, (b) T_d = 35 °C, and (c) T_d = 40 °C. For all the experiments P_c = 0.05 mbar. T_d, drying temperature; and P_c, chamber pressure.

In general, although small differences in MC and T_g with respect to vial position were observed, these differences can be considered negligible in the range of T_d and t_d studied. For FK1, MC and T_g values of the center vials were taken for further optimization analysis.

Construction of process design space (PDS) for secondary drying step

The previous analyses on the influence of the different secondary input process parameters on MC and T_g provides the foundation for the construction of the PDS for the secondary drying step of a freeze-drying process. Thus, the 2 secondary drying critical input parameters considered during the construction of the PDS were

drying temperature (T_d) and drying time (t_d). To consider the effect of vial position on the PDS construction, the results from the center vials were utilized for 2 reasons: (1) In the range of T_d and t_d studied here, the biggest difference in T_g between the center and front edge vials was around 4 °C. Thus, considering the intended storage temperature of the dried FK1 (which is 25 °C), the influence on storage stability of a 4 °C difference in a T_g value of around 64 °C is very minimal; (2) the edge vials only account for a small portion of the total number of vials, thus the additional time required to decrease the MC of the edge vials to a value similar to the MC of the center vials could be uneconomical.

The experimental results of the DoE for secondary drying (cf. Table 17) are presented in Table 18.

Table 18. Moisture content and glass transition temperature experimental results for FK1 at different secondary drying processing conditions

Input parameters		Output parameters									
		Moisture content (wt%)					Glass transition temperature (°C)				
T_d (°C)	t_d (h)	M1	M2	M3	Ave	SD	M1	M2	M3	Ave	SD
30	10	2.46	2.37	2.25	2.36	0.086	54.6	55.4	54.7	54.9	0.37
	15	1.83	1.94	1.75	1.84	0.078	61.6	60.9	61.8	61.4	0.39
	20	1.65	1.76	1.69	1.70	0.045	65.1	64.1	64.1	64.4	0.46
35	10	1.75	1.67	1.89	1.77	0.091	62.1	61.5	62.5	62.0	0.41
	15	1.25	1.36	1.39	1.33	0.060	64.7	65.5	66.9	65.7	0.93
	20	1.32	1.28	1.33	1.31	0.022	66.8	67.1	66.6	66.8	0.22
	15*	**1.40**	**1.53**	**1.52**	**1.48**	**0.059**	**65.7**	**65.8**	**64.8**	**65.4**	**0.45**
	15*	**1.30**	**1.36**	**1.46**	**1.37**	**0.066**	**65.1**	**66.4**	**65.3**	**65.6**	**0.58**
40	10	1.30	1.35	1.50	1.38	0.085	68.5	68.2	66.8	67.8	0.76
	15	1.33	1.13	1.14	1.20	0.092	70.2	70.3	70.1	70.2	0.06
	20	1.08	0.94	1.02	1.01	0.057	72.0	70.2	71.4	71.2	0.75

*Experimental central points, which were repeated for the response surface regression analysis.
T_d, drying temperature; t_d, drying time; M1, M2 and M3, three different measurements; Ave, the mathematical average of the three measurements; SD, the standard deviation of the three measurements.

Response surface regression analyses of the MC and T_g results presented in Table 18, as a function of T_d and t_d, were performed and the following equations were obtained:

$$MC = 12.94 - 0.44T_d - 0.28t_d + 0.0046T_d^2 + 0.0043t_d^2 + 0.0029T_d t_d \quad (27)$$

$$T_g = 31.3 - 2.75T_d + 3.66t_d - 0.013T_d^2 - 0.028t_d^2 - 0.062T_d t_d \quad (28)$$

where, MC[wt%] is moisture content; T_d[°C]is drying temperature; t_d[h] is drying time; and T_g[°C] is glass transition temperature.

The fitting quality of the regression analyses was assessed using the adjusted R-squared values. For Equation 27, the adjusted R-squared was 96.9%, whereas for Equation 28, it was 98.9%. Hence, the fitting and predicting quality of the regression models was statistically significant. The regression model equations were used to generate MC and T_g data within the range of T_d and t_d studied. The resulting data from the regression model equations were used to plot contour graphs of MC (Figure. 55a) and T_g (Figure 55b) as a function of T_d and t_d. The final secondary drying PDS was defined based on an appropriate range of T_g, considering the intended storage temperature of the product. For example, the intended storage temperature of FK1 was 25 °C, and a T_g value of the dried product in a range from 60 °C–68 °C was considered sufficient for up to 2 years storage time. Therefore, the PDS incorporates secondary drying processing parameters (i.e., T_d and t_d) that yield a T_g in the range of 60 °C–68 °C and the corresponding MC. In the case of FK1, the MC range that corresponds to a T_g range from 60 °C to 68 °C was 1.3 wt%–1.8 wt%. The overall PDS for the secondary drying of FK1 is shown in Figure 55c. Figure 55c illustrates that any combination of secondary drying processing parameters in the white shaded area yields the predefined T_g and MC values.

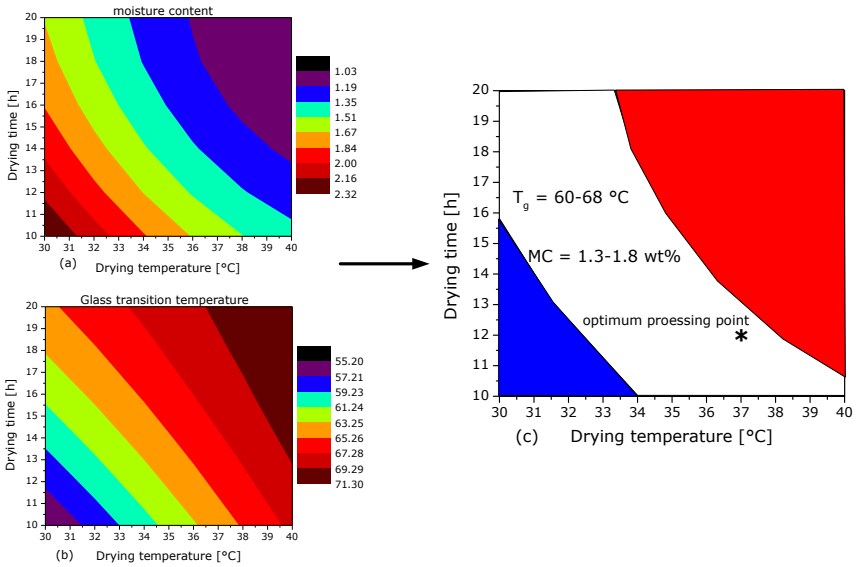

Figure 55. Process design space (PDS) for secondary drying of FK1; (a) contour plot of moisture content (MC), (b) contour plot of glass transition temperature (P_c), and (c) overall PDS for secondary drying. For all the experiments: chamber pressure (P_c) = 0.05 mbar.

Generally, selection of economically optimum secondary drying processing conditions involves high T_d and short t_d; however, the nature of the formulation should be considered when high T_d is selected. In the case of FK1, the optimum secondary drying processing conditions were selected as follows (see Figure 55c):

- Drying temperature = 37 °C
- Drying time = 12 h
- Chamber pressure = 0.05 mbar

Verification of optimum secondary drying process parameters

To confirm the accuracy of the PDS processing parameters, the output parameters from a verification experiment were compared to the PDS output parameters. The verification experiment was performed at the optimum processing parameter defined previously.

The results from the verification experiment are displayed in Table 19. As can be seen from Table 19, the average MC and T_g of the center vials were well within the

MC and T_g range defined by the PDS (cf. Figure 55c). Also, the front edge vials, which have the highest MC and lowest T_g in the vial array, had MC and T_g values in good agreement with the PDS defined values.

Table 19. Moisture content and glass transition temperature experimental results for FK1 obtained from verification experiment

Input parameters			Vial position	Output parameters									
				Moisture content (wt%)					Glass transition temperature (°C)				
T_d (°C)	t_d (h)	P_c (mbar)		M1	M2	M3	Ave	SD	M1	M2	M3	Ave	SD
37	12	0.05	Center vials	1.58	1.59	1.53	1.57	0.026	66.0	64.5	66.2	65.5	0.77
			Front edge vials	1.89	2.01	1.70	1.87	0.128	60.4	59.4	61.5	60.4	0.87

T_d, drying temperature; t_d, drying time; P_c, chamber pressure; M1, first measurement M2, second measurement M3, third measurements; Ave, mathematical average of the three measurements; SD, standard deviation of the three measurements.

This implies that the secondary drying PDS delivers reliable results and provides a scientific basis to optimize the secondary drying step. Moreover, the PDS gives a wide range of possible processing parameters from which a user can freely define the optimum process parameters. In this sense, formulation characteristics could be critical factors to select the T_d-t_d profile.

4.4.4. Conclusions

Optimization of a drug formulation from Fresenius Kabi (FK1) was performed using a design of experiments (DoE) experimental approach. The DoE was developed based on the knowledge of the critical process input parameters, such as drying temperature, drying time and chamber pressure as well as the characteristics of the drug formulation. Furthermore, the influence of vial position on residual moisture content (MC) and glass transition temperature (T_g) were studied.

Within the range of drying time studied, a 40% reduction in moisture content was observed when the drying temperature was increased from 30 °C to 40 °C, regardless of the drying time. This significant decrease in moisture content demonstrated a strong influence of the secondary drying temperature on the

moisture content of FK1. However, the effect of drying temperature on glass transition temperature was minimal. This was due to the fact that, at the drying temperatures and drying times studied, the moisture content already reached a very low level and a further reduction in moisture content yielded minimal effect on the glass transition temperature of the dried product. Thus, the minimum moisture content could be defined based on its effect on the glass transition temperature of the product. Although less significant, the effect of the drying time on moisture content and glass transition temperature of FK1 followed a similar trend to the effect of the drying temperature. Hence, from process economy perspective, a high drying temperature could significantly reduce processing time.

The chamber pressure, on the other hand, was found to have little influence on the secondary drying output parameters of FK1. Further, the effect of vial position on MC and T_g demonstrated a small difference between edge and center vials. In this regard, at all the experimental conditions studied here, the edge vials had higher MC and lower T_g than the center vials. As demonstrated by the product temperature profile of front edge and center vials during the secondary drying, there is a possible heat loss from the front edge vials to the freeze dryer walls and door. This could, at least partly, be responsible for the lower product temperature of the front edge vials, and hence lower secondary drying rate.

Based on the understanding of the influence of the drying temperature and time on MC and T_g, a secondary drying process design space (PDS) was developed for the FK1 product. The PDS incorporate possible secondary drying processing parameters (i.e., drying temperature and drying time) that yield acceptable MC and T_g for the FK1 product. These acceptable MC and T_g values could be defined based on the formulation characteristics and storage conditions. Verification results showed excellent agreement in MC and T_g with the PDS defined values. Therefore, understanding the relationship between the input and output parameters and development of PDS for the secondary drying step of FK1 significantly facilitated process optimization. Considering the effectiveness of the approach presented herein for a highly complex formulation, such as FK1, its applicability for similar

products could be very important. Further, the availability of the PDS could serve as an important tool to solve manufacturing related problems.

4.4.5. References

[1]. Abdul-Fattah AM, Lechuga-Ballesteros D, Kalonia DS, Pikal MJ. The impact of drying method and formulation on the physical properties and stability of methionyl human growth hormone in the amorphous solid state. *J Pharm Sci.* 2008;97(1):163–184.

[2]. Colandene JD, Maldonado LM, Creagh AT, Vrettos JS, Goad KG, Spitznagel TM. Lyophilization cycle development for a high-concentration monoclonal antibody formulation lacking a crystalline bulking agent. *J Pharm Sci.* 2007;96(6):1598–1608.

[3]. Fissore D, Pisano R, Barresi AA. Monitoring of the secondary drying in freeze-drying of pharmaceuticals*. J Pharm Sci.* 2011;100(2):732–42.

[4]. Konstantinidis AK, Kuu W, Otten L, Nail SL, Sever RR. Controlled nucleation in freeze-drying: effects on pore size in the dried product layer, mass transfer resistance, and primary drying rate. *J Pharm Sci.* 2011;100:3453–3470.

[5]. Liapis AI, Bruttini R. Freeze-drying of pharmaceutical crystalline and amorphous solutes in vials: dynamic multi-dimensional models of the primary and secondary drying stages and qualitative features of the moving interface. *Drying Technol.* 1995;13(1–2):43–72.

[6]. Nail SL, Jiang S, Chongprasert S, Knopp SA. Fundamentals of freeze drying. In: Nail SL, Akers MJ, eds. *Development and Manufacture of Protein Pharmaceuticals*, New York: Kluwer Academic/Plenum Publisher; 2002:281–360.

[7]. Oddone I, Barresi AA, Pisano R. Influence of controlled ice nucleation on the freeze-drying of pharmaceutical products: the secondary drying step. *Int J Pharm.* 2017;524(1–2):134–140.

[8]. Pikal MJ, Cardon S, Bhugra C, Jameel F, Rambhatla S, Mascarenhas WJ, Akay HU. The non-steady state modeling of freeze drying: in-process product temperature and moisture content mapping and pharmaceutical product quality applications. *Pharm Dev Technol.* 2005;10(1):17–32.

[9]. Pikal MJ, Shah S, Roy ML, Putman R. The secondary drying stage of freeze drying: drying kinetics as a function of temperature and chamber pressure. *Int J Pharm*. 1990;60:203–217.

[10]. Pisano R, Fissore D, Barresi AA. Quality by design in the secondary drying step of a freeze-drying process. *Drying Technol.* 2012;30(11–12):1307–1316.

[11]. Rambhatla S, Ramot R, Bhugra C, Pikal MJ. Heat and mass transfer scale-up issues during freeze drying: II. Control and characterization of the degree of supercooling. *AAPS PharmSciTech.* 2004;5(4) e58:1–9.

[12]. Sahni EK, Pikal MJ. Modeling the secondary drying stage of freeze drying: development and validation of an excel-based model. *J Pharm Sci.* 2017;106(3):779–791.

[13]. Schneid SC, Gieseler H, Kessler WJ, Luthra SA, Pikal MJ. Optimization of the secondary drying step in freeze drying using TDLAS technology. *AAPS PharmSciTech.* 2011;12(1):379–387.

[14]. Sheehan P, Liapis AI. Modeling of the primary and secondary drying stages of the freeze drying of pharmaceutical products in vials: numerical results obtained from the solution of a dynamic and spatially multi-dimensional lyophilization model for different operational policies. *Biotechnol Bioeng.* 1998;60(6):712–728.

[15]. Tréléa IC, Fonseca F, Passot S. Dynamic modeling of the secondary drying stage of freeze drying reveals distinct desorption kinetics for bound water. *Drying Technol.* 2016;34(3):335–345.

Chapter 5: Conclusions

Chapter 5: Conclusions

Form the experimental results obtained in this study, it can be concluded that:

- A strong relationship between formulation and freeze-drying process has been demonstrated. In this sense, a formulation composition has a direct impact on freeze-drying process efficiency. A formulation with low collapse temperature (less than -40 °C), for example, requires a very long primary drying time. Further, a formulation with low solubility of the active constituent may require a large amount of solvent, and hence long primary drying time. Therefore, consideration of the impact of formulation composition on process efficiency is a critical step during freeze-drying process design.

- The primary drying output parameters (i.e., product temperature, overall vial heat transfer coefficient and sublimation rate) showed significant differences with respect to the vial positions. Thus, while the center vials have the lowest primary drying output parameters, the highest values were observed for the front edge vials.

- Concerning the effect of shelf temperature on the primary drying output parameters, product temperature and sublimation rate showed a direct relationship with shelf temperature. In this sense, reducing shelf temperature, at a constant chamber pressure, reduces the heat input to the system. Thus, the energy equilibrium state of the system is achieved at lower product temperature. Furthermore, the vapor pressure of ice is reduced as product temperature decreases, and thus, at constant chamber pressure, the driving force for sublimation decreases. Consequently, the sublimation rate also decreases.

- Because of the assumptions involved in the calculation of the overall vial heat transfer coefficient, its dependence on shelf temperature was not a straightforward relationship. At low shelf temperature, for example, the

contribution of the direct conduction heat transfer mechanism (a direct result of the shelf temperature) to the overall vial heat transfer coefficient becomes weaker than the contribution from the energy input via the conduction through the gas and radiation. In such circumstances, the calculation of the overall vial heat transfer coefficient was overestimated.

- Variation in chamber pressure showed a significant influence on the primary drying output parameters. Increasing chamber pressure, at constant shelf temperature, increases all the primary drying output parameters. At high chamber pressure, sublimation of ice does not start unless the product temperature is too high to yield a vapor pressure of ice greater than the chamber pressure. Thus, due the absence of sublimation of ice at low product temperature, the energy consumption from the system is very low and, consequently, most of the energy input at the start of the primary drying is utilized to increase the product temperature. The increase in product temperature, at constant shelf temperature, increases both the overall vial heat transfer coefficient and the sublimation rate.

- Different combination of primary drying input parameters (i.e., chamber pressure and shelf temperature) yielded similar product temperatures; however, significant differences among the corresponding sublimation rate and overall vial heat transfer coefficient were observed. In general. It was demonstrated that, at a given product temperature, low chamber pressure–high shelf temperature combinations yielded the highest sublimation rate.

- A novel approach to design and optimize the primary drying section of the freeze-drying process has been developed in this study. The approach, called Temperature Ramp Approach (TRA), is an experimental based and easy-to-use approach, which requires proper formulation characterization and definition of a narrow range of target product temperatures for the primary drying step. The TRA considers variations in product temperatures and sublimation rates across a shelf, and thus assures the effectiveness and robustness of the resulting freeze-drying process.

- To address the quality-by-design concept for a freeze-drying process, a new approach for the construction of a process design space (PDS) for the primary drying step has been developed. The proposed approach uses a customized design of experiments (DoE) to perform a range of sublimation experiments and considers variations in product temperature and sublimation rate within the vial arrays. A PDS is an important tool during freeze-drying process scale-up and transfer.

- The secondary drying output parameters (i.e., moisture content and glass transition temperature) were found to be strongly influenced by the drying temperature and time. The influence of drying temperature was observed to decrease as drying time increases. This demonstrates that most of the residual moisture content, at higher drying temperature, was removed shortly after the start of the secondary drying process. On the other hand, the chamber pressure was found to have an insignificant effect on the secondary drying output parameters. Further, a process design space for the secondary drying step is proposed as a useful tool to design, optimize, scale-up, and transfer of the freeze-drying process.

List of Figures

List of Figures

List of Tables

List of Tables

Appendices

APPENDICES

El artículo **"**Understanding and optimization of the secondary drying step of a freeze-drying process: a case study" que forma parte de la sección "Appendices" ha sido retirado de la tesis debido a restricciones relativas a derechos de autor. Dicho artículo ha sido sustituido por su referencia bibliográfica, enlace al artículo y resumen.

- Assegehegn, G., Brito de la Fuente, E., Franco, J.M., Gallegos, C.: "Understanding and optimization of the secondary drying step of a freeze-drying process: a case study". Dryng Technology. DOI : 10.1080/07373937.2020.1739065

Enlace al artículo: https://doi.org/10.1080/07373937.2020.1739065

RESUMEN:

The objective of this study was to build an understanding and optimize the secondary drying step of a freeze-drying process using a drug formulation from Fresenius Kabi (FK1) as a case study. For this purpose, a design of experiments (DoE) was developed to study the influence of drying temperature, drying time, vial position, and chamber pressure on moisture content and glass transition temperature of FK1. The results obtained herein showed that the influence of drying temperature on moisture content and glass transition temperature was strong at short drying time, implying that increasing drying temperature could lead to a significant decrease in the required drying time to achieve a designed moisture content and glass transition temperature. Variation in chamber pressure from 0.05-0.40 mbar showed insignificant influence on moisture content and glass transition temperature. Small variations in moisture content and glass transition temperature with respect to vial position were also observed, where edge vials had higher moisture content and, consequently, lower glass transition temperature than center vials. Further, the results from the DoE were utilized to construct a process design space (PDS) for the secondary drying step of FK1. Experimental verification of the PDS demonstrated an excellent agreement between the PDS-defined and experimentally-determined moisture content and glass transition temperature values. Thus, the PDS facilitated process optimization of FK1 and could serve as an important tool during scale-up and transfer of the process.

Appendix A: Published articles

Appendix A.1:

The Importance of Understanding the Freezing Step and its Impact on Freeze Drying Process Performance

Getachew Assegehegn[1], Edmundo Brito-de la Fuente[1], José M. Franco[2] and Críspulo Gallegos[1]

[1]Fresenius-Kabi Deutschland GmbH, Process and Product Engineering Center, Global Manufacturing Pharmaceuticals, Bad Homburg, Germany

[2]Pro2TecS-Chemical Product and Process Technology Research Centre, Complex Fluid Engineering Laboratory. Departamento de Ingeniería Química, Universidad de Huelva, Huelva, Spain

Published in:

Journal	Journal of Pharmaceutical Sciences
Publishing company	Elsevier
Editor-in-Chief	Prof. Ronald T. Borchardt
Volume and pages	108; 1378-1395
Publication year	2019
ISSN	0022-3549
DOI	https://doi.org/10.1016/j.xphs.2018.11.039
Journal impact factor (2018)	**3.197**

Category (2017)	**Journal rank/total journal**	**Quartile**
Chemistry, medicinal	21/59	Q2
Chemistry, multidisciplinary	69/171	Q2
Pharmacology & pharmacy	93/261	Q2

Journal of Pharmaceutical Sciences 108 (2019) 1378-1395

Contents lists available at ScienceDirect

Journal of Pharmaceutical Sciences

journal homepage: www.jpharmsci.org

Review

The Importance of Understanding the Freezing Step and Its Impact on Freeze-Drying Process Performance

Getachew Assegehegn [1,*], Edmundo Brito-de la Fuente [1], José M. Franco [2], Críspulo Gallegos [1]

[1] Fresenius-Kabi Deutschland GmbH, Process and Product Engineering Center, Global Manufacturing Pharmaceuticals, Bad Homburg, Germany
[2] Departamento de Ingeniería Química, Pro2TecS-Chemical Product and Process Technology Research Centre, Complex Fluid Engineering Laboratory, Universidad de Huelva, Huelva, Spain

ARTICLE INFO

Article history:
Received 5 October 2018
Revised 24 November 2018
Accepted 27 November 2018
Available online 5 December 2018

Keywords:
freeze-drying
lyophilization
nucleation
crystal growth
crystallinity
glass transition(s)

ABSTRACT

The freeze-drying process is a combination of 2 equally important processes, freezing, and drying. In the past, the effort was mainly focused on optimizing the drying process without considering the possible effects of the freezing step. During freezing, a solution undergoes several physical changes, including a supercooling state. The degree of supercooling of a solution dictates the ice habit (size, number, and morphology) during freezing, which impacts the subsequent drying process, such as the resistance to water vapor flow. Therefore, heterogeneous degree of supercooling leads to heterogeneous ice habits and, in turn, to heterogeneous drying behavior. This poses significant challenges during freeze-drying process development, optimization, and scale up. Hence, controlling the degree of supercooling significantly improves freeze-drying process design. The aim of the current review is to gather existing information on the physicochemical phenomena involved in the freezing process and how these phenomena impact the subsequent drying step of the freeze-drying process. In addition, modification of the freezing process and different techniques used to actively control the degree of supercooling during freezing will be reviewed and discussed. Their impact on freeze-drying process performance will be also addressed.

Introduction

Drying is one of the key unit operations in pharmaceutical and biopharmaceutical industries, especially used to remove solvents (usually water) from liquid drug formulations with the purpose of converting them into solid forms without compromising their pharmaceutical and therapeutic properties. The main reason behind this conversion is that a drug formulation in its solid state allows the immobilization of the active drug substance as well as the excipients, hence significantly reducing the chemical and physical degradation pathways, such as hydrolysis, oxidation, isomerization, condensation, racemization, and reactions with other components in solution.[1] An extended stability of the formulation containing the active pharmaceutical ingredient (API), even at ambient temperature, is then achieved.[2] In addition to the stability benefits, drug formulations in solid forms have the advantages of easy handling and storage, and reducing transportation costs.[3] In contrast to the aforementioned advantages, solid or freeze-dried products have some disadvantages, such as they are not as convenient to administer as a sterile, ready-to-use solution; freeze-dried products require additional reconstitution and transfer steps during administration (because of this, sterility assurance may be compromised); and due to expensive equipment and manufacturing costs, freeze-dried products are, generally, more expensive than ready-to-use solutions.

Several drying technologies are already in use or under development in pharmaceutical and biopharmaceutical industries. These include freeze-drying,[4-6] foam drying,[7,8] spray,[9-11] spray freeze-drying,[12-14] supercritical fluid drying,[15,16] convective drying,[17] microwave drying,[18,19] and more recently electrostatic drying.[20] Shanghai Tofflon Science and Technology Co. Ltd. is currently developing a spray freeze dryer for pharmaceutical products (private communication, 2018). A detailed review of these drying technologies is given elsewhere.[3] Selection of an efficient drying process often presents challenges, because it requires the consideration and evaluation of many critical parameters. These include physical properties of the product, drying temperature, residual water content, quality and shelf-life of the dried product, ease of process design, scalability, capability to implement the technique in a good manufacturing practice environment, ease of control of

* *Correspondence to:* Getachew Assegehegn (Telephone: +49 6172 608 7381).
E-mail address: getachew.assegehegn@fresenius-kabi.com (G. Assegehegn).

https://doi.org/10.1016/j.xphs.2018.11.039
0022-3549/

critical process parameters, and investment and operational costs of the drying process. The challenges arise from the fact that all the available drying technologies only fulfill few of the factors listed previously. Therefore, the selection process requires an intensive evaluation and comparison of the different drying technologies, especially considering the final product attributes. In addition to the aforementioned factors, the cost of raw materials might also have an impact on the selection of the drying process.[3] For instance, for high-value products, as it is often the case with pharmaceuticals, the cost of the raw ingredients may be the primary driver that dictates the selection of a drying method, as low yield or product recovery less than 100% may not be acceptable.[3]

Despite the abundance of drying technologies available, the vast majority of these techniques, in their current state, are not directly applicable for the processing of pharmaceutical and biopharmaceutical products because of many reasons, including (1) unknown effect of energy source on structure or stability of the products, (2) energy efficiency, (3) scalability, and (4) inability to achieve low residual water content.[3] This might be the reason why the vast majority of the pharmaceutical and biopharmaceutical industries are currently using freeze-drying or lyophilization as a drying technique. Despite its shortcomings, such as high production costs, high investment and maintenance costs, and low throughput, lyophilization is a well-established drying method that successfully passes regulatory bottlenecks. The broad use of freeze-drying process is supported by the fact that, in 1998, lyophilized pharmaceuticals accounted for 11.9% of all new injectable or infusible drugs, but, by 2015, they made up half of all such new drug introductions.[21]

Freeze-drying is a drying unit operation with a core principle of removal of solvent from a liquid formulation, in which the formulation is first frozen and then the frozen solvent is removed by sublimation, at a reduced pressure, followed by a desorption process for the removal of the unfrozen solvent. Therefore, 2 equally important major processes are taking place during a complete freeze-drying process; (1) *freezing*, during which most of the solvent, up to 95%,[22] is converted into frozen solid, and (2) *drying*, during which almost all the solvent (frozen and unfrozen) is removed from the formulation. The drying process is further classified into 2 steps, based on the mechanism of the drying process, namely sublimation (primary drying) and desorption (secondary drying).

Freezing is the first operation in a freeze-drying process and is, of course, a critical step because if the product is impaired from the start, there is obviously no interest to go further.[23] During the freezing step, most of the water is converted into solid by forming a network of ice crystals and this step dictates ice crystal morphology, size, and size distribution, which in turn influence several critical parameters, such as dried product resistance, primary and secondary drying rates, extent of product crystallinity, specific surface area, and reconstituability of the dried product.[24] The influence of freezing on the subsequent drying process can be well described using the governing transport phenomena equations of a freeze-drying process. During the primary drying phase of a freeze-drying process, heat and mass transfer should take place in "close-equilibrium," so that the change in product temperature during the entire primary drying period remains insignificant, usually within 2°C-3°C. Therefore, for the purpose of calculations, a pseudo steady-state in product temperature can be safely assumed and, hence, the equilibrium in heat and mass transfer during primary drying is given as in Equation 1.

$$\dot{Q} = \Delta H_s \dot{m} \tag{1}$$

Where, $\dot{Q}$ [W] is the overall heat transfer rate to a given vial, ΔH_s [J/g] is the heat of sublimation of ice, and $\dot{m}$[g/s] is the overall mass transfer rate from a vial.

Furthermore, the overall heat and mass transfer rates can be expressed as in Equations 2 and 3, respectively.

$$\dot{Q} = A_v K_v (T_s - T_p) \tag{2}$$

Where, A_v [cm^2] is the outer surface area of a vial, K_v [$W/cm^2.K$] is the overall heat transfer coefficient of a vial, T_s [K] is the shelf temperature, and T_p [K] is the product temperature.

$$\dot{m} = \frac{p_i(T_p) - p_c}{R_p(r)} \tag{3}$$

Where, p_i (T_p) [mbar] is the vapor pressure of ice (function of product temperature, T_p), p_c [mbar] is the chamber pressure, and R_p (r) [mbar.s/g] is the resistance to mass transfer of the dried product (function of pore radius, r).

Substituting Equations 2 and 3 into Equation 1 gives

$$A_v K_v (T_s - T_p) = \Delta H_s \frac{p_i(T_p) - p_c}{R_p(r)} \tag{4}$$

All the parameters in Equation 4 are as described previously. Equation 4 can be used to analyze the effect of the freezing step on the primary drying of freeze-drying process.

Effect of Freezing on Resistance to Mass Transfer of the Dried Product (R_p (r))

As mentioned earlier, the predominant and direct impact of the freezing step is on the formation of ice crystal habits, such as size and morphology, and this, in turn, impacts the pore size of the dried product after the ice crystals are sublimed. Large ice crystals leave large pore radius in the dried product and, consequently, they have low resistance to mass transfer. By contrast, small ice crystals leave small pore radius, which hinder the transport of water vapor significantly. Therefore, the resistance to mass transfer of the dried product is inversely related to the size of ice crystals that are formed during the freezing step.

Effect of Freezing on Product Temperature (T_p) and Vapor Pressure of Ice (p_i)

As mentioned in the previous section, the direct impact of the freezing step is on the resistance to mass transfer of the dried product, R_p, and, as a consequence of this, many other parameters, such as product temperature, T_p, vapor pressure of ice, p_i, overall heat transfer coefficient of a vial, K_v, and mass transfer rate, $\dot{m}$, are affected. Although the effect of the freezing step on these parameters is rather complex, it can be studied by evaluating the governing heat and mass transfer equations. Rearranging Equation 4 for product temperature, the following equation is obtained:

$$T_p = T_s - \frac{\Delta H_s (p_i(T_p) - p_c)}{A_v K_v R_p(r)} \tag{5}$$

To evaluate the effect of the freezing step on product temperature, T_p, from Equation 5, the following condition must be met: the input process parameters, which means the shelf temperature, T_s, and the chamber pressure, p_c, should be kept unchanged. Now, let us consider 2 proprietary products, product A and product B. For product A, the freezing protocol produces few and large ice crystals and, hence, low R_p. On other hand, the freezing protocol for product B produces many and small ice crystals and, hence, high R_p. According to Equation 5, this results in lower product temperature for product A than for product B. This is because, at low R_p, the

endothermic mass transfer process is dominant and thus takes up substantial energy from the process. If this substantial energy take-up is not compensated by increasing the heat transfer rate (rate limiting process), the product temperature decreases. At the same time, according to the phase diagram of water, the vapor pressure of ice, p_i, decreases as product temperature decreases. Consequently, the term $(p_i(T_p)-p_c)$ in Equation 5 decreases, resulting in a reduction of mass transfer rate. The reduction in mass transfer rate reduces the energy take-up from the process, and thus the product temperature slightly increases. This cycle repeats itself until a new equilibrium in heat and mass transfer rate is achieved. This analysis implies that, for product A (with low R_p), the energy input (i.e., the shelf temperature) can be increased to shift the heat transfer rate from a rate-limiting process to a process in equilibrium with the mass transfer rate, so that the product temperature remains at the predefined target product temperature from the start of the process.

On the other hand, at high R_p, the endothermic mass transfer process becomes a rate-limiting process, and the excess energy input from the dominant exothermic heat transfer process causes the product temperature to increase. At the same time, according to the phase diagram of water, the vapor pressure of ice, p_i, increases as product temperature increases. Consequently, the term $(p_i(T_p)-p_c)$ in Equation 5 increases, resulting in an increased forced mass transfer rate. Depending on the increase in the magnitude of the forced mass transfer rate and the product temperature, a micro-collapse or a complete collapse of the product might occur. This analysis implies that, for product B (with high R_p), the energy input, which means the shelf temperature, might need to be decreased to shift the heat transfer rate from a dominant process to a process in equilibrium with the mass transfer rate, so that the product temperature remains at the predefined target product temperature, avoiding product damage. In general, the impact of the freezing step on the different parameters can be summarized as follows:

$$\left.\begin{array}{l} r \propto \text{ice crystal size} \\ R_p \propto \dfrac{1}{r} \\ R_p \propto T_p \\ p_i \propto T_p \\ T_p, p_i \propto \dfrac{1}{r} \\ \dot{m} \propto \dfrac{1}{R_p}, T_p \end{array}\right| \quad \text{Provided } T_s \text{ and } p_c \text{ are kept unchanged} \qquad (6)$$

Therefore, it is of paramount importance to study the nature of the freezing step during development, optimization, transfer, and scale-up of the freeze-drying process.

Effect of Freezing on Mass Transfer Rate ($\dot{m}$)

The effect of the freezing step on mass transfer rate is not a straightforward relationship. On one hand, mass transfer rate is inversely related to the resistance to mass transfer of the dried product, R_p. On the other hand, mass transfer rate is directly related to the product temperature, T_p, and, hence, to the vapor pressure of ice, p_i, provided that the shelf temperature and chamber pressure are kept unchanged (Eq. 6).

As can be deduced from Equation 6, large ice crystals are correlated with low dried product resistance and with low product temperature. Furthermore, Equation 6 shows the relationship of dried product resistance and product temperature with mass transfer rate and, according to this equation, the lower the dried product resistance, the higher the mass transfer rate and, on the other hand, the lower the product temperature (or the vapor pressure of ice), the lower the mass transfer rate. Therefore, the overall effect of the freezing step on mass transfer rate is dependent on the relative effect of the freezing step on the dried product resistance and the product temperature. Therefore, the advantage of having high mass transfer rate due to low dried product resistance could be offset by the low product temperature, unless the processing parameters (shelf temperature and chamber pressure) are set to keep the product temperature at the predefined target product temperature.

In addition to the forementioned impact of the freezing step on freeze-drying process, it is a critical step with regard to biological activity and stability of the API, especially for pharmaceutical proteins.[25-29] Therefore, a thorough understanding of the physicochemistry of the freezing process is essential for understanding how both formulation composition and process conditions influence the quality of the freeze-dried product.[30]

The aim of the current review is to gather existing information on the physicochemical phenomena involved during the freezing process and how these phenomena impact the subsequent drying step of the freeze-drying process. In addition, modification of the freezing process and different techniques used to actively control the degree of supercooling during freezing will be reviewed and discussed along with their impact on freeze-drying process performance. In this sense, this review stresses the importance of understanding the fundamental principles of the freezing step during the freeze-drying process, as well as its significant impact on freeze-drying process development, optimization and scale up. In addition, an update of the available techniques for the active control of the degree of supercooling is addressed.

The Freezing Process

In general, the freezing process consists of 3 stages namely, (1) *cooling stage*, in which the liquid formulation is cooled from its initial temperature to the freezing point temperature; (2) phase *change stage*, in which the first ice nucleus formation and ice crystal growth are taking place; and (3) *solidification stage*, in which all the ice crystals grow to an extent that no further ice crystal growth is possible.[31]

Cooling Stage

During the cooling stage, the temperature of the formulation is decreased until the first ice nucleus starts to be formed. The temperature at which the first ice nucleus is formed is known as ice *nucleation temperature*, T_n. When an aqueous system is cooled at atmospheric pressure, it does not freeze spontaneously at its equilibrium freezing point[32]; rather, it retains its liquid state to a certain degree. The equilibrium freezing of aqueous systems requires, among other things, that an ice crystal nucleus is made available at the equilibrium freezing point of the system and that appreciable temperature differences within the system do not exist. Supercooling arises when, at least, one of these conditions is not met.[33] *Supercooling* is therefore defined as the ability of an aqueous system to retain its liquid state below its equilibrium freezing point. During the supercooling state, which is a nonequilibrium and metastable state, water molecules form clusters with relatively long-living hydrogen bonds with similar molecular arrangements to ice crystals.[32,34] Since this process is energetically unfavorable, the molecular clusters break up rapidly until an adequate amount of molecules associate in 3 dimensions to form a thermodynamically stable aggregate, so-called critical nucleus, which provides surfaces suitable for crystal growth.[31] Depending on the cooling

rate used, 2 supercooling states can be observed. The first is *global supercooling*, in which the entire liquid volume achieves a similar level of supercooling, and the secondary nucleation zone encompasses the entire liquid volume. Solidification then progresses through the already nucleated volume.[24] Slow cooling rates, such as shelf-ramp cooling, lead to global supercooling. The second is *local supercooling*, in which a small fraction of the volume is supercooled to the point of primary and secondary nucleation. The nucleation and solidification fronts are in close proximity in space and time, with the front moving into the non-nucleated liquid.[24] Figure 1 shows a typical freezing curve of a pharmaceutical liquid formulation. The equilibrium freezing point of this formulation is shown as point A and, because freezing does not start at point A, the formulation retains its liquid state until point B, in which the first ice nucleus is formed. The state of the formulation from point A to point B is termed as *supercooling state* and the degree that the given formulation retains its supercooling state is termed as *degree of supercooling*. The degree of supercooling is quite variable and it is affected by several factors, such as foreign particles, container surface area, process conditions, sample volume, composition of the matrix, and contact area between sample and container.[31] The aforementioned and other factors are responsible for the random and stochastic nature of ice nucleation. As will be discussed later more in detail, the variation in degree of supercooling from sample to sample affects the drying behavior of these samples during primary drying and this, in turn, hinders the effort to design robust and economically optimized freeze-drying processes. Therefore, the ability to control the degree of supercooling or ice nucleation during the freeze-drying process is essential to produce batches with consistent and similar freezing behaviors. Freezing methods aiming to control the ice nucleation during the freeze-drying process are currently available. Some of them have yielded successful experimental results at laboratory scale.[35-37] However, only limited data are still available at industrial scale.[38,39] These methods will be discussed more in detail later in this review.

Phase Change Stage

Phase change stage (referring to a phase change from liquid to solid) starts once a formulation reaches its ice nucleation temperature (T_n), point B of Figure 1, in which the first ice nucleus appears. The appearance of the first ice nucleus is called *primary nucleation*.

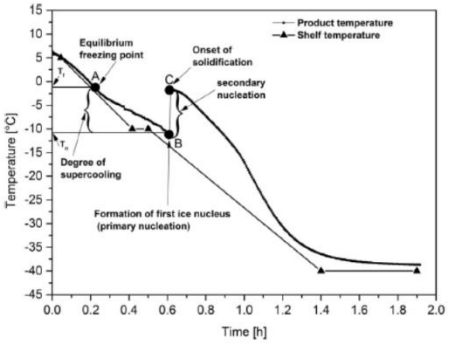

Figure 1. Freezing curve of a typical pharmaceutical formulation obtained during a shelf-ramp freezing experiment (authors' own results). T_f is the equilibrium freezing temperature; T_n is the ice nucleation temperature.

Primary nucleation is an extremely fast process and, hence, it is difficult to observe either by eye or on a cooling thermogram except as a starting point of the secondary nucleation.[24] *Secondary nucleation* (from point B to C of Fig. 1) immediately follows primary nucleation and it is characterized by the addition of ice nucleation sites.

Formation of ice crystals is an exothermic process and, for this process to continue, the heat given off must be removed. This heat is removed by the supercooled solution, which is at a certain degree below the equilibrium freezing temperature. During this process, the supercooled formulation only absorbs limited amount of heat and, hence, the temperature of the solution increases quickly to its equilibrium freezing temperature where formation of ice crystals ceases, point C of Figure 1. The amount of heat absorbed during secondary nucleation determines the total number of ice crystals formed, which, in turn, depends on the degree of supercooling. Higher degree of supercooling allows bigger amount of heat to be absorbed during the exothermic crystallization process and this grants the formation of many ice crystals.

The mass fraction of freezable water that crystallizes during nucleation (x) can be calculated according to Equation 7, in which the extent of supercooling is used to absorb the heat of crystallization up to the equilibrium freezing point[24]:

$$x = \frac{m_{wn}}{m_{wf}} = \frac{\left(T_f - T_n\right) C_{pw}}{\left(1 - C/C_g'\right) \Delta H_m} \tag{7}$$

Where, m_{wn} is the mass of water crystallized at nucleation, m_{wf} is the mass of freezable water, T_f is the equilibrium freezing temperature of water, T_n is the ice nucleation temperature, C_{pw} is the heat capacity of water (around 4.2 J/g.K), C is the mass fraction of solutes, C_g' is the mass fraction of solutes in the maximally freeze concentrated state, and ΔH_m is the latent heat of fusion of water (334 J/g).[40] The amount of total crystallizable water and unfrozen water is mainly influenced by the composition of the formulation and is not influenced by the ice nucleation temperature.[41]

In addition, the rate of ice crystal growth (freezing rate) is dependent on the degree of supercooling. At higher degree of supercooling (i.e., lower ice nucleation temperature), the ice crystal growth rate is faster. This is because the relatively colder shelves of the freeze dryer remove the heat generated during ice formation faster. The rate of crystal growth (G) can be expressed as a function of degree of supercooling, as shown in Equation 8[34]:

$$G = \beta(\Delta T_s)^n \tag{8}$$

Where, $\Delta T_s = T_f - T_n$ (degree of supercooling), and β and n are experimental constants.

On the other hand, if a solution has a low degree of supercooling, meaning small temperature difference between the equilibrium freezing point temperature and the nucleation temperature, only a small amount of the heat of crystallization can be absorbed by the supercooled water. This results in the instantaneous freezing of only a small fraction of freezable water and, hence, the formation of just a few ice crystals. In addition, the ice crystal growth rate of a solution with low degree of supercooling is slow, as the relatively warmer freeze dryer shelves have low driving force to remove the crystallization heat. A pictorial depiction of the freezing process at high and low degrees of supercooling is shown in Figure 2. Figure 2a shows the freezing phenomenon in the case of a high degree of supercooling (i.e., 13°C). As discussed earlier, higher degree of supercooling leads to a higher amount of water to crystallize during secondary nucleation (cf. Eq. 7) and to faster rate of freezing (cf. Eq. 8). This, in turn, leads to the formation of many ice

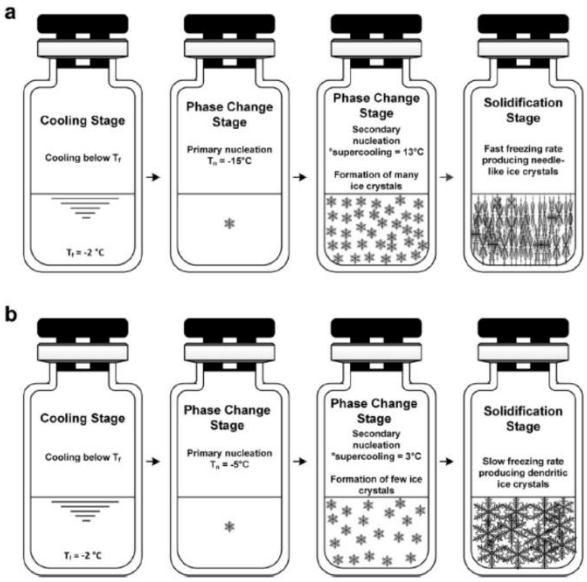

Figure 2. Pictorial depiction of the freezing phenomena: effect of the degree of supercooling on ice crystals size, number, and morphology. (a) Freezing phenomena with high degree of supercooling, and (b) freezing phenomena with low degree of supercooling. T_f is the equilibrium freezing temperature; T_n is the ice nucleation temperature.[41]

nucleation sites during secondary nucleation producing many small ice crystals. By contrast, Figure 2b shows an example of a low degree of supercooling (i.e., 3°C). In this case, it is apparent that a lower amount of water crystallizes during secondary nucleation (cf. Eq. 7), yielding very few large ice crystals.

It is also known that ice crystal morphology is a function of the degree of supercooling. Generally, 3 different types of ice crystal morphologies can be observed during freezing of a solution[34,42]: (1) at high degree of supercooling (Fig. 2a), because of the fast freezing rate, the water molecules arrange randomly around the ice nuclei, creating irregular dendrites or needle-like crystals; (2) at low degree of supercooling (Fig. 2b), the freezing rate is slower and the water molecules have sufficient time to arrange themselves to form regular hexagonal crystals, called dendrites; (3) at high cooling rates, many ice spears can originate from the center of crystallization without side branches, called spherulites. Supporting this idea, Tammann reported the influence of nucleation temperature on ice crystal morphology.[43] Specifically, samples frozen at low degree of supercooling (i.e., warmer nucleation temperature) yield dendritic structures, whereas samples frozen at high degree of supercooling (i.e., colder nucleation temperature) yield crystal filaments.[28,43]

Solidification Stage

Once stable ice nuclei are formed, their growth proceeds by the addition of water molecules to the interface, which is termed as solidification. Point C of Figure 1 shows the onset of solidification. During solidification, the ice crystals grow, reducing the availability of liquid water. This, in turn, increases the solute concentration in the formulation, which is referred to as freeze-concentration.[28] The increase in solute concentration during freezing is a function of temperature only and is independent of the initial concentration.[44] On further cooling, the solute concentration increases to a critical concentration, above which the concentrated solution undergoes either eutectic freezing or vitrification.[32]

A eutectic mixture is formed when a solute crystallizes from a freeze-concentrated solution.[30] For example, mannitol, glycine, sodium chloride, and phosphate buffers are known to crystallize on freezing if present as the major component.[28] The *eutectic temperature* (T_{eu}) is the lowest temperature at which a solution remains liquid and, at this point, the freeze-concentrate saturates and eutectic freezing or solute crystallization occurs.[32] It is only below the eutectic temperature that a crystalline system is considered completely solidified.[30]

For binary mixtures, the eutectic temperature depends on the solubility of the solute and it could generally be said that the lower the solubility of a given solute, the higher is the eutectic temperature.[30] For multicomponent systems, the general rule is that the crystallization of any component is influenced or hindered by the presence of other component.[1]

On the other hand, vitrification occurs in amorphous solutions where solutes do not crystallize during freezing. The fact that amorphous solutes do not crystallize at their eutectic temperature is due to their complex microstructures.[1] Freezing of water and, consequently, increase in solution concentration cease when the solution viscosity is close to 10^2 Pa•s.[45] At this viscosity level, the state of the freeze-concentrated solution is expected to change from a rubbery to a glassy solid, a process known as glassification or vitrification.[45] The temperature at which this transition occurs is referred to as the *glass transition temperature of the maximally*

freeze-concentrated solution (Tg'). Tg' is shown in the supplemented phase diagram, Figure 3, as the intersection of the freezing point depression curve of water in the presence of amorphous solute and the glass transition curve. Tg' is the point on the glass transition curve, representing a reversible change between a viscous rubber-like liquid and a rigid glassy system.[30,32] Tg' depends on the composition of the solution, but is independent of the initial solute concentration.[44,47,48]

The most important difference between freeze-drying a crystalline solution and an amorphous solution concerns the definition of the maximum allowable product temperature during primary drying. In a crystalline solution, complete solidification of the solution occurs below the eutectic temperature and, hence, the eutectic temperature is defined as the maximum allowable product temperature during primary drying. On the other hand, complete solidification of an amorphous solution occurs below the glass transition temperature of the maximally freeze-concentrated solution (Tg'). Although, in most cases, Tg' is used to define the maximum allowable product temperature during primary drying, the collapse temperature (Tc) of an amorphous solution more precisely defines the temperature at which a structural loss of the product occurs. In addition, Tc is several degrees higher than Tg', as the high viscosity of the sample at a temperature close to Tg' prevents viscous flow.[22] Thus, to maximize process efficiency, Tc can be used to define the maximum allowable product temperature during primary drying. Eutectic melting temperatures are relatively high compared to glass transition temperatures, allowing a higher product temperature during primary drying and resulting in much shorter drying processes.[32] If the product temperature during primary drying exceeds either the eutectic temperature (for a crystalline solution) or the collapse temperature (for amorphous solutions), a structural breakdown of the dried product occurs. This structural breakdown is commonly known as meltback (for a crystalline solution) or collapse (for amorphous solutions).[30] In relation to this, the physical state of some drugs, that means crystalline versus amorphous, may have a significant effect on drug potency loss; crystalline drugs are more prone to lose potency.[49,50] Drug potency and insolubility share a common origin: structural and thermodynamic drug properties. A potent drug forms a stable complex, that is, a complex with an unfavorable free energy of dissociation. Similarly, an insoluble drug forms a stable crystal, that is, a crystal with an unfavorable free energy of dissolution.[49,50] Because amorphous drugs are markedly more soluble than their crystalline counterparts, they represent the most energetic solid state of a material, and thus they provide the biggest advantage in terms of solubility and bioavailability.[51,52] The higher aqueous solubility can potentially translate into higher bioavailability compared to a formulation consisting of the crystalline form of the drug substance. Recently, amorphous solid dispersions have been used as formulation solutions to improve drug solubility and bioavailability.[53]

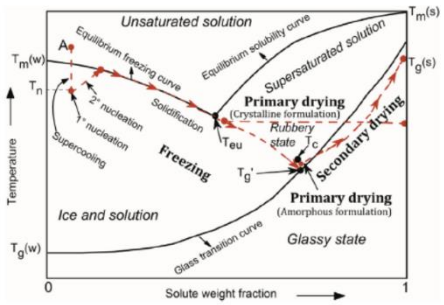

Figure 3. Supplemented phase diagram describing the low temperature behavior of a selected proprietary solution "A". $T_m(w)$: melting or freezing temperature of pure water; T_n: ice nucleation temperature; $T_g(w)$: glass transition of pure water; $T_m(s)$: melting or freezing temperature of solute; $T_g(s)$: glass transition temperature of solute; T_g': glass transition temperature of maximally freeze-concentrated solution (for an amorphous solution); Tc: collapse temperature; T_{eu}: eutectic temperature of a frozen crystalline solution.[28,32,33,44,46]

Moreover, the microstructural differences between crystalline and amorphous frozen solutions result in significantly different behaviors during the freeze-drying process. Thus, the interstices among the ice crystal matrices of a crystalline solution consist of an intimate mixture of small crystals of ice and solute, whereas the interstitial region in amorphous solutes consists of solid solution and unfrozen, amorphous water. Therefore, in a crystalline solution, nearly all water is frozen and can be easily removed during primary drying without requiring secondary drying. However, in an amorphous solution, up to 20% of unfrozen water is associated with the solid solution, which must be removed by desorption during secondary drying.[30] Characterization of a lyophilization formulation is therefore essential to better understand the effect of the freezing step on the subsequent drying process. Several techniques are available to characterize a lyophilization formulation in its frozen state. Differential scanning calorimetry, modulated differential scanning calorimetry, and differential thermal analysis are used for the determination of glass transition temperature of the maximally freeze-concentrated solution (Tg'), and eutectic temperature (T_{eu}),[48,54-58] whereas freeze-drying microscopy is used for the determination of the collapse temperature (Tc).[59-62]

It is common that crystalline bulking agents, such as mannitol, polyethylene glycol (PEG), and glycine, are added to amorphous lyophilization formulations to facilitate the primary drying.[63] In such circumstances, a thorough understanding of the extent of crystallinity of the crystalline bulking agents is crucial in terms of process performances as well as storage stability. Bhatnagar et al.[64] studied the effect of sucrose concentration on the crystallization of PEG. They reported that sucrose concentration above 5 (% w/v) effectively hindered PEG crystallization during freeze-drying, whereas PEG was crystallized in a formulation with sucrose concentration up to 10 (% w/v) when PEG was covalently linked with recombinant human growth hormone. While PEG crystallization during freezing allows primary drying to be performed at elevated temperature and decreases primary drying time, failure of PEG crystallization during freeze-drying leads to crystallization during storage, which might affect protein stability. Low temperature X-ray powder diffractometry is one of the techniques used for qualitative determination of crystallinity on mixed frozen formulation.[65]

The illustration of the supplemented phase diagram (see Fig. 3) summarizes all the physicochemical changes that occur during freezing and the subsequent drying process for a selected proprietary formulation, named as A.

As can be observed in Figure 3, a solution "A," having a certain initial solute weight fraction, is cooled down according to a typical freezing protocol (red broken line starting at "A"). The freezing line crosses the equilibrium freezing curve, demonstrating the fact that solutions do not instantaneously freeze at their equilibrium freezing temperatures. As discussed in Cooling Stage section, the solution passes through a supercooling state before the formation of the first ice nucleus. After the formation of the first ice nucleus, additional ice crystals are created during the secondary nucleation, until the temperature of the supercooled water reaches the equilibrium freezing curve. The number of ice crystals formed during

the secondary nucleation is dependent on the degree of supercooling (cf. Phase Change Stage section).

Once the secondary nucleation is completed, additional heat is removed by cooling the solution further and the remaining water freezes and solidifies when the previously formed ice crystals grow.[32] If the cooling rate is slow, the solidification process follows the equilibrium freezing curve of the solution until it intersects the equilibrium solubility curve and this demonstrates that solidification is only proceeding by the growth of ice crystals formed during secondary nucleation. During the solidification process, the concentration of the solution increases as more water is removed by ice crystal growth and this increase in concentration is independent of the initial concentration (it only depends on temperature).[45] At the point of intersection of the equilibrium freezing curve and the equilibrium solubility curve, the solution reaches a critical concentration, above which the supersaturated solution undergoes, depending on the nature of the formulation, either eutectic freezing or vitrification.

Crystalline formulations undergo eutectic freezing, in which the solute crystallizes below the eutectic temperature. During the eutectic freezing, the unfrozen water is released from the supersaturated solution as the solute continues crystallizing and this free water immigrates to the frozen water and further crystallizes. If 100% solute crystallization is assured, it could be concluded that all the available water is also frozen. This means that, during freeze-drying of a crystalline formulation, all the water can be removed by sublimation, as shown in Figure 3. Crystalline formulations can be freeze-dried a few degrees below their eutectic temperatures without the need for secondary drying.

Amorphous formulations, on the other hand, undergo vitrification, in which the solute concentration continues to increase as more water freezes below the eutectic temperature. Freezing of water ceases when the freeze-concentrated solution changes from a rubbery to a glassy solid. This transition is marked by the intersection of the freezing curve and the glass transition curve in Figure 3. The temperature at which a transition from rubbery state to glassy solid is taking place is known as the glass transition of the maximally freeze-concentrated solution, Tg'. In amorphous formulations, the glassy solid consists of amorphous solutes and frozen (as well as unfrozen) water. Depending on the initial concentration of the solute, the unfrozen water in the glassy solid can be as high as 20%.[30]

Primary drying of amorphous formulations can be performed at a few degrees below Tc (as seen in Fig. 3) until all the frozen water is removed. At the end of primary drying, the water content of the dried product is still significantly high, which accounts for the unfrozen water. During the freeze-drying process, the unfrozen water is removed by a desorption process (more commonly known as secondary drying). During the secondary drying, the temperature of the formulation is increased to facilitate desorption of unfrozen water through the pores of the dried cake. It is, however, important to note here that the increase in temperature during the secondary drying should not lead to a temperature of the sample above the glass transition temperature, and hence the secondary drying curve should remain below the glass transition curve during the complete process (Fig. 3).

As demonstrated in Figure 3 and in the above sections, the random nature of the degree of supercooling is the main factor for the formation of heterogeneous ice habits during freezing. These heterogeneous ice crystals have significant effect during the drying process, as they impose differences in resistance to water vapor flow, which lead to heterogeneous product temperatures and drying behaviors. In addition, freezing may affect the physicochemical properties of a formulation, such as protein denaturation, pH shifts, and degradation reaction. Therefore, the knowledge of the freezing step and its impact on the product quality and process performance is a critical step for a successful process development and scale-up. In this context, the ability to control the degree of supercooling during the freezing step is essential in achieving consistent ice crystal habits and, hence, drying behaviors. Several technologies are available with the aim of controlling the degree of supercooling (nucleation) during the freezing step of a freeze-drying process, which will be discussed in the next section in detail.

Technological Alternatives for the Active Control of Ice Nucleation and Their Impact on the Freeze-Drying Process

The impact of the freezing step on the whole freeze-drying process is yet the least understood topic mainly because: (a) freezing a given formulation is not the final goal of a freeze-drying process and, as a consequence, it may be thought that achieving just a solidified formulation is sufficient for the subsequent drying process. This leads to the exclusion of the freezing step from discussions of freeze-drying process optimizations and failures; (b) the freezing step accounts, in most of the cases, for less than 15% of the total freeze-drying time and this turns the attention of many product development engineers and scientists to the optimization of the primary and secondary drying steps, neglecting the potential impact of the freezing step; and (c) the complexity of the freezing process, lack of variety of freezing methods equipped with freeze driers, and the difficulty of controlling the ice nucleation make it difficult to investigate the effect of different freezing methods on the freeze-drying process. This is why many freeze-drying process designers use the most easily available freezing method, the shelf-ramp method.

Nevertheless, the freezing step has been identified by some researchers as a particularly important step, which must also be monitored and controlled, as it impacts both the primary and the secondary drying steps. With this regard, there are several studies that deal with the effect of the freezing step on the freeze-drying process.[24,35,37,66-85] The primary reasons that explain this influence rely on the structure (morphology), size, and number of ice crystals formed during freezing (cf. Fig. 2). When the ice crystals sublime during primary drying, they leave a porous structure behind, through which water vapor flows. The size of the pores determines the resistance to water vapor flow (mass transfer) during primary and secondary drying, as shown in Equation 6. Larger ice crystals leave larger pores behind, and during primary drying, this means less resistance to mass transfer and faster drying rate. On the other hand, larger pore sizes reduce the surface area available for diffusion of the unfrozen solvent and decrease the rate of desorption during secondary drying.

The correlation between ice nucleation temperature (T_n) and ice crystal size or morphology was established many years ago. In 1925, Tammann reported that samples frozen at a high nucleation temperature yielded dendritic ice crystals, whereas samples frozen at a low nucleation temperature yielded crystal filaments.[43] In 1969, Thijssen and Rulkens reported that the freezing rate is an important determinant of pore size and drying rate in freeze-drying of liquid food products. For a 20% dextran solution freeze-dried in slabs, a faster cooling rate during freezing resulted in smaller pores and therefore higher resistance and slower drying rates.[86] Roy and Pikal[66] reported that the ice nucleation temperature in vials with thermocouples was higher than in vials without thermocouples, resulting in a higher primary drying rate. Recently, Searles et al.[24] demonstrated a strong correlation between the ice nucleation temperature and primary drying rate. They showed that an increase in ice nucleation temperature by approximately 12°C increased the primary drying rate of a model formulation by approximately 37%. A decrease in product resistance with increasing ice nucleation

temperature has been reported by Rambhatla et al.[70] In their study, they used the ice fog method to obtain different ice nucleation temperatures for 4 model formulations. They observed up to 38% reduction in product resistance when increasing the ice nucleation temperature by 8°C. Nakagawa et al.[74] demonstrated a clear relationship between ice nucleation temperature and ice morphology. In their study, they used ultrasounds to control the ice nucleation temperature. They reported that an increase in nucleation temperature from −8°C to −2°C changed the ice habit from small, many, and heterogeneous ice crystals to large and dendrite ice crystals. Similarly, Awotwe-Otoo et al.[36] and Esfandiary et al.[37] observed a significant primary drying time reduction because of a higher ice nucleation temperature achieved by using the controlled ice nucleation method.

During freezing, the cooling rate and the ice nucleation temperature can be controlled by means of different technologies, aiming to improve the impact of the freezing step on the subsequent primary and secondary drying processes, as well as on the final product quality, such as physical state of the sample, residual moisture content, and reconstitution time. Various methods that allow for the direct control of the freezing step have been proposed. Although such methods have demonstrated potential for process improvement at laboratory and pilot plant scales, their applicability to commercial-scale manufacturing of regulated products seems to be very difficult to achieve, due to economic, sterility, and safety concerns.[36] These different technological alternatives are discussed in detail in the following.

Precooled Shelf Freezing

In the precooled shelf freezing method, samples are placed on shelves, which are cooled to a predefined temperature. Searles et al.[24] used shelves precooled between −40 and −44°C and they found that the median nucleation temperature for the precooled shelf frozen samples was increased by around 3.5°C as compared to samples frozen using a shelf ramp freezing. They also demonstrated that samples placed on a shelf at −44°C nucleated over a wide range of temperature, indicating the limitation of the precooled shelf method to enable a consistent nucleation temperature across the vials. The effect of different loading shelf temperatures was studied by Hottot et al.[76] In their study, they measured the mean ice crystal size in the frozen matrix and reported insignificant effect of the loading temperatures on ice crystal sizes.

Comparing precooled shelf freezing to quench freezing, Dawson and Hockely demonstrated that 1%(w/v) trehalose formulation frozen by liquid nitrogen exhibited a fine filamentous directional network of ice crystals, had less resistance to vapor flow during drying and reconstituted faster, whereas freezing by placement on a −50°C shelf yielded a leafy mixed-orientation appearance with a higher resistance to vapor flow compared to liquid nitrogen–frozen samples.[87]

In general, the effect of different loading temperatures on subsequent process parameters, such as nucleation temperature, ice morphology, and drying rates should be systematically assessed if this method is going to be used.

Freezing with Annealing

Annealing is a process step in which samples are maintained at a specified temperature for a period. Annealing can be carried out as a holding temperature during the initial cooling but, more commonly, it is a postfreezing warming and holding step, followed by recooling.[28,88] More often, annealing is used to facilitate crystallization of active or bulking agents, but it also has a profound effect on improving consistency in inter-vial ice crystal size and drying behaviors.[22,28,46,67] The mechanism of ice crystal morphological change during annealing, as demonstrated by Searles,[28] is due to the difference in surface free energy between small and large ice crystals. According to Kelvin's equation, ice crystals with smaller radii of curvature induce a higher vapor pressure and, hence, on increased bulk mobility due to annealing, ice crystal regions with smaller radii will melt preferentially as a consequence of their higher vapor pressure, which induces higher free energy compared to ice crystal regions with larger radii.[88] In addition, higher temperature during annealing increases the diffusional mobility of the annealed species and, in turn, increases the diffusion of the melted ice crystals into the surviving ice crystals in the time scale of the annealing process. Therefore, the choice of temperature and time during an annealing process is a critical step. Furthermore, annealing can also promote the completion of freeze-concentrate (devitrification), as rewarming up to a temperature above Tg' allows amorphous water to crystalize.[32,67] However, annealing is not a suitable process for formulations susceptible for denaturation and degradation above their glass transition temperature. In addition, the benefits of shorter drying time may be offset by the additional time required for the annealing cycle.

The reported data on the impact of annealing on the subsequent drying processes are, until recently, controversial. Pikal et al.[89] found that annealing resulted in larger ice crystal sizes for small (5 μL) samples that were frozen rapidly between glass coverslips. With sublimation studies in a 13-μL microbalance apparatus, Pikal et al. also showed that annealing resulted in circa 50% decrease in the area-normalized dry product resistance for an amorphous formulation and up to 60% for a crystalline formulation, but actual drying rates were not presented. However, annealing was not tested on products frozen and dried in vials. On the other hand, Lu and Pikal[69] reported that annealing of a mannitol-trehalose-sodium chloride formulation increased the dried product resistance and hence the primary drying time. They hypothesized that the increase in dried product resistance of the annealed samples was because of the crystallization of solutes during annealing, preventing microcollapse during drying. Liu et al.[71] reported 10% and 17% primary drying time reduction when comparing a shelf ramp freezing with freezing and annealing at −10°C for 4 h and with freezing and annealing at −2.5°C for 4 h, respectively. Unfortunately, the source of the reduction in primary drying time in the study by Liu et al. is not clear, as the average product temperatures during primary drying for the 3 freezing protocols were identical while using the same shelf temperature and chamber pressure. This is because if annealing had helped to reduce the resistance to vapor flow, one would expect to see a reduction in product temperature if the shelf temperature and chamber pressure were identical. Searles et al.[67] reported that a 3.5-fold enhancement in primary drying rate can be achieved after annealing of amorphous sucrose, hydroxyethyl starch or mixture of both. On the other hand, a recent study by Esfandiary et al.[37] showed that, compared to a freezing protocol without annealing, up to 20% increase in primary drying time was observed when the same formulation was annealed at −15°C for 2 h. As demonstrated by these authors, the reason for this increase in primary drying time was the strong top crust formed in the annealed samples. In addition, Assegehegn et al.[90] recently reported insignificant effect of annealing on amorphous formulation with high solid content (18.5 wt%). They showed that the increase in cycle time due to the annealing step was higher than any reduction in cycle time in the subsequent drying process.

Quench Freezing

Quench freezing refers to the process of immersing sample containers either into liquid nitrogen, liquid propane, dry ice-

acetone, or dry ice-ethanol for a period that assures complete solidification.[32]

Quench freezing is characterized by a fast cooling and fast freezing. Fast cooling tends to stabilize metastable states by retaining greater quantities of unfrozen water, whereas fast freezing tends to promote a finer subdivision of the ice. High cooling rates tend to increase both nucleation and crystal growth rates.[33] It has also been reported that quench freezing results in a directional freezing. Thus, Hsu et al.[91] observed that freezing of vials in dry ice-isopropanol yielded directional solidification. Dawson and Hockely also demonstrated that a 1% (w/v) trehalose formulation frozen by liquid nitrogen exhibited a fine filamentous directional network of ice crystals.[87]

The impact of quench freezing on freeze-drying process optimization is not a well-studied subject yet; however, as the quench freezing promotes the formation of heterogeneous ice crystals, its applicability in manufacturing scale processes is minimal.[32]

Vacuum-Induced Surface Freezing

The concept of vacuum-induced surface freezing was introduced by Kramer et al.,[92] based on the mechanism that favors evaporation of cold water when the pressure of a solution is reduced at a given temperature. In these circumstances, the associated enthalpy of vaporization causes sufficient cooling of the solution surface to produce a thin film of ice. Kramer et al. proposed the following procedure to perform vacuum-induced surface freezing: the vials were placed on a precooled shelf at +10°C and the chamber pressure was reduced to a predefined value required to cause incipient surface freezing of the solution. This pressure was determined by visual observations and they set it at 1 mbar. After 5 min under these conditions, the solution exhibited a surface freezing to form an ice layer thickness of 1-3 mm. To avoid further boiling of water and melting of the ice surface film, the chamber pressure was released to atmospheric pressure as quickly as possible and, simultaneously, the shelf temperature was reduced to 3°C-4°C below the onset of melting of ice in the frozen formulation. After holding the solution at these conditions for 1 h, ice crystal growth was completed and the shelf temperature was further reduced to −40°C to complete the solidification phase of the freezing step. These authors claimed that the vacuum-induced surface freezing method produced large chimney-like ice crystals, which in turn yielded a reduction of up to 20% in primary drying time.

Liu et al.[71] also studied the impact of vacuum-induced surface freezing on subsequent primary drying. They reported up to 12% primary drying time reduction compared to a standard shelf ramp freezing. Contrary to the method by Kramer et al. described previously, Liu et al. modified the vacuum-induced surface freezing method as follows: the shelf temperature was first lowered down to −10°C and the chamber pressure to 0.8 mbar. After a visual observation of ice crystals on the top surface, the freezing step was completed by quickly lowering the shelf temperature to −45°C and holding. The reason for the lower shelf temperature, as compared to the original procedure, was because the latent heat of vaporization at higher shelf temperatures was not sufficient to lower the temperature of the sample at the bottom of the vial. In this case, complete nucleation might take longer than 5 min and "puff-off" of the sample could take place.

A recent study by Oddone et al.[93,94] reported that the vacuum-induced surface freezing method improves intra-vial and inter-vial drying behavior uniformity, as well as moisture content of model formulations. These authors also reported that the effective pressure to induce ice nucleation was formulation dependent. In addition, Oddone et al.[95] studied the effect of vacuum-induced surface freezing on secondary nucleation. Although the time required to achieve the same moisture content during secondary drying was longer for samples frozen using vacuum-induced surface freezing as compared to normal freezing, the overall time (primary and secondary) was shorter. In addition, consistency in vial-to-vial moisture content was improved using vacuum-induced surface freezing as freezing protocol.

In general, this method is associated with a high water boiling risk if some processing parameters, such as shelf temperature and chamber pressure, are not carefully selected. Moreover, only few experimental results are available so far to support its effectiveness and scalability.

Ice Fog Freezing Technique

The use of ice fog to nucleate ice crystals was first proposed by Rowe[96] and implemented for the freeze-drying process by Rambhatla et al.[70] The concept of ice fog technique relies on the use of cold nitrogen as a heat exchange medium. When cold nitrogen gas enters the product chamber, ice crystals are formed from the water vapor inside the chamber. These ice crystals are then forced into the vials, due to the slightly higher pressure outside the vials, and serve as nucleation seeds. The primary advantage of this technique is the improvement of the uniformity of ice nucleation among vials. In addition, Rambhatla et al. reported that the ice fog technique can also be used to perform freezing at a defined nucleation temperature. With this aim, Rambhatla et al. used ice fog technique to nucleate samples at different nucleation temperatures ranging from −1°C to −12°C.[70] As a first approach, they used nitrogen at −40°C and reported a successful nucleation at 3 different temperatures (−3°C, −7°C, and −12°C). However, complete nucleation of all vials took as long as 30 min. In addition, they found no significant differences in dried product resistance of the samples nucleated at the 3 nucleation temperatures, although a 10% increase in primary drying time, resulting from 8°C increase in nucleation temperature, was reported.[70] The reason for this, according to the authors, is that the long time required for complete nucleation of the samples at a temperature far above their Tg' favors annealing and Ostwald ripening, which increases the ice crystal size and, hence, reduces the dried product resistance of samples nucleated at low temperatures. To tackle this problem, the same authors modified the technical setup of the ice fog technique and the temperature of the nitrogen entering the chamber was reduced from −40°C to −50°C. These improvements enabled them to achieve complete nucleation, in all the vials studied, in less than 5 min. Using this setup, they reported nearly 30% reduction in primary drying time when comparing samples nucleated at −11°C with samples nucleated at −1°C.[70]

In a follow-up study, Patel et al.[97] used a modified version of the ice fog technique called reduced pressure ice fog technique. In this technique, before the introduction of cold nitrogen, the pressure inside the chamber was evacuated at a desired nucleation temperature, as shown in Figure 4. Different reduced pressures, namely from 800 to 64 mbar, were tested. However, the results obtained at high pressures were not satisfactory at all. They reported that, in a pressure range from 66.7 to 64 mbar, complete nucleation of one shelf load was achieved in less than a minute. However, there was no explanation given on why the higher pressure range was not successful or why the reduced pressure technique shortened the nucleation time. The most probable reason could be that, owing to the large pressure difference between the cold nitrogen chamber and the drying chamber, the high suction power of the drying chamber was able to draw a large amount of cold nitrogen gas. This amount of cold nitrogen gas was then able to nucleate much more water vapor inside the chamber, which was sufficient to seed all the

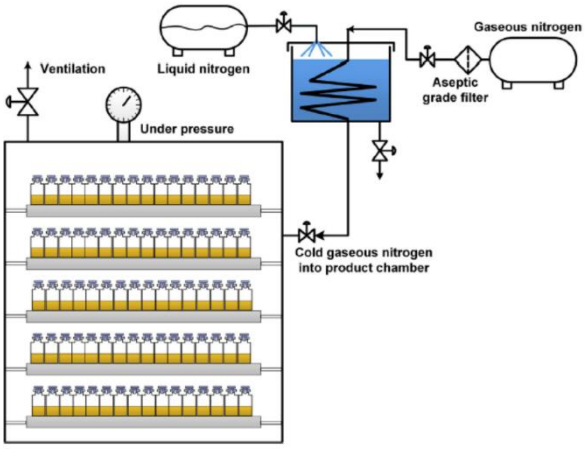

Figure 4. Pictorial depiction of the original ice fog method, as described by Patel et al.[97] In this method, once the vials reach the desired nucleation temperature, cold nitrogen gas is introduced into the product chamber. The ice fog is generated from the humidity inside the chamber.

vials within short periods of time. This could also explain the reason why high drying chamber pressure ranges were not successful. High chamber pressure reduces the pressure difference between the cold nitrogen chamber and the drying chamber, thus limiting the amount of cold nitrogen entering into the drying chamber. Therefore, the amount of cold nitrogen introduced into the chamber, either via reduced drying chamber pressure or increased cold nitrogen chamber pressure, and the ability to uniformly distribute the nitrogen within the drying chamber, especially for manufacturing freeze-driers with many and large shelves, define the success of the ice fog technique. The aforementioned reasoning is also supported by the full load experiment (3 fully loaded shelves) performed by Patel et al.,[97] in which the reduced pressure ice fog technique was not able to nucleate all the vials uniformly and in a short period, even at the lowest chamber pressure.

An industrial scale ice fog technique is currently available from Linde Gases, in collaboration with IMA Life North America, under the trade name of VERISEQ® nucleation technology,[38,39,98] and from Millrock Technology, Inc., under the trade name of FreezeBooster® Controlled Nucleation Technology. In the case of industrial scale ice fog method, the ice crystals are first formed by mixing cold nitrogen and water vapor in a device, such as an ejector, outside the product chamber. The ice fog is then introduced into the product chamber once the vials reach the desired nucleation temperature,[38] as shown in Figure 5. It has been reported that, for freeze dryers having 1.1 m^2 and 2.5 m^2 shelf area, introduction of ice fog for 30-50 s was sufficient to nucleate all the vials.[38] However, the number of vials used in these tests was far away from the full capacity of the freeze dryers and the success of ice fog technique cannot be guaranteed yet. In another study, Azzarella et al.[39] reported successful ice fog controlled nucleation in industrial scale freeze dryers with shelf areas of 15 m^2, 39 m^2 (45,540 vials), and 56 m^2 (195,960 vials), yielding a reduction of up to 19% in product primary drying time and up to 40% improvement in batch homogeneity. They have also reported that, to successfully induce nucleation for bigger freeze dryers, jacketed walls are required to reduce thermal gradient across the shelf stacks.

In general, even though the ice fog freezing technique is a promising method for the active control of nucleation, especially from inter-vial and intra-vial homogeneity points of view, more studies are needed to support its success at industrial scale.

High-Pressure Shift or Depressurization Freezing

High-pressure shift freezing has been a common practice in freeze conservation of foods.[99] In this method, the samples are exposed to high pressure while their temperature is lowered. According to the phase diagram of water, liquid water can be kept unfrozen well below its equilibrium freezing temperature under high pressure conditions. When the desired temperature is reached in the product, pressure is released, inducing uniform supercooling throughout the sample. This is due to the fact that the increase in pressure affects the whole sample instantaneously and at the same time. Thus, this supercooling induces uniform formation of nuclei throughout the sample (regardless of its shape or size), so that the latent heat is released, raising the sample temperature to the corresponding equilibrium freezing temperature. Freezing is then completed at constant pressure, usually at atmospheric conditions, and by lowering the shelf temperature. The higher the pressure and the lower the product temperature before expansion, the more is the ice formed.[99-102] This is consistent with the fact that a higher degree of supercooling produces many ice crystals.

The main advantage of high-pressure shift freezing in the food industries is related to the big amount of ice instantaneously formed after expansion.[102] By contrast, formation of few and large ice crystals is the main goal in the freeze-drying process. This can be achieved by manipulating the parameters of the high-pressure shift freezing method, such as the pressure difference before and after expansion and the product temperature before expansion. A small pressure difference and high product temperature produce few and large ice crystals.

Application of high-pressure shift freezing to a freeze-drying process was first introduced by Gasteyer et al.[103] The procedures of the freezing method they have used in their patent are identical

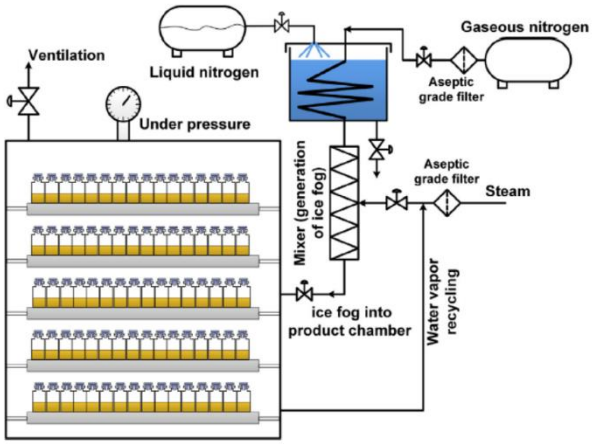

Figure 5. Pictorial depiction of the modified (industrial) ice fog method, as described by Chakravarty et al.[38] In this modified method, ice fog is generated outside the product chamber in a mixer, mixing cold nitrogen gas with water vapor. The ice fog is then introduced into the chamber once the vials reach the desired nucleation temperature.

to the one described previously, which comprise (1) cooling the materials to near or below their equilibrium freezing temperature in an elevated pressure; (2) decreasing the pressure to induce ice nucleation; and (3) further cooling the materials up to complete solidification. As described by these authors, the possible mechanisms for inducing ice nucleation using high-pressure shift freezing are (1) an initial elevated pressure increases the concentration of dissolved gas in a solution and a rapid decrease in pressure at low temperature reduces the gas solubility. As a consequence, the gas is released from the supercooled solution, forming cold bubbles, which trigger nucleation; (2) depressurization causes evaporation of some liquid in the solution and the resultant cooling from the endothermic evaporation process may initiate the nucleation; and (3) on depressurizing, the cold gas in a close proximity to the solution freezes some vapor and these ice crystals re-enter the solution and act as seeds or surfaces to initiate nucleation. As part of the patent supporting examples, Gasteyer et al. reported a reduction in primary drying time, stating an average difference in water loss of about 21% when comparing samples frozen using high-pressure shift freezing with samples frozen using shelf-ramp freezing. The primary drying conditions in both freezing methods were identical.[103] One of the main advantages of controlled ice nucleation is to improve vials freezing behavior consistency and, consequently, to achieve uniform ice sublimation. However, this was not achieved in the example provided by these authors.[103] In their example, the averages plus or minus standard deviations of the water loss for the vials studied were 86.1 ± 3%, in the case of samples frozen using high-pressure shift freezing, and 65.2 ± 0.93%, in the case of shelf-ramp frozen samples. This demonstrates that shelf-ramp freezing produces a better ice sublimation uniformity than high-pressure shift freezing.

The applicability of high-pressure shift freezing was demonstrated both at laboratory (1 m^2 shelf area) and small industrial scale (5 m^2 shelf area) freeze dryers by performing repeated tests, where the ice nucleation temperature was controlled within 1°C of their equilibrium freezing point.[104] Bursac et al.[104] reported a 27% decrease in primary drying time for 5 wt% sucrose freeze-dried by applying high-pressure shift freezing as compared to shelf-ramp freezing. In addition, the same authors reported improved dried product uniformity, demonstrating a reduction in absolute standard deviation in the residual moisture content of the sucrose cakes from 4.6% down to 2.1%. In another study, Konstantinidis et al.[35] reported 40% reduction in primary drying time for a 5 wt% mannitol solution when using high-pressure shift or depressurization controlled nucleation. In other more recent studies by Awotwe-Otoo et al., the advantage of controlling ice nucleation using high-pressure shift or depressurization technique has been demonstrated.[36,80] For the formulations studied, they reported up to 21% reduction in primary drying time, although the difference in residual moisture content was insignificant.

The high-pressure shift or depressurization freezing technique at industrial scale is available from Praxair, Inc., under the trade name of ControLyo™, Nucleation On-Demand Technology. However, experimental studies demonstrating the success of this technique at this scale are not yet available.

In general, it could be said that high-pressure shift or depressurization freezing technique is an effective tool for controlling the degree of supercooling or ice nucleation during the freeze-drying process. That is because this technique relies on inducing ice nucleation based on pressure manipulation, and the isostatic nature of pressure (i.e., even application of pressure to all containers under treatment) offers significant advantage in terms of (1) covering a wide range of sample sizes (potential for ease of scalability); and (2) inducing ice nucleation over a wide range of sample sizes instantaneously and simultaneously (potential for improving freezing uniformity within as well as between batches and potential for reducing freezing time). In addition, as described by Rampersad et al.,[105] a freeze dryer requires minimum adaptation to accommodate the high-pressure shift or depressurization freezing technique.

Ultrasound-Powered Freezing

The application of power ultrasounds for active control of freezing food products has been proven to be effective.[34,106-108]

Many authors have reported that ultrasound vibration can be used to initiate ice nucleation at a desired freezing temperature.[74,109-111] Ultrasound-powered freezing process is generally accomplished according to the following steps[74,77,110]: (1) cooling the sample down to a desired nucleation temperature; (2) applying ultrasound power at a certain frequency and for a period; and (3) further reducing the temperature until complete solidification, as shown pictorially in Figure 6. The mechanism of inducing ice nucleation by using ultrasounds remains uncertain. However, regardless of the mechanism, it has been clearly demonstrated that the application of ultrasounds has a notable and quantifiable effect on ice nucleation.[110] Different theories have been proposed to describe the mechanism of ultrasounds-induced ice nucleation. The first proposal was provided by Hickling.[112] Based on this proposal, extensive collapse of cavitation bubbles produced by ultrasounds generates local zones of high pressure for a very short period of time. These high-pressure zones increase the local degree of supercooling, which acts as a driving force for ice nucleation. On the other hand, Zhang et al.[113] reported a delay on the onset of ice nucleation after the application of ultrasound irradiation. They attributed this delay not only to the collapse of cavitation bubbles, but also to some other variables responsible for ice nucleation. A complete different mechanism of ultrasound-triggered ice nucleation was reported by Dodds et al.[114] This mechanism is based on a molecular segregation theory, which explains that the driving force for nucleation is the pressure gradient around the cavitation bubble, resulting in a pressure-controlled diffusion of particles. These particles are composed of a number of molecules, which, on segregation, create a nucleus. In addition to the aforementioned mechanisms, Chow et al.[115-117] reported that ultrasound irradiation may also trigger secondary nucleation. They hypothesized that the movement of fast and powerful cavitation bubbles fragments the ice crystals already created, producing additional new ice crystals (termed as secondary nucleation). Because of these phenomena, ultrasound irradiation creates numerous and small ice crystals even at relatively high ice nucleation temperature.

The use of ultrasound-powered controlled ice nucleation for freeze-drying applications was first reported by Nakagawa et al.,[74] who implemented an ultrasound system to control the freezing step during freeze-drying of proteins in vials. These authors reported that ultrasound power can be used to initiate ice nucleation of model pharmaceutical formulations at a preselected ice nucleation temperature. However, the relationship between the ice nucleation temperature and the ultrasound process parameters was not described. Other studies suggested that pulse or acoustic power,[109-111,115] ultrasound duration,[106,111] number of cavitation bubbles,[117] and initial oxygen content[118] influence the ice nucleation temperature, and ice crystal size and shape. Nakagawa et al.[74] reported a clear correlation between ice nucleation temperature and ice crystal size during ultrasound-powered controlled ice nucleation. Small and numerous ice crystals were obtained at low nucleation temperature (higher supercooling degree), whereas large and directional ice crystals (dendrite type) were obtained at high nucleation temperature (lower supercooling degree). They also reported a significant reduction in primary drying time, up to 60%, when the ice nucleation temperature was increased from −8°C to −2°C. In another study, Passot et al.[79] reported an improved intra-vial homogeneity in sublimation by using ultrasound-controlled ice nucleation. In addition, up to 14% reduction in primary drying time was reported by changing the freezing protocol from shelf-ramp freezing to ultrasound-controlled freezing.[79]

In general, ultrasound-powered controlled ice nucleation could be considered a promising alternative for controlling ice nucleation during freeze-drying. However, some drawbacks associated with the ultrasound technology need to be addressed. These include (1) the heat dissipated during ultrasounds application may alter the freezing process. Hence, optimum acoustic power and duration should be determined, which could represent a challenge; (2) Nakagawa et al.[74] reported that vials having poor mechanical contact with the shelf surface might be less affected by the ultrasound vibration. In addition to this, application of uniform ultrasound vibration across a single shelf surface, as well as across the shelf stack, might be a challenge in an industrial scale freeze drier; (3) scalability of the freeze-drying process to industrial scale. In this regard, the optimum ultrasound power and duration obtained in a laboratory scale freeze dryer might not be directly applied to an industrial scale freeze dryer. This means that scaling up the ultrasound process could present a huge challenge; and (4) the application of strong and intensive vibration on the freeze dryer shelves obviously creates particulate matters, which jeopardize the sterility of the process.

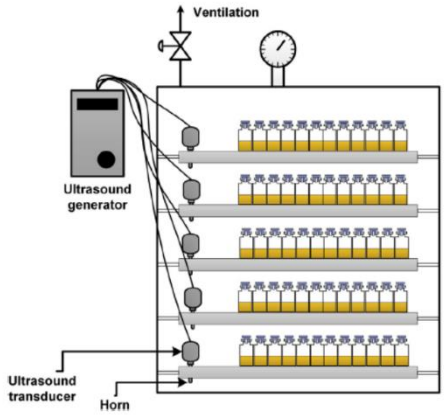

Figure 6. Pictorial depiction of ultrasound-powered freezing as described by Nakagawa et al.[74] In this method, controlled ultrasound power is applied to the shelves, once the vials reach the desired nucleation temperature.[74]

Electrofreezing

Although the effect of electrofreezing on the freezing of water droplets in the atmosphere was reported as early as 1861,[119] the first trials to induce ice nucleation in supercooled water droplets by high-voltage electric fields were carried out by Rau[120] in 1951. Electrofreezing is generally carried out according to the following protocol[121,122]: (1) cooling the sample to a desired nucleation temperature; (2) applying an electric field, in a continuous or pulsed manner, to the supercooled sample to induce ice nucleation; and (3) further reducing the temperature up to complete solidification. Although many scientists tried to study the mechanism of electrofreezing to induce ice nucleation experimentally[121,123-125] and theoretically,[126-128] the basic mechanism is still controversial. However, bubble formation and breakdown induced by the electric field are believed to be the most accepted mechanisms.[121,122]

Application of electrofreezing in the freeze-drying process is still not a well-developed technology because of many drawbacks associated with an electrofreezing process in typical freeze-drying applications. These include its relative complexity and high costs

associated to its implementation and maintenance, the invasive nature of the method, and the incompatibility with solutions containing ionic species (e.g., NaCl). In addition, the effectiveness of electrofreezing is also electrode-dependent,[125] which adds more complexity to the method. In relation to the applicability of electrofreezing in the freeze-drying process, Petersen et al.[122] reported that electrofreezing can be used to selectively choose nucleation temperature during the freezing step and hence reduce the primary drying time.

In general, electrofreezing is a method that needs a thorough study for its applicability in freeze-drying application. This method requires the need of an electrode in each container system, questioning the application of this method in a freeze-drying process at industrial scale, as well as introducing apparent sterility concerns.

Ice Crystals Distribution From Condensed Frost

Controlled ice nucleation using pressure differential ice fog distribution from a cold condenser was first introduced by Ling.[129] This method is based on the following steps: (1) cooling down a product placed inside a product chamber to a predetermined temperature; (2) creating sufficient volume of ice fog in a separate condenser chamber, which is connected to the product chamber using a vapor port; and (3) opening the vapor port between the condenser chamber (which is at a pressure higher than the product chamber pressure) and the product chamber. During this operation, ice fog from the condenser distributes rapidly and evenly through the vapor port into the product chamber, which acts as nucleating agent.

In the original ice fog method, the ice fog is created from the humidity inside the product chamber by introducing cold nitrogen gas, which, according to Ling, has some drawbacks. These include inability to nucleate large number of vials simultaneously at a controlled time and temperature, producing significant vial-to-vial heterogeneity in nucleation temperature (owing to the time difference between the first and the last frozen vials), and requirement of significant retrofit to implement it.[129] Ling reported that creating a sufficient amount of ice fog, according to the size of the product, in an external chamber (such as a condenser chamber), resolves the aforementioned drawbacks of the original ice fog method. In contrast to the aforementioned advantage of ice fog from an external condenser chamber reported by Ling,[129] the same author[130] reported, in an accompanying patent, that the amount of ice fog produced in a limited volume of condenser chamber was insufficient to nucleate large number of vials. In the new patent, Ling reported that volume limitation of the condenser chamber can be tackled by producing a condensed frost (solid) instead of a suspended ice fog (gas),[130] as shown in Figure 7. During the opening of the isolation valve between the product chamber and the condenser chamber, the sudden change in pressure creates strong gas turbulence in the condenser chamber. This turbulence is capable of breaking any loosely attached condensed frost into ice crystals and these ice crystals travel to the product chamber and act as nucleating agent. However, Ling's patents[129,130] do not contain experimental results to support any of the claims and advantages, as well as to prove the effectiveness of the methods in a large-scale freeze-drying process.

With this regards, Geidobler et at.[131] reported a similar approach of controlled nucleation. This approach is based on the following steps: (1) cool down and equilibrate the product inside the product chamber to a desired temperature; (2) Cool down the condenser to around −50°C to −80°C and spray sterile water to load the condenser with ice; (3) depressurize the freeze dryer (both product and condenser chambers) to a predefined vacuum set point; (4) Repressurize the freeze dryer using a venting valve connected to the condenser. During repressurization, the venting gas passes through the cold condenser to the product chamber, carrying ice crystals.[131] According to these authors, the predominant mechanism for induction of nucleation is that loosely attached ice from the condenser surface is blown into the product chamber during repressurization, even though in situ generated ice crystals might also have contribution.[131] The success of nucleation in this approach, according to these authors, was nearly 100% for small scale batch sizes. In addition, Geidobler et al.[81] reported a significant improvement in specific surface area and primary drying time of several formulations containing bovine serum albumin and monoclonal antibody, when comparing shelf ramp freezing and precooled shelf methods with the previously stated controlled nucleation approach.

The approach developed by Geidobler et al.[131] is under development by different companies, such as GEA Lyophil GmbH, under the trade name of LYOSPARK™ controlled nucleation, and Martin Christ Gefriertrocknungsanlagen GmbH, under the trade name of LyoCoN controlled nucleation.

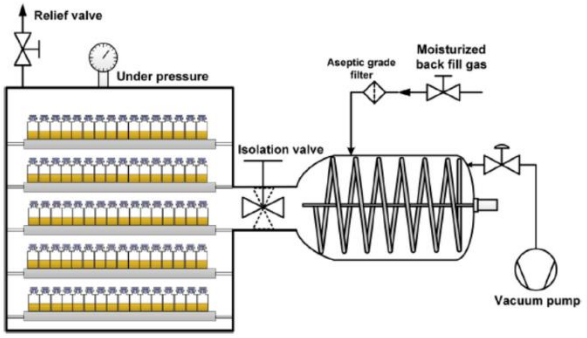

Figure 7. Pictorial depiction of ice crystals distribution from condensed frost, as described by Ling.[130] In this method, the condenser chamber is used to create ice crystals by introducing moisturized gas after cooling it down to below −50°C. Once the isolation valve is open, the ice crystals are distributed to the product chamber due to the pressure difference between the 2 chambers.[130]

In general, the most significant limitation of this approach, as it is in almost all controlled nucleation techniques, is the ability to uniformly and instantly trigger nucleation at large-scale freeze dryers. It is therefore crucial that freeze dryer–manufacturing companies deliver reliable and useful experimental data regarding the effectiveness of this approach at industrial scale freeze dryers.

Gap Freezing

Gap freezing is a relatively recent concept introduced by Kuu et al.,[132,133] which is performed according to the following steps: (1) creating a gap between the cooling shelves and the vials by using low thermal conductivity spacers and a stainless steel tray; (2) placing the vials on the tray; and (3) applying a step change of temperature, usually directly up to the final temperature. During the step change in temperature, the actual cooling rate of the samples is determined by the heating and cooling capabilities of the freeze dryer.[82] The gap freezing concept is designed to eliminate directional freezing of solutions, which, as the authors claim, happens when vials are directly sitting on the cooling shelves. This is due to the fact that the much higher heat transfer rate from the bottom shelf to the vials than from the top shelf to the vials causes freezing to start at the bottom of the vials, moving then upward. During this upward freezing phenomenon, solutes are pushed upward in the vials, resulting in a solute concentration at the top of the vials, which can eventually form a "skin layer" at the cake surface and, subsequently, increasing the dried product resistance to vapor flow during primary drying.[82] Therefore, Kuu et al.[82,133] reported that the gap freezing method can avoid the upward freezing phenomenon and promote a uniform freezing of solutions both from bottom and top directions, avoiding formation of a highly concentrated skin layer. Even though the exact mechanism for increasing the ice nucleation temperature was not described, the authors also reported an increase in ice nucleation temperature of samples frozen by using the gap freezing method as compared to samples frozen by conventional shelf ramp freezing.[82]

Kuu et al.[82,134] performed different studies to explain the effect of gap freezing on freeze-drying performance, mainly by comparing the results obtained with those from the conventional shelf ramp freezing method. However, more studies are still needed to explain the advantages of gap freezing over the other controlled ice nucleation methods, in terms of freeze-drying process performance, ease of scaling up, and ease of implementation in an industrial scale freeze-drying process.

Summary

Freeze-drying is a very commonly used drying unit operation in pharmaceutical and biopharmaceutical industries, mainly for the purpose of removing solvents from unstable liquid formulations. The shelf life of unstable liquid formulations can be significantly extended if the solvents, which facilitate chemical and physical degradation pathways, are removed from these formulations. During a freeze-drying process, the formulation is first frozen and, then, the frozen solvent is removed by a sublimation process at a reduced pressure, followed by a desorption process for the removal of the unfrozen solvent. Therefore, 2 equally important major processes are taking place during a complete freeze-drying process: (1) freezing, during which most of the solvent is converted into a frozen solid; and (2) drying, during which almost all the solvent (frozen and unfrozen) is removed from the formulation. The drying process is further classified into 2 steps, based on the mechanism of the drying process, namely sublimation process (primary drying) and desorption process (secondary drying).

Freezing is the first step in the freeze-drying process and the fundamental understanding of the physicochemical changes during freezing is of paramount importance due to the fact that the freezing step dictates ice crystal morphology, size, and size distribution, which in turn influence several critical parameters, such as dried product resistance, primary and secondary drying rates, extent of product crystallinity, and reconstituability of the dried product. In addition, freezing is a critical step with regard to biological activity and stability of the APIs, especially pharmaceutical proteins.

Physical changes during freezing take place in 3 distinct phases: (1) cooling stage; (2) phase change stage; and (3) solidification stage. During the cooling stage, the temperature of the solution is lowered below its equilibrium freezing temperature until the first ice nucleus starts to be formed. The temperature at which the first ice nucleus is formed is known as ice nucleation temperature. The physical state of a solution below its equilibrium freezing temperature is called supercooling and the degree to which a solution retains its supercooling state before formation of the first ice nucleus is called degree of supercooling. In other words, the degree of supercooling is the temperature difference between the equilibrium freezing temperature and the ice nucleation temperature. The degree of supercooling determines the number, size, and morphology of ice crystals and, consequently, many other critical parameters during the drying phase of the freeze-drying process. The degree of supercooling is quite variable and it significantly differs from container to container, being affected by several factors such as foreign particles, container surface area, process conditions, sample volume, composition of the matrix, and contact area between sample and container. This random nature of the degree of supercooling affects the ice habit and results in vial-to-vial and batch-to-batch ice habit heterogeneity. This, in turn, adds a significant challenge during development, optimization, and scale-up of the freeze-drying process. In addition, the degree of supercooling at different manufacturing scales can be affected due to the differences in particulate levels, which adds additional challenges to the scale-up of a freeze-drying process. During the phase change stage, formation of ice nuclei is taking place. The number of ice nuclei formed, the rate of ice growth, and the ice crystals size depend on the degree of supercooling. The higher the degree of supercooling, the more crystallization heat can be absorbed by the supercooled solution, and the more fraction of water instantly freezes, resulting in many ice crystals. Solutions with small degree of supercooling, on the other hand, absorb only a small amount of the heat of crystallization. This results in a small fraction of freezable water to instantly freeze and, hence, the formation of very few ice crystals is favored. During the solidification stage, the ice crystals formed during the phase change stage grow in size, increasing the concentration of the solution. Solidification stops when, for a crystalline solution, all the solute and the solvent crystallize, whereas, for an amorphous solution, the increase in concentration of the solution prevents further growth of ice. For crystalline solutions, complete solidification is achieved below the eutectic temperature of the solution, whereas, for amorphous solutions, complete solidification is achieved below the glass transition of the maximally freeze-concentrated solution.

The variation in degree of supercooling is the major challenge during the freeze-drying process development and scale-up. Therefore, its control during the freezing step is of paramount importance. Several alternative technologies, developed with the aim of controlling the degree of supercooling during the freeze-drying process, have been reviewed here and are summarized in Table 1.

Most of these technologies have been successfully tested at laboratory scale, but their potential use at industrial scale is still

Table 1
Summary of Alternative Freezing Technologies and Their Advantages and Disadvantages with Regard to the Active Control of Ice Nucleation for Freeze-Drying Applications

Freezing Methodologies	Method Description	Advantages[a]	Disadvantages[a]	References
Precooled shelf freezing	Vials are placed on shelves cooled to a predefined temperature	Increases Tn Easy to scale-up Noninvasive Retrofit not needed	Inability to select Tn Formation of heterogeneous ice crystals	24,76
Freezing with annealing	Vials are held at a specified temperature above Tg' during cooling or rewarmed after freezing	Increases ice crystals size Increases drying rate Increases intra-batch and inter-batch ice crystal homogeneity Easy to scale up Noninvasive Retrofit not needed	Inability to select Tn Sensitive to annealing temperature and time May promote degradation of sensitive APIs Additional process time due to annealing step	22,28,37,46,67,69,71,88,89
Quench freezing	Vials are immersed in a cold bath	Increases Tn Noninvasive	Inability to select Tn Difficult to scale up Formation of heterogeneous ice crystals Retrofit needed	33,87,91
Vacuum-induced surface freezing	Vials are placed on a pre-cooled shelf and chamber pressure is reduced to promote surface freezing of the solution	Increases Tn Increases drying rate Increases intra-batch and inter-batch ice crystal homogeneity Retrofit not needed Noninvasive	Inability to select Tn Risk of "puff-off" and boiling Difficult to scale up	71,92-95
Ice fog freezing technique	Ice fog is injected into cold vials as nucleating agents	Ability to select Tn Increases drying rate Increases intra-batch and inter-batch ice crystal homogeneity Good repeatability Possible to scale up	Retrofit needed Invasive Less effective at industrial scale (needs more experimental support) Expensive	38,39,70,97,98
High-pressure shift or depressurization freezing	Instant nucleation is induced by reducing the pressure after vials are cooled to a desired nucleation temperature at an elevated pressure	Ability to select Tn Increases drying rate Increases intra-batch and inter-batch ice crystal homogeneity Good repeatability Easy to scale up Could be effective at industrial scale (needs more experimental support)	Retrofit needed Invasive Expensive	35,36,80,103-105
Ultrasound-powered freezing	Instant nucleation is induced by applying ultrasound power after vials are cooled to a desired nucleation temperature	Ability to select Tn Increases drying rate	Retrofit needed Strong vibration creates particulate matter and thus sterility concern Difficult to scale-up Difficult to optimize the process	34,74,77,79,106,107,109,110
Electrofreezing	Nucleation is induced by applying electric pulse after vials are cooled to a desired nucleation temperature	Ability to select Tn Increases drying rate	Retrofit needed Invasive Incompatibility with solutions containing ionic species Expensive	121,122,125
Ice crystals distribution from condensed frost	Ice crystals are injected into cold vials as nucleating agents	Ability to select Tn Increases drying rate Increases intra-batch and inter-batch ice crystal homogeneity Good repeatability Possible to scale up	Retrofit needed Invasive Less effective at industrial scale (needs more experimental support) Expensive	81,129-131
Gap freezing	Vials are placed and cooled in a stainless tray, which is in a certain gap from the shelf	Reduces "skin layer" at the top Increases drying rate Possible to scale-up	Inability to select Tn Slow freezing process might offset benefits of drying rate Retrofit needed Increases equipment height	82,132-134

TN, nucleation temperature.
[a] Advantages and disadvantages sections include author's opinion.

under progress. The lack of experimental data concerning the effectiveness of these technologies at industrial scale, as well as the potential expensive investment are the major factors preventing companies from implementing them. It is therefore evident that more research and experimental data are necessary to justify their effectiveness, especially at industrial scale.

References

1. Franks F. *Freeze Drying of Pharmaceuticals and Biopharmaceuticals*. Cambridge: The Royal Society of Chemistry: RSC Publishing; 2007.
2. Bosca S, Fissore D. Monitoring of a pharmaceuticals freeze-drying process by model-based process analytical technology tools. *Chem Eng Technol*. 2014;37(2):240-248.
3. Walters RH, Bhatnagar B, Tchessalov S, Izutsu K, Tsumoto K, Ohtake S. Next generation drying technologies for pharmaceutical applications. *J Pharm Sci*. 2014;103(9):2673-2695.
4. Pikal MJ. Freeze drying. In: Swarbrick J, ed. *Encyclopedia of Pharmaceutical Technology*. 3rd ed. New York: Informa Healthcare, Inc.; 2006:1807-1833.
5. Bhatnagar BS, Tchessalov S, Lewis LM, Johnson R. Freeze drying of biologics. In: Swarbrick J, ed. *Encyclopedia of Pharmaceutical Science and Technology*. 4th ed. New York: Taylor and Francis; 2013:1673-1722.
6. Kharaghani A, Tsotsas E, Wolf C, Beutler T, Guttzeit M, Oetjen G. Freeze drying. In: *Ullmann's Encyclopedia of Industrial Chemistry*. Weinheim: Wiley-VCH Verlag GmbH & Co. KGa; 2017.
7. Ohtake S, Martin RA, Saxena A, et al. Formulation and stabilization of Francisella tularensis live vaccine strain. *J Pharm Sci*. 2011;100(8):3076-3087.
8. Jangle RD, Pisal SS. Vacuum foam drying: an alternative to lyophilization for biomolecule preservation. *Indian J Pharm Sci*. 2012;74(2):91-100.
9. Cheow WS, Li S, Hadinoto K. Spray drying formulation of hollow spherical aggregates of silica nanoparticles by experimental design. *Chem Eng Res Des*. 2010;88(5-6):673-685.
10. Ohtake S, Martin RA, Yee L, et al. Heat-stable measles vaccine produced by spray drying. *Vaccine*. 2010;28(5):1275-1284.
11. Cortés-Rojas DF, Fernandes Souza CR, Pereira Oliveira W. Optimization of spray drying conditions for production of Bidens pilosa L. dried extract. *Chem Eng Res Des*. 2015;93:366-376.
12. Sonner C, Maa YF, Lee G. Spray-freeze-drying for protein powder preparation: particle characterization and a case study with trypsinogen stability. *J Pharm Sci*. 2002;91(10):2122-2139.
13. Cheow WS, Ng ML, Kho K, Hadinoto K. Spray-freeze-drying production of thermally sensitive polymeric nanoparticle aggregates for inhaled drug delivery: effect of freeze-drying adjuvants. *Int J Pharm*. 2011;404(d1-2):289-300.
14. Dolly P, Anishaparvin A, Joseph GS, Anandharamakrishnan C. Microencapsulation of Lactobacillus plantarum (mtcc 5422) by spray-freeze-drying method and evaluation of survival in simulated gastrointestinal conditions. *J Microencapsul*. 2011;28(6):568-574.
15. Reverchon E, Adami R, Cardea S, Della Porta G. Supercritical fluids processing of polymers for pharmaceutical and medical applications. *J Supercrit Fluids*. 2009;47(3):484-492.
16. Jin HY, Xia F, Zhao YP. Preparation of hydroxypropylmethyl cellulose phthalate nanoparticles with mixed solvent using supercritical anti-solvent process and its application in co-precipitation of insulin. *Adv Powder Technol*. 2012;23(2):157-163.
17. Gabel RD, Mattern M, Winter G, Wirl A, Woog H. *Process for the Manufacture of Dry, Amorphous Products Comprising Biologically Active Material by Means of Convection Drying and Products Obtainable by the Process*. Patent. Munich: European Patent Office; 1998. EP0913178.
18. Farrel G, McMinn WAM, Magee TRA. Microwave-vacuum drying kinetics of pharmaceutical powders. *Dry Technol*. 2005;23(9):2131-2146.
19. de Jesus SS, Filho RM. Optimizing drying conditions for the microwave vacuum drying of enzymes. *Dry Technol*. 2011;29(15):1828-1835.
20. Xie J, Jiang J, Davoodi P, Srinivasan MP, Wang CH. Electrohydrodynamic atomization: a two-decade effort to produce and process micro-/nanoparticulate materials. *Chem Eng Sci*. 2015;125:32-57.
21. Shanley A. Modernizing lyophilization. *Biopharm Int*. 2017;30(12):50-52.
22. Tang X, Pikal MJ. Design of freeze-drying processes for pharmaceuticals: practical advice. *Pharm Res*. 2004;21(2):191-200.
23. Rey L. Glimpses into the realm of freeze-drying: classical issues and new ventures. In: Louis R, Joan CM, eds. *Freeze Drying/Lyophilization of Pharmaceutical and Biological Products*. 3rd ed. London: Informa Healthcare; 2010:1-28.
24. Searles JA, Carpenter JF, Randolph TW. The ice nucleation temperature determines the primary drying rate of lyophilization for samples frozen on a temperature-controlled shelf. *J Pharm Sci*. 2001;90(7):860-871.
25. Carpenter JF, Prestrelski SJ, Anchordoguy TJ, Arakawa T. Interactions of stabilizers with proteins during freezing and drying. In: Jeffrey LC, Robert L, eds. *Formulation and Delivery of Proteins and Peptides*. Volume 567. Washington D.C: American Chemical Society; 1994:134-147.
26. Bhatnagar BS, Bogner RH, Pikal MJ. Protein stability during freezing: separation of stresses and mechanisms of protein stabilization. *Pharm Dev Technol*. 2007;12(5):505-523.
27. Bhatnagar BS, Pikal MJ, Bogner RH. Study of the individual contributions of ice formation and freeze-concentration on isothermal stability of lactate dehydrogenase during freezing. *J Pharm Sci*. 2008;97(2):798-814.
28. Searles JA. Freezing and annealing phenomena in lyophilization. In: Louis R, Joan CM, eds. *Freeze Drying/Lyophilization of Pharmaceutical and Biological Products*. 3rd ed. London: Informa Healthcare; 2010:52-81.
29. Connolly BD, Le L, Patapoff TW, Cromwell ME, Moore JMR, Lam P. Protein aggregation in frozen trehalose formulations: effects of composition, cooling rate, and storage temperature. *J Pharm Sci*. 2015;104(12):4170-4184.
30. Nail SL, Jiang S, Chongprasert S, Knopp SA. Fundamentals of freeze drying. In: Nail SL, Akers MJ, eds. *Development and Manufacture of Protein Pharmaceuticals*. New York: Kluwer Academic/Plenum Publisher; 2002:281-360.
31. Dalvi-Isfahan M, Hamdami N, Xanthakis E, Le-Bail A. Review on the control of ice nucleation by ultrasound waves, electric and magnetic fields. *J Food Eng*. 2017;195:222-234.
32. Kasper JC, Friess W. The freezing step in lyophilization: physico-chemical fundamentals, freezing methods and consequences on process performance and quality attributes of biopharmaceuticals. *Eur J Pharm Biopharm*. 2011;78:248-263.
33. MacKenzie AP, Derbyshire W, Reid DS. Non-equilibrium freezing behavior of aqueous systems. *Philos Trans R Soc Lond B Biol Sci*. 1977;278(959):167-189.
34. Petzold G, Aguilera J. Ice morphology: fundamentals and technological applications in foods. *Food Biophys*. 2009;4:378-396.
35. Konstantinidis AK, Kuu W, Otten L, Nail SL, Sever RR. Controlled nucleation in freeze-drying: effects on pore size in the dried product layer, mass transfer resistance, and primary drying rate. *J Pharm Sci*. 2011;100(8):3453-3470.
36. Awotwe-Otoo D, Agarabi C, Khan MA. An integrated process analytical technology (PAT) approach to monitoring the effect of supercooling on lyophilization product and process parameters of model monoclonal antibody formulations. *J Pharm Sci*. 2014;103(7):2042-2052.
37. Esfandiary R, Gattu SK, Stewart JM, Patel SM. Effect of freezing on lyophilization process performance and drug product cake appearance. *J Pharm Sci*. 2016;105(4):1427-1433.
38. Chakravarty P, Ron L, DeMarco F, Renzi E. Ice fog as a means to induce uniform ice nucleation during lyophilization. *Biopharm Int*. 2012;25(1):33-38.
39. Azzarella J, Mudhivarthi VK, Wexler E, Ganguly A. Increasing vial-to-vial homogeneity: an analysis of using VERISEQ® nucleation on production-scale freeze dryers. *Biopharm Int*. 2016;29(12):36-41.
40. Kumano H, Asaoka T, Saito A, Okawa S. Study on latent heat of fusion of ice in aqueous solutions. *Int J Refrig*. 2007;30(2):267-273.
41. Geidobler R, Winter G. Controlled ice nucleation in the field of freeze-drying: fundamentals and technology review. *Eur J Pharm Biopharm*. 2013;85:214-222.
42. Shibkov AA, Golovin YI, Zheltov MA, Korolev AA, Leonov AA. Morphology diagram of non-equilibrium patterns of ice crystals growing in supercooled water. *Physica A Stat Mech Appl*. 2003;319:65-79.
43. Knight CA. *The Freezing of Supercooled Liquids*. Princeton: D. Van Nostrand and Co. Ltd.; 1967.
44. Franks F. Freeze-drying of bioproducts: putting principles into practice. *Eur J Pharm Biopharm*. 1998;45:221-229.
45. Blond G, Simatos D, Catte M, Dussap CG, Gros JB. Modeling of the water-sucrose state diagram below 0°C. *Carbohydr Res*. 1997;298:139-145.
46. Liu J. Physical characterization of pharmaceutical formulations in frozen and freeze-dried solid states: techniques and applications in freeze-drying development. *Pharm Dev Technol*. 2006;11:3-28.
47. Hatley RHM, Mant A. Determination of the unfrozen water content of maximally freeze-concentrated carbohydrate solutions. *Int J Biol Macromol*. 1993;15:227-232.
48. Her LM, Nail SL. Measurement of glass transition temperatures of freeze-concentrated solutes by differential scanning calorimetry. *Pharm Res*. 1994;11:54-59.
49. Gupta P, Chawla G, Bansal AK. Physical stability and solubility advantage from amorphous celecoxib: the role of thermodynamic quantities and molecular mobility. *Mol Pharm*. 2004;1(6):406-413.
50. Connelly PR, Snyder PW, Zhang Y, et al. The potency-insolubility conundrum in pharmaceuticals: mechanism and solution for hepatitis C protease inhibitors. *Biophys Chem*. 2015;196:100-108.
51. Hancock BC, Parks M. What is the true solubility advantage for amorphous pharmaceuticals? *Pharm Res*. 2000;17(4):397-404.
52. Rumondor ACF, Dhareshwar SS, Kesisoglou F. Amorphous solid dispersions or prodrugs: complementary strategies to increase drug absorption. *J Pharm Sci*. 2016;105(9):2498-2508.
53. Purohit HS, Trasi NS, Sun DD, et al. Investigating the impact of drug crystallinity in amorphous tacrolimus capsules on pharmacokinetics and bioequivalence using discriminatory in vitro dissolution testing and physiologically based pharmacokinetic modeling and simulation. *J Pharm Sci*. 2018;107(5):1330-1341.
54. Ma X, Wang DQ, Bouffard R, MacKenzie A. Characterization of murine monoclonal antibody to tumor necrosis factor (TNF-MAb) formulation for freeze-drying cycle development. *Pharm Res*. 2001;18:196-202.
55. Schawe EK. A quantitative DSC analysis of the metastable phase behavior of the sucrose-water system. *Thermochim Acta*. 2006;451:115-125.
56. Sacha GA, Nail SL. Thermal analysis of frozen solutions: multiple glass transitions in amorphous systems. *J Pharm Sci*. 2009;98(9):3397-3405.

57. Ward KR, Matejtschuk P. The use of microscopy, thermal analysis, and impedance measurements to establish critical formulation parameters for freeze-drying cycle development. In: Louis R, Joan CM, eds. *Freeze Drying/Lyophilization of Pharmaceutical and Biological Products*. 3rd ed. London: Informa Healthcare; 2010:112-135.
58. Knopp MM, Löbmann K, Elder DP, Rades T, Holm R. Recent advances and potential applications of modulated differential scanning calorimetry (mDSC) in drug development. *Eur J Pharm Sci*. 2016;87:164-173.
59. Passot S, Fonseca F, Alarcon-Lorcab M, Rolland D, Marina M. Physical characterization of formulations for the development of two stable freeze-dried proteins during both dried and liquid storage. *Eur J Pharm Biopharm*. 2005;60:335-348.
60. Meister E, Gieseler H. Freeze-dry microscopy of protein/sugar mixtures: drying behavior, interpretation of collapse temperatures and a comparison to corresponding glass transition data. *J Pharm Sci*. 2009;98(9):3072-3087.
61. Depaz RA, Pansare S, Patel SM. Freeze-drying above the glass transition temperature in amorphous protein formulations while maintaining product quality and improving process efficiency. *J Pharm Sci*. 2016;105(1):40-49.
62. Horn J, Friess W. Detection of collapse and crystallization of saccharide, protein, and mannitol formulations by optical fibers in lyophilization. *Front Chem*. 2018;6:4.
63. Johnson RE, Kirchhoff CF, Gaud HT. Mannitol-sucrose mixtures-versatile formulations for protein lyophilization. *J Pharm Sci*. 2002;91(4):914-922.
64. Bhatnagar BS, Martin SWH, Hodge TS, et al. Investigation of PEG crystallization in frozen and freeze-dried PEGylated recombinant human growth hormone-sucrose systems: implications on storage stability. *J Pharm Sci*. 2011;100(8):3062-3075.
65. Cavatur RK, Suryanarayanan R. Characterization of frozen aqueous solutions by low temperature X-ray powder diffractometry. *Pharm Res*. 1998;15:194-199.
66. Roy M, Pikal MJ. Process control in freeze-drying: determination of the end point of sublimation drying by an electronic moisture sensor. *J Parenter Sci Technol*. 1989;43(2):60-66.
67. Searles JA, Carpenter JF, Randolph TW. Annealing to optimize the primary drying rate, reduce freezing-induced drying rate heterogeneity, and determine Tg' in pharmaceutical lyophilization. *J Pharm Sci*. 2001;90(7):872-887.
68. Pikal MJ, Rambhatla S, Ramot R. The impact of the freezing stage in lyophilization: effects of the ice nucleation temperature on process design and product quality. *Am Pharmaceut Rev*. 2002;5:48-52.
69. Lu X, Pikal MJ. Freeze-drying of mannitol-trehalose-sodium chloride-based formulations: the impact of annealing on dry layer resistance to mass transfer and cake structure. *Pharm Dev Technol*. 2004;9(1):85-95.
70. Rambhatla S, Ramot R, Bhugra C, Pikal MJ. Heat and mass transfer scale-up issues during freeze drying: ii. Control and characterization of the degree of supercooling. *AAPS Pharm Sci Tech*. 2004;5(4):e58.
71. Liu J, Viverette T, Virgin M, Anderson M, Dalal P. A study of the impact of freezing on the lyophilization of a concentrated formulation with a high fill depth. *Pharm Dev Technol*. 2005;10:261-272.
72. Abdelwahed W, Degobert G, Fessi H. Freeze-drying of nano-capsules: impact of annealing on the drying process. *Int J Pharm*. 2006;324:74-82.
73. Hawe A, Friess W. Impact of freezing procedure and annealing on the physicochemical properties and the formation of mannitol hydrate in mannitol-sucrose-NaCl formulations. *Eur J Pharm Biopharm*. 2006;64:316-325.
74. Nakagawa K, Hottot A, Vessot S, Andrieu J. Influence of controlled nucleation by ultrasounds on ice morphology of frozen formulations for pharmaceutical proteins freeze-drying. *Chem Eng Process*. 2006;45:783-791.
75. Petersen A, Schneider H, Rau G, Glasmacher B. A new approach for freezing of aqueous solutions under active control of the nucleation temperature. *Cryobiology*. 2006;53:248-257.
76. Hottot A, Vessot S, Andrieu J. Freeze drying of pharmaceuticals in vials: influence of freezing protocol and sample configuration on ice morphology and freeze-dried cake texture. *Chem Eng Process*. 2007;46:666-674.
77. Hottot A, Nakagawa K, Andrieu J. Effect of ultrasound-controlled nucleation on structural and morphological properties of freeze-dried mannitol solutions. *Chem Eng Res Des*. 2008;86(2):193-200.
78. Nakagawa K, Murakami W, Andrieu J, Vessot S. Freezing step controls the mannitol phase composition heterogeneity. *Chem Eng Res Des*. 2009;87(8):1017-1027.
79. Passot S, Trelea IC, Marin M, Galan M, Morris GJ, Fonseca F. Effect of controlled ice nucleation on primary drying stage and protein recovery in vials cooled in a modified freeze-dryer. *J Biomech Eng*. 2009;131(7):74511-74515.
80. Awotwe-Otoo D, Agarabi C, Read EK, et al. Impact of controlled ice nucleation on process performance and quality attributes of a lyophilized monoclonal antibody. *Int J Pharm*. 2013;450(1-2):70-78.
81. Geidobler R, Konrad I, Winter G. Can controlled ice nucleation improve freeze-drying of highly-concentrated protein formulations? *J Pharm Sci*. 2013;102(11):3915-3919.
82. Kuu WY, Doty MJ, Rebbeck CL, Hurst WS, Cho YK. Gap-freezing approach for shortening the lyophilization cycle time of pharmaceutical formulations-demonstration of the concept. *J Pharm Sci*. 2013;102(8):2572-2588.
83. Ullrich S, Seyferth S, Lee G. Measurement of shrinkage and cracking in lyophilized amorphous cakes. Part IV: effects of freezing protocol. *Int J Pharm*. 2015;495(1):52-57.
84. Pisano R, Capozzi LC. Prediction of product morphology of lyophilized drugs in the case of vacuum induced surface freezing. *Chem Eng Res Des*. 2017;125:119-129.
85. Fang R, Tanaka K, Mudhivarthi V, Bogner RH, Pikal MJ. Effect of controlled ice nucleation on stability of lactate dehydrogenase during freeze-drying. *J Pharm Sci*. 2018;107(3):824-830.
86. Thijssen H, Rulkens W. Effect of freezing rate on rate of sublimation and flavor retention in freeze-drying. *Int J Refrig*. 1969;10:99-113.
87. Dawson P, Hockley D. Scanning electron microscopy of freeze-dried preparations: relationship of morphology to freeze-drying parameters. *Dev Biol Stand*. 1992;74:185-192.
88. Randolph TW, Searles JA. Freezing and annealing phenomena in lyophilization: effect upon primary drying rate, morphology, and heterogeneity. *Am Pharmaceut Rev*. 2002;5(4):40-46.
89. Pikal MJ, Shah S, Senior D, Lang JE. Physical chemistry of freeze-drying: measurement of sublimation rates for frozen aqueous solutions by a microbalance technique. *J Pharm Sci*. 1983;72(6):635-650.
90. **Assegehegn G, Brito-de la Fuente E, Franco JM, Gallegos C. Effect of annealing on freeze drying of amorphous pharmaceutical formulations with high solid content. Poster presented at 21st International Drying Symposium, Valencia, September 2018.**
91. Hsu CC, Nguyen HM, Yeung DA, et al. Surface denaturation at solid-void interface: a possible pathway by which opalescent particulates form during the storage of lyophilized tissue-type plasminogen-activator at high-temperatures. *Pharm Res*. 1995;12(1):69-77.
92. Kramer M, Sennhenn B, Lee G. Freeze-drying using vacuum-induced surface freezing. *J Pharm Sci*. 2002;91(2):433-443.
93. Oddone I, Pisano R, Bullich R, Stewart P. Vacuum induced nucleation as a method for freeze-drying cycle optimization. *Ind Eng Chem Res*. 2014;53:18236-18244.
94. Oddone I, Van Bockstal PJ, de Beer T, Pisano R. Impact of vacuum-induced surface freezing on inter-and intra-vial heterogeneity. *Eur J Pharm Biopharm*. 2016;103:167-178.
95. Oddone I, Barresi AA, Pisano R. Influence of controlled ice nucleation on the freeze-drying of pharmaceutical products: the secondary drying step. *Int J Pharm*. 2017;524(1-2):134-140.
96. Rowe TD. A technique for the nucleation of ice. In: *International Symposium on Biological Product Freeze-drying and Formulation, Geneva*. 1990.
97. Patel S, Bhugra C, Pikal MJ. Reduced pressure ice fog technique for controlled ice nucleation during freeze-drying. *AAPS Pharm Sci Tech*. 2009;10:1406-1411.
98. Brower J, Lee R, Wexler E, Finley S, Caldwell M, Studer P. New developments in controlled nucleation: commercializing VERISEQ® nucleation technology. In: Varshney D, Singh M, eds. *Lyophilized Biologics and Vaccines: Modality Based Approach*. New York: Springer Science+Business Media; 2015:73-90.
99. Otero L, Sanz PD. High pressure shift freezing. Part 1. Amount of ice instantaneously formed in the process. *Biotechnol Prog*. 2000;16:1030-1036.
100. Zhu S, Ramaswamy HS, Le Bail A. Ice crystal formation in gelatin gel during pressure shift versus conventional freezing. *J Food Eng*. 2005;66(1):69-76.
101. Fernandez PP, Otero L, Guignon B, Sanz PD. High-pressure shift freezing versus high-pressure assisted freezing: effects on the microstructure of a food model. *Food Hydrocoll*. 2006;20:510-522.
102. Otero L, Sanz PD, Guignon B, Aparicio C. Experimental determination of the amount of ice instantaneously formed in high-pressure shift freezing. *J Food Eng*. 2009;95(4):670-676.
103. Gasteyer TH, Sever RR, Hunek B, Grinter N, Verdone ML. *Lyophilization System and Method*. Alexandria, VA: United States Patent and Trademark Office; 2007. US 2007/0186437 A1.
104. Bursac R, Sever RR, Hunek B. A practical method for resolving the nucleation problem in lyophilization. *Bioproc Int*. 2009;7:66-72.
105. Rampersad BM, Sever RR, Hunek B, Gasteyer TH. *Freeze-dryer and Method of Controlling the Same*. Alexandria, VA: United States Patent and Trademark Office;; 2010. US 2010/0242301 A1.
106. Li B, Sun DW. Effect of power ultrasound on freezing rate during immersion freezing of potatoes. *J Food Eng*. 2002;55(3):277-282.
107. Sun DW, Li B. Microstructural change of potato tissues frozen by ultrasound-assisted immersion freezing. *J Food Eng*. 2003;57(4):337-345.
108. Kiani H, Zhang Z, Sun DW. Effect of ultrasound irradiation on ice crystal size distribution in frozen agar gel samples. *Innov Food Sci Emerg Technol*. 2013;18:126-131.
109. Inada T, Zhang X, Yabe A, Kozawa Y. Active control of phase change from supercooled water to ice by ultrasonic vibration 1. Control of freezing temperature. *Int J Heat Mass Transf*. 2001;44:4523-4531.
110. Saclier M, Peczalski R, Andrieu J. Effect of ultrasonically induced nucleation on ice crystals' size and shape during freezing in vials. *Chem Eng Sci*. 2010;65:3064-3071.
111. Kiani H, Sun DW, Delgado A, Zhang Z. Investigation of the effect of power ultrasound on the nucleation of water during freezing of agar gel samples in tubing vials. *Ultrason Sonochem*. 2012;19(3):576-581.
112. Hickling R. Nucleation of freezing by cavity collapse and its relation to cavitation damage. *Nature*. 1965;206:915-917.
113. Zhang X, Inada T, Tezuka A. Ultrasonic-induced nucleation of ice in water containing air bubbles. *Ultrason Sonochem*. 2003;10(2):71-76.
114. Dodds J, Espitalier F, Louisnard O, et al. The effect of ultrasound on crystallization-precipitation processes: some examples and a new segregation model. *Part Part Syst Charact*. 2007;24(1):18-28.
115. Chow R, Blindt R, Chivers R, Povey M. The sono-crystallisation of ice in sucrose solutions: primary and secondary nucleation. *Ultrasonics*. 2003;41:595-604.
116. Chow R, Blindt R, Kamp A, Grocutt P, Chivers R. The microscopic visualisation of the sono-crystallisation of ice using a novel ultrasonic cold stage. *Ultrason Sonochem*. 2004;11:245-250.

117. Chow R, Blindt R, Chivers R, Povey M. A study on the primary and secondary nucleation of ice by power ultrasound. *Ultrasonics*. 2005;43:227-230.
118. Amira JH, Romann P, Pierre L. Ultrasonically triggered freezing of aqueous solutions: influence of initial oxygen content on ice crystals' size distribution. *J Cryst Growth*. 2014;402:78-82.
119. Dufour L. Über das Gefrieren das Wassers and Über die Bildung des Hagels. *Ann Phys*. 1862;114:530-554.
120. Rau W. Eiskeimbildung durch Dielektrische Polarisation. *Z Naturforsch A*. 1951;6:649-657.
121. Shichiri T, Araki Y. Nucleation mechanism of ice crystals under electrical effect. *J Cryst Growth*. 1986;78:502-508.
122. Petersen A, Rau G, Glasmacher B. Reduction of primary freeze-drying time by electric field induced ice nucleus formation. *Heat Mass Transf*. 2006;42:929-938.
123. Shichiri T, Nagata T. Effect of electric currents on the nucleation of ice crystals in the melt. *J Cryst Growth*. 1981;54:207-210.
124. Mandal G, Kumar PP. A laboratory study of ice nucleation due to electrical discharge. *Atmos Res*. 2002;61:115-123.
125. Hozumi T, Saito A, Okawa S, Watanabe K. Effects of electrode materials on freezing of supercooled water in electric freeze control. *Int J Refrig*. 2003;26(5):537-542.
126. Xia X, Berkowitz ML. Electric-field induced restructuring of water at a platinum-water interface: a molecular dynamics computer simulation. *Phys Rev Lett*. 1995;74(16):3193-3196.
127. Vaitheeswaran S, Yin H, Rasaiah JC. Water between plates in the presence of an electric field in an open system. *J Phys Chem B*. 2005;109(14):6629-6635.
128. Wei S, Zhong C, Su-Yi H. Molecular dynamics simulation of liquid water under the influence of an external electric field. *Mol Simul*. 2005;31(8):555-559.
129. Ling W. *Controlled Nucleation during Freezing Step of Freeze Drying Cycle Using Pressure Differential Ice Fog Distribution*. Alexandria, VA: United States Patent and Trademark Office; 2014. Patent US2014/8839528B2.
130. Ling W. *Controlled Nucleation during Freezing Step of Freeze Drying Cycle Using Pressure Differential Ice Crystals Distribution from Condensed Frost*. Alexandria, VA: United States Patent and Trademark Office; 2014. Patent US2014/8875413B2.
131. Geidobler R, Mannschedel S, Winter G. A new approach to achieve controlled ice nucleation of supercooled solutions during the freezing step in freeze-drying. *J Pharm Sci*. 2012;101(12):4409-4413.
132. Kuu WY. *Optimization of Nucleation and Crystallization for Lyophilization Using Gap Freezing*. Alexandria, VA: United States Patent and Trademark Office; 2012. Patent US2012/0077971A1.
133. Kuu WY, Doty MJ, Hurst WS, Rebbeck CL. *Optimization of Nucleation and Crystallization for Lyophilization Using Gap Freezing*. Alexandria, VA: United States Patent and Trademark Office; 2012. Patent US2012/0192448 A1.
134. Kuu WY, Doty MJ, Nisipeanu E, Rebbeck CL, Cho YK, Smit MH. Modeling of heat and mass transfer processes for the gap-lyophilization system using the mannitol-trehalose-NaCl formulation. *J Pharm Sci*. 2014;103(9):2784-2796.

Appendix A.2:

Use of a Temperature Ramp Approach (TRA) to Design an Optimum and Robust Freeze-drying Process for Pharmaceutical Formulations

Getachew Assegehegn[1], Edmundo Brito-de la Fuente[1], José M. Franco[2] and Críspulo Gallegos[1]

[1]Fresenius-Kabi Deutschland GmbH, Process and Product Engineering Center, Global Manufacturing Pharmaceuticals, Bad Homburg, Germany

[2]Pro2TecS-Chemical Product and Process Technology Research Centre, Complex Fluid Engineering Laboratory. Departamento de Ingeniería Química, Universidad de Huelva, Huelva, Spain

Published in:

Journal	International Journal of Pharmaceutics
Publishing company	Elsevier
Editor-in-Chief	Prof. Jürgen Siepmann
Volume and pages	---
Publication year	----
ISSN	0378-5173
DOI	---------
Journal impact factor (2018)	**4.213**

Category (2017)	**Journal rank/total journal**	**Quartile**
Pharmacology & pharmacy	46/261	Q1
Pharmacology & toxicology	3/274	Q1

Research Article

Use of a Temperature Ramp Approach (TRA) to Design an Optimum and Robust Freeze-drying Process for Pharmaceutical Formulations

Getachew Assegehegn[1], Edmundo Brito-de la Fuente[1], José M. Franco[2], and Críspulo Gallegos[1]

[1]Fresenius-Kabi Deutschland GmbH, Product and Process Engineering Center, Global Manufacturing Pharmaceuticals, Bad Homburg, Germany
[2]Pro2TecS-Chemical Product and Process Technology Research Centre, Complex Fluid Engineering Laboratory. Departamento de Ingeniería Química, Universidad de Huelva, Huelva, Spain

Abstract

Freeze-drying, until now, has been a process that was designed using a trial and error experimental approach. This approach is often material and time consuming, and the resulting freeze-drying processes are neither optimum nor robust. Accordingly, the objective of this study was to develop a simple-to-use and experimental-based approach to design an optimum and robust freeze-drying process for any given formulation. The temperature ramp approach (TRA) detailed in this study involves the implementation of a customized design of experiments (DoE) to perform few (three or four) experiments using a given drug formulation. The DoE results are analyzed to define optimum processing conditions (i.e., shelf temperature and chamber pressure) based on a predefined range of target product temperature for primary drying, which could be defined from formulation characterization at its frozen state. In this study, a successful freeze-drying process of two model formulations using the TRA was designed. Verification experiments at the optimum processing conditions showed excellent agreement in both product temperature and sublimation rate with the values obtained using the TRA. Thus, the TRA detailed in this study offers a significant advantage to reduce development time and material and enhance the efficiency and robustness of the resulting freeze-drying process.

Key words: Freeze-drying; Lyophilization; Process design; Quality by design; Optimization; design of experiments; Pharmaceuticals

Nomenclature

Ave	Average
C	Center vials
DoE	Design of experiments
FE	Front edge vials
L_{R_p}	Dried layer thickness
$\dot{m}$	Overall mass transfer rate (sublimation rate) from a vial
Max	Maximum
MF1	Model formulation 1 (10% (w/w) trehalose solution)
MF2	Model formulation 2 (20% (w/w) sucrose solution)
Min	Minimum

P_c	Chamber pressure
P_i	Ice vapor pressure
SD	Standard deviation
T_c	Collapse temperature of an amorphous formulation
t_d	Drying time of primary drying
T_{eu}	Eutectic temperature
T_g'	Glass transition temperature of the maximally freeze-concentrated solution
T_p	Product temperature
T_pave	Average product temperature during primary drying
T_pt	Target product temperature for primary drying
TRA	Temperature ramp approach
T_s	Shelf temperature

1. Introduction

Although the entire freeze-drying process is an energy intensive, time consuming, and economically expensive process, the primary drying step is the longest and most critical step (Patel et al., 2010; Mortier et al., 2016) As a result, this step significantly influences the product quality, such as physical appearance and reconstituability, and process economy of the freeze-drying process. Consequently, there is growing interest in the pharmaceutical and biopharmaceutical industries to optimize the primary drying step with regard to both product quality and processing time. Optimization of the primary drying step requires significant knowledge of the process, the formulation, and the interrelationship between the process and the formulation.

Fig. 1 displays the interrelationship between the formulation properties and the freeze-drying process. As shown in Fig. 1, there are several formulation properties and process parameters that could play an important role during the optimization of the primary drying step.

Figure 1. Interrelationship between the formulation and freeze-drying process, and its role during the freeze-drying process design and optimization.

As displayed in Fig. 1, characterization of the formulation in its frozen state provides critical formulation properties, such as the glass transition temperature of the maximally freeze-concentrated solution, T_g', collapse temperature of an amorphous formulation, T_c, eutectic melting temperature of a crystalline formulation, T_{eu}, and degree of crystallinity of the formulation. Such information is useful to define the target product temperature for the primary drying step (T_pt). A formulation with very low T_g' or T_c might need to be reformulated with the addition of collapse temperature modifiers to facilitate the sublimation rate during primary drying. Alternatively, crystalline bulking agents with high T_{eu} can be added to support the amorphous formulation. With such modifications, primary drying can be performed at product temperatures higher than T_g' or T_c, and the processing time can be shortened (Depaz et al., 2016; Bjelošević et al., 2018, Hom et al., 2018; Anko et al., 2019; Pansare & Patel, 2019).

Freeze-drying process design and optimization could be initiated once the optimum formulation is defined. Notably, understanding the freezing step is also essential to design and optimize the primary drying step (Kasper & Friess, 2011; Awotwe-Otoo et al., 2015; Ullrich et al., 2015; Esfandiary et al., 2016; Fonte et al., 2016; Goshima et al., 2016; Pisano & Capozzi, 2017; Assegehegn et al., 2019a; Colucci et

al., 2019; Vollrath et al., 2019). From the perspective of a freeze-drying process, optimization of the primary drying step implies working at a chamber pressure (P_c) and a shelf temperature (T_s) that yield the $T_p t$ of a given formulation. Performing the primary drying above $T_p t$ leads to product damage and, hence, to the rejection of the product. Whereas, performing the primary drying below the $T_p t$ leads to an unnecessarily long drying time and to an unoptimized and economically expensive freeze-drying process.

Heat and mass transfers are the core principle of the sublimation process during the primary drying step. The driving force for the mass transfer is the pressure difference between the ice vapor pressure at the sublimation front (P_i) and the chamber pressure (i.e., $P_i(T_p) - P_c$). To initiate the vapor mass transport during the primary drying, the P_c is lowered to a pressure less than the P_i at a target product temperature ($T_p t$). The sublimation of ice is an endothermic process, and thus, it takes up energy from the system. It is therefore necessary to have an exothermic process to counterbalance the energy consumption due to the mass transfer process and to keep the system in an energy equilibrium state. An energy equilibrium state is a state where the input and output energies are equilibrated to keep the system at a constant T_p. The exothermic process during the primary drying refers to an energy transport in the form of heat to the system. This is usually performed by manipulating the temperature of the shelves (T_s) on which the sublimating product rests. The driving force for the heat transfer is the temperature difference between T_s and T_p (i.e., $T_s - T_p$). To initiate heat transfer during primary drying, T_s is increased above T_p. However, depending on the processing conditions (i.e., T_s and P_c), the formulation (i.e., solid content), and the freezing step (i.e., ice crystal size and morphology), the energy equilibrium state could be achieved at a T_p far from $T_p t$. Therefore, the aim of the primary drying optimization is to achieve the energy equilibrium state of the system at $T_p t$. In the freeze-drying process, T_p is indirectly controlled through the manipulation of the processing conditions (i.e., T_s and P_c). In the majority of cases, the optimum processing conditions are achieved through a trial and error approach, which leads to unnecessarily long experimental setups. Furthermore, the resulting freeze-drying processes are neither robust nor efficient. In an attempt to minimize the trial and error experiments, researchers have developed mathematical models for the determination of the optimum processing conditions based on the governing heat and mass transfer equations (Schoen et al., 1995; Brülls & Rasmuson, 2002; Pikal et al., 2005; Gieseler et al., 2007; Velardi & Barresi, 2008; Kuu & Nail, 2009; Giordano et al., 2011; Koganti et al., 2011; Fissore et al., 2011; Bosca et al., 2013; Kodama et al., 2013 & 2014; Fissore & Pisano, 2015; Chen et al., 2015; Mortier et al., 2016; Zhu et al., 2018; Sharma et al., 2019). The mathematical models provide an opportunity to simulate several combinations of input process parameters during the freeze-drying process design; however, their success is highly dependent on the accuracy of model input parameters and on the assumptions of the model equations. Furthermore, since some input parameters are obtained from non-drug experimental trials, verification of the resulting optimum processing conditions may require the execution of several freeze-drying experiments using the actual drug formulation.

Considering the broad use of the freeze-drying process in the pharmaceutical and biopharmaceutical industries (Shanley, 2017), there is a huge interest to develop a simple-to-use and reliable approach to design an optimum and robust freeze-drying process for any given drug formulation. To address this issue, this study presents an approach, called *Temperature Ramp Approach (TRA)*. This simple-to-use experimental-based TRA could be applied to design an effective freeze-drying process using a few experimental setups. The TRA considers some important general issues and experimental procedures, as described below:

- Defining the target product temperature for the primary drying step. As discussed previously, knowledge of a formulation and its critical properties are vital during freeze-drying process

design. The sublimation rate is dependent on several parameters, namely P_i or T_p, P_c, and the resistance to mass transfer of the dried product (Assegehegn et al., 2019a). To maximize the sublimation rate during primary drying, it is important to work at the highest P_i (this corresponds to the highest T_p) and at the lowest P_c. However, the maximum allowable T_p during the primary drying is limited by the T_c of amorphous formulations or by the T_{eu} of crystalline formulations. Such parameters are obtained from formulation characterization in its frozen state (cf. Fig. 1). Several techniques are available to characterize a lyophilization formulation in its frozen state. Differential scanning calorimetry, modulated differential scanning calorimetry, and differential thermal analysis are used for the determination of T_g', and T_{eu} (Her & Nail, 1994; Ma et al., 2001; Schawe, 2006; Sacha & Nail, 2009; Knopp et al., 2016; Ward & Matejtschuk, 2019), whereas freeze-drying microscopy is used for the determination of T_c (Passot et al., 2005; Meister & Gieseler, 2009). On the other hand, the minimum P_c is limited by the capability of the freeze-drying equipment (Ganguly et al., 2013 & 2017; Kshirsagar et al., 2019). Patel and Pikal reported that most manufacturing dryers cannot control chamber pressures below 0.06 mbar and there is no additional advantage in sublimation rate for chamber pressures above 0.40 mbar (Patel & Pikal, 2013).

- Designing experimental setups to perform the temperature ramp experiments. An effective design of experiments (DoE) is essential to avoid repeated experimental setups. Thus, it is recommended to gather literature knowledge about similar formulations and, if necessary, to perform some preliminary freeze-drying experiments. This study demonstrated that, using an effective DoE, only three temperature ramp experiments are needed to design an optimum freeze-drying process of a model formulation.

- Defining optimum processing conditions after analyzing the results obtained from the temperature ramp experiments. It is well-known that vials located at the periphery of a tray, commonly known as edge vials, have higher T_p and sublimation rate compared to vials located at the center of a tray (Pikal et al., 2016; Scutellà et al., 2017a; 2017b & 2018a; Pikal et al., 2018; Assegehegn et al., 2019b). These heterogeneities in T_p and drying rate pose significant challenges during freeze-drying process design and scale-up. On one hand, defining the process variables based on center vials T_p could cause the edge vials to exceed the maximum allowable T_p and, consequently, suffer product damage. On the other hand, defining the drying time based on the sublimation rate of the edge vials could cause significant damage to the center vials as they generally need longer drying times during the primary drying step. The approach detailed in this study incorporates such T_p and sublimation rate variations caused due to vial location on a shelf. This guarantees the robustness of the process and facilitates process scale-up and transfer.

- Performing a sublimation rate determination experiment. The purpose of this experiment is to define the optimum drying time (t_d) during the primary drying step. Because center vials have the lowest sublimation rate, a gravimetric approach could be utilized to determine the sublimation rate of the center vials at the previously defined optimum processing conditions.

- Performing a verification experiment. This experiment aims to verify the previously defined optimum T_s-P_c-t_d profile. Visual inspection of the dried products and product temperature profiles could be used to assess the success of the freeze-drying process.

Therefore, the primary objective of this study was to utilize the aforementioned TRA to design a freeze-drying process of two model formulations. It has been demonstrated that the successful design of a

robust and optimum freeze-drying process using only three temperature ramp experiments was possible for the two model formulations studied. Thus, compared to expensive and time-consuming trial and error experimental approach, the TRA detailed in this study has several advantages with respect to development time and material savings. Furthermore, considering the simple and effective design strategy of the TRA, developmental engineers and scientists at any level of experience and lyophilization knowledge could utilize it to design an effective freeze-drying process for any given drug formulation.

2. Materials and methods

2.1 Materials

All vials used in this study were 10-mL tubing vials purchased from SCHOTT AG (Mainz, Germany). The stoppers were Igloo single vented gray stoppers from West Pharmaceutical Services, Inc. (West Pharmaceutical Services, Inc., Exton, PA, USA). The temperature ramp approach was used to design a freeze-drying process of two model formulations. Model formulation 1 (MF1) represents a formulation with an intermediate solid content and is a solution containing 10% (w/w) trehalose. Trehalose was purchased from Pfanstiehl, Inc. (Pfanstiehl, Inc., Waukegan, IL, USA). The second model formulation (MF2) represents a formulation with a high solid content and is a solution containing 20% (w/w) sucrose. Sucrose was purchased from VWR (Darmstadt, Germany). The two model formulations were prepared using water for injection obtained from Fresenius Kabi Deutschland GmbH (Friedberg, Germany). The trehalose and sucrose powders were used without further treatment. All the solutions used in this study were filtered using 0.22-µm pore size filters (PALL Corporation, Port Washington, NY, USA) before filling into the vials, aiming to remove any particulate matter that might have been introduced during preparation.

2.2 Methods

2.2.1 Differential Scanning Calorimetry (DSC)

A TA instruments Q2000 series differential scanning calorimetry (DSC) with a refrigerated cooling system (RCS) (TA Instruments, New Castle, DE, USA) was used to determine the T_g' of frozen samples. The following program was employed to determine the T_g' of MF1 and MF2. A nitrogen supply at 50 mL/min was provided to the system using the continuous mode of the RCS. A sample of 10-15 mg of MF1 or MF2 was weighed into aluminum sample pans, and the pans were hermetically sealed. An empty hermetically sealed pan was used as a reference. Once the sample and reference pans were placed on the sample chamber of the DSC, the samples were equilibrated at 40 °C for 2 min and then frozen to -60 °C at a rate of 20 °C/min. To assure complete solidification of the frozen samples, they were held at -60 °C for 10 min. The T_g' values were obtained during the heating period from -60 °C to 40 °C at a rate of 10 °C/min. These T_g' values were analyzed using Universal Analysis software, and they were reported as the midpoint of the glass transition curve.

2.2.2 Freeze-Drying Microscopy (FDM)

A Lyostat 2 freeze-drying microscopy (Biopharma Technology Ltd., Winchester, UK) was used to determine the T_c of the model formulations studied. The following program was used to determine T_c of MF1 and MF2. A sample of 2 µL was placed on a quartz cover slip and covered using a glass cover slip. A 70-µm thick metal spacer was placed between the quartz and the glass cover slips to allow sublimation

of the samples. The solution samples were frozen to -40 °C at a rate of 20 °C/min, and the frozen solution was held for 5 min to allow complete solidification. Once solidification was completed, the pressure inside the cooling stage was evacuated to around 0.10 mbar. The samples were held at -40 °C and 0.10 mbar until an approximately 2–3-mm dry layer thickness was achieved. The samples were then heated at a rate of 5 °C/min to a temperature slightly less than the T_g' obtained from the DSC. Aiming to observe a structural change at a higher temperature resolution, the heating rate was lowered to 0.5 °C/min, and the samples were further heated until a complete structural damage was observed. Images of the samples were captured throughout the experiment, and the T_c was defined as the temperature at which a clearly observable structural change of the frozen solution was observed.

2.2.3 *Freeze-drying experiment*

HOF laboratory freeze dryer (HOF Sonderanlagenbau GmbH, Lohra, Germany) was used to perform all the freeze-drying experiments. The freeze dryer had four shelves with a total usable shelf area of 0.36 m^2 and a Pirani gauge for P_c control. All the freeze-drying experiments were carried out using 10-mL tubing vials, and for each of the experiments, 176 vials (one fully loaded shelf) were filled with 5-mL solution and placed on one of the four shelves of the freeze dryer. To reduce the effect of atypical radiation, a 4-mm thick polystyrene foam block and an aluminum foil were used to cover the acrylic chamber door of the dryer door. Product temperature measurement was performed using eight wireless thermologgers (Lives International, Timis, Romania), which were set to record product temperatures every 20 s. The freezing step was kept identical for all the TRA experiments, as follows: cooling from +5 °C to -10 °C at 1 °C/min, 90 min holding at -10 °C; further freezing to -40 °C at 1 °C/min and 240 min holding at -40 °C. During the primary drying, the shelf temperature was ramped down at 1 °C/min within the shelf temperature range given in the DoE (see Table 1). During the ramping down period, a 3-hour holding time was defined at different shelf temperature points, and the steady state product temperature was recorded at these shelf temperature points (see Table 1). Product temperatures of the front edge vials and center vials were measured using four thermologgers for each vial group. At each of the shelf temperature points, the product temperature measurements obtained from the four thermologgers were used to calculate the minimum, maximum, average, and standard deviation of the product temperature.

2.2.4 *Design of Experiments (DoE)*

DoE allows the simultaneous determination of the effects of all potential input variables on the output responses. In addition, it allows investigations on how the process response changes as input variables fluctuate within allowable limits. DoE requires a profound scientific background of the formulation and the process. In addition, preliminary experiments using the specified drug formulation could be necessary to facilitate the development of an effective DoE. For the primary drying step of the freeze-drying process, the critical input process parameters are T_s and P_c, whereas the critical output parameters are T_p, t_d, and sublimation rate (Assegehegn et al., 2019b). Therefore, based on prior knowledge and few preliminary experiments using the model formulations, a customized DoE for both model formulations was developed and is presented in Table 1. The biggest advantage of the TRA is that the T_s range during the DoE can be extended to any desired range, as long as the upper T_s limit does not lead to product collapse. Furthermore, the entire TRA experiment should be completed before the frozen ice is completely sublimed.

Table 1.

2.2.5 *Determination of sublimation rate*

In order to define the optimum drying rate for any fill volume, determination of sublimation rate at the optimum processing conditions (processing conditions that yield the highest possible product temperature of the edge vials and, at the same time, the highest possible sublimation rate of the center vials) is important. Sublimation rate was determined gravimetrically. For this purpose, 16 selected sample vials, which were systematically placed to represent vial groups with the lowest sublimation rates, were weighed before and after the freeze-drying experiments. It has been experimentally determined that, at the optimum processing conditions, center vials yield the lowest product temperature and, thus, the lowest sublimation rate. Therefore, the 16 sample vials were placed at the center of the vial array. A laboratory analytical balance (Sartorius AG, Göttingen, Germany) was used to weigh the sample vials. To stop the sublimation process immediately, the vacuum of the product chamber was released using dry nitrogen. At the end of the sublimation process, the product chamber was too cold to cause condensation of the surrounding moisture into the cold stoppers and into the extremely hygroscopic dried product. To prevent this issue, the vials were heated to 20 °C before the product chamber door was opened. Once the product chamber door was opened, the sample vials were immediately fully stoppered and re-weighed. The minimum sublimation rate of the 16 sample vials was taken to calculate the drying time of the primary drying step. To avoid any effect of the freezing step, the freezing protocol used during the TRA experiments and the sublimation experiments was identical.

It has been reported that the resistance of the dried product increases as the length of the dried layer of the product increases (Kuu et al., 2006; Fissore et al., 2011; Kodama et al., 2014; Scutellà et al., 2018b). This implies that the sublimation rate decreases by increasing the product dried layer. Therefore, to consider the minimum sublimation rate, the sublimation process was stopped when a reasonable dried layer thickness of the center vials was achieved. Since the dried layer of the center vials was not visible, the dried layer of the front edge vials, which was visible through the acrylic door of the dryer, was used as a guide to stop the sublimation process. Thus, the sublimation process was stopped after the dried layer of the front edge vials reached the vial bottom. The exact drying time for the calculation of the sublimation rate was obtained from the center vials product temperature profile. The definition of the starting and finishing time for the sublimation process is given elsewhere (Assegehegn et al., 2019b).

3. Results and Discussion

3.1 Characterization of frozen formulations

The T_g' of both model formulations, as determined using the DSC experiment described previously, were in excellent agreement with literature reported data (Her & Nail, 1994; Chang & Randall, 1992). The T_c of the model formulations were determined from a subjective assessment of images that were captured during the experiment. Although the determination of the T_c values involves subjective evaluation of images, they provide important information on the structural change of a formulation at a microscopic scale, which is similar to a structural change that could occur during a freeze-drying process. Thus, the T_c can precisely define the $T_p t$ during the primary drying step of the freeze-drying process. The T_c of both model formulations were in excellent agreement with literature reported values (Adams & Ramsay, 1996). The T_g', T_c, and $T_p t$ of both model formulations are summarized and presented in Table 2.

Table 2.

3.2 Optimization of primary drying using TRA

The main objective of optimizing the primary drying step of a freeze-drying process is to balance the heat and mass transfer of the process during the sublimation step so that T_p remains within a desired range during the entire primary drying step. Even knowing T_g' and T_c, the optimization of the primary drying step is challenging. On one hand, T_p, which depends on formulation properties, processing conditions, and container-closure system, cannot be directly controlled during the primary drying step. This leads to several trial and error experimental studies aiming to achieve the optimum processing conditions. Although several mathematical models available today are helpful in reducing the experimental burdens necessary to optimize the primary drying step, several time- and material-consuming verification experimental studies could still be required. On the other hand, differences in product temperature and sublimation rate of vials located at the periphery and at the center of the vial array make the optimization effort even more challenging. In this sense, the challenge arises from defining an optimum T_s-P_c-t_d profile, considering all vials in the array. In addition to being optimum, robustness of the process is an important factor. Accordingly, the process should withstand small deviations in T_s and P_c, and considering such deviations, the drying time should allow all vials to complete the sublimation of the ice before proceeding to the secondary drying step.

The TRA developed in this study uses few experimental studies to define optimum processing conditions of a given formulation during primary drying. In addition, the approach is developed to consider the differences in product temperature and sublimation rate of vials at different locations. Because the TRA works better for formulations that show insignificant change in T_p as thickness of the dried layer (L_{R_p}) increases, determination of the relationship between T_p and L_{R_p} of a given formulation is an important part of the TRA. This could be easily performed by following the change in T_p during the progress of primary drying at a selected T_s-P_c combination. As long as T_p during this experiment stays lower than T_{eu}, T_g', or T_c of the formulation, any T_s-P_c combination can be used. For the two model formulations studied here, once T_p reached pseudo steady-state conditions, the change in T_p as a function of L_{R_p} was insignificant, demonstrating that the dried layer imposes similar resistance to vapor transport regardless of its thickness (see Fig. 2). On the other hand, for formulations that show strong dependency of T_p on L_{R_p}, the TRA gives vital information to examine how T_p changes as L_{R_p} increases and T_s decreases. In such circumstances, multiple T_s during primary drying could be employed. The two model formulations described previously (cf. Table 1) were used to discuss the use of the TRA to design an effective freeze-drying process. The detailed steps of the TRA are discussed below.

Figure 2: Dependency of product temperature (T_p) on dried layer thickness of model formulations (MF)1 and MF2.

Determination of product temperature (T_p): As discussed previously, T_p is a key variable during TRA process development. Thus, correct determination of the T_p is very important. Nail et al. described some recommended best practices for product temperature measurement (Nail et al., 2017). The factors that significantly influence T_p are T_s and P_c, and the primary goal of TRA is to evaluate the effect of these factors on T_p for a given formulation and at a given container-closure system. The core advantage of TRA is its ability to analyze several combinations of T_s and P_c in a single experimental setup, thus minimizing the number of experimental studies. Some representative T_p profiles of both model formulations for front edge vials (FE) and center vials (C), measured during the TRA experiments, are displayed in Fig. 3. In these experiments, the container-closure systems used were identical; therefore, the influence of

variation in vial heat transfer coefficient on product temperature can be safely assumed as negligible. Table 3 presents results and statistical analyses of the T_p for FE and C of both model formulations. For each vial group, four thermologgers were used to measure T_p, from which the minimum (Min), maximum (Max), average (Ave), and standard deviation (SD) of the T_p were calculated (cf. Table 3). The calculation of the Min, Max, Ave, and SD at each T_s point considers a pseudo steady-state condition in T_p (except at the first T_s point). Thus, because the first few T_p measurements at each T_s point showed transient behavior, they were not considered for the calculation of Min, Max, Ave, and SD. The T_p range used for the calculation of Min, Max, Ave, and SD at each T_s point are displayed in Fig. 3. For each vial group and at each T_s point, the Min, Max, Ave, and SD were calculated from T_p measurements (approximately 1800 data points) obtained using the four thermologgers. Thus, in addition to being statistically significant, the reported T_p values are accurate representations of the experiments studied herein.

Figure 3. Product temperature profiles of selected temperature ramp approach experiments; (a) model formulation (MF)1 at P_c = 0.10 mbar, (b) MF2 at P_c = 0.10 mbar. C, center vials; FE, front edge vials, T_p, product temperature; P_c, chamber pressure.

The statistical results (Table 3) show that regardless of the processing conditions and the formulation, the differences between the maximum and minimum T_p and the standard deviation at the first T_s point were higher than those at the rest of the T_s points. This was attributed to the longer time required to reach a pseudo steady-state condition in T_p at the start of the primary drying. For this reason, the first T_s point was not included in further analysis of the TRA results. Differences in maximum and minimum T_p at the rest of the T_s points (see Table 3) were consistent and small (less than 1 °C), demonstrating that, at all T_s points, the change in T_p was insignificant. The SD of the T_p measures the precision or uniformity of the data points at each of the T_s points. As presented in Table 3, the SD for all combinations of T_s and P_c studied, except for the first T_s point, was well below 1 °C. Since the SD values are calculated based on statistically significant numbers of data, the average product temperature ($T_p ave$) values presented in Table 3 can be considered as accurate representation of the T_p at the given T_s and P_c values.

Table 3.

Determination of optimum processing conditions: As discussed previously, optimum processing conditions during primary drying define values of T_s and P_c, which allow the energy equilibrium of the system to be achieved at $T_p t$. As shown in Table 3 and reported in the literature (Pikal et al., 2016 & 2018; Scutellà et al., 2017a; 2017b & 2018a; Assegehegn et al., 2019b), the front edge vials have higher T_p compared to the center vials. Thus, the $T_p ave$ values of the front edge vials (Table 3) were utilized to analyze the $T_p t$ during the primary drying step. Evaluation of the optimum processing conditions was performed using regression analyses of the T_p of the front edge vials as a function of T_s at the P_c studied (Fig. 4). As can be deduced from Fig. 4, the experimental data fit the regression analysis equations (polynomial curve fitting equations) fairly well ($R^2 \geq 0.97$). Thus, accurate determination of the optimum processing conditions is possible. The shade area of Fig. 4 displays the range of $T_p t$, as defined previously (cf. Table 2), and the corresponding optimum T_s range at a given P_c. For example, the range of the $T_p t$ for MF1 was defined from -29.5 °C to -28.5 °C (cf. Table 2). As displayed in Fig. 4a, the optimum range of T_s at a P_c of 0.10 mbar was obtained from -17.0 °C to -11.5 °C. The optimum range of T_s at a given P_c was defined on the basis that the T_p of the front edge vials remained within the predefined range of $T_p t$ (Fig. 4). Similarly, at the optimum T_s, the range of T_p for the center vials varied between -31.1 °C

and -30.4 °C (arrow lines, Fig. 4a). Alternatively, the regression equations from Fig. 4 could be used to calculate the optimum T_s at the corresponding P_c. Using similar analyses, the optimum range of T_s for MF1 and MF2 at all the P_c studied are summarized and presented in Table 4.

Figure 4. Product temperature dependence on shelf temperature for front edge and center vials at a selected chamber pressure; (a) Model formulation (MF)1 at P_c = 0.10 mbar, (b) MF1 at P_c = 0.15 mbar, (c) MF2 at P_c = 0.10 mbar, and (d) MF2 at P_c = 0.15 mbar. P_c, chamber pressure.

Table 4:

It is well known that the sublimation rate depends on P_c. Thus, depending on P_c, similar T_p values could produce different sublimation rates. Consider, for example, two optimum processing conditions of MF2 from Table 4: (1) P_c = 0.05 mbar and T_s = -28.5 (at this processing condition, T_p of the center vials was -35.8 °C); (2) P_c = 0.15 mbar and T_s = -29.5 (at this processing condition, T_p of the center vials was -34.9 °C). The driving force for the sublimation of ice $(P_i(T_p) - P_c)$ for both selected processing conditions can be calculated from the knowledge of the ice vapor pressure (P_i) at the corresponding product temperatures (T_p). At processing condition 1, $P_i(T_p) - P_c$ = 0.155 mbar, whereas at processing condition 2, $P_i(T_p) - P_c$ = 0.076 mbar. Furthermore, for the same formulation and similar T_p, it could be safely assumed that the dried product resistance is the same. With such a valid assumption, the terms $P_i(T_p) - P_c$ and sublimation rate have similar qualitative and quantitative meanings. Thus, a higher $P_i(T_p) - P_c$ is directly translated into a higher sublimation rate. This analysis implies that although processing conditions 1 and 2 are defined as optimum processing conditions for MF2 from a T_p perspective, they yield significantly different sublimation rates. In this particular example, although the energy equilibrium state of the system at processing condition 2 is achieved within $T_p t$ (cf. Table 4), the corresponding sublimation rate is significantly lower than that at processing condition 1. This leads to a prolonged primary drying time and, hence, to an unoptimized primary drying step. Given the importance of such knowledge and information during the optimization of the primary drying step, it is therefore essential to identify the range of P_c that yields the highest sublimation rate. This is done by plotting the driving force for the sublimation of ice $(P_i(T_p) - P_c)$ against T_p of the front edge vials, as displayed in Fig. 5. It is important to mention here that because the center vials have the lowest T_p and, thus, the lowest P_i in the vial array, the P_i values in Fig. 5 were calculated from T_p of the center vials.

Figure 5. Dependency of the driving force for sublimation of ice, $P_i(T_p) - P_c$, on chamber pressure and product temperature; (a) Model formulation (MF)1 and (b) MF2. P_i, ice vapor pressure; T_p, product temperature; P_c, chamber pressure

Fig. 5 shows that for both model formulations, enhanced sublimation rates are obtained at lower P_c and higher T_p. Furthermore, $P_i(T_p) - P_c$ at P_c of 0.15 mbar was very low, suggesting that performing the primary drying at a chamber pressure above 0.10 mbar would not provide any advantage in terms of sublimation rate. Therefore, the optimum chamber pressure for MF1 and MF2 could be defined in the range of 0.05 to 0.10 mbar (shaded area of Fig. 5).

Hence, referring to Table 4 and considering the aforementioned analyses, the final optimum processing conditions (i.e., T_s and P_c) for both model formulations were defined and are presented in Table 5.

Table 5.

Determination of optimum primary drying time: Once the optimum processing conditions of a formulation were defined, the next step in the TRA scheme was to define the primary drying time of a given fill volume. Therefore, experimental determination of the sublimation rate at a set point, selected from any of the previously defined ranges of optimum processing conditions (see Table 5), should be performed. In this study, the following set points were chosen to determine the primary drying time of MF1 and MF2:

- For MF1: P_c = 0.075 mbar, T_s = -7.0°C
- For MF2: P_c = 0.075 mbar, T_s = -16.0°C

As outlined in the materials and methods section, sublimation rates of the center vials were determined gravimetrically, and the results are presented in Table 6. As shown in Table 6, the $T_p ave$ of the front edge vials for both model formulations were well within the $T_p t$ ranges (cf. Table 2). This demonstrates the accuracy and reliability of the TRA design strategy, which was also supported by the fact that the standard deviations of the sublimation rate for both model formulations were also very low. Once reliable sublimation rates of the center vials were determined, the optimum primary drying time could be calculated either from the minimum or average sublimation rates.

Table 6.

Verification experiment: Aiming to confirm the reliability of the freeze-drying process design strategy detailed in this study, the selected optimum processing conditions were experimentally verified. During the verification experiments, the previously selected optimum processing set point and the minimum sublimation rate (cf. Table 6) were employed. To assess the success and reliability of the TRA design strategy, T_p was checked, and a visual inspection of the dried products was performed. To minimize possible variations in the drying behavior due to the freezing step, the freezing protocol during both verification and TRA experiments were kept identical.

Fig. 6 shows product temperature profiles of the verification experiments. There are different techniques to define the end of primary drying and, hence, to evaluate the adequacy of the selected primary drying time (Patel et al., 2010). One technique is to use the product thermocouples response. In general, the point where the thermocouple response starts to offset from steady-state represents the end of the primary drying. However, a more conservative approach is to use the point where T_p approaches the shelf set point temperature. As shown in Fig. 6a and 6b, the T_p responses of the center vials started to offset from their steady-state values before the start of the secondary drying, demonstrating that the drying time allocated to the process was adequate.

Figure 6. Experimental verification of the optimum processing conditions obtained using TRA. (a) Product temperature profiles of front edge vials (FE) and center vials (C) for model formulation (MF)1; (b) Product temperature profiles of front edge vials (FE) and center vials (C) for MF2. P_c, chamber pressure.

Furthermore, the completion of primary drying was supported by the physical appearance (damage-free) of the dried cakes, as displayed in Fig. 7a and 7b. Although assessment of the physical appearance of a dried cake is subjective, some literature guidelines (Ullrich et al., 2015; Patel et al., 2017; Haeuser et al., 2018; Ohori et al., 2019) have been followed to determine an acceptable appearance of a freeze-dried cake.

Figure 7. Physical appearance of the dried product after the verification experiments: (a) Model formulation (MF)1 and (b) MF2.

Table 7 presents the comparison between the T_p estimated from the TRA experiments and determined from the verification tests. The TRA estimated values presented in Table 7 represent the T_p values obtained from Table 5 at P_c = 0.10 mbar.

Table 7.

As can be deduced from Table 7, the average T_p of both the front edge and center vials obtained from the verification experiment remained well within the range of the T_p values estimated from the TRA tests. This demonstrates that the TRA freeze-drying process design strategy described in this study produces very accurate and reproducible results. This enables process scientists to design the freeze-drying process of a given pharmaceutical drug formulation based on a scientific and experimental-based approach rather than through a trial and error approach. Furthermore, the TRA employs a few and well-defined experimental runs, providing remarkable potential for savings in terms of development time and material.

4. Conclusions

The design strategy of a freeze-drying process for pharmaceuticals and biopharmaceuticals is far from optimum. In most cases, a trial and error experimental approach is employed during the designing, scaling-up, and transfer of the freeze-drying process. This approach is often material and time consuming, and the resulting freeze-drying processes are neither optimum nor robust. In this study, we described a novel simple-to-use and experimental-based approach, called TRA, for the design of an optimum and robust freeze-drying process for any pharmaceutical and biopharmaceutical drug formulations. Proper formulation characterization and definition of a narrow range of target product temperatures during the primary drying step are necessary before performing the TRA experiments. An effective DoE that contains a reliable range of process parameters (i.e., shelf temperature and chamber pressure) was developed based on a profound scientific understanding of the model formulations and the freeze-drying process. Furthermore, a few preliminary experiments were performed to better define the range of shelf temperatures at a given chamber pressure. One of the core advantages of the TRA is that a wide range of shelf temperatures can be tested in a single experiment, provided the complete TRA experiment is performed before the completion of sublimation. DoE was used to perform temperature ramp experiments, from which all necessary information to define optimum processing conditions for the primary drying step was obtained.

The proposed TRA considers variations in product temperatures and sublimation rates across a shelf. Accordingly, product temperature of the front edge vials and sublimation rate of the center vials were used to define the optimum processing conditions. In this sense, the optimum processing conditions were selected on the basis that product temperature of the front edge vials was kept within a pre-defined target product temperature and, at the same time, the highest possible sublimation rate of the center vials was achieved. This assures the effectiveness and robustness of the resulting freeze-drying process. Compared to the mathematical models that may require several freeze-drying experiments for optimization and verification, the TRA detailed in this study produced more realistic, reliable, and accurate results, demonstrating the potential for significant savings in terms of development time and material. Experimental verification with both model formulations at the optimum processing conditions showed

excellent agreement between the TRA-estimated and the experimentally determined product temperature and sublimation rate values. Finally, coupled with an effective DoE, the proposed TRA for the freeze-drying process design considerably reduces development time and material, and, at the same time, significantly improves the effectiveness and robustness of the resulting freeze-drying process.

5. References

[1]. Patel SM, Jameel F, Pikal MJ. The effect of dryer load on freeze-drying process design. *J Pharm Sci.* 2010;99:4363-4379.

[2]. Mortier STFC, Van Bockstal PJ, Corver J, Nopens I, Gernaey KV, De Beer T. Uncertainty analysis as essential step in the establishment of the dynamic Design Space of primary drying during freeze-drying. *Eur J Pharm Biopharm*. 2016;103:71-83.

[3]. Depaz RA, Pansare S, Patel SM. Freeze-drying above the glass transition temperature in amorphous protein formulations while maintaining product quality and improving process efficiency. *J Pharm Sci.* 2016;105:40-49.

[4]. Bjelošević M, Seljak KB, Trstenjak U, Logar M, Brus B, Ahlin Grabnar P. Aggressive conditions during primary drying as a contemporary approach to optimise freeze-drying cycles of biopharmaceuticals. *Eur J Pharm Sci.* 2018;122:292-302.

[5]. Horn J, Schanda J, Friess W. Impact of fast and conservative freeze-drying on product quality of protein-mannitol-sucrose-glycerol lyophilizates. *Eur J Pharm Biopharm.* 2018;127:342-354.

[6]. Anko M, Bjelošević M, Planinšek O, Trstenjak U, Logar M, Ahlin Grabnar P, Brus B. The formation and effect of mannitol hemihydrate on the stability of monoclonal antibody in the lyophilized state. *Int J Pharm.* 2019;564:106-116.

[7]. Pansare SK, Patel SM. Lyophilization process design and development: A single-step drying approach. *J Pharm Sci.* 2019;108:1423-1433.

[8]. Kasper JC, Friess W. The freezing step in lyophilization: Physico-chemical fundamentals, freezing methods and consequences on process performance and quality attributes of biopharmaceuticals. *Eur J Pharm Biopharm.* 2011;78:248-263.

[9]. Awotwe-Otoo D, Agarabi C, Read EK, Lute S, Brorson KA, Khan MA. Product and process understanding to relate the effect of freezing method on glycation and aggregation of lyophilized monoclonal antibody formulations. *Int J Pharm.* 2015;490(1-2):341-50.

[10]. Ullrich S, Seyferth S, Lee G. Measurement of shrinkage and cracking in lyophilized amorphous cakes. Part IV: Effects of freezing protocol. *Int J Pharm.* 2015;495(1):52-57.

[11]. Esfandiary R, Gattu SK, Stewart JM, Patel SM. Effect of freezing on lyophilization process performance and drug product cake appearance. *J Pharm Sci.* 2016;105:1427-1433.

[12]. Fonte P, Lino PR, Seabra V, Almeida AJ, Reis S, Sarmento B. Annealing as a tool for the optimization of lyophilization and ensuring of the stability of protein-loaded PLGA nanoparticles. *Int J Pharm.* 2016;503(1-2):163-73.

[13]. Goshima H, Do G, Nakagawa K. Impact of ice morphology on Design Space of pharmaceutical freeze-drying. *J Pharm Sci.* 2016;105:1920-1933.

[14]. Pisano R, Capozzi LC. Prediction of product morphology of lyophilized drugs in the case of vacuum induced surface freezing. *Chem Eng Res Des.* 2017;125:119-129.

[15]. Assegehegn G, Brito-de la Fuente E, Franco JM, Gallegos C. The importance of understanding the freezing step and its impact on freeze drying process performance. *J Pharm Sci.* 2019a;108:1378-1395.

[16]. Colucci D, Maniaci R, Fissore D. Monitoring of the freezing stage in a freeze-drying process using IR thermography. *Int J Pharm.* 2019;566:488-499.

[17]. Vollrath I, Friess W, Freitag A, Hawe A, Winter G. Comparison of ice fog methods and monitoring of controlled nucleation success after freeze-drying. *Int J Pharm.* 2019;558:18-28.

[18]. Schoen MP, Braxton BK, Gatlin LA, Jefferis III RP. A simulation model for the primary drying phase of the freeze-drying cycle. *Int J Pharm.* 1995;114(2):159-170.

[19]. Brülls M, Rasmuson A. Heat transfer in vial lyophilization. Int J Pharm. 2002;246(1-2):1-16.

[20]. Pikal MJ, Cardon S, Bhugra C, Jameel F, Rambhatla S, Mascarenhas WJ, Akay HU. The non-steady state modeling of freeze-drying: in-process product temperature and moisture content mapping and pharmaceutical product quality applications. *Pharm Dev Technol.* 2005;10:17-32.

[21]. Gieseler H, Kramer T, Pikal MJ. Use of Manometric Temperature Measurement (MTM) and SMARTTM freeze dryer technology for development of an optimized freeze-drying cycle. *J Pharm Sci.* 2007;96:3402-3418.

[22]. Velardi SA, Barresi AA. Development of simplified models for the freeze-drying process and investigation of the optimal operating conditions. *Chem Eng Res Des.* 2008;86:9-22.

[23]. Kuu WY, Nail SL. Rapid freeze-drying cycle optimization using computer programs developed based on heat and mass transfer models and facilitated by Tunable Diode Laser Absorption Spectroscopy (TDLAS). *J Pharm Sci.* 2009;98:3469-3482.

[24]. Giordano A, Barresi AA, Fissore D. On the use of mathematical models to build the design space for the primary drying phase of a pharmaceutical lyophilization process. *J Pharm Sci.* 2011;100:311-324.

[25]. Koganti VR, Shalaev EY, Berry MR, Osterberg T, Youssef M, Hiebert DN, Kanka FA, Nolan M, Barrett R, Scalzo G, Fitzpatrick G, Fitzgibbon N, Luthra S, Zhang L. Investigation of design space for freeze-drying: Use of modeling for primary drying segment of a freeze-drying cycle. *AAPS PharmSciTech.* 2011:12;854-861.

[26]. Fissore D, Pisano R, Barresi AA. Advanced approach to build the design space for the primary drying of a pharmaceutical freeze-drying process. *J Pharm Sci.* 2011;100:4922-4933.

[27]. Bosca S, Barresi AA, Fissore D. Fast freeze-drying cycle design and optimization using a PAT based on the measurement of product temperature. *Eur J Pharm Biopharm.* 2013;85:253-62.

[28]. Kodama T, Sawada H, Hosomi H, Takeuchi M, Wakiyama N, Yonemochi E, Terada K. Determination for dry layer resistance of sucrose under various primary drying conditions using a novel simulation program for designing pharmaceutical lyophilization cycle. *Int J Pharm.* 2013;452:180-187.

[29]. Kodama T, Sawada H, Hosomi H, Takeuchi M, Wakiyama N, Yonemochi E, Teradad K. Optimization of primary drying condition for pharmaceutical lyophilization using a novel simulation program with a predictive model for dry layer resistance. *Chem Pharm Bull.* 2014;62:153-159.

[30]. Fissore D, Pisano R. Computer-aided framework for the design of freeze-drying cycles: optimization of the operating conditions of the primary drying stage. *Processes*. 2015;3:406-421.

[31]. Chen X, Sadineni V, Maity M, Quan Y, Enterline M, Mantri RV. Finite element method (FEM) modeling of freeze-drying: monitoring pharmaceutical product robustness during lyophilization. *AAPS PharmSciTech*. 2015;16:1317-1326.

[32]. Zhu T, Moussa EM, Witting M, Zhou D, Sinha K, Hirth M, Gastens M, Shang S, Nere N, Somashekar SC, Alexeenko A, Jameel F. Predictive models of lyophilization process for development, scale-up/tech transfer and manufacturing. *Eur J Pharm Biopharm*. 2018;128:363-378.

[33]. Sharma P, Kessler WJ, Bogner R, Thakur M, and Pikal MJ. Applications of the tunable diode laser absorption spectroscopy: In-process estimation of primary drying heterogeneity and product temperature during lyophilization. *J Pharm Sci*. 2019;108:416-430.

[34]. Shanley A. Modernizing lyophilization. *BioPharm Int*. 2017;30:50-52.

[35]. Her LM, Nail SL. Measurement of glass transition temperatures of freeze-concentrated solutes by differential scanning calorimetry. *Pharm Res*. 1994;11:54-59.

[36]. Ma X, Wang DQ, Bouffard R, MacKenzie A. Characterization of murine monoclonal antibody to tumor necrosis factor (TNF-MAb) formulation for freeze-drying cycle development. *Pharm Res*. 2001;18:196-202.

[37]. Schawe EK. A quantitative DSC analysis of the metastable phase behavior of the sucrose-water system. *Thermochimica Acta*. 2006;451:115-125.

[38]. Sacha GA, Nail SL. Thermal analysis of frozen solutions: multiple glass transitions in amorphous systems. *J Pharm Sci*. 2009;98:3397-3405.

[39]. Knopp MM, Löbmann K, Elder DP, Rades T, Holm R. Recent advances and potential applications of modulated differential scanning calorimetry (mDSC) in drug development. *Eur J Pharm Sci*. 2016;87:164-7.

[40]. Ward K.R., Matejtschuk P. (2019) Characterization of Formulations for Freeze-Drying. In: Ward K., Matejtschuk P. (eds) Lyophilization of Pharmaceuticals and Biologicals. Methods in Pharmacology and Toxicology. Humana Press, New York, NY.

[41]. Passot S, Fonseca F, Alarcon-Lorcab M, Rolland D, Marina M. Physical characterization of formulations for the development of two stable freeze-dried proteins during both dried and liquid storage. *Eur J Pharm Biopharm.* 2005;60:335-348.

[42]. Meister E, Gieseler H. Freeze-dry microscopy of protein/sugar mixtures: drying behavior, interpretation of collapse temperatures and a comparison to corresponding glass transition data. *J Pharm Sci.* 2009;98:3072-3087.

[43]. Ganguly A, Alexeenko AA, Schultz SG, Kim SG. Freeze-drying simulation framework coupling product attributes and equipment capability: toward accelerating process by equipment modifications. *Eur J Pharm Biopharm.* 2013;85:223-35.

[44]. Ganguly A, Varma N, Sane P, Bogner R, Pikal M, Alexeenko A. Spatial variation of pressure in the lyophilization product chamber. Part 1: Computational modeling. *AAPS PharmSciTech.* 2017;18:577-585.

[45]. Kshirsagar V, Tchessalov S, Kanka F, Hiebert D, Alexeenko A. Determining maximum sublimation rate for a production lyophilizer: Computational modeling and comparison with ice slab tests. *J Pharm Sci.* 2019;108:382-390.

[46]. Patel SM, Pikal MJ. Lyophilization Process Design Space. *J Pharm Sci.* 2013;102:3883-3887.

[47]. Pikal MJ, Bogner R, Mudhivarthi V, Sharma P, Sane P. Freeze-drying process development and scale-up: Scale-up of edge vial versus center vial heat transfer coefficients, Kv. *J Pharm Sci.* 2016;105:3333-3343.

[48]. Scutellà B, Plana-Fattoric A, Passota S, Bourlès E, Fonseca F, Flick D, Tréléa IC. 3D mathematical modelling to understand atypical heat transfer observed in vial freeze-drying. *Appl Therm Eng.* 2017a;126:226-236.

[49]. Scutellà B, Passot S, Bourlés E, Fonseca F, Tréléa IC. How vial geometry variability influences heat transfer and product temperature during freeze-drying. *J Pharm Sci.* 2017b;106:770-778.

[50]. Scutellà B, Bourlès E, Plana-Fattori A, Fonseca F, Flick D, Trelea IC, Passot S. Effect of freeze dryer design on heat transfer variability investigated using a 3D mathematical model. *J Pharm Sci.* 2018a;107:2098-2106.

[51]. Pikal MJ, Pande P, Bogner R, Sane P, Mudhivarthi V, Sharma P. Impact of natural variations in freeze-drying parameters on product temperature history: Application of quasi steady-state heat and mass transfer and simple statistics. *AAPS PharmSciTech.* 2018;19:2828-2842.

[52]. Assegehegn G, Brito-de la Fuente E, Franco JM, Gallegos C. An experimental based approach to construct Process Design Space (PDS) of a freeze-drying process: An effective tool to design an optimum and robust freeze-drying process for pharmaceuticals. *J Pharm Sci.* 2019b; Article in press, DOI: https://doi.org/10.1016/j.xphs.2019.07.001.

[53]. Kuu WY, Hardwick LM, Akers MJ. Rapid determination of dry layer mass transfer resistance for various pharmaceutical formulations during primary drying using product temperature profiles. *Int J Pharm.* 2006;313(1-2):99-113.

[54]. Scutellà B, Trelea IC, Bourlès E, Fonseca F, Passot S. Determination of the dried product resistance variability and its influence on the product temperature in pharmaceutical freeze-drying. *Eur J Pharm Biopharm.* 2018b;128:379-388.

[55]. Chang BS, Randall CS. Use of sub-ambient thermal analysis to optimize protein lyophilization. *Cryobiology.* 1992;29:632-656.

[56]. Adams GDJ, Ramsay JR. Optimizing the lyophilization cycle and the consequences of collapse on the pharmaceutical acceptability of Erwinia L-Asparaginase. *J Pharm Sci.* 1996;85:1301-1305.

[57]. Nail S, Tchessalov S, Shalaev E, Ganguly A, Renzi E, Dimarco F, Wegiel L, Ferris S, Kessler W, Pikal M, Sacha G, Alexeenko A, Thompson TN, Reiter C, Searles J, Coiteux P. Recommended best practices for process monitoring instrumentation in pharmaceutical freeze drying-2017. *AAPS PharmSciTech.* 2017;18:2379-2393.

[58]. Patel SM, Doen T, Pika MJ. Determination of end point of primary drying in freeze-drying process control. *AAPS PharmSciTech.* 2010;11:73-84.

[59]. Patel SM, Nail SL, Pikal MJ, Geidobler R, Winter G, Hawe A, Davagnino J, Rambhatla GS. Lyophilized drug product cake appearance: What is acceptable? *J Pharm Sci.* 2017;106:1706-1721.

[60]. Haeuser C, Goldbach P, Huwyler J, Friess W, Allmendinger A. Imaging techniques to characterize cake appearance of freeze-dried products. *J Pharm Sci.* 2018;107:2810-2822.

[61]. Ohori R, Akita T, Yamashita C. Mechanism of collapse of amorphous-based lyophilized cake induced by slow ramp during the shelf ramp process. *Int J Pharm.* 2019;564:461-471.

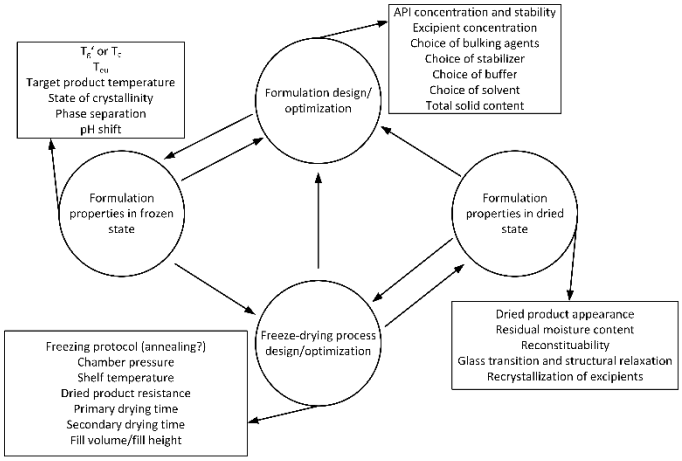

Figure 1. Interrelationship between the formulation and freeze-drying process, and its role during the freeze-drying process design and optimization.

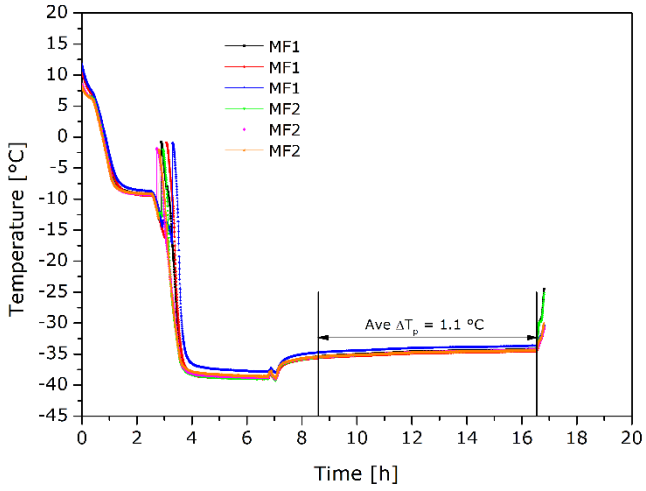

Figure 2: Dependency of product temperature (T_p) on dried layer thickness of model formulations (MF)1 and MF2.

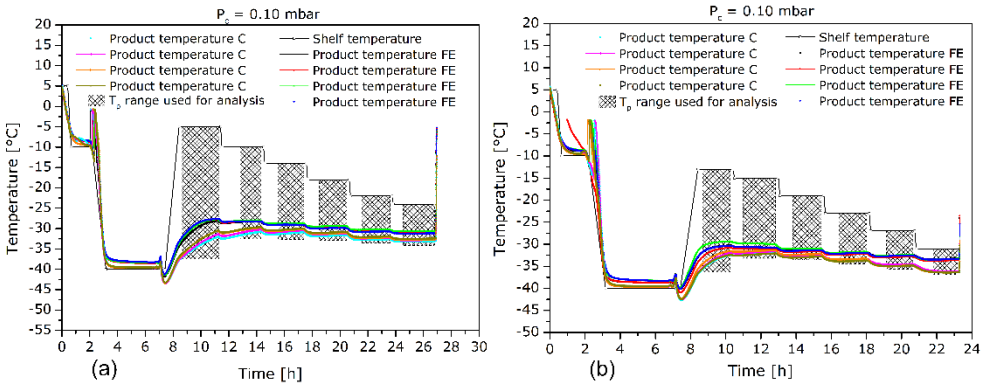

Figure 3. Product temperature profiles of selected temperature ramp approach experiments; (a) model formulation (MF)1 at P_c = 0.10 mbar, (b) MF2 at P_c = 0.10 mbar. C, center vials; FE, front edge vials, T_p, product temperature; P_c, chamber pressure.

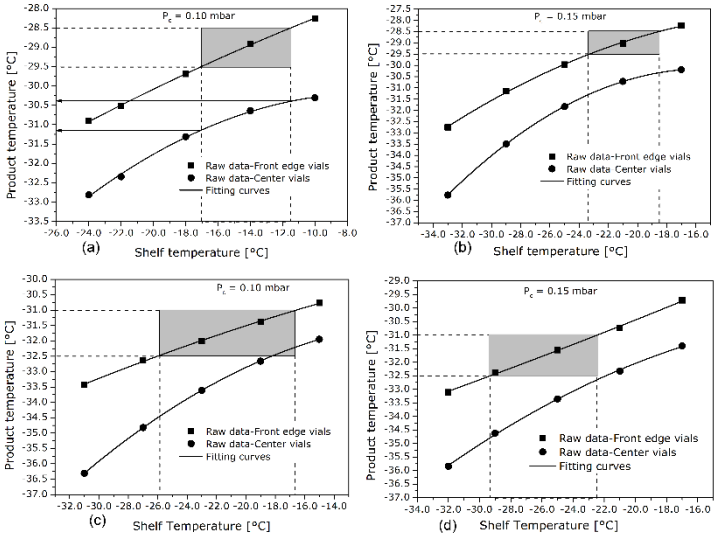

Figure 4. Product temperature dependence on shelf temperature for front edge and center vials at a selected chamber pressure; (a) Model formulation (MF)1 at P_c = 0.10 mbar, (b) MF1 at P_c = 0.15 mbar, (c) MF2 at P_c = 0.10 mbar, and (d) MF2 at P_c = 0.15 mbar. P_c, chamber pressure.

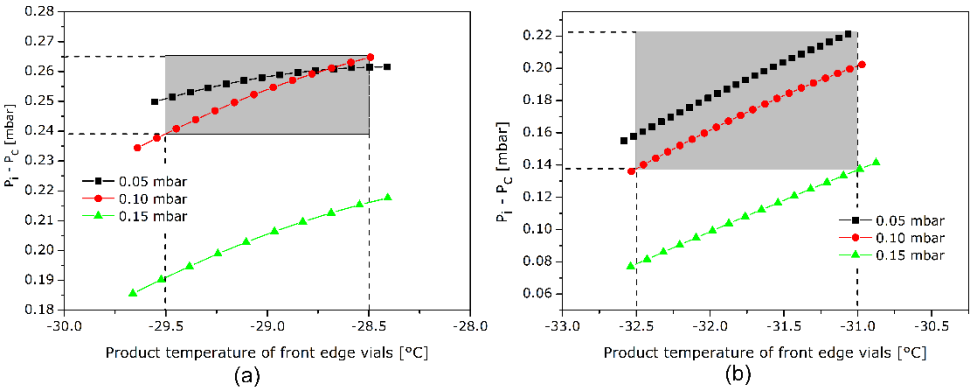

Figure 5. Dependency of the driving force for sublimation of ice, $P_i(T_p) - P_c$, on chamber pressure and product temperature; (a) Model formulation (MF)1 and (b) MF2. P_i, ice vapor pressure; T_p, product temperature; P_c, chamber pressure.

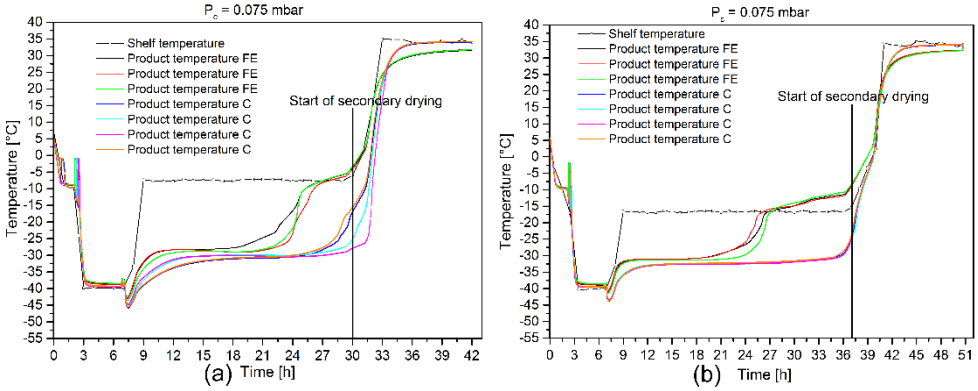

Figure 6. Experimental verification of the optimum processing conditions obtained using TRA. (a) Product temperature profiles of front edge vials (FE) and center vials (C) for model formulation (MF)1; (b) Product temperature profiles of front edge vials (FE) and center vials (C) for MF2. P_c, chamber pressure.

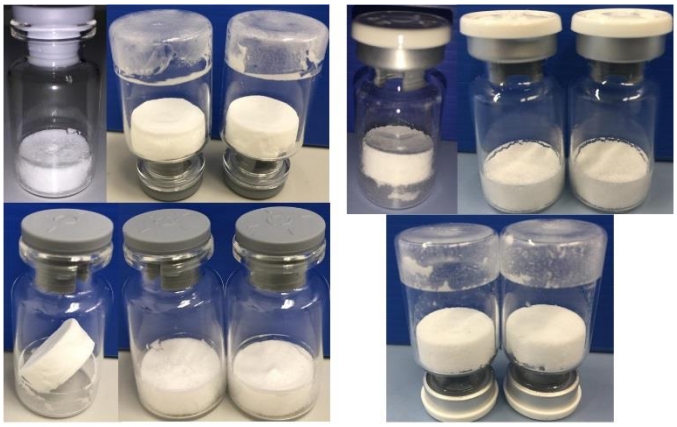

Figure 7. Physical appearance of the dried product after the verification experiments: (a) Model formulation (MF)1 and (b) MF2.

Table 1. Customized design of experiments (DoE) for MF1 and MF2

Experiment number	Primary drying input parameters		T_s points for TRA (°C)[a]
	P_c (mbar)	Range of T_s (°C)	
10% (w/w) trehalose solution (MF1)			
1	0.05	[0.0, -20.0]	0, -4, -8, -12, -16, and -20
2	0.10	[-5.0, -24.0]	-5, -10, -14, -18, -22, and -24
3	0.15	[-15.0, -33.0]	-15, -17, -21, -25, -29, and -33
20% (w/w) sucrose solution (MF2)			
1	0.05	[-8.0, -24.0]	-8, -10, -14, -18, -22, and -24
2	0.10	[-13.0, -31.0]	-13, -15, -19, -23, -27, and -31
3	0.15	[-15.0, -32.0]	-15, -17, -21, -25, -29, and -32

[a]T_s points are selected from the predefined range of T_s to perform a holding step during the TRA experiments. The quantity and value of the T_s points within a given range are user defined.
MF, model formulation; TRA, temperature ramp approach; P_c, chamber pressure; T_s, shelf temperature

Table 2. Summary of formulation critical properties for MF1 and MF2.

Formulation	Solid content (mg/g)	T_g' (°C)	T_c (°C)	$T_p t$ (°C)
MF1	100	-29.2	-27.5	[-29.5, -28.5]
MF2	200	-32.4	-31.1	[-32.5, -31.0]

MF, model formulation; T_g', glass transition temperature of the maximally freeze-concentrated solution; T_c, collapse temperature of an amorphous formulation; $T_p t$, target product temperature for primary drying

Table 3. Product temperature results and statistical analyses of MF1 and MF2 obtained from TRA experiments according to the DoE (Table 1). Statistical analysis includes minimum (Min), maximum (Max), average (Ave), and standard deviation (SD) of T_p at each T_s point studied.

		Statistical analysis of product temperatures (°C)							
		Front edge vials				Center vials			
P_c (mbar)	T_s points (°C)	Min[a]	Max[b]	Ave[c]	SD[d]	Min[a]	Max[b]	Ave[c]	SD[d]
					MF1				
0.05	0.0	-34.8	-27.7	-30.4	1.90	-40.4	-33.2	-36.7	1.77
	-4.0	-28.8	-27.8	-28.2	0.23	-34.4	-31.2	-31.9	0.76
	-8.0	-29.0	-28.5	-28.8	0.16	-32.8	-31.1	-32.0	0.42
	-12.0	-29.8	-29.2	-29.5	0.18	-32.6	-31.5	-32.2	0.31
	-16.0	-30.6	-30.0	-30.3	0.26	-33.1	-32.3	-32.8	0.25
	-20.0	-31.4	-30.6	-31.0	0.29	-34.0	-33.2	-33.7	0.22
0.10	-5.0	-33.9	-27.5	-29.5	1.62	-37.6	-30.5	-33.7	1.81
	-10.0	-28.7	-28.0	-28.3	0.15	-31.3	-29.6	-30.3	0.50
	-14.0	-29.1	-28.7	-28.9	0.11	-31.5	-30.0	-30.6	0.40
	-18.0	-29.9	-29.4	-29.7	0.16	-31.9	-30.8	-31.3	0.30
	-22.0	-30.8	-30.2	-30.5	0.17	-32.8	-31.9	-32.4	0.26
	-24.0	-31.2	-30.6	-30.9	0.16	-33.2	-32.4	-32.8	0.23
0.15	-15.0	-33.2	-28.1	-30.3	1.24	-35.5	-31.0	-33.1	1.09
	-17.0	-28.8	-27.8	-28.2	0.27	-31.1	-29.4	-30.2	0.42
	-21.0	-29.5	-28.7	-29.0	0.22	-31.3	-30.2	-30.7	0.27
	-25.0	-30.5	-29.6	-30.0	0.24	-32.1	-31.4	-31.8	0.19
	-29.0	-31.6	-30.7	-31.1	0.23	-33.7	-33.2	-33.5	0.14
	-33.0	-33.2	-32.4	-32.8	0.23	-36.0	-35.5	-35.8	0.10
					MF 2				
0.05	-8.0	-35.1	-29.5	-30.8	1.26	-40.8	-32.9	-35.6	2.00
	-10.0	-30.3	-29.7	-30.1	0.13	-32.9	-32.0	-32.3	0.21
	-14.0	-31.1	-30.9	-30.9	0.05	-33.0	-32.5	-32.8	0.12
	-18.0	-31.5	-31.2	-31.3	0.08	-33.7	-33.2	-33.5	0.11
	-22.0	-31.9	-31.4	-31.8	0.12	-34.4	-34.1	-34.3	0.08
	-24.0	-32.1	-31.5	-31.9	0.19	-34.7	-34.4	-34.6	0.07
0.10	-13.0	-34.1	-30.3	-31.2	0.84	-36.8	-31.6	-33.7	1.26
	-15.0	-31.0	-30.6	-30.8	0.14	-32.5	-31.4	-32.0	0.34
	-19.0	-31.8	-31.1	-31.4	0.21	-33.1	-32.2	-32.7	0.25
	-23.0	-32.4	-31.7	-32.0	0.19	-33.9	-33.3	-33.6	0.18
	-27.0	-33.0	-32.4	-32.6	0.18	-35.0	-34.5	-34.8	0.14
	-31.0	-33.8	-33.2	-33.4	0.15	-36.4	-36.1	-36.3	0.09
0.15	-15.0	-30.5	-29.0	-29.6	0.34	-34.1	-30.9	-31.9	0.73
	-17.0	-30.1	-29.4	-29.7	0.24	-31.8	-31.1	-31.4	0.14
	-21.0	-31.1	-30.4	-30.7	0.26	-32.6	-32.1	-32.3	0.12
	-25.0	-31.9	-31.1	-31.6	0.25	-33.6	-33.1	-33.4	0.11
	-29.0	-32.8	-31.9	-32.4	0.23	-34.8	-34.4	-34.6	0.09
	-32.0	-33.4	-32.6	-33.1	0.23	-36.0	-35.6	-35.8	0.09

[a]Minimum value for each vial group represents the minimum T_p considering all four thermologgers used.
[b]Maximum value for each vial group represents the maximum T_p considering all four thermologgers used.
[c]Average value for each vial group represents the average T_p considering all four thermologgers used.
[d]Standard deviation value for each vial group represents the standard deviation considering all four thermologgers used.
MF, model formulation; TRA, temperature ramp approach; DoE, design of experiments; T_p, product temperature; T_s, shelf temperature; P_c, chamber pressure

Table 4: Range of optimum T_s as a function of the P_c studied and the corresponding range of T_p for MF1 and MF2 fluids.

P_c (mbar)	Range of optimum T_s (°C)[a]	Range of T_p at optimum processing conditions (°C)[b]	
		Front edge vials	Center vials
		MF1	
0.05	[-12.0, -6.0]	[-29.5, -28.5]	[-32.3, -31.9]
0.10	[-17.0, -11.5]	[-29.5, -28.5]	[-31.1, -30.4]
0.15	[-22.5, -19.0]	[-29.5, -28.5]	[-31.1, -30.4]
		MF2	
0.05	[-28.5, -15.0]	[-32.5, -31.0]	[-35.8, -33.0]
0.10	[-26.0, -16.5]	[-32.5, -31.0]	[-34.5, -32.3]
0.15	[-29.5, -22.0]	[-32.5, -31.0]	[-34.9, -32.5]

[a]The range of optimum T_s was calculated using the regression equations (curve fitting equations) on the basis that the corresponding front edge vials T_p range remained within the predefined $T_p t$ (shaded area in Fig. 4).
[b]The range for center vials T_p was calculated using the regression equations (curve fitting equations) in the optimum T_s range (cf. Fig. 4a).
MF, model formulation; P_c, chamber pressure; T_s, shelf temperature; T_p, product temperature; $T_p t$, target product temperature.

Table 5. Final optimum processing conditions for MF1 and MF2.

Optimum P_c (mbar)	Range of optimum T_s (°C)	Range of T_p at optimum processing conditions (°C)	
		Front edge vials	Center vials
		MF1	
0.05	[-12, -6.0]	[-29.5, -28.5]	[-32.3, -31.9]
0.10	[-17.0, -11.5]	[-29.5, -28.5]	[-31.1, -30.4]
		MF2	
0.05	[-28.5, -15.0]	[-32.5, -31.0]	[-35.8, -33.0]
0.10	[-26.0, -16.5]	[-32.5, -31.0]	[-34.5, -32.3]

MF, model formulation; P_c, chamber pressure; T_p, product temperature; T_s, shelf temperature.

Table 6. Results of the sublimation rate determination experiments at the selected processing set point.

Formulation	Front edge vials		Center vials					
	T_p[a] (°C)		T_p[b] (°C)		$\dot{m}$[c] (g/h·vial)			
	Ave	SD	Ave	SD	Min	Max	Ave	SD
MF1	-29.10	0.70	-32.44	1.51	0.130	0.151	0.140	0.007
MF2	-31.06	0.20	-32.94	1.09	0.086	0.105	0.095	0.005

[a]The average and standard deviation values were calculated from temperature measurements obtained from three thermologgers (approximately 4500 data points).
[b]The average and standard deviation values were calculated from temperature measurements obtained from four thermologgers (approximately 6000 data points).
[c]The Min, Max, Ave and SD of the sublimation rate were calculated from 16 center vials.
MF, model formulation; Ave, average; SD, standard deviation; Min, minimum; Max, Maximum; T_p, product temperature; $\dot{m}$, overall mass transfer rate from a vial.

Table 7. Comparison of the TRA estimated and experimentally determined parameters at the selected optimum processing set point.

Formulation	TRA estimated values		Experimentally determined values			
	Front edge vials	Center vials	Front edge vials T_p(°C)[a]		Center vials T_p(°C)[b]	
	T_p(°C)	T_p(°C)	Ave	SD	Ave	SD
MF1	[-29.5, -28.5]	[-31.1, -30.4]	-28.8	0.45	-31.1	1.35
MF2	[-32.5, -31.0]	[-34.5, -32.3]	-31.3	0.45	-32.4	1.09

[a]The average and standard deviation values were calculated from temperature measurements obtained from three thermologgers (approximately 4800 data points).
[b]The average and standard deviation values were calculated from temperature measurements obtained from five thermologgers (approximately 10300 data points).
TRA, temperature ramp approach; T_p, product temperature.

Appendix A.3:

An Experimental-Based Approach to Construct the Process Design Space of a Freeze-Drying Process: An Effective Tool to Design an Optimum and Robust Freeze-Drying Process for Pharmaceuticals.

Getachew Assegehegn[1], Edmundo Brito-de la Fuente[1], José M. Franco[2] and Críspulo Gallegos[1]

[1]Fresenius-Kabi Deutschland GmbH, Process and Product Engineering Center, Global Manufacturing Pharmaceuticals, Bad Homburg, Germany

[2]Pro2TecS-Chemical Product and Process Technology Research Centre, Complex Fluid Engineering Laboratory. Departamento de Ingeniería Química, Universidad de Huelva, Huelva, Spain

Published in:

Journal	Journal of Pharmaceutical Sciences
Publishing company	Elsevier
Editor-in-Chief	Prof. Ronald T. Borchardt
Volume and pages	108; 1378-1395
Publication year	2019
ISSN	0022-3549
DOI	https://doi.org/10.1016/j.xphs.2018.11.039
Journal impact factor (2018)	**3.197**

Category (2017)	**Journal rank/total journal**	**Quartile**
Chemistry, medicinal	21/59	Q2
Chemistry, multidisciplinary	69/171	Q2
Pharmacology & pharmacy	93/261	Q2

ARTICLE IN PRESS

Journal of Pharmaceutical Sciences xxx (2019) 1-12

Contents lists available at ScienceDirect

Journal of Pharmaceutical Sciences

journal homepage: www.jpharmsci.org

Pharmaceutics, Drug Delivery and Pharmaceutical Technology

An Experimental-Based Approach to Construct the Process Design Space of a Freeze-Drying Process: An Effective Tool to Design an Optimum and Robust Freeze-Drying Process for Pharmaceuticals

Getachew Assegehegn [1,*], Edmundo Brito-de la Fuente [1], José M. Franco [2], Críspulo Gallegos [1]

[1] Fresenius-Kabi Deutschland GmbH, Product and Process Engineering Center, Global Manufacturing Pharmaceuticals, Bad Homburg, Germany
[2] Departamento de Ingeniería Química, Pro2TecS-Chemical Product and Process Technology Research Centre, Complex Fluid Engineering Laboratory, Universidad de Huelva, Huelva, Spain

ARTICLE INFO

Article history:
Received 28 May 2019
Revised 2 July 2019
Accepted 2 July 2019

Keywords:
freeze-drying
lyophilization
quality-by-design
formulation
processing
mathematical models(s)

ABSTRACT

The application of quality by design (QbD) is becoming an integral part of the formulation and process development for pharmaceutical products. An essential feature of the QbD philosophy is the design space. In this sense, a new approach to construct a process design space (PDS) for the primary drying section of a freeze-drying process is addressed in this paper. An effective customized design of experiments (DoE) is developed for freeze-drying experiments. The results obtained from the DoE are then used to construct the product-based PDS. The proposed product-based PDS construction approach has several advantages, including (1) eliminating assumptions on the heat transfer coefficient and dried product resistance, as it is constructed from experimental results specifically obtained from a given formulation, yielding more realistic and reliable results and (2) PDS construction based on a narrow range of product temperatures and considering the variations in product temperature and sublimation rate of vials across a shelf. This guarantees the effectiveness and robustness of the process and facilitates the process scale-up and transfer. The PDS developed herein was experimentally verified. The PDS predicted parameters were in excellent agreement with the experimentally obtained parameters.

Introduction

Freeze-drying or lyophilization is a drying unit operation that is frequently used in pharmaceutical and biopharmaceutical industries to convert labile liquid formulations into a solid state with the aim of improving their long-term storage stability.[1,2] Despite being a method of high relevance for these industries, freeze-drying is an energy intensive, time consuming, and economically expensive process.[3,4] Therefore, the rational design and optimization of the freeze-drying process is of paramount importance. It is understandable that a sound knowledge of a formulation and its critical properties are essential for the efficient and rational design of a freeze-drying process.[5-9] Formulation critical properties include the freezing behavior of the formulation (phase separation, protein denaturation, and pH shift), glass transition temperature of the maximally freeze-concentrated solution (T_g'), collapse temperature of the amorphous formulation (T_c), eutectic temperature of the crystalline formulation (T_{eu}), stability of the active ingredients during preparation, and properties of the excipients. Knowledge of such formulation properties and the freeze-drying process itself significantly eases the design of a robust and optimum process. Whereas an optimum process minimizes the process time, a robust process addresses minor process deviations and maintains the predefined quality target product profiles (QTPP).

The primary drying step of the freeze-drying process is, typically, the most critical and longest processing step. Consequently, the majority of the optimization efforts are performed in this step. As reviewed in previous papers,[10,11] the freezing step has a significant effect on the primary drying rate; this is attributed to the morphology, and the number and size of ice crystals formed during the freezing step. The ice crystals leave a porous structure of dried product upon sublimation, which determines the permeability and resistance to water vapor flow through the dried product. The larger the ice crystals formed during the freezing, the larger the pore radius of the porous dried product and, hence, the lower the resistance to water vapor flow. This facilitates the drying rate during the sublimation step of the freeze-drying process. In general, the influence of the freezing step on the different freeze-

* *Correspondence to:* Getachew Assegehegn (Telephone: +4961726087381).
E-mail address: getachew.assegehegn@fresenius-kabi.com (G. Assegehegn).

https://doi.org/10.1016/j.xphs.2019.07.001
0022-3549/

Nomenclature

CQAs	Critical quality attributes
DoE	Design of experiments
DS	Design space
K_v	Vial heat transfer coefficient
MF1	Model formulation 1 (10% (w/w) trehalose solution)
MF2	Model formulation 2 (20% (w/w) sucrose solution)
$\dot{m}$	Overall mass transfer rate (sublimation rate) from a vial
P_c	Chamber pressure
PDS	Process design space
P_i	Vapor pressure of ice
QbD	Quality by design
QTPP	Quality target product profiles
r	Pore radius of a dried product
R_p	Resistance to mass transfer of the dried product
T_c	Collapse temperature of an amorphous formulation
t_d	Drying time of primary drying
T_{eu}	Eutectic temperature
T_g'	Glass transition temperature of the maximally freeze-concentrated solution
T_p	Product temperature
T_pave	Average product temperature during primary drying
T_pt	Target product temperature
T_s	Shelf temperature

drying parameters can be summarized as shown in Equation 1. A more detailed analysis of Equation 1 is given in reference.[11]

$$\begin{aligned} r &= f(\textit{ice crystal size}) \\ R_p &= f\left(\frac{1}{r}\right) \\ T_p &= f\left(R_p, \frac{1}{r}\right) \\ P_i &= f(T_p, R_p) \\ \dot{m} &= f\left(\frac{1}{R_p}, T_p\right) \end{aligned} \quad \textit{Provided } T_s \textit{ and } P_c \textit{ are held constant} \qquad (1)$$

where, r(cm) is the pore radius of the dried product; R_p(mbar•s/g) is the resistance to mass transfer of the dried product; T_p(°C) is the product temperature, P_i(mbar) is the vapor pressure of ice; T_s(°C) is the shelf temperature; P_c(mbar) is the chamber pressure; and $\dot{m}(g/s)$ is the overall mass transfer rate from a vial.

During the primary drying step, the chamber pressure, P_c, is reduced to trigger the sublimation of the ice crystals and, simultaneously, the shelf temperature, T_s, is increased to provide energy to the sublimation process. The endothermic sublimation of ice and the exothermic heat input processes are occurring in "close equilibrium". Thus, the change in product temperature during the primary drying is insignificant, provided that the shelf temperature and chamber pressure are held constant. One major factor for a slight change in product temperature during the primary drying could be the increase in dried product resistance caused by an increase in dried layer thickness.

In a freeze-drying process, the product temperature is indirectly controlled through the manipulation of the shelf temperature and chamber pressure. In the majority of cases, the manipulation of the shelf temperature and chamber pressure is realized through a trial and error approach, which leads to unnecessary long experimental setups. Further, the resulting freeze-drying process is neither robust nor efficient. In an attempt to minimize the trial and error experiments, researchers have developed mathematical models for the determination of the optimum processing conditions based on the governing heat and mass transfer equations.[4,12-28] In these mathematical models, 2 input parameters, namely the overall vial heat transfer coefficient and the resistance to mass transfer of the dried product, are experimentally determined. The overall vial heat transfer coefficient is typically determined from a water sublimation test, whereas the resistance to mass transfer of the dried product is determined using the drug formulation. The determination of these parameters from a nondrug formulation and from a single experimental run could lead to a significant error during the optimization of the process.[22] The authors' experimental results show up to 18% difference in the overall vial heat transfer coefficient determined from water sublimation tests and from drug formulation sublimation tests (see Table 1). Further, determination of the dried product resistance from a single experimental run may not represent different processing conditions. Processing at a product temperature close to the T_c could introduce a microcollapse on the dried structure, yielding a considerably reduced dried product resistance compared with the dried products without microcollapse.

Following the roll out of the International Conference on Harmonization (ICH) Q8(R2), the application of quality by design (QbD) has become an integral part of the formulation and process development for pharmaceutical products.[29] An essential feature of the QbD philosophy is the design space, which is defined, according to ICH Q8(R2), as a multidimensional combination and interaction of input variables and process parameters that have been demonstrated to provide the assurance of critical product quality.[30] Given the high interest of the pharmaceutical industries in implementing the QbD concept in their formulation and process development platforms, there exists a requirement for a systematic, scientific, and result-based design space construction strategy.

To address this point for a freeze-drying process, this study presents a new approach for the construction of a process design space (PDS) using a customized design of experiments (DoE). A PDS is a space enclosed by critical input process parameters of a given process, within which the output parameters and the critical quality attributes (CQAs) of the product remain within the desired limit. A PDS ensures both process efficiency and product quality,

Table 1
Differences in Overall Vial Heat Transfer Coefficients (K_v) of a Drug Formulation and Water for Injection

P_c (mbar)	T_s (°C)	Overall Vial Heat Transfer Coefficient, K_v*10^4 (cal/s.cm^2.K)		
		Drug Formulation	Water for Injection	Difference (%)
0.05	−10.0	1.895	1.934	2.06
	−17.0	1.952	1.871	4.15
	−20.0	2.127	1.869	12.1
0.10	−10.0	3.044	3.044	0.00
	−15.0	2.847	3.093	8.64
	−20.0	3.131	3.165	1.09
	−24.0	2.764	3.182	15.1
0.15	−15.0	4.169	4.624	10.9
	−18.0	4.508	4.229	6.19
	−25.0	3.485	4.144	18.9

Note that the experiments were performed using identical vials and stoppers. Authors' own experimental results. P_c is chamber pressure and T_s is shelf temperature.

and, hence, its advantages and applications during the freeze-drying of pharmaceutical products are significant. Because freeze-drying is an energy intensive process, designing the most optimum freeze-drying process is certainly one of the highest priorities for pharmaceutical industries. In this regard, a PDS provides an opportunity to define optimum process parameters while maintaining product quality. Further, a PDS significantly eases the freeze-drying process scale-up and transfer and ensures consistent product quality during large-scale commercial manufacturing. A PDS provides information on how possible process deviations during scale-up, transfer, or manufacturing influence the output parameters and CQAs and offers an opportunity for an early and systematic mitigation system for the case where the output parameters and CQAs are outside the PDS. Possible process deviations during scale-up, transfer, or manufacturing could be caused by differences in freezing conditions at lab and manufacturing scale and differences in equipment design. In such circumstances, equipment characterization is necessary to assess the differences between equipment and to adjust the processing conditions. Adjustment of the processing conditions could be significantly facilitated using the PDS.

In a freeze-drying process, it is important to consider that a PDS contains the input parameters that provide the maximum possible sublimation rate during the primary drying step. As can be deduced from Equation 1, the sublimation rate is dependent on several parameters, namely, ice vapor pressure or product temperature, chamber pressure, and dried product resistance to mass transfer. To maximize the sublimation rate during primary drying, it is important to execute at the highest vapor pressure of ice (this corresponds to the highest product temperature) and at the lowest chamber pressure. However, the maximum product temperature during primary drying is limited by the T_c of the amorphous formulations or the T_{eu} of the crystalline formulations. Conversely, the minimum chamber pressure is limited by the capability of the freeze-drying equipment.[31-33] In this sense, a PDS offers a method to identify the product and equipment limitations and to select the most optimized and robust process parameters for a given formulation.

Although profound prior scientific knowledge of both formulation and process is indispensable for building an effective DoE, it also significantly assists in minimizing the number of experiments necessary to construct a PDS. Using an effective DoE, less than 20 freeze-drying experiments can be performed to develop the PDS of a pharmaceutical formulation. As mentioned earlier, the primary drying is the most critical phase in terms of process economics and overall product quality. Thus, the focus of this study is on the construction of the PDS for the primary drying phase of the freeze-drying process. Although the mathematical models provide an opportunity to simulate several combinations of input process variables during the PDS construction, their success is highly dependent on the accuracy of the model input parameters and the assumptions of the model equations. In this sense, the experimental-based PDS construction approach detailed in this study offers an alternative method for the construction of a freeze drying PDS. In addition, although the mathematical models may need fewer experimental setups than the experimental approach presented herein, the advantages of the experimental approach over the mathematical models are several folds. These include (1) the utilization of unique and easy procedures to construct a PDS using the data obtained solely from freeze-drying experiments of a given drug product. This eliminates the assumptions on heat transfer coefficient and dried product resistance, thus providing highly accurate results. For this reason, the PDS developed in this study is termed a product-based PDS; (2) unlike the current representation of a freeze-drying PDS, this study uses shelf temperature versus chamber pressure curves with narrow ranges of product temperatures as contour lines. This facilitates the selection of the most effective and optimized process parameters for a given formulation; and (3) the PDS presented herein incorporates the variation in product temperatures and sublimation rates of vials at different locations of a shelf. This guarantees the robustness of the process and facilitates the process scale-up and transfer. Moreover, presenting a product-based PDS offers more realistic and reliable results if there is an intention of using the PDS for regulatory purposes.

Finally, it is worth pointing out that Chang and Fischer reported construction of a freeze-drying PDS based on experimental approach, aiming to explain the use of a single-step freeze drying cycle for a crystalline formulation (i.e., use of high shelf temperature [as high as 40°C] and low chamber pressure to avoid using secondary drying).[34] Consequently, it is apparent that the approach followed by Chang and Fischer is based on a rather different concept.

Materials and Methods

Materials

Sucrose was purchased from VWR (Darmstadt, Germany), and trehalose was purchased from Pfanstiehl, Inc. (Waukegan, IL). The 2 raw materials were used without further treatment. Water for injection was obtained from Fresenius Kabi Deutschland GmbH (Friedberg, Germany). All vials used in this study were 10-mL tubing vials purchased from SCHOTT AG (Mainz, Germany). The stoppers were Igloo single vented gray stoppers from West Pharmaceutical Services, Inc. (West Whiteland Township, PA).

Two model formulations were used for the development of the PDS. Model formulation 1 (MF1) was a 10% (w/w) trehalose solution; model formulation 2 (MF2) was a 20% (w/w) sucrose solution. Water for injection was used to prepare all the solutions used in this study. Aiming to remove particulate matters that could be introduced during preparation, the model formulations were filtered using 0.22 μm pore-size filters (PALL Corporation, Port Washington, NY) prior to filling the vials.

Methods

Differential Scanning Calorimetry

The glass transition temperature of the frozen samples (T_g') was measured using a TA Instruments Q2000 series differential scanning calorimetry (DSC) with refrigerated cooling system (RCS) (TA Instruments, New Castle, DE). Sucrose and trehalose solutions were prepared as described previously, and a sample of 10-15 mg was weighed into aluminum sample pans, which were then hermetically sealed. An empty, hermetically sealed, pan was used as a reference. The RCS was set on continuous mode, and the nitrogen supply was set to 50 mL/min. The solution samples were first equilibrated at 40°C for 2 min and then frozen to −60°C at a rate of 20°C/min. The frozen samples were held at −60°C for 10 min before heating to 40°C at a rate of 10°C/min. The T_g' values were determined using Universal Analysis software and were reported as the midpoint of the glass transition curve.[35]

Freeze-Drying Microscopy

The collapse temperature (T_c) of the model formulations was determined using a Lyostat 2 freeze-drying microscopy (Biopharma Technology Ltd., Winchester, UK). Sucrose and trehalose solutions were prepared as described previously, and a sample of 2 μL was placed on a quartz cover slip and covered using a glass cover slip. To allow sublimation of the sample, a 70 μm thick metal spacer was placed between the quartz and glass cover slips. The solution samples were frozen to −40°C at a rate of 20°C/min and held for

5 min. After freezing, the vacuum was reduced to approximately 0.1 mbar and maintained at this condition until an approximately 2-3 mm dry layer thickness was achieved. The samples were further heated at 5°C/min to a temperature marginally less than the T_g' obtained from DSC, and then the heating rate was decreased to 0.5°C/min, aiming to observe a structural change at a higher temperature resolution. The samples were heated until complete structural damage was observed. Images of the samples were captured throughout the experiment, and the collapse temperature (T_c) was defined as the temperature where a clearly observable structural change of the frozen solution was observed.

Freeze-Drying Experiment

All freeze-drying experiments were performed using an HOF laboratory freeze dryer with a total usable shelf area of 0.36 m^2 (HOF Sonderanlagenbau GmbH, Lohra, Germany). The freeze dryer was equipped with a Pirani gauge for chamber pressure control and 3 type K thermocouples for the measurement of the product temperature. Freeze-drying experiments of both model formulations were performed using 10-mL tubing vials. For each of the model formulations, 176 vials (1 fully loaded shelf) were filled with 4 mL solution and placed on 1 of the 4 shelves of the freeze dryer. During the sublimation rate determination experiments, the fill volume was selected to be higher than the design fill volume (3 mL) to bring equivalence in dried product resistance and sublimation rate. For example, consider a sublimation experiment that was stopped after an average 60% of a given (5 mL) fill volume was sublimed. This is equivalent to a complete sublimation of 3 mL fill volume and, thus, brings equivalence in dried layer thickness (i.e., dried layer resistance) and sublimation rate. The freeze dryer had an acrylic chamber door, and to reduce the effect of radiation, the door was covered with a 4-mm thick polystyrene foam block and an aluminum foil. Eight wireless thermologgers (Lives International, Timis, Romania) and the 3 type K thermocouples were used to measure product temperatures. Although the presence of temperature probes could impact the freezing and drying behavior of the probed vials, such impact could be minimized by using thin temperature probes. Thus, both the type K thermocouples and wireless thermologgers used in this study were less than 1 mm thick. Product temperatures using the wireless thermologgers were measured every 20 s. The freezing step was held constant for all freeze-drying experiments as follows: 1°C/min down to −10°C and 90 min holding time; further freezing to −40°C at 1°C/min and 240 min holding time. Conversely, the primary drying was changed according to the DoE, as indicated in Table 2. The shelf surface temperatures (Fig. 4) were measured using the wireless thermologgers in a fully loaded shelf. For this purpose, the thermologgers were inserted into bottomless 10-mL vials, and they were arranged to have a clear contact with the shelf surface.

Determination of Sublimation Rate

The sublimation rate was determined gravimetrically. For this purpose, 50 selected sample vials were weighed before and after the freeze-drying experiments. The sample vials were systematically placed to represent different vial groups, which could have different sublimation rates and product temperatures, within the vial array. Figure 1 displays the placement of the sample vials and thermocoupled vials for all the experiments performed in this study. For example, in Figure 1, vials numbered 1-8 represent a vial group referred to as "*front edge*", vials 9-17 represent "*side edge outer*", vials 18-26 represent "*side edge inner*", vials 27-42 represent "*center*", and vials 43-50 represent "*rear edge*". Maximum, minimum, and average sublimation rates of each vial group were calculated from the sublimation rates obtained from the numbered vials of the same group (cf. Fig. 1). A laboratory analytical balance (Sartorius AG, Göttingen, Germany) was used to weigh the sample vials. The sublimation process was terminated by backfilling the product chamber using dry nitrogen, and the vials were heated to 20°C before the product chamber door was opened. This step was included to prevent condensation from the surrounding moisture from forming on the cold stoppers and penetrating into the extremely hygroscopic dried product. The freeze dryer available did not have an automatic stoppering mechanism. As a result, once the product chamber door was opened, the sample vials were taken out of the chamber, immediately fully stoppered and re-weighed.

Table 2
Custom Designed Full-Factorial Design of Experiments for Model Formulation 1 and Model Formulation 2

Experiment Number	Primary Drying Input Parameters		Primary Drying Output Parameters
	P_c (mbar)	T_s (°C)	
1	0.05	−5.0[a]	• Product temperature of front edge and center vials • Sublimation rate of front edge and center vials
2		−10.0	
3		−13.0[b]	
4		−15.0	
5		−20.0	
6	0.08	−10.0	
7		−15.0	
8		−20.0	
9		−25.0	
10	0.10	−15.0	
11		−17.0	
12		−20.0	
13		−25.0	
14	0.15	−17.0	
15		−20.0	
16		−25.0	
17		−30.0	
18	0.20	−20.0	
19		−25.0	
20		−30.0	

P_c is chamber pressure and T_s is shelf temperature.
[a] Experiment only for model formulation 1.
[b] Experiment only for model formulation 2.

It is well-known that dried product resistance and product temperature increase when product dried layer thickness increases.[19,22,36] Therefore, to include the maximum effect of the dried product resistance during the determination of the sublimation rate, the sublimation experiments were stopped once the dried layer of the front edge vials was close to the vial bottom. This was performed by visually observing the dried layer of the front edge vials. At the end of the sublimation experiments, up to 70 wt% of the initial water content of the edge vials was removed, whereas, for center vials, up to 50 wt% of the initial water content was removed. Further, this procedure allows determination of consistent loss of water during the different sublimation experiments. The exact drying time for the calculation of the sublimation rate was obtained from the product temperature profile of the wireless thermologgers. Primary drying time, by definition, starts when the shelf temperature attains the desired shelf set point temperature for primary drying. Thus, regardless of the product temperature, the starting time for the calculation of the sublimation rates was defined as the time at which the shelf temperature attained the desired set point temperature. It was experimentally determined that at low chamber pressure and low shelf temperature, up to 4 h were required to achieve a pseudo steady-state condition in product temperature. Whereas, up to 2 h were required to attain a pseudo steady-state condition in product temperature at high chamber pressure and high shelf temperature conditions. Although the time required to achieve a pseudo steady state in product temperature was highly dependent on the processing conditions and formulation solid content, the values obtained in this study

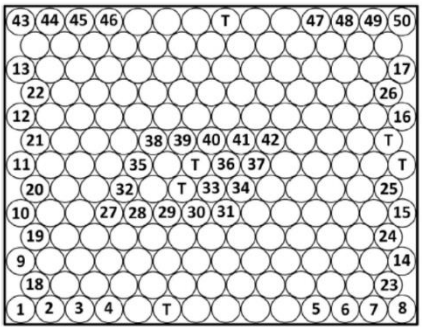

Figure 1. Vial placement for the sublimation experiments of this study. "Numbered vials" represent vials weighed before and after the freeze-drying experiment. "T-signed vials" represent vials with thermocouples for product temperature measurement of the different groups of vial arrays.

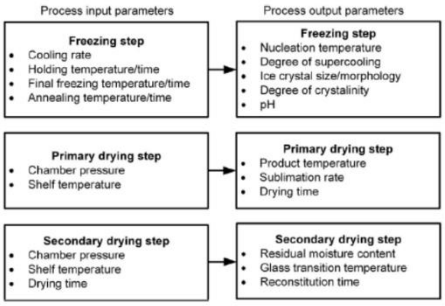

Figure 2. Critical input and output process parameters of a typical freeze-drying process.

were significantly longer than the values reported in the literature.[37] Therefore, such definition of the starting time considers the real effect of different processing conditions and formulations on the sublimation rate before the product temperature attained a pseudo steady-state condition. That is, the calculation of the sublimation rates considered the transition period at the beginning of the primary drying. Thus, any bias in sublimation rate calculation that could occur due to the transition period was avoided.

Design of Experiments

DoE is a structured analysis of experiments wherein input parameters are changed, and differences and variations in output parameters are measured. DoE allows the simultaneous determination of the effects of all potential input variables on the output responses, as well as investigations on how the process response changes as input variables fluctuate (random and systematic variation of the process parameters) within allowable limits. This requires a profound scientific background of the formulation and process, and, further, preliminary experiments using the specified drug formulation could be required to facilitate the development of an effective DoE. For a freeze-drying process, the critical process input and output parameters of the 3 steps are well known. They are depicted in Figure 2.

As the focus of this study was on the PDS development for the primary drying step, the DoE only considered the input and output parameters of the primary drying step of the freeze-drying process. Based on prior knowledge and preliminary experiments using the model formulations, a customized full-factorial DoE for both model formulations was developed as displayed in Table 2.

Results and Discussion

Characterization of Frozen Formulations

Representative DSC thermograms for MF1 and MF2 are displayed in Figure 3i. For MF1, T_g' was observed at a temperature of −29.2°C; for MF2, T_g' was observed at a temperature of −32.4°C. The T_g' values of MF1 and MF2 obtained in this study were in excellent agreement with previously reported values.[35,38]

Freeze-drying microscopy images of MF1 and MF2 are displayed in Figure 3ii. The T_c of both model formulations obtained in this study were also in excellent agreement with the values reported in the literature.[39] Table 3 presents the results of T_g', T_c, and the range of maximum product temperature during primary drying for the two model formulations.

Construction of Process Design Space for MF1

During the construction of the freeze-drying PDS, the limitations imposed by the freeze-dryer and formulation were considered. Patel and Pikal[40] reported that the majority of manufacturing dryers cannot control chamber pressures less than 0.06 mbar and that there is no additional advantage in sublimation rate for chamber pressures greater than 0.40 mbar. To verify these limitations, preliminary experiments were performed as follows: (1) a sublimation test using pure water at a chamber pressure of 0.05 mbar and a shelf temperature of −10°C. This test provided an average sublimation rate of 0.319 g/h·vial, which exceeds the expected average sublimation rate of the model formulations at the same chamber pressure. Therefore, it can be safely assumed that 0.05 mbar and greater chamber pressures would not experience chocking flow for the expected sublimation rates of the model formulations studied and (2) sublimation tests using both model formulations at a chamber pressure of 0.25 mbar and a shelf temperature of −25°C. Although these processing conditions yielded average product temperatures close to T_c (−29.7°C for MF1 and −31.0°C for MF2), the corresponding average sublimation rates (0.074 g/h·vial for MF1 and 0.089 g/h·vial for MF2) were considerably less than the sublimation rates obtained at lower chamber pressures and similar product temperatures. Therefore, chamber pressures greater than 0.25 mbar would have no benefit from a sublimation rate point of view.

The DoE displayed in Table 2 was developed considering the information obtained from the previously mentioned preliminary experiments. Representative results of the freeze-drying experiments are presented in Table 4. The results for all the processing conditions displayed in the DoE (Table 2) were obtained in a similar manner (not indicated herein) and further processed.

The results displayed in Table 4 indicate remarkable differences in $T_p ave$ and the sublimation rates between the front edge and center vials. As supported by the experimental results displayed in Figure 4 and in the literature,[41–44] even in a freeze-drying process with a minimum effect of radiation, there could be significant spatial variation in the shelf surface temperature. Cold spots were observed at the center of the shelf, indicating a temperature of approximately 4°C colder than the hot spots, which were observed at the front edge

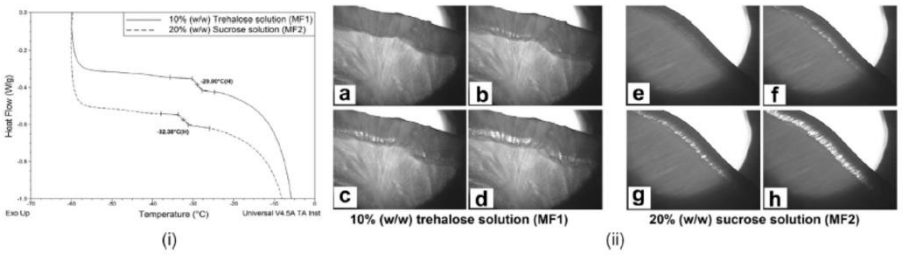

Figure 3. Characterization of frozen formulations. (i) DSC thermograms for MF1 (solid line) and for MF2 (dashed line). (ii) Freeze-drying microscopy images for MF1, (a) intact structure at T = −28.5°C, (b) onset of collapse at T = −28.0°C, (c) collapse at T = −27.5°C, and (d) significant damage at T = −27.0°C and for MF2, (e) intact structure at T = −31.8°C, (f) onset of collapse at T = −31.4°C, (g) collapse at T = −31.1°C, and (h) significant damage at T = −30.6°C.

of the shelf. These spatial shelf surface temperature variations could be attributed to the large thermal demand of the vials located at the center of the shelf compared with the vials located at the edge. The center vials have a higher vial packing density (number of vials per unit area). Hence, they absorb much larger energy during ice sublimation compared with edge vials. This, in turn, leads to different product temperatures and sublimation rates of the vials placed at different locations across a shelf (see Fig. 4).

Therefore, consideration of such variations during the construction of a PDS is critical in the design of a robust freeze-drying process. Further, as indicated in Table 4, the sublimation rate is dependent on the chamber pressure. Thus, depending on the chamber pressure, similar product temperatures can produce different sublimation rates. As displayed in Table 4 for MF1, a similar $T_p ave$ for front edge vials was obtained at Condition 1 ($T_s = -20°C/P_c = 0.10$ mbar) and Condition 2 ($T_s = -30°C/P_c = 0.20$ mbar). Analyzing Conditions 1 and 2, similar $T_p ave$ were obtained at different T_s values. Thus, to yield similar $T_p ave$, a higher P_c requires a lower T_s. This is because (1) when the chamber pressure increases, the heat transfer rate owing to gas conduction increases, leading to an increase in product temperature[45] and (2) at constant P_i, high chamber pressures reduce the driving force for mass transfer rate, $P_i(T_p) - P_c$. The reduction in the endothermic mass transfer rate decreases the energy consumption from a vial, leading to an increase in product temperature, unless T_s is adjusted. It is important to note here that, although similar $T_p ave$ can be obtained at different P_c values, the corresponding sublimation rate values can be significantly different. Referring to the aforementioned conditions, the sublimation rates of the front edge vials under Condition 1 are significantly greater than under Condition 2. Similarly, although the center vials at Condition 1 had reduced $T_p ave$, their sublimation rates were considerably greater compared with the center vials under Condition 2. This is attributed to the fact that at a given T_p, the driving force for mass transfer rate, $P_i(T_p) - P_c$, decreases as P_c increases. Thus, for a given T_p, low P_c and high T_s produce a high mass transfer rate. Such knowledge and information for a specific drug product is essential to design the most optimized and robust freeze-drying process. A PDS can be used as a tool to choose the optimum process variables that yield the maximum possible mass transfer rate, without exceeding the maximum allowable product temperature during primary drying.

The construction of the PDS was started by plotting isotherms for the product temperature on a graph of shelf temperature versus chamber pressure, as displayed in Figure 5b. The product temperature isotherms were calculated from data obtained experimentally and represented the average product temperature of the front edge vials. The reason for selecting the front edge vials to define the product temperature was that this vial group had the highest product temperature in the vial arrays. Product temperatures were collected every 20 s. The average product temperature represents an average value of the product temperatures collected during the entire period of the sublimation test. Figure 5a presents the average product temperature of the front edge vials at the selected shelf temperature and chamber pressure. The results demonstrate an excellent linear relationship ($R^2 > 0.94$) of the average product temperature and shelf temperature at any given chamber pressure. Using regression analyses of the data points (solid lines, Fig. 5a), possible combinations of chamber pressure and shelf temperature that produce any desired product temperature can be calculated. This information was used to construct the graph of chamber pressure versus shelf temperature with the isotherms of the product temperatures (Fig. 5b).

As can be observed in Figure 5a, a change in the slope of the curves with increasing chamber pressure was observed. At relatively low chamber pressures, less than 0.08 mbar, the driving force for the sublimation rate is large, and thus the heat transfer becomes a rate-limiting factor of the drying process. In this case, as the excess sublimation process consumes additional input energy, large changes in shelf temperature are required to produce an observable change in product temperature. Conversely, although high chamber pressures enhance the heat transfer rate, which is attributed to improved heat transfer via gas conduction,[45] they significantly reduce the driving force for mass transfer. Thus, the mass transfer becomes a rate-limiting factor of the drying process, and any additional input energy, that is an increase in shelf temperature, has significant influence on the product temperature. This is evident from Figure 5a, where it can be observed that the curves at

Table 3
Values of T_g', T_c, and the Range of Maximum Product Temperature During Primary Drying for MF1 and MF2

Formulation	T_g' (°C)	T_c (°C)	Range of Maximum Product Temperature During Primary Drying (°C)
MF1	−29.2	−27.5	−28.5 to −29.5
MF2	−32.4	−31.1	−31.5 to −32.5

T_g' is the glass transition temperature of the maximally freeze-concentrated solution and T_c is the collapse temperature.

Table 4
Results of Average Product Temperatures and Sublimation Rates at Selected Combinations of Chamber Pressure and Shelf Temperatures for MF1 and MF2

P_c (mbar)	T_s (°C)	Formulation	Front Edge Vials				Center Vials			
			$T_p ave$[a] (°C)	Sublimation Rate (g/h·vial)			$T_p ave$[a] (°C)	Sublimation Rate (g/h·vial)		
				Max[b]	Min[c]	Ave[d]		Max[b]	Min[c]	Ave[d]
0.10	−15.0	MF1	−30.1	0.229	0.170	0.191	−32.6	0.137	0.115	0.121
	−17.0		−30.7	0.202	0.147	0.171	−33.5	0.113	0.102	0.107
	−20.0		−31.7	0.181	0.137	0.156	−34.2	0.110	0.088	0.099
	−25.0		−32.1	0.159	0.114	0.129	−36.6	0.087	0.069	0.076
0.20	−20.0		−28.9	0.223	0.175	0.193	−29.9	0.134	0.120	0.125
	−25.0		−29.8	0.165	0.125	0.138	−31.4	0.085	0.081	0.078
	−30.0		−31.7	0.094	0.069	0.078	−33.5	0.046	0.026	0.042
	−35.0		−34.7	0.055	0.035	0.044	−36.6	0.018	0.015	0.016
0.10	−15.0	MF2	−30.3	0.258	0.201	0.221	−31.4	0.150	0.121	0.131
	−17.0		−30.7	0.231	0.173	0.193	−32.8	0.127	0.102	0.109
	−20.0		−31.1	0.210	0.160	0.177	−33.2	0.115	0.086	0.091
	−25.0		−32.0	0.156	0.127	0.137	−35.0	0.072	0.059	0.067
0.20	−20.0		−30.1	0.272	0.208	0.232	−30.8	0.153	0.138	0.144
	−25.0		−31.3	0.174	0.145	0.157	−32.3	0.105	0.081	0.092
	−30.0		−32.2	0.131	0.095	0.108	−33.8	0.052	0.041	0.045
	−35.0		−34.5	0.077	0.046	0.057	−36.7	0.018	0.014	0.016

P_c is chamber pressure; T_s is shelf temperature; $T_p ave$ is the average product temperature.
[a] The average product temperatures ($T_p ave$) for each vial group were calculated as the arithmetic average of the temperature measurements in the time range used for sublimation rate calculation.
[b] The maximum sublimation rates were the maximum value of the sublimation rates from each vial group.
[c] The minimum sublimation rates were the minimum value of the sublimation rates from each vial group.
[d] The average sublimation rates were calculated as the arithmetic average of the sublimation rates from each vial group.

low chamber pressure have larger slopes than the curves at high chamber pressures. This fact has a quantifiable effect from a process robustness point of view. That is, a freeze-drying process designed at relatively low chamber pressure is more robust to small shelf temperature variations than a freeze-drying process designed at relatively high chamber pressure.

The range of maximum product temperature during primary drying for MF1 was defined from −29.5°C to −28.5°C (see Table 3). Further, lower and higher chamber pressure limits were defined based on the equipment and process constraints. This information was used to impose formulation, process, and equipment constraints, and the PDS was defined as displayed in Figure 5b. From Figure 5b, the process parameters that yielded a low product temperature space and high product temperature space can be easily identified. In the former, the product temperature is less than the desired range and leads to an unnecessarily long primary drying time (inefficient process), whereas in the latter, the resulting high product temperature leads to product damage (collapse or meltback), which compromises product CQAs. Although it has been reported that collapse does not lead to a loss of CQAs for drug products,[40] additional experimental studies are required to study the effect of collapse on drug stability during storage.[46-53] Further, regulatory agencies require consistent, reproducible, and uniform cake appearance to ensure drug stability.[8]

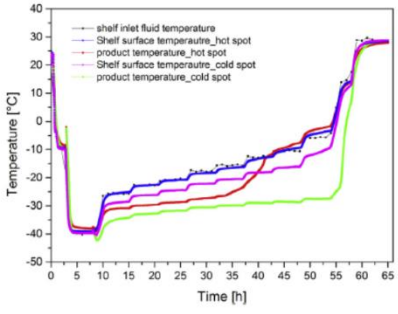

Figure 4. Experimental data showing significant spatial shelf surface temperature and product temperature differences across a shelf. Chamber pressure = 0.1 mbar.

From the PDS defined in Figure 5b, one would choose to use "high chamber pressure-low shelf temperature" or "low chamber pressure-high shelf temperature" combinations to achieve the same product temperature. However, depending on the chamber pressure, the same product temperature can produce different sublimation rates. At a given product temperature, low chamber pressure yields a high sublimation rate. Thus, a further definition of the PDS including values for sublimation rate is necessary. To include such information, the data of sublimation rates are plotted against experimental product temperatures, as displayed in Figure 6a. Figure 6a contains the average product temperature of the front edge vials in the x-axis and the minimum sublimation rate of the center vials in the y-axis. As reported in the literature[42-44,54] and determined experimentally in this study, the center vials have the lowest sublimation rate in the vial arrays. Therefore, Figure 6a allows consideration of the minimum sublimation rate during the construction of the PDS. This, in turn, avoids possible product damage owing to premature change to the secondary drying step. The choice of the average product temperature of the front edge vials in Figure 6a is because the product isotherms of the PDS (see Fig. 5b) are based on this parameter. Therefore, information on the sublimation rate of the center vials when the front edge vials achieve the target product temperature is required.

As indicated in Figure 6a, there is an excellent fitting of the experimental data ($R^2 > 0.95$) and regression analyses of the data were used to calculate the minimum sublimation rate of the center vials at a given chamber pressure and product temperature of the front edge vials. The initial PDS (Fig. 5b) was redefined after the sublimation rate values obtained from Figure 6a were included. The final PDS for MF1 is presented in Figure 6b.

The PDS defined in Figure 6b encompasses a wide range of T_s, P_c, and sublimation rate values. Thus, a control space within the PDS can be defined when the range of process parameters is small and well controlled. The control space is defined to encompass the

highest sublimation rates within the PDS. However, it is recommended that the consideration of edge process parameters to account for batch-to-batch process variations be avoided. Process parameters for the primary drying step can be defined within the control space as a set point. The set point can be selected anywhere within the control space. However, to consider intrabatch and interbatch variation in the process parameters, it is recommended to select the set point as the midpoint of the control space. At the set point, the minimum sublimation rate within the control space can be used to calculate the primary drying time.

Construction of Process Design Space for MF2

The experimental data obtained for MF2 were analyzed in a similar manner to the method followed for MF1. Accordingly, the PDS for the second formulation was obtained. It is presented in Figure 7.

Experimental Verification of the PDSs for MF1 and MF2

Because the calculations of the product temperatures and sublimation rates involve linear regression analyses, minor inaccuracies in the corresponding values could occur. Therefore, it is important to verify, experimentally, that the PDS obtained in this study yields the expected product temperatures and sublimation rates of the model formulations. Freeze-drying experimental runs were performed at selected set point values for both model formulations. The values of the set point parameters were selected from Figures 6b and 7, as follows:

- For MF1: $P_c = 0.075$ mbar, $T_s = 3$ °C, Fill volume = 3 mL
- For MF2: $P_c = 0.075$ mbar, $T_s = -16$ °C, Fill volume = 3 mL

The freezing protocol in these verification experiments was the same as the freeze protocol used for the construction of the PDS. This minimizes any possible variation of drying behavior owing to the freezing protocol. The product temperatures of the center and front edge vials were measured using wireless thermologgers (4 for each vial group). The sublimation rates of the center vials were determined gravimetrically and, for this purpose, 16 center vials were weighed before and after the experiment.

Figure 8 displays the product temperature profiles of MF1 and MF2 obtained from the verification experiments. Further, the estimated parameters from the PDS were compared with the parameters obtained from the verification experiments. They are presented in Table 5.

As indicated in Figure 8 and Table 5, there is an excellent agreement between the PDS-estimated and the experimentally determined values for both model formulations. This demonstrates that the procedures described in this article for the construction of an effective and product-based PDS, coupled with an effective DoE, produce highly accurate and reproducible results. This can enable process scientists to design freeze-drying processes for a given pharmaceutical drug formulation based on a scientific approach, using limited well-defined experimental runs.

Utilization of the Lab PDS for Process Scale-Up and Transfer

Equipment Capability

Mainly owing to their large capacity, chocking flow could be more pronounced at manufacturing scale freeze dryers. Therefore, it is critical to determine the capability of the target freeze dryer to control the P_c at full load capacity and at typical freeze-drying sublimation rates. The determination of the capability of a target freeze dryer could be carried out using a one-point water sublimation test as follows: (1) fully load the target freeze dryer with pure water placed on a tray made from plastic; (2) freeze the water and allow complete solidification; (3) set the P_c to 0 and increase the T_s to +30°C or +40°C; and (4) observe the minimum P_c and its stability, attained by the freeze dryer after the T_s setpoint has been reached. Although the calculation of the exact value of the total vapor flow rate could be difficult, it could be assumed that the total vapor flow rate of pure water, at a T_s value ranging from +30°C to +40°C and a controllable low P_c is much higher than most of the typical vapor flow rates obtained using drug formulations. Thus, if a freeze dryer is able to attain and control a minimum P_c of, for example, 50 μbar when pure water at a T_s of +30°C or +40°C is used, it could be safely concluded that the occurrence of chocked flow for P_c up to 50 μbar is highly unlikely when a drug formulation at typical primary drying T_s values is used.

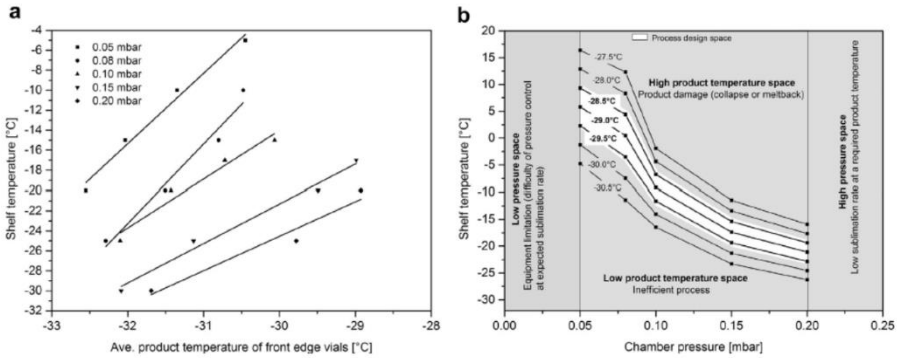

Figure 5. (a) Relationship between average product temperature of front edge vials and shelf temperature (at different chamber pressures) for MF1 and (b) PDS for primary drying of MF1 after formulation, process and equipment constraints.

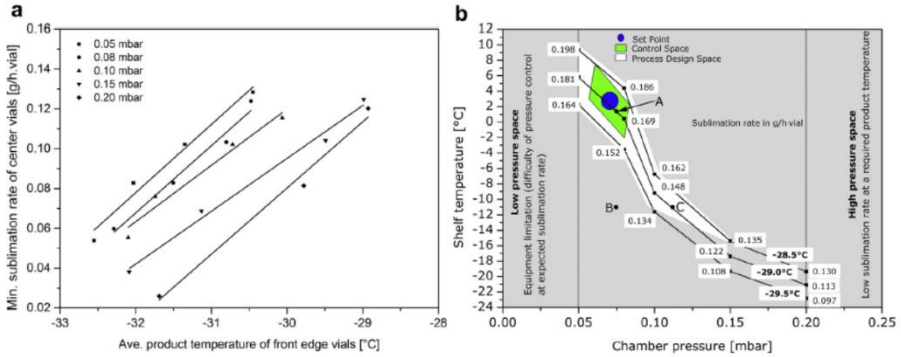

Figure 6. (a) Relationship of average product temperature of front edge vials and minimum sublimation rate of center vials (at different chamber pressures) for MF1. (b) Final process design space (PDS) for primary drying of MF1, taking into consideration minimum sublimation rate of center vials. Relatively minimum values of sublimation rate (mostly in the region of high chamber pressure) were removed from the originally defined PDS (Fig. 5b).

Differences in Resistance to Mass Transfer of the Dried Product (R_p) and Overall Vial Heat Transfer Coefficient (K_v)

The differences in R_p and K_v between laboratory and manufacturing scale freeze dryers are the major freeze-drying process scale-up and transfer factors. Differences in R_p could be caused by variations in the degree of supercooling, which could be affected by differences in cleanness between laboratory and manufacturing environments. On the other hand, differences in K_v could arise from differences in design and performance of the dryers. Differences in R_p and K_v during scale-up or transfer could be easily detected from T_p response, provided that identical primary drying processing conditions (i.e., T_s and P_c) are used. Thus, at the same processing conditions, an increase in R_p is reflected by an increase in T_p. Because the vapor flow is more restricted at higher R_p, there is less energy consumption from the system, and most of the heat input is utilized to increase the T_p. Conversely, at low R_p, most of the heat input is consumed by the relatively higher sublimation rate (attributed to the lower resistance to vapor flow), and hence the T_p becomes lower. An increase in K_v at the same T_s and P_c leads to an increase in T_p and vice versa. However, the influence of K_v on freeze-drying process scale-up and transfer could be significantly minimized by using the same container-closure system and a laboratory scale freeze dryer with similar design and performance to a manufacturing scale freeze dryer. Therefore, the most important factor that could cause differences in T_p during scale-up or transfer is R_p.

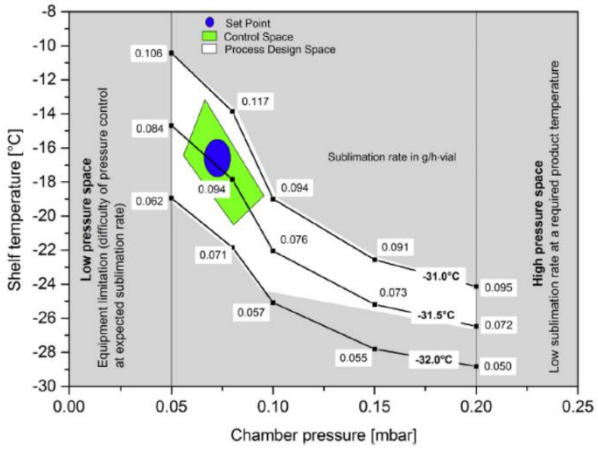

Figure 7. Final process design space (PDS) for primary drying of MF2, taking into consideration the minimum sublimation rate. Relatively minimum values of sublimation rate (mostly in the region of high chamber pressure) were removed from the originally defined PDS.

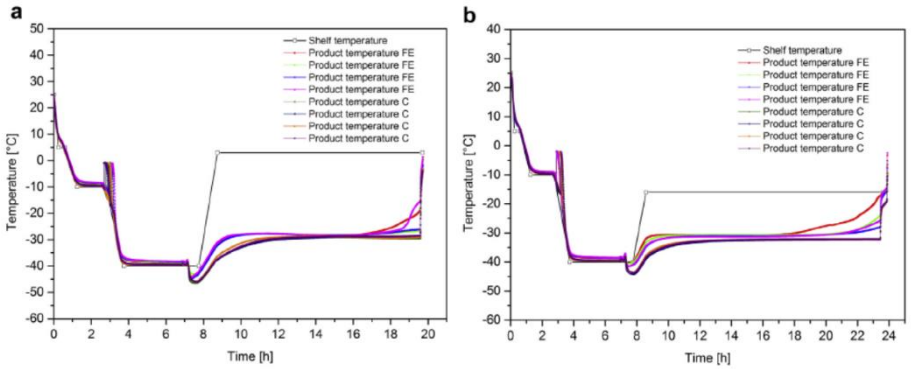

Figure 8. Experimental verification of the process design space (PDS). (a) Product temperature profiles of front edge vials (FE) and center vials (c) for MF1; (b) Product temperature profiles of front edge vials (FE) and center vials (c) for MF2.

From the above discussion, the T_s (keeping P_c constant) at the target freeze dryer that is needed to obtain the target product temperature (T_pt) could be different, and thus determination of the new T_s and adjustment of the drying time (t_d) would be the major scale-up or transfer experiments. With this regard, the PDS developed at lab scale provides important information that could be utilized during the scale-up or transfer experiments: (1) the range of possible T_s values that could be used to determine the new T_s; (2) the robustness of the formulation to T_s changes; and (3) variation of sublimation rates at different processing conditions. Considering possible variations in R_p, a T_s range from −12°C to +12°C at a P_c = 0.075 mbar could yield the T_pt for MF1 (cf. Fig. 6b). Such information could be utilized to perform a temperature ramp experiment using the target freeze drier to obtain the new T_s value. Point A of Figure 6b shows that, at P_c = 0.075 mbar, a T_s around +1°C was required to yield a T_p of −29.0°C. Assuming that the new T_s value, at the target freeze dryer and P_c = 0.075 mbar, required to yield a T_p of −29.0°C was −11°C (Point B, Fig. 6b), the corresponding differences in sublimation rates and thus in t_d, of point A and point B could be adjusted using the PDS developed at lab scale. The reduction in sublimation rate caused by an increase in R_p (thus a decrease in T_s) at constant P_c (Point B, Fig. 6b) is equivalent to a reduction in sublimation rate caused by an increase in P_c (thus a decrease in T_s) at constant R_p, provided that the T_p is the same for both cases. Considering the same formulation, product temperature, and processing environment, the R_p at laboratory scale can be assumed as fairly constant at the different processing conditions. Furthermore, assuming the reduction in T_s at the target freeze dryer is due entirely to the increase in R_p, the sublimation rate at the new T_s value (i.e., −11°C) and T_p = −29.0°C from the PDS (point C, Fig. 6b) could be used to adjust the sublimation rate and the t_d at the target freeze dryer.

Conclusions

A new step-by-step procedure for the construction of a product-based PDS for the primary drying step was described. An effective DoE was developed, which could then be used to experimentally determine the necessary information for the construction of the PDS. The development of an effective DoE requires a profound scientific understanding of the formulation and process and perhaps requires only limited preliminary experiments. The proposed product-based PDS considers variations in product temperatures and sublimation rates within the vial arrays. With this regard, the product temperature of the front edge vials and sublimation rate of the center vials were used. This assures the effectiveness and the robustness of the PDS. Compared with the mathematical models that could require several freeze-drying experiments for optimization and verification, the product-based PDS detailed herein produced highly accurate results, demonstrating the potential for significant development time and material savings. Further, the PDS of a drug formulation based on experimental results presents more realistic and reliable data if there is an intention of using the PDS for regulatory agencies. Experimental

Table 5
Comparison of PDS-Estimated and Experimentally Determined Parameters at Set Point

Formulation	PDS Estimated Values				Experimentally Determined Values				Differences (%)			
	FE	C			FE	C			FE	C		
	T_pave (°C)	T_pave (°C)	$\dot{m}$(g/h·vial)	t_d[c] (h)	T_pave[a] (°C)	T_pave[a] (°C)	$\dot{m}$[b] (g/h·vial)	t_d[d] (h)	T_pave	T_pave	$\dot{m}$	t_d
MF1	−28.7	−31.0	0.169	16.0	−28.4	−30.1	0.177	15.3	1.05	2.90	4.73	4.38
MF2	−31.2	−33.4	0.094	25.5	−31.3	−32.8	0.104	23.1	0.32	1.80	10.64	9.41

T_pave is average product temperature; $\dot{m}$ is sublimation rate; t_d is drying time of primary drying; FE is front edge vials; and C is center vials.
[a] T_pave was obtained by averaging product temperatures obtained from 4 thermologgers.
[b] $\dot{m}$ is the minimum value of 16 sublimation rate values.
[c] t_d is calculated based on the minimum sublimation rate within the control space and based on 3 mL fill volume.
[d] t_d is calculated based on the minimum sublimation rate of the 16 experimentally determined sublimation rate values and based on 3 mL fill volume.

verifications of the PDS for the 2 formulations studied in this research were performed, and an excellent agreement between the PDS predicted values and experimentally determined values were achieved. Finally, coupled with an effective DoE, the proposed procedure for the construction of a product-based PDS considerably reduces development time and material requirements and significantly improves the accuracy, effectiveness, and robustness of the resulting freeze-drying process. Thus, process scale-up problems are minimized with the development of a PDS. Further, the resulting optimum and robust freeze-drying process has significant advantages in process cost and energy savings and in maintaining product quality consistency during a large-scale manufacturing process.

Acknowledgment

Each of the authors confirms that there was no financial aid from an organization or technical assistance outside the authors themselves.

References

1. Pikal MJ. Freeze-drying of proteins. Part I: process design. *BioPharm*. 1990;3:18-27.
2. Pikal MJ. Freeze-drying of proteins. Part II: formulation selection. *BioPharm*. 1990b;10:26-30.
3. Patel SM, Jameel F, Pikal MJ. The effect of dryer load on freeze drying process design. *J Pharm Sci*. 2010;99:4363-4379.
4. Mortier STFC, Van Bockstal PJ, Corver J, Nopens I, Gernaey KV, De Beer T. Uncertainty analysis as essential step in the establishment of the dynamic design space of primary drying during freeze-drying. *Eur J Pharm Biopharm*. 2016;103:71-83.
5. Tang X, Pikal MJ. Design of freeze-drying processes for pharmaceuticals: practical advice. *Pharm Res*. 2004;21:191-200.
6. Liu J. Physical characterization of pharmaceutical formulations in frozen and freeze-dried solid states: techniques and applications in freeze-drying development. *Pharm Dev Technol*. 2006;11:3-28.
7. Wang DQ. Formulation characterization. In: Rey L, May JC, eds. *Freeze Drying/Lyophilization of Pharmaceutical and Biological Products*. 3rd ed. London, UK: Informa Healthcare; 2010:233-253.
8. Goldman JM, More HT, Yee O, et al. Optimization of primary drying in lyophilization during early-phase drug development using a definitive screening design with formulation and process factors. *J Pharm Sci*. 2018;107:2592-2600.
9. Ward KR, Matejtschuk P. Characterization of formulations for freeze-drying. In: Ward K, Matejtschuk P, eds. *Lyophilization of Pharmaceuticals and Biologicals. Methods in Pharmacology and Toxicology*. New York: Humana Press; 2019:1-32.
10. Goshima H, Do G, Nakagawa K. Impact of ice morphology on design space of pharmaceutical freeze-drying. *J Pharm Sci*. 2016;105:1920-1933.
11. Assegehegn G, Brito-de la Fuente E, Franco JM, Gallegos C. The importance of understanding the freezing step and its impact on freeze drying process performance. *J Pharm Sci*. 2019;108:1378-1395.
12. Pikal MJ, Cardon S, Bhugra C, et al. The non-steady state modeling of freeze-drying: in-process product temperature and moisture content mapping and pharmaceutical product quality applications. *Pharm Dev Technol*. 2005;10:17-32.
13. Gieseler H, Kramer T, Pikal MJ. Use of Manometric Temperature Measurement (MTM) and SMART™ freeze dryer technology for development of an optimized freeze-drying cycle. *J Pharm Sci*. 2007;96:3402-3418.
14. Velardi SA, Barresi AA. Development of simplified models for the freeze-drying process and investigation of the optimal operating conditions. *Chem Eng Res Des*. 2008;86:9-22.
15. Kuu WY, Nail SL. Rapid freeze-drying cycle optimization using computer programs developed based on heat and mass transfer models and facilitated by Tunable Diode Laser Absorption Spectroscopy (TDLAS). *J Pharm Sci*. 2009;98:3469-3482.
16. Sundaram J, Shay YHM, Hsu CC, Sane SU. Design space development for lyophilization using DOE and process modeling. *Biopharm Int*. 2010;23:26-36.
17. Giordano A, Barresi AA, Fissore D. On the use of mathematical models to build the design space for the primary drying phase of a pharmaceutical lyophilization process. *J Pharm Sci*. 2011;100:311-324.
18. Koganti VR, Shalaev EY, Berry MR, et al. Investigation of design space for freeze-drying: use of modeling for primary drying segment of a freeze-drying cycle. *AAPS PharmSciTech*. 2011;12:854-861.
19. Fissore D, Pisano R, Barresi AA. Advanced approach to build the design space for the primary drying of a pharmaceutical freeze-drying process. *J Pharm Sci*. 2011;100:4922-4933.
20. Bosca S, Barresi AA, Fissore D. Fast freeze-drying cycle design and optimization using a PAT based on the measurement of product temperature. *Eur J Pharm Biopharm*. 2013;85:253-262.
21. Kodama T, Sawada H, Hosomi H, et al. Determination for dry layer resistance of sucrose under various primary drying conditions using a novel simulation program for designing pharmaceutical lyophilization cycle. *Int J Pharm*. 2013;452:180-187.
22. Kodama T, Sawada H, Hosomi H, et al. Optimization of primary drying condition for pharmaceutical lyophilization using a novel simulation program with a predictive model for dry layer resistance. *Chem Pharm Bull*. 2014;62:153-159.
23. Fissore D, Pisano R. Computer-aided framework for the design of freeze-drying cycles: optimization of the operating conditions of the primary drying stage. *Processes*. 2015;3:406-421.
24. Chen X, Sadineni V, Maity M, Quan Y, Enterline M, Mantri RV. Finite element method (FEM) modeling of freeze-drying: monitoring pharmaceutical product robustness during lyophilization. *AAPS PharmSciTech*. 2015;16:1317-1326.
25. Van Bockstal PJ, Mortier STFC, Corver J, Nopens I, Gernaey KV, De Beer T. Quantitative risk assessment via uncertainty analysis in combination with error propagation for the determination of the dynamic design space of the primary drying step during freeze-drying. *Eur J Pharm Biopharm*. 2017;121:32-41.
26. Arsiccio A, Pisano R. Application of the quality by design approach to the freezing step of freeze-drying: building the design space. *J Pharm Sci*. 2018;107:1586-1596.
27. Zhu T, Moussa EM, Witting M, et al. Predictive models of lyophilization process for development, scale-up/tech transfer and manufacturing. *Eur J Pharm Biopharm*. 2018;128:363-378.
28. Sharma P, Kessler WJ, Bogner R, Thakur M, Pikal MJ. Applications of the tunable diode laser absorption spectroscopy: in-process estimation of primary drying heterogeneity and product temperature during lyophilization. *J Pharm Sci*. 2019;108:416-430.
29. Patel S, Jameel F, Sane S, Kamat M. Lyophilization process design and development using QbD principles. In: Jameel F, Hershenson S, Khan M, Martin-Moe S, eds. *Quality by Design for Biopharmaceutical Drug Product Development. AAPS Advances in the Pharmaceutical Sciences Series*. 18. New York: Springer; 2015:303-329.
30. US Department of Health and Human Services, Food and Drug, Administration. Center for drug evaluation and research(CDER), center for biologics evaluation and research (CBER). In: *ICH Q8(R2) Pharmaceutical Development*. Silver Spring, MD: Food and Drug Administration (FDA); 2009.
31. Ganguly A, Alexeenko AA, Schultz SG, Kim SG. Freeze-drying simulation framework coupling product attributes and equipment capability: toward accelerating process by equipment modifications. *Eur J Pharm Biopharm*. 2013;85:223-235.
32. Ganguly A, Varma N, Sane P, Bogner R, Pikal M, Alexeenko A. Spatial variation of pressure in the lyophilization product chamber part 1: computational modeling. *AAPS PharmSciTech*. 2017;18:577-585.
33. Kshirsagar V, Tchessalov S, Kanka F, Hiebert D, Alexeenko A. Determining maximum sublimation rate for a production lyophilizer: computational modeling and comparison with ice slab tests. *J Pharm Sci*. 2019;108:382-390.
34. Chang BS, Fischer NL. Development of an efficient single-step freeze-drying cycle for protein formulations. *Pharm Res*. 1995;12:831-837.
35. Her LM, Nail SL. Measurement of glass transition temperatures of freeze-concentrated solutes by differential scanning calorimetry. *Pharm Res*. 1994;11:54-59.
36. Scutellà B, Trelea IC, Bourlès E, Fonseca F, Passot S. Determination of the dried product resistance variability and its influence on the product temperature in pharmaceutical freeze-drying. *Eur J Pharm Biopharm*. 2018;128:379-388.
37. Pikal MJ. Use of laboratory data in freeze-drying process design: heat and mass transfer coefficients and the computer simulation of freeze-drying. *J Parenter Sci Technol*. 1985;39:115-139.
38. Chang BS, Randall CS. Use of sub-ambient thermal analysis to optimize protein lyophilization. *Cryobiology*. 1992;29:632-656.
39. Adams GDJ, Ramsay JR. Optimizing the lyophilization cycle and the consequences of collapse on the pharmaceutical acceptability of Erwinia l-Asparaginase. *J Pharm Sci*. 1996;85:1301-1305.
40. Patel SM, Pikal MJ. Lyophilization process design space. *J Pharm Sci*. 2013;102:3883-3887.
41. Pikal MJ, Bogner R, Mudhivarthi V, Sharma P, Sane P. Freeze-drying process development and scale-up: scale-up of edge vial versus center vial heat transfer coefficients, Kv. *J Pharm Sci*. 2016;105:3333-3343.
42. Scutellà B, Plana-Fattoric A, Passota S, et al. 3D mathematical modelling to understand atypical heat transfer observed in vial freeze-drying. *Appl Therm Eng*. 2017;126:226-236.
43. Scutellà B, Passot S, Bourlès E, Fonseca F, Tréléa IC. How vial geometry variability influences heat transfer and product temperature during freeze-drying. How vial geometry variability influences heat transfer and product temperature during freeze-drying. *J Pharm Sci*. 2017;106:770-778.
44. Scutellà B, Bourlès E, Plana-Fattori A, et al. Effect of freeze dryer design on heat transfer variability investigated using a 3D mathematical model. *J Pharm Sci*. 2018b;107:2098-2106.
45. Pikal MJ, Roy ML, Shah S. Mass and heat transfer in vial freeze-drying of pharmaceuticals: role of the vial. *J Pharm Sci*. 1984;73:1224-1237.
46. Wang DQ, Hey JM, Nail SL. Effect of collapse on the stability of freeze-dried recombinant factor VIII and a-amylase. *J Pharm Sci*. 2004;93:1253-1263.
47. Schersch K, Betz O, Garidel P, Muehlau S, Bassarab S, Winter G. Systematic investigation of the effect of lyophilizate collapse on pharmaceutically relevant proteins I: stability after freeze-drying. *J Pharm Sci*. 2010;99:2256-2278.

48. Schersch K, Betz O, Garidel P, Muehlau S, Bassarab S, Winter G. Systematic investigation of the effect of lyophilizate collapse on pharmaceutically relevant proteins, part 2: stability during storage at elevated temperatures. *J Pharm Sci*. 2012;101:2288-2306.
49. Schersch K, Betz O, Garidel P, Muehlau S, Bassarab S, Winter G. Systematic investigation of the effect of lyophilizate collapse on pharmaceutically relevant proteins III: collapse during storage at elevated temperatures. *Eur J Pharm Biopharm*. 2013;85:240-252.
50. Ullrich S, Seyferth S, Lee G. Measurement of shrinkage and cracking in lyophilized amorphous cakes. Part I: final-product assessment. *J Pharm Sci*. 2015;104:155-164.
51. Patel SM, Nail SL, Pikal MJ, et al. Lyophilized drug product cake appearance what is acceptable? *J Pharm Sci*. 2017;106:1706-1721.
52. Duralliu A, Matejtschuk P, Williams DR. Humidity induced collapse in freeze dried cakes: a direct visualization study using DVS. *Eur J Pharm Biopharm*. 2018;127:29-36.
53. Haeuser C, Goldbach P, Huwyler J, Friess W, Allmendinger A. Imaging techniques to characterize cake appearance of freeze-dried products. *J Pharm Sci*. 2018;107:2810-2822.
54. Pikal MJ, Pande P, Bogner R, Sane P, Mudhivarthi V, Sharma P. Impact of natural variations in freeze-drying parameters on product temperature history: application of quasi steady-state heat and mass transfer and simple statistics. *AAPS PharmSciTech*. 2018;19:2828-2842.

Appendix A.4:

Understanding and optimization of the secondary drying step of a freeze-drying process: A case study

Getachew Assegehegn[1], Edmundo Brito-de la Fuente[1], José M. Franco[2] and Críspulo Gallegos[1]

[1]Fresenius-Kabi Deutschland GmbH, Process and Product Engineering Center, Global Manufacturing Pharmaceuticals, Bad Homburg, Germany

[2]Pro2TecS-Chemical Product and Process Technology Research Centre, Complex Fluid Engineering Laboratory. Departamento de Ingeniería Química, Universidad de Huelva, Huelva, Spain

Published in:

Journal	Drying Technology
Publishing company	Taylor & Francis
Editor-in-Chief	Dr. Arun S. Mujumdar
Volume and pages	---
Publication year	----
ISSN	0737-3937
DOI	---------
Journal impact factor (2018)	**2.307**

Category (2017)	**Journal rank/total journal**	**Quartile**
Chemical Engineering		Q1
Physical and Theoretical Chemistry		Q2